

35TH
INTERNATIONAL
GEMMOLOGICAL
CONFERENCE

October 8 - 19, 2017
Namibia

IGC 2017



NAMIBIA



35th International Gemmological Conference IGC

**October 2017
Windhoek, Namibia**

Dear colleagues of IGC,

It is our great pleasure to host the 35th International Gemmological Conference in Windhoek, Namibia. The spectacular landscape, the species-richness of wildlife and the variety of cultures and traditions make Namibia a very popular country to visit. For gemmologists Namibia is of highest interest because of its unique geology, mineral resources and gemstone potential. IGC is an important platform for distinguished gemmologists from all over the world to present and discuss their latest research works but also to cultivate friendship within the gemmological family. It is our great desire to thank the local organizer Andreas Palfi for his extraordinary work to realize the IGC in Namibia.

The organizers of 35th International Gemmological Conference wish you an exciting and memorable conference.

Dr. Ulrich Henn, Prof. Dr. Henry A. Hänni, Andreas G. Palfi MSc



The organizers of the 35th International Gemmological Conference in Namibia. From the left: Andreas Palfi, Ruth Palfi, Ulrich Henn, Annamarie Peyer, Henry A. Hänni at Okapuka Ranch, Namibia in 2016.

Organization of the 35th International Gemmological Conference

Organizing Committee

Dr. Ulrich Henn (German Gemmological Association)

Prof. Dr. Henry A. Hänni (Swiss Gemmological Institute SSEF)

Andreas G. Palfi MSc (local organizer, Consulting Exploration Geologist, Palfi, Holman and Associates, Geo Tours Namibia and Namibia Minerals)

Dr. Jayshree Panjekar (IGC Secretary)

IGC Executive Committee

Guest Programme

Ruth Palfi (Windhoek, Namibia) and Annamarie Peyer (Hong Kong)

Homepage

Dr. Michael Krzemnicki (Swiss Gemmological Institute SSEF)

Dr. Laurent Cartier (Swiss Gemmological Institute SSEF)

Proceedings

Dr. Michael Krzemnicki (Swiss Gemmological Institute SSEF)

Dr. Laurent Cartier (Swiss Gemmological Institute SSEF)

Abstract Review Board

Prof. Dr. Henry A. Hänni

Prof. Dr. Emmanuel Fritsch

Dr. Ulrich Henn

Dr. Karl Schmetzer

Dr. Hanco Zwaan

Special thanks

Mrs. Martina Bank (German Gemmological Association) for organizing registrations, general administration and financial management.

Acknowledgements

Ministry of Mines and Energy Namibia:

The Honourable Minister Obeth Kandjoze, MP

The Honourable Deputy Minister Kornelia Shilunga, MP

Permanent Secretary Simeon Negumbo

Mining Commissioner Mr. Erasmus Shivolo

Department Geological Survey: Ms. Gloria Simubali, Acting Deputy Permanent Secretary

Chamber of Mines of Namibia: Mr. Veston Malango CEO

Green Dragon Mine: Mag. Stephan Reif

Kristall Gallerie and Otjua Tourmaline Mine: Kleynhans family

Usakos Tourmaline Mine: Mr. Hannes Brunner

Namibia Diamond Trading Company (NDTC): Mr. Shihaleni Ndjaba CEO

Namdeb Diamond Corporation: Mr. Riaan Burge, General Manager and Dr. Jurgen Jacob, Head of Mineral Resource and Environment

Namcot Diamonds: Mr. Ofer Babluky, General Manager

About the IGC Executive Committee



Members of the IGC Executive Committee at the Closing Ceremony of the 34th IGC in Vilnius, Lithuania.

- Dr. Jayshree Panjikar, Executive Secretary, India (fourth from the left)
- Prof. Dr. Emmanuel Fritsch, France (first from the left)
- Dr. J. C. Hanco Zwaan, The Netherlands (second from the left)
- Tay Thye Sun, Singapore (third from the left)
- Prof. Dr. Henry A. Hänni, Switzerland (fourth from the right)
- Dr. Karl Schmetzer, Germany (third from the right)
- Gamini Zoysa, Sri Lanka (second from the right)
- Willow Wight, Canada (first from the right)
- Dr. Michael Krzemnicki, Switzerland
- Dr. Dietmar Schwarz, Germany

About the venue



Windhoek

Windhoek downtown



Safari Court Hotel

Otjua Tourmaline Mine

Windhoek

Windhoek is the capital of the Republic of Namibia and located at the geographical centre of the country. More than 320,000 people live in Namibia's largest city which is the social, economic, political and cultural centre.

The conference will be held at the Safari Hotels with well-equipped conference facilities.

Pre- and post-conference tours will lead to the diamond operations at Oranjemund and near Lüderitz and to tourmaline and garnet mining areas near Karibib and Usakos as well as to the historic place Swakopmund at the Atlantic Ocean with its unique museum and Kristall Galerie.

Sponsors



INTERNATIONAL GEMMOLOGICAL CONFERENCE

History of the IGC

The International Gemmological Conference (IGC) owes much of its origin to BIBOA (*Bureau International pour la Bijouterie, Orfevrene, Argenterie*), the International Jewellery and Gemstone Federation, the first Congress of which in 1926 recommended and defined use of the term cultured pearl.

Experts from various European gem testing laboratories were invited to attend a series of expert meetings that aimed to formulate the policies of BIBOA. In 1936, at the fifth conference of experts, collaboration among laboratories was acclaimed by traders and they encouraged Laboratory Directors to meet each other at a technical conference from which all commercial delegates would be excluded.

Technical meetings were held annually, and in 1951 a Technical Conference was held in Idar Oberstein to prepare for the next London Congress in 1952. Those attending the 1951 conference included Mr B.W. Anderson, Mr G. Gobel, Dr E. Gübelin, Mr F. Wolf, Mr A. Bonebakker, Mr H. Tillander, Mr A. Strondahl, and Mr O. Dragstead. It has been suggested that the future framework of the IGC was established at this meeting in Idar Oberstein.

The London Congress saw the restructuring of BIBOA in which Gemmological Associations were replaced by National Federal Committees, and BIBOA evolved into BIBOAH – the forerunner of CIBJO, now known as The World Jewellery Confederation.

A Technical Conference met at Lugano from 23rd to 25th October 1952 at the initiative of Prof. K. Schlossmacher and Dr. E. Gübelin. Also present at this conference were Messrs B.W. Anderson, A. Bonebakker, O. Dragstead, G. Gobel, K. Siess and H. Tillander. At this historic meeting Dr E. Gübelin proposed creation of a “Committee of an International Gemmological Association” that would consist of one member per country; this member being the Director of a Gem Testing Laboratory, or a gemmologist of the calibre who could attend that meeting. This was agreed to, and this meeting was later considered to be the inaugural meeting of the IGC.

The first meeting of the IGC in Lugano was followed by subsequent meetings in Amsterdam, The Netherlands (1953), Copenhagen, Denmark (1954), London, UK (1955), Munich, Germany (1956), Oslo, Norway (1957), Paris, France (1958), Milano, Italy (1960), Helsinki, Finland (1962), Vienna, Austria (1964); Barcelona, Spain (1966); Stockholm, Sweden (1968); Brussels, Belgium (1970); Vitznau, Switzerland (1972); Washington D. C., USA (1975), The Hague, The Netherlands (1977), Idar Oberstein, Germany (1979), Kashiko-Jima, Japan (1981), Beruwela, Sri Lanka (1983); Sydney, Australia (1985); Rio de Janeiro, Brazil (1987), Tremezzo, Italy (1989); Stellenboch (1991), Paris, France (1993); Bangkok, Thailand (1995); Idar Oberstein, Germany (1997); Goa, India (1999); Madrid, Spain (2001), Wuhan, China (2004); Moscow, Russia (2007); Arusha, Tanzania (2009), Interlaken, Switzerland (2011); Hanoi, Vietnam, (2013); Vilnius, Lithuania (2015); the 35th IGC will be held in Windhoek, Namibia in 2017.

Over the history of the IGC, that now in its fourth decade, it can therefore be seen that the International Gemmological Conference is the longest surviving gemmological conference to remain largely in its original format. Over its history, invited delegates representing 33 countries or areas – including Australia, Austria, Belgium, Brazil, Canada, China, Czech Republic, Denmark, England, Finland, France, Greece, Germany, Hong Kong, Israel, India, Italy, Japan, Kenya, Korea, Netherlands, Norway, Russia, Singapore, South Africa, Spain, Sri Lanka, Switzerland, Sweden, Thailand, U.S.A. and Zimbabwe – have been invited to participate in IGC meetings.

During the 20th IGC, which was held in Sydney, Australia, the members present elected nine members to Honorary Members status. The first Honorary Members of the IGC were Oliver Chalmers (Australia), Prof. A. Chikayama (Japan), and Mr R. Crowningshield (U.S.A), Mr. O. Dragsted (Sweden), Prof. Gübelin (Switzerland), Mr. R. T. Liddicoat (U.S.A), Mr. M. Masso (Spain), Dr. F. H. Pough (U.S. A) and Dr. J. M. Saul (Kenya).

In Italy, the IGC logo was designed by Roberto Sambonet and made in gold by Roberto Cusi offered to the conference delegates during the Tremezzo 1989.

In Italy, in 1989, the following rules were agreed for future meetings of the IGC:

1. The prime objective was to be the exchange of gemmological experiences.
2. Gemmology was to be the platform for all topics and was to be regarded as the principal theme.
3. It was decided that attendance at all further Conferences should be by invitation that would be determined where necessary by the Conference Secretary and the Executive Committee.
4. All delegates were to be encouraged to present papers; but this would not be mandatory.
5. All delegates must have a publishing record and all papers at IGC meetings must presented in English, both when written or spoken.
6. The Conference must keep foremost in mind the prime objectives and avoid dilution/confusion of this objective which, if not maintained, could result in a blank organization without true status or credibility.
7. Peripheral commercial activity must be kept to a minimum, and there should be no blatant sponsorship of any kind.

These rules, combined with the original concepts, have been kept as the basis for all conferences since. Any invitation is specific to the person invited and is not transferable.

Rules/Standard Operating Procedures of the IGC

Membership

Membership of the IGC shall consist of:

1. **Honorary Members** are those who are senior members of the IGC and are elected by Delegates on an as-required basis.
2. **Delegates** are those who are elected from Observers, on the recommendation of the Executive Committee, from those Observers who have presented (in English) worthwhile presentations (either lectures, and/or posters) at three successive IGC meetings before becoming eligible for election as a Delegate.
3. **Observers** are those who shall be well published, internationally recognised gemmologists who are invited to attend IGC meetings on the invitation of either the Executive Committee, Delegate/s from the country in which they are resident, or the Conference Secretary of the country in which the IGC meeting is to be held.

Applications for Observer status, which shall be supported by a pertinent CV and list of publications, should be submitted to the Executive Committee for consideration before any invitation to attend an IGC is offered by the Conference Secretary.

Executive Committee

The day-to-day administration and decision making of the IGC shall be overseen by an Executive Committee that meets formally at IGC meetings, and in between meetings conducts the routine business of the IGC electronically by email. Following nomination, new members of the Executive Committee shall be elected by majority vote of Delegates at the Business Meeting that follows each IGC.

From time to time, the Executive Committee shall elect a **Chairman** and also one **Honorary Secretary**, who will be responsible for detailed administration and the distribution of decisions of the Executive Committee to Honorary Members and Delegates.

Written minutes shall be kept for all meetings of the Executive Committee and General Business Meetings of Delegates. Copies of these minutes shall be circulated by the Honorary Secretary to eligible Honorary Members and Delegates.

Meetings of the IGC

IGC meetings should be held every two years in a host country approved by Honorary Members and Delegates. Historically these meetings have been held in odd calendar years.

IGC meeting should be timed so as not to clash with other meetings (e.g. IMA meetings) that Delegates are likely to attend.

The venue for IGC meetings should alternate between European and non-European countries.

A country wishing to host an IGC meeting shall submit their proposal first to the Executive Committee and then formally present their proposal to Delegates. The decision to accept or reject a proposal to host an IGC meeting will be made by majority vote of Honorary Members and Delegates present at the IGC Business Meeting, or electronically if an IGC meeting is not being held at the time a decision needs to be made.

Countries hosting IGC meetings shall establish their own administrative structures to ensure the efficient planning and operation of the IGC. Costs involved in hosting an IGC shall be met by Registration Fees paid by Honorary Members, Delegates and Observers attending the meeting, and financial sponsorship from private, institutional and government sources. Day-to-day administration for an IGC shall be the responsibility of an elected Conference Secretary, who shall be either an Honorary Member or Delegate of the IGC.

General responsibilities of the Conference Secretary of each IGC include:

- Planning and implementation for the IGC of:
 - pre-conference activities
 - post-conference activities
 - the formal IGC conference
 - associated cultural activities and events
 - guest entertainment program
 - all finances
 - receipt and compilation of abstracts of papers
 - publication of proceedings of IGC conference
 - implementation of poster presentations

- Obtaining the necessary government permissions and other political factors
- Organisation of formalities required for different foreign visitors in the host country e.g. visas, special permissions etc.

Attendance at IGC meetings, of Delegates and Observers from countries other than the host country, shall be restricted to a maximum of five registrations per country. This restriction does not include Honorary Members.

Each IGC shall consist of a minimum of:

1. Two to three day pre-and post-conference study excursions to areas and facilities of gemmological interest.
 2. A 1-day session, prior to the IGC, at which previously nominated delegates and/or observers will be invited to give presentations to gemmologist members of the country hosting the IGC.
 3. A five-day professional conference that shall consist of: Formal papers of 15 minutes duration, followed by 5 minutes of questions and answers; and, Poster presentations that shall be scheduled independently so that adequate time is allowed for each poster to be presented by its author/s and then have its content available for discussion by interested delegates.
1. A Business Meeting for Delegates of a maximum of 1 hour duration that traditionally follows closure of the IGC professional conference.
 2. A 1-hour General Discussion session to allow Honorary Members, Delegates and Observers time to exchange opinions on future directions of the IGC.

If feasible, future meetings of the IGC should be held at the hotel/institution in which the accommodation for Honorary Members, Delegates and Observers has been arranged by the Host country organising committee.

If sufficient seating is available at the venue/s for future IGC lectures, gemmology students from the country hosting the IGC shall be encouraged to attend lectures presented at that IGC.

IGC 2017 Programme

| | |
|----------------------|-------------------------------------|
| 8 - 11 October 2017 | Pre-conference tour |
| 11 – 15 October 2017 | Conference, Safari Hotels, Windhoek |
| 16 – 19 October 2017 | Post-conference tour |

Conference Programme

Windhoek, Namibia 11 – 15 October 2017

Wednesday 11 October 2017

| | |
|---------------|--|
| 18.00 | Registration at Safari Court Hotel |
| 18.00 - 20.30 | Welcome Reception at Safari Court Hotel – Pool Area |
| 20.30 | Dinner (individually) |
| 20.30 - 21.30 | Executive Committee (EXECO) Meeting, Flamingo Room No. 2, Safari Hotel |

Thursday 12 October 2017

| | |
|---------------|--|
| 9.00 – 10.00 | Registration, Namib Room 1, Safari Hotel |
| 10.00 - 10.45 | Opening Ceremony, Namib Room 1, Safari Hotel |
| 10.45 - 11.15 | Coffee Break |

Sessions at Namib Room 1, Safari Hotel

| | |
|---------------|---|
| Session 1 | Invited lectures – Chairman: Henry A. Hänni |
| 11.15 – 12.00 | <u>Gabi Schneider</u> : The History of Diamond Mining in Namibia |
| 12.00 – 12.30 | <u>Andreas Palfi</u> : Colour and Ornamental Stones of Namibia |
| 12.30 - 14.00 | Lunch at Welwitschia Restaurant, Safari Hotel |
| Session 2 | Gemstones of Namibia and South Africa – Chairlady: Jayshree Panjekar |
| 14.00 - 14.20 | <u>Ulrich Henn</u> , Tom Stephan, Thomas Lind, Fabian Schmitz: A Gemmological Study on Tourmaline from the Karibib and Usakos Region, Namibia |
| 14.20 – 14.40 | <u>Edward W. Boehm</u> : Spessartine Garnets from Namibia: Geology, Gemology, Market |
| 14.40 – 15.00 | <u>Harmony K. Musiyarira</u> , Ditend Tesh, Mallikarjun Pillalamarry, Nikowa Namate: Growth Strategy for the Namibian Jewellery Industry and Coloured Gemstone Value Chain |
| 15.00 – 15.20 | <u>Brendan M. Laurs</u> : Recent Mining of some Alluvial Diamond Deposits in South Africa |

15.20 – 15.50 Coffee Break
 15.50 Poster Session
 19.00 – 21.00 Buffet Dinner at Acacia Restaurant, Safari Court Hotel

Friday 13 October 2017

8.00 – 8.45 Executive Committee (EXECO) Meeting, Flamingo Room No. 2, Safari Hotel

Session 3 **Corundum** – Chairman: Karl Schmetzer

9.00 – 9.20 Terrence Coldham: An Examination of the Morphology of Grains of Crystalline Corundum from Lava Plains Northern Queensland; A Rare Example of an “in situ” Pyroclastic Sapphire Deposit

9.20 – 9.40 Franck Notari, Emmanuel Fritsch, Candice Caplan, Thomas Hainschwang: Are Boehmite Needles in Corundum Rose Channels?

9.40 – 10.00 Shane F. McClure: Sapphire Mining in Montana

10.00 – 10.20 W. Atichat, J. Jakkawanvibul, M. Maneekrajangsaeng, T. Sripoonjan, T. Leelawatanasuk, V. Pisutha-Arnond, N. Narudeesombat, P. Chanthayod, B. Sriprasert: Padparadscha Color Grading for Gem Trade

10.20 – 11.10 Coffee Break

Session 4 **Diamond** – Chairman: Emmanuel Fritsch

11.10 – 11.30 Hiroshi Kitawaki, Kentaro Emori, Mio Hisanaga, Masahiro Yamamoto: Two Kinds of Synthetic Diamonds Having Features Similar to Natural Diamonds

11.30 – 11.50 R. Serov, Y. Shelementiev, A. Serova: Hybrid Diamonds: Natural Diamonds Overgrown with CVD Synthetic

11.50 – 12.10 Rainer Schultz-Güttler: Skins, Stains, Spots and Ruts: Green Diamonds from Brazil

12.10 – 12.30 Andy H. Shen, Tay Thye Sun, Ye Luo, J.T. van Gorsel, Mega Rosana Fatimah, Tay Kunming, Wilyanto Deng: Kalimantan Diamonds from Landak: Gemmological Characteristics, FTIR and Photoluminescence Spectroscopy

12.30 - 14.00 Lunch at Welwitschia Restaurant, Safari Hotel

14.00 - 17.00 Poster Session

Exhibition and sale of Namibian minerals and gemstones by small-scale miners, gemstone auction, Namibian jewellery exhibition
 Organized by Industry Growth Strategy (IGS) for the Gemstone and Jewellery Industry of Namibia

18.30 – 22.00 Dinner at Joe’s Beerhouse, Windhoek

Saturday 14 October 2017

- Session 5 **Spinel, Tourmaline, Garnet** – Chairman: Gamini Zoysa
- 9.00 – 9.20 Jayshree Panjikar, Aatish Panjikar: Study and Investigation of Spinel from Kermunda in Odisha, India
- 9.20 – 9.40 Cheng-Si Wang, Andy H. Shen: Reversibility of Photoluminescence Spectra of Spinel with Heat Treatment
- 9.40 – 10.00 Claudio C. Milisenda, Stefan Müller: REE Photoluminescence in Paraiba Type Tourmaline from Mozambique
- 10.00 – 10.20 Karl Schmetzer, H. Albert Gilg, Ulrich Schüssler, Jayshree Panjikar: Origin Determination of Garnets: Search for Historical Trade Routes
- 10.20 – 11.10 Coffee Break
- Session 6 **Corundum** – Chairlady: Willow Wight
- 11.10 – 11.30 J.C. (Hanco) Zwaan, Leo M. Kriegsman, Jorien L.N. van der Wal, Richard J.M. Taylor, E. Gamini Zoysa: Characterization and Formation of ‘Metamorphic’ Sapphires – Examples from Sri Lanka
- 11.30 – 11.50 E. Zoysa Gamini, Liu Shang I, Edward, Arūnas Kleišmantas: Preliminary Report on New Corundum Deposits of Sri Lanka
- 11.50 – 12.10 Sutas Singbamroong, Aisha Rashid Almazrooei, Nazar Ahmed: Lead Glass-Filled Padparadscha
- 12.10 – 12.30 Seung Kwon Lee, Kiran Kwon: Raman Study for Heat-Treated Sapphires Based on the Structural Relaxation by Impurities and Thermal Energy
- 12.30 - 14.00 Lunch at Welwitschia Restaurant, Safari Hotel
- Session 7 **Investigation Techniques** – Chairman: Hanco Zwaan
- 14.00 – 14.20 Michael S. Krzemnicki, Hao A. O. Wang, Walter A. Balmer, Jean-Pierre Chalain, Pierre Lefèvre, Wei Zhou, and Laurent Cartier, Henry A. Hänni: GemTOF: A New and Highly Versatile Method to Analyse Trace Elements and Isotopes of Gemstones and Pearls
- 14.20 – 14.40 Kentaro Emori, Hiroshi Kitawaki: Identification of Natural and Synthetic Amethyst Using Multivariate Analysis
- 14.40 – 15.00 Masaki Furuya: The Efficiency and Limitation of the Phosphorescence Imaging for Screening Current Melee Sized Synthetic Diamonds
- 15.00 – 15.20 Bahareh Shirdam, Soheila Aslani: Origin determination of Iran Excellent-Quality Turquoise Based on Trace Element Analysis Using ICP-MS and Micro XRF

| | |
|---------------|---|
| 15.20 – 15.50 | Coffee Break |
| 15.50 | Poster Session |
| 19.00 – 22.00 | Gala Dinner at Omatako Room 2, Safari Court Conference Centre |

Sunday 15 October 2017

| | |
|---------------|--|
| Session 8 | Pearls and Amber – Chairman: Tay Thye Sun |
| 9.00 – 9.20 | <u>Nick Sturman</u> , Areeya Manustrong, Kwanruen Lawanwong, Promlikit Kessrapong, Nanthaporn Somsa-ard, Artitaya Homkrajae: “Golden” Pinctada Maxima Non-Bead Cultured Pearls with an Emphasis on their Internal Structures |
| 9.20 – 9.40 | <u>Stefanos Karampelas</u> , Abeer Tawfeeq Al-Alawi, Ali Al-Attawi, Kenneth Scarratt: Natural Pearls Found from Pinctada Radiata in the Kingdom of Bahrain: Characteristic Structures, Comparison and Identification |
| 9.40 – 10.00 | <u>Elisabeth Strack</u> : Past and Present Situation of Freshwater Pearls from North Western Russia |
| 10.00 – 10.20 | Liu Shang I, Edward: Feather and Insect Inclusions in Burmese Amber and its Impact on Origin Determination |
| 10.20 – 10.50 | Coffee Break |
| Session 9 | Miscellaneous – Chairman: John Saul |
| 11.10 – 11.30 | <u>Willow Wight</u> : Ammolite, Canada’s Unique Fossil Gemstone |
| 11.30 – 11.50 | <u>Anette Juul-Nielsen</u> , Arent Heilmann: A Gemstone Occurrence Map for Greenland |
| 11.50 – 12.10 | <u>Stephen Kennedy</u> , Jens Najorka: Imitations of Tianhuang and Shoushan sSones |
| 12.10 – 12.30 | <u>Çiğdem Lüle</u> : Gemological Terminology issues: An Ongoing Battle... |
| 12.30 - 14.00 | Lunch at Welwitschia Restaurant, Safari Hotel |
| Session 10 | Beryl, Cordierite, Jade – Chairman: Ulrich Henn |
| 14.00 – 14.20 | Klaus Schollenbruch, <u>Lore Kiefert</u> , Klemens Link, Tewodros Sintayehu: Gem Quality Emeralds from Ethiopia |
| 14.20 – 14.40 | <u>Karen E. Fox</u> , Chris Yakymchuk: Canadian Gem-Grade Cordierite |
| 14.40 – 15.00 | <u>Ahmadjan Abduriyim</u> , Kazuko Saruwatari, Yusuke Katsurada: Jadeite Jade from Japan: Its History, Gemmology and Comparison with Jadeite from other Sources |
| 15.00 – 15.40 | Coffee Break |

| | |
|---------------|--|
| 15.40 – 16.40 | Closing Ceremony, Namib Room 1, Safari Hotel |
| 19.00 – 21.00 | Buffet Dinner at Acacia Restaurant, Safari Court Hotel |

Posters

Daniel Barchewitz:
GemRam for Simple Gem ID

Laurent E. Cartier, Michael S. Krzemnicki, H.A.O. Wang, Henry A. Hänni:
Traceability of Gemstones: Challenges and Opportunities

Gagan Choudhary:
Aquaprase™: An Interesting Green-Blue Variety of Chalcedony

Henry A. Hänni, Leander Franz, Wei Zhou:
Sannan-Skarn: a New Ornamental Gemstone from Pakistan

Arūnas Kleišmantas, Gamini E. Zoysa, Edward Liu Shang I:
Chemistry and Gemmological Features of Spinel from Sri Lanka and Vietnam

Michael Krzemnicki, Hao A. O. Wang, Tom Stephan, Ulrich Henn:
Cobalt Diffusion-Treated Spinel

Leander Franz, Michael Krzemnicki, Kristina Ernst, Christian de Capitani, George E. Harlow, Nicolai Kouznetsov:
Kosmochlor-Bearing Jadeite Rocks from Kenterlau-Itmurundy (Lake Balkhash, Kazakhstan)

Thanong Leelawatasuk, Tasnara Sripoonjan, Namrawee Susawee, Pornsawat Wathanakul, Visut Pisutha-Arnond:
Rare Fancy Sapphires from Bo Phloi Gem Field, Kanchanaburi, Western Thailand

Thanapong Lhuaamporn, Saengthip Saengbuangamlam, Nataya Nilhud, Thanong Leelawatanasuk:
Characteristics of Exceptionally Gem-Quality Untreated Blue Sapphires from Bo-Phloi Gemfield, Kanchanaburi-Thailand

John M. Saul:
Transparent Gemstones and the Most Recent Supercontinent Cycle

Andy H. Shen, Cuihong Liu, Tian Shao, Min Ye:
Color Origin of Color-Changing Diaspore from Turkey

Jian Mao, Elizabeth Su:
Research of Jadeite Inclusions: Graphite and Zircon

Panjawan Thanasuthipitak, Kanyarat Kwansirikul, Weerapan Srichan, Phisit Limtrakun, Opor Saidum and Theerapongs Thanasuthipitak:
Gem Materials from Upper Northern Thailand: Potential in Jewellery

The History of Diamond Mining in Namibia

Gabi Schneider

Namibian Uranium Association
director@namibianuranium.org

Despite their sparkle, the treasures of the Namibian coast remained hidden for a long time. By the beginning of the 1900s Namibia had already developed a number of mines that had been producing a range of metals for many years, but diamond mining had remained a dream. Prospectors had been looking for the “blue ground”, since this was the rock hosting the famous South African diamond discoveries made in 1866. No one, however, had imagined that the precious stone could be found in a rather different environment, and that the gems lay on the desert floor, right under the feet of those who were daring enough to venture there. This all changed in April 1908, when Zacharias Lewala found the first diamond in Namibia. Since then, the stretch southwards from Lüderitz to Oranjemund has developed into one of the most important diamond-producing areas in the world. Indeed, even north of Lüderitz and all the way to the Kunene mouth on the border between Namibia and Angola, diamonds have been located by prospectors and mined intermittently.

Following Lewala’s find, a diamond rush broke out in what was then the German colony of Deutsch-Südwestafrika, hundreds of prospectors flocked into the area, and a plethora of small companies formed, many of them trading on the Lüderitz stock exchange! Many people made money very quickly, and the sleepy town of Lüderitz changed overnight into a luxury place. However, the German government put a sudden end to all of this, when it declared the area of limits barely 6 months after the first stone had been found. It gave all the mineral rights to the state-owned Deutsche Kolonialgesellschaft für Südwestafrika, as Germany wanted the riches for itself, and not for its individual subjects in the colony. In the long run, the Deutsche Kolonialgesellschaft für Südwestafrika proved to be underfunded and unable to mine the wealth it was given, and sub-leased its rights to the larger companies that had been founded. They mined the deposits very profitably, and sold the stones to the German government. Soon, the area produced 15% of the world’s total production in diamonds.

Everything changed on the diamond fields when World War I broke out in 1914. The German miners were enlisted, and the local miners sent home. But fighting in the German colony only lasted for about a year. Due to the surrender of the German troops, the diamond companies came under the control of the South African government. In contrast to other occupying forces, South Africa did not confiscate private properties, and the mines were re-opened. But unlike before the war, the diamonds now had to be sold to the South African government, through the diamond syndicate of Cecil Rhodes in London. Following the signing of the Treaty of Versailles, Sir Ernest Oppenheimer took over almost all of the German diamond companies and founded the Consolidated Diamond Mines of South West Africa (CDM) under his Anglo American Corporation of South Africa. This was a stepping stone for him to become the chairperson of DeBeers Consolidated Mines, the richest diamond company of all times, in 1929, and DeBeers bought CDM from Anglo American in 1930.

An important advance in the 1920s was the development of CDM’s Elizabeth Bay Diamond Mine which had the most modern treatment plant in the world at the time. However, the Eureka moment came in 1928, when the diamonds in the beach terraces at the mouth of the Orange River were discovered. This discovery dwarfed all earlier discoveries and revealed stones of extraordinary quality in what is without doubt the largest diamond placer in the world. Nevertheless, large scale development would not take place until after the Great Depression of the early 1930s. In 1941, CDM eventually moved its headquarters to Oranjemund. Since then numerous technical innovations, including the moving of the coastline westwards have produced millions of carats of diamonds with more than 95% of them being of gemstone quality.

The History of Diamond Mining in Namibia

Gabi Schneider

As early as the German colonial days, some adventurous minds suggested the possibility of diamonds on the floor of the sea. If they are in beach terraces onshore, why should they not be in submerged older terraces formed when the sea level was lower during the various ice ages? But the technical constraints were immense. This changed when Samuel Vernon Collins, a Texas oil and pipeline man known as Sammy, entered the scene. He managed to recover the first diamonds in commercial quantities from the sea floor, albeit with immense technical and financial efforts. Collins's company was taken over by DeBeers in 1965, and systematic exploration and development of marine mining technology have since made Namibia the leading nation worldwide when it comes to sea bed mining of diamonds.

Following Namibian Independence, CDM was transformed into a 50:50 partnership between the Namibian government and DeBeers aptly named Namdeb. This was the start of a new lease of life, and technical innovation took to new heights. The last frontier, the shallow water that cannot be mined from land or from the sea is today conquered with dredges, beach accretion and sampling devices that can walk into the surf zone. Diamonds have been mined in Namibia for more than a century, which is an extraordinary period for the life of any mine, and this one's secret lies in the large extent of the deposit and the extraordinary quality of its stones. The diamond industry remains the single most important source of income for Namibia and is positioned well to continue to play this important role.

Colour and Ornamental Stones of Namibia

Andreas G. Palfi

Palfi, Holman and Associates, Geo Tours Namibia,
Windhoek, Namibia, pha@mweb.com.na

Introduction

Namibian gemstones are subdivided into two subgroups, as per the Mineral Act, 1992;

1. Precious Stones such as diamond, sapphire, ruby and emeralds of which diamonds are a major export earner to the country, whilst no sapphire and ruby localities were found and only two minor and uneconomic emerald occurrences were discovered. Dealing with rough precious stones requires special permits and illegal purchase/sale of roughs may result in hefty fines and imprisonment.
2. "Semi-precious stones" group of minerals of the Namibian Mineral Act, 1992 is corresponding of the Colour and Ornamental Stones as per CIBJO Trade Rules and includes all the other gemstones ranging from the high value tourmalines, pietersite and garnets (demantoid, spessartite) to the lower value silica varieties.

Another group of well known Namibian minerals, that is mineral specimens, often found with colour stones and thus also included in the same group of minerals.

The geological setting of the Namibian colour and ornamental stones is very similar to the one of Brazil (we have been close neighbours in the geological past) with abundant tourmaline-bearing pegmatites and basalt hosted amethysts. Brazilian pegmatites, due to high rainfalls suffered far greater host-rock weathering, allowing much easier mining by small-scale operators. In Namibia, gemstone mining unfortunately requires the immediate use of surface drilling, blasting, thus additional finances are often out of reach of the small-scale mining community. In addition due to scarcity of water any prospecting and mining is far more difficult in the country. Colour and ornamental stone production and export figures of the country, especially for the higher value minerals, are not reliable due to un- or under-reported direct sales to local or overseas dealers (Palfi, 2001). Whilst the direct GDP contribution of these minerals to the Namibian economy is minimal, nevertheless at least three thousand otherwise unemployed people making a living by small-scale mining and selling their gems as well as mineral specimens to local/overseas dealers and mostly to the foreign tourists visiting the country.

Namibia is rich in colour and ornamental stone occurrences but unfortunately none of them would make a world class deposit. However, as far as mineral specimens are concerned the Tafelkop amethyst, Erongo aquamarine and the secondary copper minerals, including diopside of Kaokoland are well known by mineral collectors around the world.

In the followings there will be a brief discussion of the most important colour and ornamental stone mines/occurrences in the country.

Tourmaline mineralisation associated with pegmatite intrusions

Most of the tourmaline bearing pegmatites occur within a broad triangle between small towns of Omaruru, Karibib and Usakos. The first reported major tourmaline find was near Usakos where prior to World War I, at the end of a cassiterite mining operation, a large cavity was discovered containing gem tourmalines (Geological Survey, 1992). The material, without knowing the actual value, was stored in old cement barrels to be eventually re-discovered by a gemstone dealer from Idar-Oberstein. At the same locality the *Usakos Tourmaline Mine*, just south of Usakos, is mechanised, but workings are getting more difficult due to depth of operation. Hopefully, time permitting, the post-conference tour will be able to visit this mine.

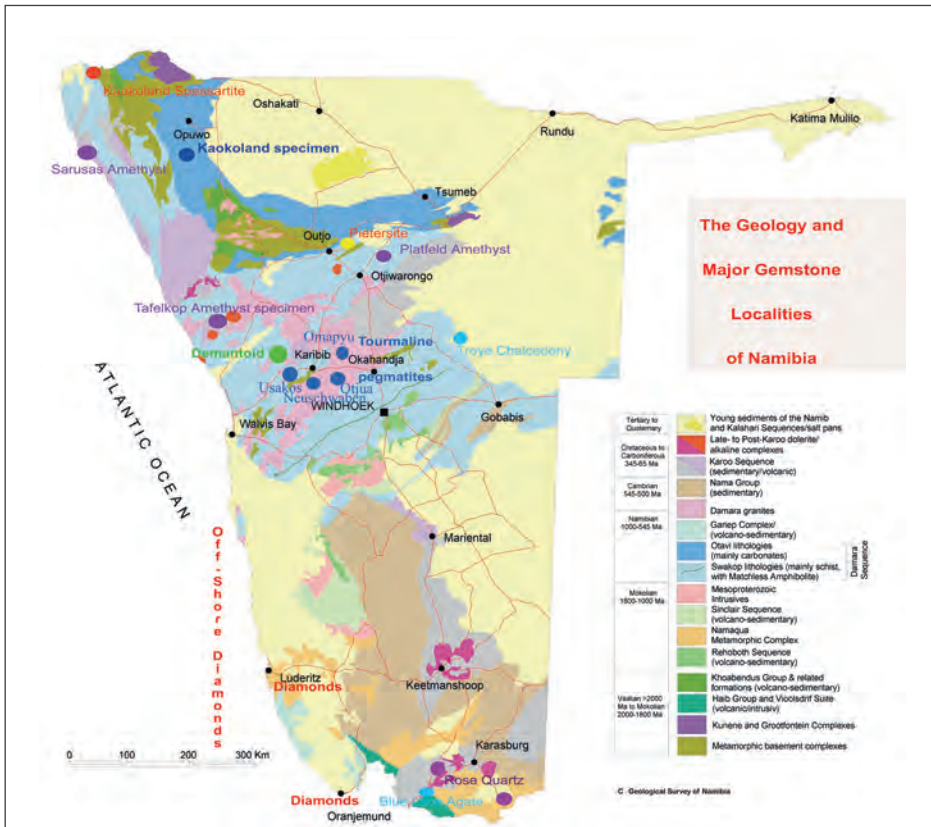


Figure 1. Geological map of Namibia.



Figure 2. Otjua tourmaline pegmatite.



Figure 3. Neuschwaben artisanal miner.

The *Otjua Tourmaline Mine*, south-east of Karibib will also be visited during the post-conference tour. Operations presently suspended as the owners are waiting for a mining licence approval. This was a site where some years ago a large cavity with huge quartz crystals, as well as gem quality tourmalines was discovered (Palfi, 2014). Some of the finds are displayed in the Kristal Galerie, Swakopmund, to be visited by the post conference tour.

The *Neuschwaben Tourmaline Mine*, the largest and richest tourmaline deposit in Namibia, is owned by an association of small-scale miners. The area is subdivided into small parcels and individuals or group of individuals carrying out inefficient and at times dangerous artisanal mining. Most of the production is sold to local or foreign dealers.

Another important tourmaline producing area, *Omapyu*, is located between Wilhelmstal and Omaruru, where numerous mining claims are intermittently operated by small-scale miners.

Garnet mineralisation within metamorphic rocks

Demantoid mineralisation is associated with marbles and calc-silicates on the western side of Erongo Mountains (Palfi, 2009). The *Green Dragon Mine*, to be visited by the post-conference tour, was a constant source of demantoid to the world markets but presently operations are scaled down as the owners are waiting for the granting of a mining licence. There are numerous other mining claims in the area but most of them worked sporadically or not at all.

Spessartite (mandarin garnet):

There are two well known occurrences (Palfi, 2006) close to the Kunene River in Kaokoland, the remotest north-western corner of Namibia. The mineralisation is in quartz, biotite schist and associated with thin stratiform manganese bands. Some years ago there were two mechanised operations but both of them closed down due to costly transport problems associated with the worst four-wheel drive tracks of the country. Presently there are some valid mining claims in the area, held by artisanal miners but production, if any, is minimal. The area still has a strong potential for an investor.

Silica gem mineralisation associated with various rock types

Pietersite, a unique and highly priced blue/golden colour brecciated tiger-eye, (Palfi, 2014) is mined just north of Outjo over the last few decades. It is probably the only occurrence in the world although there were some references (Hu et al., 2010) to similar material found in China.

Amethyst mines:

There are two sporadically operating mining areas for gem amethyst; one of them located just north of Otjiwarongo (Platveld) and the other, Sarusas, far north of Swakopmund in the remote Skeleton Coast Park.

Whilst *rose quartz* is abundant in Namibia there are only two small mining operations situated in the southern part of the country close to Karasburg.

The well-known Ysterputz *Blue Lace Agate mine*, (Palfi, 2014) also close to Karasburg, recently suspended operations due to depth of mining and resulting safety issues. However, the *Troye Chalcedony* mine, east of Okahandja is in operation for the last few decades.

Most important Namibian mineral specimen localities

There are numerous mineral specimen occurrences, often with gem potential in the country (Bezing, 2007) but only a few of them will be mentioned.

The Tafelkop amethyst and other minerals in various forms are well known and sought after by collectors. The Erongo Mountain area produced some excellent specimens of often gemmy aquamarine, topaz, schorl, fluorite and jeremejevite. The Spitzkoppe, on the western side of Erongo has outstanding topaz, phenakite and bertrandite crystals. The Kaokoland area, south of Opuwo is known for its superb diopside, malachite and shattuckite specimens. Tsumeb Copper Mine (now closed) was a collector's paradise and unfortunately there are more Tsumeb specimens around the world than in Namibia.



Figure 4. Demantoid garnet processing plant at Green Dragon mine.



Figure 5. Kaokoland spessartite mining area in 2006.



Figure 6. Gem spessartite from Kaokoland.



Figure 7. Blue lace agate mine.

References

Bezing, von, L., 2007. Namibia minerals and localities. Bode Verlag GmbH. 856pp.

Geological Survey of Namibia, 1992. The Mineral Resources of Namibia, Chapter 5.2, Semi-precious stones. 1-19.

Hu, K., Heaney, P.J., 2010. A microstructural study of pietersite from Namibia and China. *Gems & Gemology*, 46(4), 280-286.

Palfi, A.G., 2001. An assessment of the gemstone sector of Namibia. Unpublished report. 49pp.

Palfi, A.G., 2006. Report on the progress of exploration on EPL 3106, (spessartite) Hartmann Mountains, Northern Kunene Region, Namibia. Unpublished report. 11pp.

Palfi, A.G., 2009. Report on the Green Dragon (demantoid) mine. Unpublished report. 12pp.

Palfi, A.G., 2014. Blue Lace Agate Mine Mining Licence ML89, a technical report (unpublished).15pp.

Palfi, A.G., 2014. Hoanib Exploration (Pty) Ltd, mining licence (Otjua tourmaline pegmatite) application. Unpublished report. 20pp.

Palfi, A.G., 2014. Hoanib Exploration (Pty) Ltd, mining licence ML57 (pietersite) renewal application. Unpublished report. 21pp.

A gemmological study on tourmaline from the Karibib and Usakos Region, Namibia

Ulrich Henn, Tom Stephan, Thomas Lind, Fabian Schmitz

German Gemmological Association, Idar-Oberstein
ulihenn@dgemg.com

The first discovery of tourmaline in Namibia occurred in the Usakos region, in a mine for tin recovery (cassiterite) from quartz-rich pegmatites, at the beginning of the 20th century. A huge pocket delivered fine green to blue-green tourmalines, which - after reaching Idar-Oberstein - would soon be popular as "African Tourmaline" all around the world (Falz, 1939).

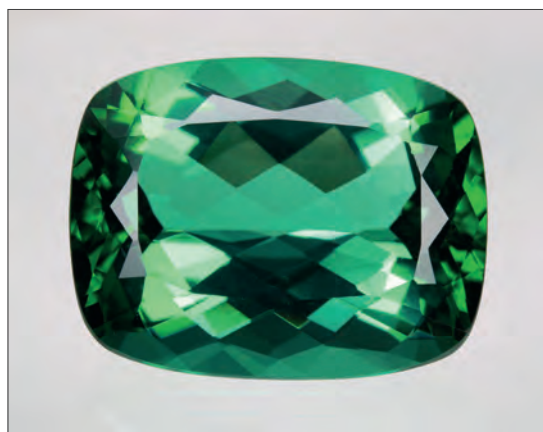


Figure 1. Green tourmaline from Otjua, Namibia. 17.51 ct, collection of Karl Egon Wild, Kirschweiler, Germany.



Figure 2. Green-blue tourmaline from Namibia. 4.40 ct, collection of DGemG, Idar-Oberstein.

Already in 1932 it was discovered that the blue-green material can be modified to bright emerald-green colours by heat treatment at 650°C and dark green stones turn lighter at 600-650°C (Wild, 1932).

In addition to the typical green to blue-green tourmalines the occurrences around Usakos produce light blue, pink, yellow, brownish and colourless stones as well as multi-coloured specimens (Jahn, 2001).

A number of interesting tourmaline occurrences are located in the area of Karibib. Since 1923 a particular strongly kaolinized Li-Be-pegmatite produces remarkable greenish-blue to deep blue tourmaline, well-known as "Neu Schwaben Tourmaline" on the international market. Additionally green and red material is found in that area (Jahn, 2001).

For quite some time the so-called „Becker pegmatite“ at Otjua intermittently produced green, brown, red, blue and black as well as "watermelon" tourmaline beside giant quartz crystals (Schneider, 2001).



Figure 3. Blue tourmaline (indicolite) from Namibia. 22.32 ct, collection of Paul Wild, Kirschweiler, Germany.



Figure 4. Watermelon tourmaline from Otjua, Namibia. 50 x 40 mm, collection of Karl Egon Wild, Kirschweiler, Germany.

Refractive indices, birefringence and density of the Namibian tourmalines are in the known range: $n_o = 1.620-1.622$, $n_e = 1.640-1.642$, $\Delta n = 0.020$, $D = 3.06-3.12 \text{ g/cm}^3$.

According to the nomenclature of Henry et al. (2011) the chemical composition classify the Namibian tourmalines as alkali group species, in fact as elbaite.

In relation to their absorption spectra the green, blue-green, green-blue to blue tourmalines from Namibia can be attributed to the Fe^{2+} -type. The pink to red specimens belong to the Mn^{3+} -type (see Lind & Stephan, 2016).

Blue tourmaline: the absorption spectrum of the blue Namibian tourmalines (indicolite) is dominated by the Fe^{2+} -absorption band with a maximum at 720 nm, absorbing the red spectral range, with the blue-violet region showing no absorption, resulting in a blue colour. In the o-direction the green is more absorbed, causing a blue (o) – greenish-blue (e) pleochroism.

Green tourmaline: As is the case with blue tourmalines, the red region of the visible spectrum of green tourmaline (Figure 5) is strongly absorbed by the short-wave tail of the strong Fe^{2+} -band with its maximum at 720nm.

Additionally, the visible spectrum shows strong absorption in the blue violet region of the spectrum, with increasing intensity towards the UV, establishing a transmission window in the green spectral range.

This absorption is much more intense in the o-spectrum than in the e-spectrum, leading to a pleochroism green (o) to blue green (e).

In the spectral region between 430 nm and the UV strong broad absorption has been attributed to IVCT ($\text{Fe}^{2+}\text{-Ti}^{4+}$), ($\text{Mn}^{2+}\text{-Ti}^{4+}$) as well as OMCT ($\text{O}^{2-}\text{-Fe}^{2+}$), ($\text{O}^{2-}\text{-Fe}^{3+}$) and $\text{Mn}^{2+}\text{-CF}$ bands.

Blue-green to green-blue tourmaline: shows the same absorption spectra as the green specimens, but the blue-violet region is less absorbed resulting in a more blue-green to green-blue colour.

The blue-green tourmaline can be modified to a more green colour by heat treatment at about 600 to 650°C, due to a decrease of absorption in the green spectral range between 500 and 600 nm.

Pink tourmaline: the absorption spectrum is dominated by a strong and two less intense bands of Mn^{3+} (o>e) with maxima at 460 and 530 and 700 nm, respectively. The pink colour is the result of two transmission ranges in the red and blue-violet spectral regions.

Studies with the gemological microscope yielded film-like fluid inclusions and two-phase inclusions typical for tourmalines.

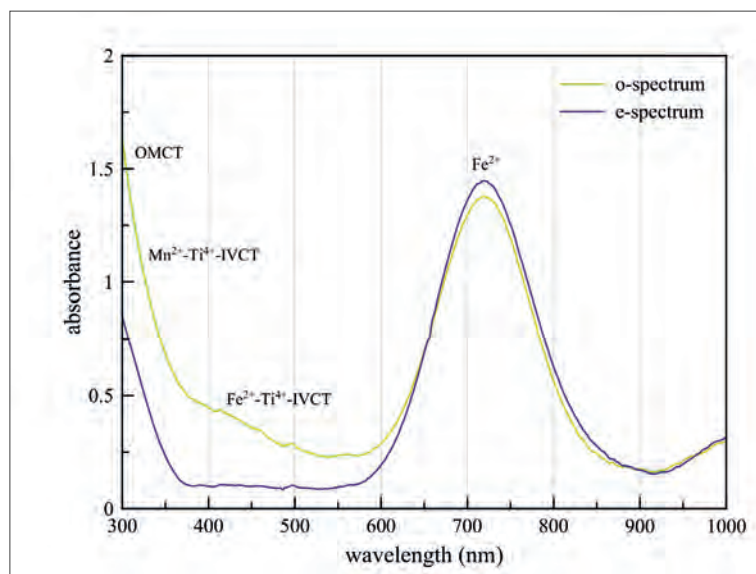


Figure 5. Visible absorption spectra of green iron-bearing tourmaline.

References

- Falz, E., 1939. Von Menschen und edlen Steinen. Reprint 1990, Charivari, Idar-Oberstein (in German).
- Henry, D. J., Novak, M., Hawthorne, F. C., Ertl, A., Dutrow, B. L., Uher, P., Pezzotta, F., 2011. Nomenclature of the tourmaline-super group minerals. *American Mineralogist* 96, 895-913.
- Jahn, S., 2001. Die Edelstein-Minen rund um Usakos und Karibib. In: Bahmann, U. & A. (Ed.): *Namibia – Zauberwelt edler Steine und Kristalle*. p. 102-109. Bode-Verlag, Haltern (in German).
- Lind, Th., Stephan, T., 2016. Spektrentypen und Farben von Turmalinen. *Z. Dt. Gemmol. Ges.* 65, 19-40 (in German).
- Schneider, G., 2001. Edelstein-Turmaline und Riesenquarze von Otjua. In: Bahmann, U. & A. (Ed.): *Namibia – Zauberwelt edler Steine und Kristalle*. p. 110-111. Bode-Verlag, Haltern (in German).
- Wild, G. O., 1932. The treatment of gem stones by heat. *Rocks and Minerals* 7, 9.

Spessartine Garnets from Namibia: Geology, Gemology, Market

Edward W. Boehm

RareSource Chattanooga, TN USA
Edward@RareSource.com

Spessartine (also called spessartite) garnets from Northwest Namibia were initially found at the Otomongo Mine just south of the confluence of the Marienfluss and Kunene Rivers. The Kunene River forms the northern border between Namibia and Angola. This region lies within the Pan-African Kaoko belt that formed by the collision of the Rio de La Plata craton of South America with the Congo craton of West Africa (F.F. Luft et al 2006). The spessartites, $Mn_3Al_2(-SiO_4)_3$, formed in a quartz-biotite-muscovite schistose gneiss in a metamorphic region of manganese-rich calcic amphiboles within the Kunene intrusive complex. These manganese-rich zones are black, providing a sharp contrast to the bright orange garnets. The crystals form as subhedral and euhedral rhombic dodecahedrons (12 faces) giving them an almost spherical appearance (figure 1).



Figure 1. Spessartine in rock

Spessartine garnets from Namibia are highly prized for their vivid orange color that seems to glow from within (figure 2). This unique characteristic is attributed to the idiochromatic presence of manganese (Mn^{2+}) with little or no iron coupled with fibrous crystalline inclusions that disperse light throughout the gem. In the past, the fibrous crystalline inclusions have been referred to as tremolite (G&G 1995) or tirodite (Photoatlas Vol.II, 2005). These two names are plausible because both are amphiboles. However, the transparent crystalline inclusions (figures 3 & 4) were recently identified by Raman analysis (figure 5) as cummingtonite (Renfro, 2017), a magnesium-rich monoclinic amphibole that is part of the tremolite-cummingtonite-actinolite series. Cummingtonite, $Mg_2Mg_5Si_8O_{22}(OH)_2$, is part of the magnesium-iron-manganese amphibole subgroup (Hawthorne et al., 2012).

Until 1997, tirodite was a name used to describe manganese-rich cummingtonite but is no longer recognized as a separate mineral. Many of the crystals and gems also have a “roiled” effect that diminishes their transparency but may also contribute to the dispersion of light. Small black manganese oxide inclusions and growth tubes are also often present. Spessartites from other localities often contain primary fluid inclusions, two and three-phase inclusions, albite and apatite crystals, etc (Laurs et al., 2001). Only the Namibian spessartites have diagnostic locality specific fibrous inclusions (Gübelin & Koivula, 2005). The Namibian spessartine garnets examined by the author exhibited refractive index, specific gravity, and spectral absorption properties that are consistent with those in published literature (Lind et al. 1993 and G&G 1995).

A local farmer discovered these bright orange garnets in 1992 in an extremely remote area at what became later known as the Otomongo or Marienfluss mine. The only access is by private plane to the closest village Opuwo and then another 9-10 hour journey by four-wheel drive vehicle to the mining area, which lies approximately 300 km northwest of the village. In late 1992, Eli Eliezri of Colgem Ltd. and Alan Roup formed a partnership with Namibian mining company Chromecorp Holdings Ltd. who owned the concession to the area. Colgem introduced the new spessartite garnets into the global market at the Tucson Gem & Mineral Show in February of 1993 (Eliezri, 1993, 2017 & Hanni, 1996, Rapaport, 2002).

These vivid orange garnets were initially marketed as Hollandine, in honor of the Dutch royal family, the House of Orange but Mandarin garnet was preferred by many US and Asian firms. “Mandarin Garnet” eventually became the default marketing name when it was discovered that a very similar term hollandite was already an accepted mineral species name for a barium-manganese oxide mineral found in India (Eliezri 2017). Other color descriptive terms that have been used are tangerine, pumpkin, or “Fanta” orange. Colgem started with approximately 5,000 carats of rough, which yielded just over 1,000 carats of faceted material. Gems of up to 30 carats were reported but most were 2 carats

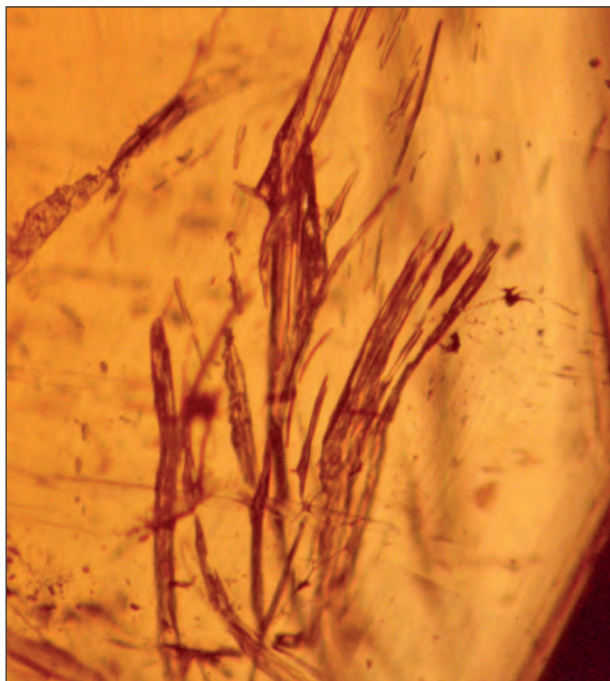


Figure 3. Cummingtonite in 3.16ct round Spessartine from Namibia by E. Boehm



Figure 2. Faceted spessartine

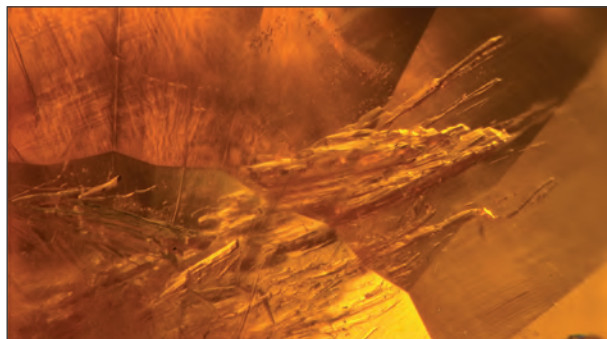


Figure 4. Cummingtonite in Namibian Spessartite 2.81mm by Nathan Renfro GIA

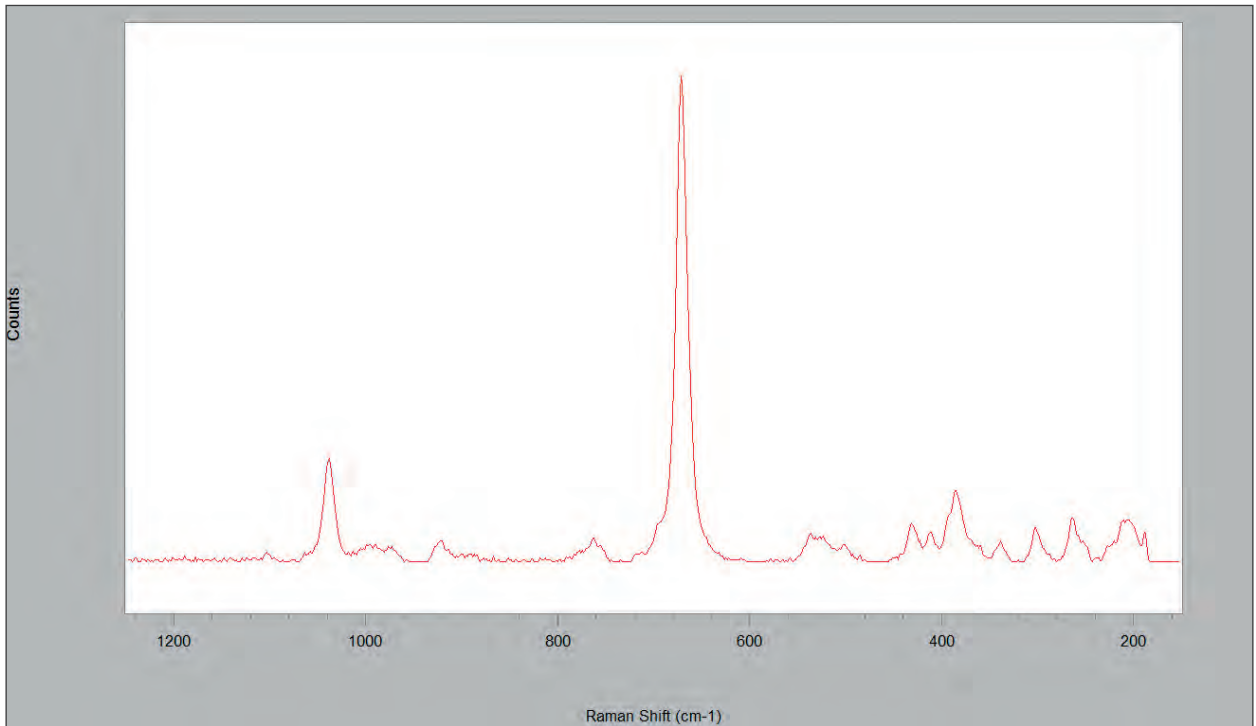


Figure 5. Raman spectrum of Cummingtonite by GIA



Figure 6. 31.92ct cushion cut spessartine garnet from Nigeria

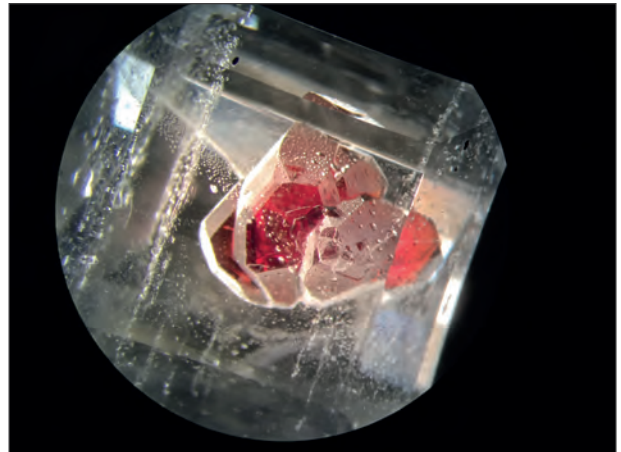


Figure 7. Spessartine inclusion

and under in size (Eliezri 1994, Lind et al. 1994, G&G 1996). A second mine called Gem Namibia was later discovered 30 km to the south, which Alan Roup owned and operated under G.E.M. Namibia Pty. Ltd. for a number of years. Both mines stopped producing in the late 1990's and only a few pieces have trickled out since. Today fine material is difficult to find, even in the second hand market, and prices range from US \$300-500/ct, for smaller or included gems up to \$4,000/ct for fine quality clean gems over 10 carats.

Other spessartite sources include United States, Brazil, Madagascar, Sri Lanka, Kenya, Zambia, Tanzania, Nigeria, and Burma. Nigeria, which began producing in 1999, just as Namibian production ceased, is currently the production leader with high quality gems up to over 50 carats in size (figure 6). The U.S. sources in Virginia and California are no longer producing so most of this material is found only in collector circles. These spessartites tend to be more yellowish-orange in color and thus do not command the same price as other sources with richer pure orange colors. Material from Brazil, Madagascar and Mozambique tends to be more of a burnt orange color while those from Zambia, Tanzania, and Nigeria are often more pumpkin orange or what the locals call “Fanta” orange in color. Some spessartite crystals can even be found as inclusions in topaz and quartz from Brazil (figure 7). The darker, burnt-orange color spessartites are considered less desirable and thus sell for approximately US \$200-500/ct, while the bright orange material in finer larger gems over 10 carats can sell for as much as \$2500/ct. Because much of the recent material found in Zambia and Tanzania is heavily included, these are often cut into cabochons, which sell for \$25-150/ct.

References:

Bank H., Henn U., Milisenda C.C. (1996) Gemmological News: Spessartite garnet from Namibia. *Gemmologie: Zeitschrift der Deutschen Gemmologischen Gesellschaft*, Vol. 45, No. 2, p. 43.

Eliezri, I., 1993, New Spessartite Garnet Occurrence in Namibia. XXIV International Gemmological Conference, Paris, France.

Eliezri, I., 1994, Hollandine – Mandarin Garnet creates stir in world gem market, Colgem marketing circular.

Eliezri, I, personal communication, 2017

Gübelin, E.J., Koivula, J.I., 2005, Photoatlas of Inclusions in Gemstones, Vol. 2, 448-454.

Koivula, J. et al., Spring 1993, Spessartine garnet from Africa, *Gems & Gemology*, *Gem News* (pp. 61-62).

Koivula, J. et al., Winter 1993, Garnet, *Gems & Gemology*, *Gem News* (p. 293).

Hänni, H., Summer 1995, Spessartine garnet from Namibia, *Gems & Gemology*, *Gem News* (p. 134).

Hänni, H., Spring 1996, Update on Namibian Spessartine, *Gem News*, *Gems & Gemology* (pp. 56-57)

Hawthorne, F.C., Oberti, R., Harlow, G.E., Maresch, W.V., Martin, R.F., Schumacher, J.C., Welch, M.D. (2012) Nomenclature of the amphibole supergroup. *American Mineralogist*: 97: 2031-2048.

Laur, B., Knox, K., Winter 2001, Spessartine Garnet from Ramona, San Diego County, California, *Gems & Gemology* (pp. 278-295).

Lind, Th., Bank H., Henn, U., 1993, Spessartine aus Namibia, *N. Jb. Miner. Mh.*, H.12, 569-576.

Lind, Th, Henn, U., Bank, H., 1994. Bright orange colored Spessartine from a new occurrence in Namibia. *Z. Dt. Gemmol. Ges.* 43 (1/2), 39-47.

Luft, F.F., Raab, M.J., Brown, R.W., Kohn, B.P., Gleadow, A.J.W., 2006, Tectono-thermal history of the Kaoko Belt, Namibia: An integrated low temperature thermochronology study, *Geochemica et Cosmochimica Acta*, Vol. 70, Issue 18, Supplement 1.

Rapaport Diamond Report, March 1, 2002

GROWTH STRATEGY FOR THE NAMIBIAN JEWELLERY INDUSTRY AND COLOURED GEMSTONE VALUE CHAIN

Harmony. K. Musiyarira, Ditend Tesh, Mallikarjun Pillalamarry, Nikowa Namate

Department of Mineral and Process Engineering, Namibia University of Science and Technology, Windhoek, Namibia;
hmusiyarira@nust.na

Abstract

With its abundant resources in diamonds and coloured gemstones, Namibia has been unable to develop an internationally competitive coloured gemstone and related industry due to the fact that the sector's value chain does not function in a way that maximises value addition. An uncoordinated supply of equipment to stone centers without a broader coloured stone sector growth strategy has constrained the growth of the sector. The main aim of this study was to establish the essential building blocks for the sector growth for the coloured gemstones and related industries. Three independent but complementary methodologies were used which included a desktop study, baseline study and data analysis and report writing. Relevant senior officials in key government ministries, public institutions, private sector organisations, small scale miners and key individuals in the mining sector were consulted through interviews. The linking up of the baseline study with the utilisation of the logical framework approach coupled with the SWOT analysis were essential techniques used in the formulation of a set of seven strategic interventions. The main thrust in formulating the interventions was to move the coloured stone and jewellery industry in Namibia from a raw resources export focused sector to a value-added and competitive brand on the global market. These strategic interventions are expected to have a significant impact on productivity and income. A holistic approach was used in coming up with these initiatives. The seven strategic interventions included conducting geological assessments to identify new deposits and quantify the existing ones, investing in education and training, improving exploration and mining practices and improving the local processing and jewellery manufacturing activities and creating an enabling environment for the sector to flourish.

Introduction

With its abundant resources in diamonds and coloured gemstones, Namibia is poised to have a significant competitive advantage in this sector. The vision of the Namibian government is to expand the range and value of coloured gemstones and jewellery products, processed within Namibia, while curbing illicit flows of the coloured gemstones and simultaneously securing the maximum benefit for its citizens, through value addition. However, there has been a fragmented approach to address the challenges facing the coloured gemstone industry in Namibia. Various government arms and donor organisations have utilised piecemeal approaches in the past in trying to make improvements on productivities across the value chain.

These attempts have brought very little results. The delivery of equipment to gemstone centers without a broader coloured gemstones sector growth strategy has not contributed to the development of the sector (Musiyarira et al. 2016). The lack of structured and formalised coordination between different government ministries has cost the government money which could have been put to good use by combining efforts across various ministries. Namibia has been unable to develop an internationally competitive coloured gemstone and related industry due to the fact that the sector's value chain does not function in a way that maximises value addition. The overall objective of this study was to establish the essential building blocks for the sector growth for the coloured gemstones and related industries.

Background

Namibia hosts a variety of quality coloured gemstones. The list of coloured gemstones includes and is not limited to quartz (rock crystal, smoky quartz, amethyst, rose quartz, strawberry quartz), tourmaline, sodalite, topaz, varieties of beryl (aquamarine, heliodore and morganite), garnet etc. The coloured gemstones are mainly mined by artisanal and small scale miners. These gemstones are disseminated within three regions of Namibia, namely Karas (South), Erongo (East) and Kunene (North West). Musiyarira et al. (2016) found that Namibia has not been benefiting fully from its rich coloured gemstones' potential due mainly to the fact that the value chain of the sector does not function in a way that maximizes value addition.

Coloured gemstones value chain in Namibia

According to Kaplinsky & Morris (2001), *value chain* describes the full range of activities which are required to bring a product or service from conception, through the different phases of production (involving a combination of physical transformation and the input of various producer services), delivery to final consumers, and final disposal after use. The coloured gemstones value chain can be summarised as: *prospecting, mining and sorting, processing, jewellery manufacturing and marketing*, and these steps are illustrated in Figure 1. The following paragraphs will analyse in detail these steps. The challenges at each stage of the value chain are outlined in the following sections.

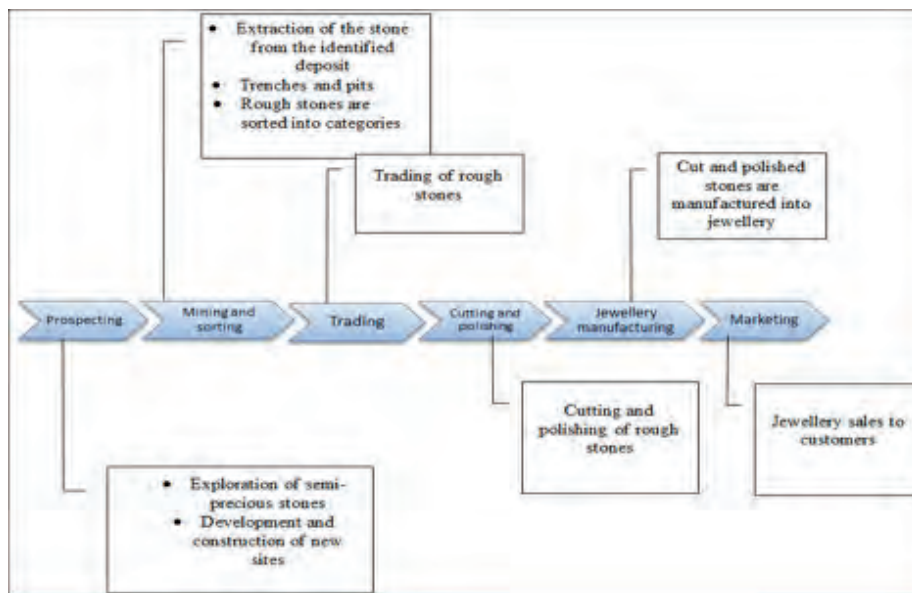


Figure 1. General value chain for coloured gemstones

Through consultative forums coupled with field visits, and interviews of the key stakeholders, there was an unequivocal agreement that selling raw stones is counterproductive to Namibia's aspiration under Vision 2030 and as per the National Development Plans (NDP4). Looking at the value chain processes and the potential for more value addition, it was agreed among the stakeholders that areas of processing, jewellery manufacturing, marketing and trading are the least utilised and hold the most potential in many respects. In light of this realisation, it was put forward that these are the general promising steps of the value chain selected for the coloured gemstones sector to be targeted for further examination. In order to better deal with the benefits or the lack thereof of value addition within the chain, it will be convenient to do an analysis through product groups which are classified in no particular order of preference into three viz: (i) finished gemstone products, (ii) collector pieces and (iii) finished jewellery products.

The following strategic interventions were identified as key in ensuring sustainability of the small mining sector in Namibia; conducting geological assessment to identify new deposits and quantify the existing ones, improving exploration and mining practices, investing in education and training, creating an enabling environment and improving the sector governance and strengthening the sector organisation and supporting the infrastructure. It was found that the main catalyst for the growth of the coloured stone sector is to consider all the unit chains/processes within the value chain as being part of the systems which need to be improved at each and every stage for the common good of the whole sector (holistic approach). These interventions and their outcomes are summarised in Figure 2 below.



Figure 2. Strategic interventions and their outcomes.

References

- Kaplinsky, R., Morris, M., 2001. A handbook for value chain analysis. Ottawa: International Development Research Centre.
- Musiyarira, H., Tesh, D., Namate, N., Pillalamarry, M., 2016. Establishing the essential building blocks for the Semi-precious industry. Proceedings of the Mining Communities 2016 Conference, 5 to 8 June 2016, Vancouver, Canada.

Recent Mining of Some Alluvial Diamond Deposits in South Africa

Brendan M. Laurs

Gem-A-The Gemmological Association of Great Britain
Encinitas, California, USA
brendan@gem-a.com

During a field excursion lead by geologist Dr Mike C. J. De Wit in August 2016, this author visited some active alluvial diamond mines in the North West Province and in the Lower Vaal-Middle Orange Basin of South Africa. This report focuses on three active mining areas: Tirisano and London Run in the North West Province, and Saxendrift on the Middle Orange River.

Alluvial diamond deposits in the North West Province (i.e., Lichtenburg–Ventersdorp and Southern Fields) have been mined for up to ~90 years, and yet their origin is not well established. The diamonds are hosted by sinuous gravel ridges (or ‘runs’) on the flat erosional surface. These gravels are not fluvial, but show characteristics in common with diamictites (unsorted, matrix-supported with sand-to-boulder sized clasts) and were recently interpreted to represent proximal eskers that formed under glaciers during the Carboniferous (280 Ma) glaciation of the area (de Wit, 2016a,b). The diamonds were likely derived locally from 500 million-year-old dikes and ‘blows’ of kimberlite that presently are not exposed on the ground surface. The deposition of the eskers was controlled by the karst terrain and ridges within dolomite host rocks of the Transvaal Supergroup (Malmani Subgroup).

The Lower Vaal River and Middle Orange River systems drain southern Africa’s interior plateau westward into the Atlantic Ocean, and may include diamonds from several sources, including those from Permo-Carboniferous sedimentary sequences described above and the large cluster of Cretaceous diamond-bearing pipes in central-southern Africa. Placer deposits developed where the rivers leave the Karoo base and flow through pre-Karoo rocks, particularly the resistant Ventersdorp Supergroup, where the irregularly weathered base effectively trapped coarse material (cobbles and boulders) that created ideal trap-sites for diamonds.

Tirisano mine (Badenhorst Diamante)

The Tirisano mine is located in the Lichtenburg–Ventersdorp Field ~35 km north of Ventersdorp (26° 5.218’ S; 26° 47.121’ E), and has been mined most recently by Badenhorst Diamante (since 2012). The deposit has produced a total of ~100,000 carats, with a current average value of US\$400–\$500/ct and an overall diamond grade of 1–2 carats per hundred tonnes (CPHT). Several gravel horizons have been defined within the main Nooitgedacht gravel run, and the lower layers constitute the main diamond ore, although some of the horizons contain abundant clay and require the use of a scrubber or trommel for processing. Most of the gravels appear to have been preserved in a sinkhole at the intersection of two major structural features, and are overlain by sandy clay.



Figure 1. This large open pit at the Tirisano diamond mine is being expanded with excavators and dump trucks. Photo by B. M. Laurs.

At the time of our visit, the operation employed 50 people and included seven trucks and two excavators. Two open pits were being mined, with the lowest gravel horizon being exploited. The pits were being dug in a series of benches with an overall pit-wall angle of 45° (i.e. Figure 1). The gravels were trucked to a washing plant (Figure 2), where the material was fed into screening equipment that removed +100 mm clasts. The remaining material passed into a scrubber and was sized to 2–32 mm. This gravel fraction was then fed into rotary washing pans, and the heavy material that accumulated along the outer edges of the pans was then routed into a secure area for X-ray and hand sorting. Most of the diamonds are near-colourless (typically H colour) with some fancy yellow and very rare pink and green stones. The typical daily production is around 5 carats, but may range up to 300 carats in a 16-hour shift. The diamonds consist mostly of octahedrons and some broken blocky pieces, and approximately 60% are of gem quality. The largest diamond was found in June 2016 and weighed ~100 ct; the second largest weighed 68 ct, and some additional significant stones weighed 13–30 ct. All of the diamonds are sold at a monthly tender in Johannesburg.

London Run (Namakwa Diamonds Ltd.)

The London Run deposit is located north of the Vaal River (27° 20.380' S; 25° 25.662' E). The area is part of the Southern Field, which is marked approximately by the towns of Schweizer-Reneke, Wolmaransstad, Bloemhof and Christiana (Wilson et al., 2006). Until 1984, the production was some 2.0 million carats (Marshall, 1987), with an additional estimated 2.5–3.0 million carats produced in 1985–2016; overall, the Southern Field is a source of some 5 million carats, with the London Run producing approximately 500,000 carats (J. Ward, pers. comm., 2017).

The gravels of the London Run are 200–400 m wide, generally 5 m thick, and are situated mainly on lavas of the Ventersdorp Supergroup. The matrix-supported, coarsening-upward gravels (with sand at the bottom) consist mostly of rounded clasts of brown quartzite derived from the Dwyka Formation. In the area that we visited, the gravel horizon was buried by ½–1 m of topsoil. In general, the upper portion of the gravel is cemented by calcrete (Figure 3) and must be blasted in places, and then bulldozers run over the blasted material to break it up for further processing. Below the calcrete horizon is an additional ~2 m of gravel, with the best diamond production coming from the bottom portion.

The diamonds produced at this deposit (e.g. Figure 4) average 0.8–0.9 ct each with a value of slightly below US\$1,000/ct. Grades are fairly constant, yielding 0.8 CPHT in the regolith and 1+ CPHT in the gravel runs. The largest stone produced in the past year weighed 62 ct. Other notable stones include a 26.74 ct D-colour internally flawless diamond and a flat-shaped 55 ct type II stone that was recovered in early 2015. Compared to the Lichtenburg–Ventersdorp Field, this area produces more fancy-coloured diamonds (i.e. yellow, pink, purple, orange, rare blue). Among those produced in recent years was a 7.55 ct vivid orange stone.



Figure 2. The processing plant at the Tirisano mine employs vibrating screens (centre-right), a scrubber/trommel (right), washing pans (center) and a secure area for X-ray and hand sorting (white container on the left). Photo by B. M. Laurs.



Figure 3. Diamond-bearing gravels in this mining trench at the London Run diamond deposit are locally cemented by calcrete (centre) and overlain by a dark soil horizon. Photo by B. M. Laurs.

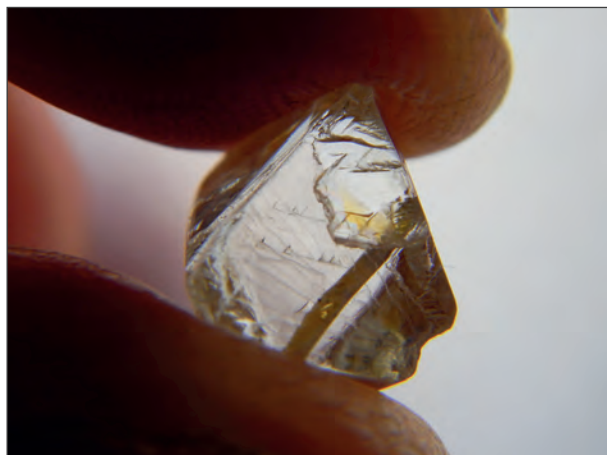


Figure 4. This London Run diamond weighs 5.52 ct, and is therefore significantly larger than most of the stones produced from this deposit. Courtesy of John Ward, Namakwa Diamonds Ltd.

At the time of our visit, a total of approximately 55 mining operations were active in the Southern Field, and seven of them (in partnership with Namakwa Diamonds Ltd.) were mining in the London Run area as of May 2017 (J. Ward, pers. comm., 2017). Our group visited one of these operations, which had 12 employees and produced 300–400 carats per month (average 10 carats/day). The processing plant consisted of two vibrating screens (used to size the material to 2–32 mm) and two rotary washing pans, with a throughput of 4,000 tonnes in a 24-hour period. The plant produced 4 tonnes of concentrate in each 12-hour shift, which was taken to a nearby privately operated facility for further processing (dense media separation and X-ray sorting). The diamonds are sold at tender in Kimberley, South Africa.

Middle Orange River (Rockwell Diamonds)

Between the towns of Douglas and Prieska (e.g. 29° 19.308' S; 23° 15.257' E) are the Middle Orange River deposits, which have yielded many large diamonds over 100 ct and several over 200 ct. The flat-lying fluvial-alluvial gravels are developed on terraces along the banks of the present Orange River, in a sequence comprising basal gravels 2–4 m thick that are overlain by <5 m of variably calcreted sands and silts. These Miocene-age gravels are typical of braided bars, and have migrated through an area up to 30 km wide. The cobble-sized clasts consist mostly of lava and quartzite, with variable amounts of banded iron formation (BIF) in a sandy matrix.

Numerous diamond mining projects have exploited the terraces along ~100 km of the Middle Orange River since the mid-1920s. At the time of our visit, Rockwell Diamonds was reworking the tailings piles (stockpiled upper gravels) from the Saxendrift mine that had not been processed by the previous company, Trans Hex Group. They also were preparing for a new mining operation at a nearby deposit called Wouterspan. Rockwell uses trommels to remove oversized material (Figure 5), and then mobile screening equipment is employed for de-sanding and magnets remove clasts of banded iron formation (which forms most of the concentrate as it has a higher density than diamond) before it is processed through washing pans. The resulting concentrate was passed through X-ray sorting machines. During the past five years, more than 10 diamonds weighing 100+ ct have been recovered by Rockwell from newly mined gravels and tailings. Although diamond grades are highly irregular, the overall grade varies from 0.3 to 2 carats per hundred cubic metres, with better grades from the lower gravel layers. Despite the low grade, the deposit has a very high diamond value of \$1,800–\$2,000/ct. About 70–80% of the value of the deposit lies in 10–20+ ct stones, so relatively large-sized material (5–36 mm) is processed.



Figure 5. Trommels are used to remove oversized material at Rockwell Diamonds' Saxendrift mine. Photo by B. M. Laurs.

The diamonds are sent to Johannesburg, where most of the production is sold in sights that are held every two weeks; large diamonds (+10 ct, referred to as 'specials') are sold separately. The largest diamond found at the Saxendrift mine by Rockwell weighed 287 ct, and was recovered in 2014.

References

de Wit, M.C.J., 2016a. Dwyka eskers along the northern margin of the main Karoo Basin. In B. Linol and M.J. de Wit, Eds., *Origin and Evolution of the Cape Mountains and Karoo Basin*, Regional Geology Reviews, Springer International Publishing, Switzerland, 87–99, http://dx.doi.org/10.1007/978-3-319-40859-0_9.

de Wit, M.C.J., 2016b. Early Permian diamond-bearing proximal eskers in the Lichtenburg/Ventersdorp area of the North West Province, South Africa. *South African Journal of Geology*, 119(4), 585–606, <http://dx.doi.org/10.2113/gssajg.119.4.585>.

Marshall, T.R., 1987. *Alluvial Diamond Occurrences of the Western and Southwestern Transvaal – A Compilation of Production Data*. Information Circular 194, Economic Geology Research Unit, University of the Witwatersrand, Johannesburg, South Africa, 238 pp.

Wilson, M.G.C., Henry, G. and Marshall, T.R., 2006. A review of the alluvial diamond industry and the gravels of the North West province, South Africa. *South African Journal of Geology*, 109(3), 301–314, <http://dx.doi.org/10.2113/gssajg.109.3.301>.

Acknowledgments

Dr Mike C. J. De Wit (Tsodilo Resources Ltd. and University of Pretoria, South Africa) is thanked for introducing this author—together with 25 other participants from at least six countries—to many historical and currently active alluvial diamond deposits in South Africa on a five-day pre-conference field trip associated with the 35th International Geological Congress. John Ward (Namakwa Diamonds, Johannesburg, South Africa) is thanked for providing photos and information on the alluvial diamonds of the Southern Field.

An examination of the morphology of grains of crystalline corundum from Lava Plains Northern Queensland; A rare example of an “in situ” pyroclastic sapphire deposit

Terrence Coldham

Sydney, Australia; terry@intogems.com.au

At many locations around the world corundum is found associated with extrusive alkaline volcanic events of the Tertiary period. Such material is often referred to as BGY (Blue Green Yellow) sapphires and is commonly found associated with a specific group of heavy minerals sometimes referred to as the zircospilic suite (zircon, corundum, spinel, ilmenite) (Hollis, 1985). Many gemmological articles concerning the occurrences of BGY sapphires comment on the apparent intimate association of the zircospilic minerals and Cenozoic alkali basalt flows. Rare xenocrysts of all these minerals have been found encased in basalt. Most of these occurrences are summarised in Hughes' book Ruby and sapphire – a Gemmologist's Guide (Hughes, 2017).

At Present the accepted theory is that most of the BGY sapphire, found in deposits at diverse locations around the globe, are shedding from extrusive basalt flows. They are released by weathering processes and then concentrated in alluvials. During the last four decades more emphasis has been placed by researchers on the suggestion that corundum also sheds from the pyroclastic phase of volcanism and that these rocks might in fact be a major source of BGY sapphire. (Pecover, 1987).

Finding evidence that pyroclastic deposits are an important source of BGY sapphire has been difficult, as such deposits are rapidly eroded away and their presence, even after a geologically short time may be difficult to recognise. Most BGY sapphire deposits are associated with volcanism active over the last 80 million years. It is not surprising that, in-situ pyroclastic deposits unaffected by weathering processes are rarely identified. In Australia evidence of sapphire bearing pyroclastic deposits have been identified as such but due to their age they have been subject to considerable weathering, fluvial action and re-deposition. (Pecover, 1987)

Geology of the Lava Plains gem field

The Lava Plains sapphire occurrence is situated within the Cainozoic McBride Volcanic Province of North Queensland Australia. Situated some 250 kilometres SSW from Cairns (Griffin & McDougall, 1975). Surface mining has been conducted in an area of basaltic lava flows and pyroclastic beds intersected by an immature drainage system containing Corundum and other minerals of the ZIRCOSPILIC suite are recovered, not only from fluvial deposits, but also directly from what appear to be remanent pyroclastic deposits. (Figure 1). Volcanic activity has continued up until very recent times in the area. Zircon, sourced directly from the pyroclastic beds have been given extrusive dates of 2-4 million years. (Sutherland et al., 2015) further 20 zircon megacryst grains sampled from the Lava Plains gem field suggest an age of 2.1 ±0.2Ma for 18 grains. (Sutherland, 2017).

During the period from 1975 to 1985 mining operations recovered sapphire from two quite different areas, one was from alluvial deposits in Wyandotte creek which has it's headwaters draining areas of pyroclastic deposits and the other from extensive surface mining of the of pyroclastic deposits themselves.

In 2015 a new mining operation started producing sapphire from the pyroclastic beds providing an excellent opportunity to examine the surface morphology of BGY corundum grains that have not been subject to the abrasion that normally results from material being transported from their source. This is quite unlike the situation for most BGY sapphire recovered from deposits around the world as they are almost invariably abraded to some extent. At Lava Plains the material is mined by simple scraping the surface of the pyroclastic beds appears and they appear to carry much higher quantities of corundum and associated minerals than any of the weathered basaltic areas non of which have shown evidence of containing corundum xenocrysts. The Lava Plains sapphire field provides us with an insight into just how important a part pyroclastic phases of volcanism play in the deposition BGY sapphires not only in Australia but elsewhere across the globe.



Figure 1. Dipping beds of pyroclastic deposits exposed after mining of the loose surface material. Scot's mine Lava plains. Photo 2016 T.Coldham.



Figure 2. Blue rough sapphire production from Lava plains sapphire fields. Photo 2015 T.Coldham.

Corundum Morphology

The first thing noticeable about a parcel of rough sapphire from the Lava Plains area is the small average size of the grains (averaging from less than one to five carats in the rough), the predominance of fine blue colour and the presence of internal and external fractures (Figure 2). Closer examination reveals the fine detail present in the surface features as they are unaffected by any form of abrasion. These features vary greatly, ranging from very etched and corroded (Figure 3), to surfaces of high lustre. Material recovered from the alluvial areas of Wyandotte Creek usually display some slight evidence of abrasion indicating a brief period of fluvial transportation, however material mined directly from the pyroclastic beds exhibit virtually no evidence of abrasion or "water wearing".

Pinacoids and prism faces are often very well developed but are often "rounded off" due to chemical corrosion prior to reaching the surface (Figure 3). Some crystals do however exhibit perfectly formed highly lustrous crystal faces that display clear horizontal growth lines and other original features developed during crystallization. Some crystal faces are so "glass like" as to allow viewing of internal features just as if they were polished surfaces (Figure 4).

Basal parting planes are very evident, some with etched surfaces evidencing the breakage occurred prior to leaving the volcano, and some with glassy fresh surfaces most likely indicating breakage at the point of or straight after ejection from the volcano. Some xenocrysts show clear evidence of intergrowth of corundum crystals with both corundum and other minerals during initial crystallisation. Other features include evidence of multi stage growth of crystals.



Figure 3. Showing the pinacoids termination and prism faces of a heavily etched Lava Plains sapphire. The junctions of the prism faces are very rounded giving the appearance of water wearing, which it is not. Evidence of three inclusions can be seen on the photo, the position of each and its surrounds suggesting various events in the history of this stone's passage to the earth's surface. (5.2x4.4x2mm, 0.78 carats).

Photo 2017 G. Henry GAA NSW Division.



Figure 4. A tiny well formed crystal of corundum displaying almost perfect crystal faces, with clean sharp undisturbed junctions. Such a crystal must have been protected from chemical corrosion after formation and on its journey to the earth's surface. (4.0x3.5mm, 0.43 carats). Photo. 2017 G. Henry GAA NSW division.

A study of these external features of the corundum xenocrysts provides proof that they were brought to the surface in a pyroclastic phase of the volcanism. Study of the features of certain individual grains provides clues to the journey taken by individual grains of sapphire from crystallization deep in the earth's crust to their expulsion onto the earth's surface.

References

Hollis, J. D., F.L. Sutherland F. L., 1985. Occurrences and origins of gem zircons in eastern Australia. Records of the Australian Museum, 36(6), 299-311.

Hughes W. H., 2017. Ruby and Sapphire: A Gemologist's Guide. Lotus Publishing. ISBN 9780964509719

Pecover, S.R., 1987. New concepts on the origin of sapphire in Northeastern New South Wales. Journal of Gemmology, 16.

Griffin, T. J., McDougall I., 1975. Geochronology of the cainozoic McBride Volcanic Province, Northern Queensland. Journal of the Geological Society of Australia, 22, 4.

Sutherland F.L., Coenraads R.R., Abduriyim A., Meffre S., Hoskin P.W.O., Giuliani G., Beattie R., Wuhler R., Sutherland G.B., 2015. Corundum (sapphire) and zircon relationships, Lava Plains gem fields, NE Australia: Integrated mineralogy, geochemistry, age determination, genesis and geographical typing. Mineralogical Magazine, 79(3), 545–581.

Sutherland F.L., 2017. Personal communication.

Acknowledgements

Graham Henry and the Gemmological Association of Australia for micrographs.

Dr. Lin Sutherland for advice and discussion of content.

Are boehmite needles in corundum Rose channels?

Franck Notari¹, Emmanuel Fritsch², Candice Caplan¹, Thomas Hainschwang³

¹GGTL-Laboratories Switzerland, Geneva, Switzerland;
Franck.Notari@ggtl-lab.org; candice.caplan@ggtl-lab.org

²Institut des Matériaux Jean Rouxel & University of Nantes, Nantes, France; emmanuel.fritsch@cncrs-imn.fr

³GGTL-Laboratories Liechtenstein, Balzers, Liechtenstein;
thomas.hainschwang@ggtl-lab.org

Crystallographically-oriented, rectilinear inclusions in corundum are often referred to as “boehmite needles” (Keller et al., 1985; Hughes, 1997; Stather, 2008; Kan-Nyunt et al., 2013). These inclusions are oriented along the edges of the rhombohedral faces “r” (10-11), that is edges $[r - r']$, $[r' - r'']$ et $[r'' - r]$ (Figure 1). They form angles of 86.1° and 93.9° (Hughes, 1997). They are actually found at the intersection of twin lamellae, formed by twinning along the rhombohedral faces. These twin lamellae can be recognized by the interference colors seen in partially polarized light, or pleochroic colors, different in the lamellae and around it. In the following pages, “needles” refers to the volume created by the intersection of such twin lamellae, even if it is not strictly a needle.

These needles contain apparently polycrystalline material tentatively identified as boehmite, at least in some cases (Schmetzer, 1986). These are common in natural corundum and sometimes used as a criterion to separate natural from synthetic corundum. Twin lamellae observed in corundum most often form via deformation twinning (Belyaev, 1974; Schmetzer, 1986). They result thus from post growth events, and are the proof that strain was applied to the crystal. Hence comes their common occurrence in natural gems and scarcity in synthetic ones.

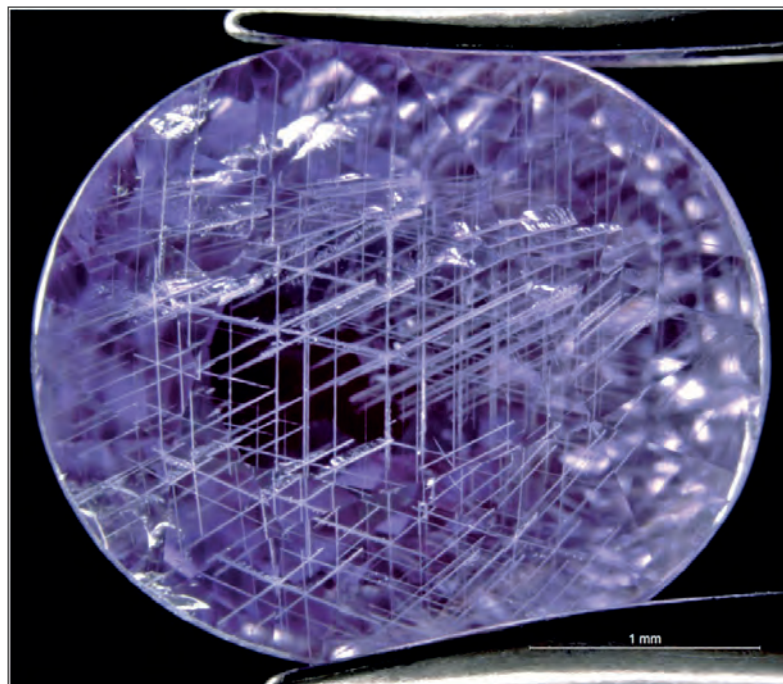


Figure 1. Purple sapphire (unheated) from the Uмба valley in Tanzania with a large number of « boehmite needles », oriented in all three possible orientations (Ref. FN-1103; Field of view: 3.34 mm).

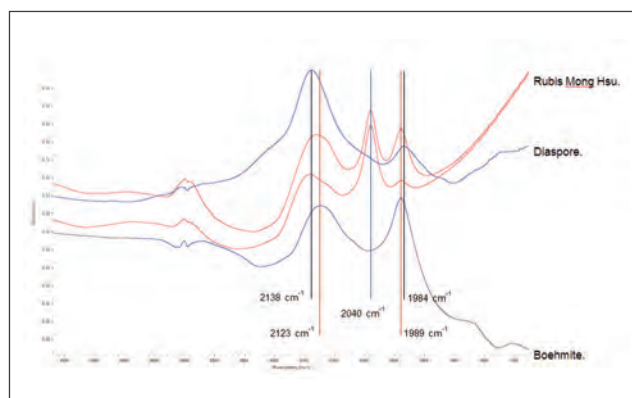


Figure 2. The infrared absorption spectra of boehmite, diaspore, and two Mong Hsu rubies with boehmite (and minor diaspore) inclusions.

Boehmite is the aluminum hydroxide γ -AlOOH, and crystallizes in the orthorhombic system. It is found in corundum as a syngenetic inclusion, often also epigenetic, and finally as an exsolution product provoking parting (White, 1979). It can be identified through an easily recognizable infrared signal with two broad bands at about 2123 and 1989 cm^{-1} , differing only slightly in position from those of diaspore (Figure 2).

Materials and methods

Gemological observation and imaging was done using a variety of Leica microscopes, including the M205C and MZ6. Infrared spectra were obtained on a variety of Fourier Transform spectrometers, including a Bruker IFS and a Thermo Nicolet Nexus at a resolution of 4 cm^{-1} generally accumulating 100 scans. Hundreds of stones containing boehmite needles (as defined above) have been investigated by infrared absorption spectroscopy. Of particular interest is a Ramaura flux synthetic ruby containing a small number of such needles (Figure 3).

To investigate the nature and aspect of the material inside the needles, three samples from Vatomaniry, Madagascar, were prepared with the needle axis near perpendicular to the plate, one with parallel windows (Figure 3). Scanning electron microscope (SEM) images were obtained on a Jeol-5800LV.

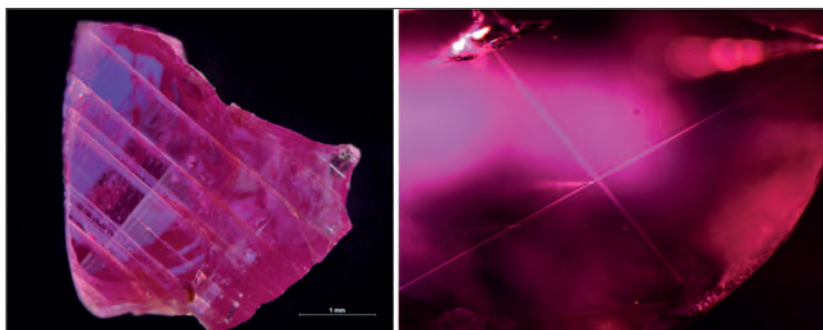


Figure 3. Some of the samples studied: (left) The parallel window Malagasy sample (Field of view, 4.83 mm) for SEM investigation with two series of twin lamellae (one dominates) and (right) a micrograph of the Ramaura synthetic ruby containing "boehmite needles" at the intersection of two twin lamellae (partially polarized light; Field of view 2.3 mm).

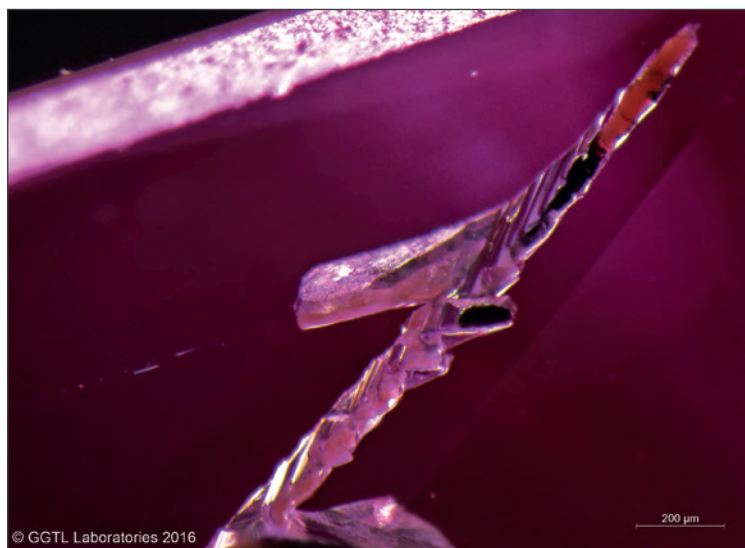


Figure 4. Unusually large “needles” in a purple sapphire from Ilakaka, Madagascar, demonstrate that these cavities are corundum negative crystals at intersecting twin lamellae (Field of view 1.65 mm).

Results

Observation with the microscope reveals two aspects for the boehmite needles: some are lath- or ribbon-shape. Others are clearly negative crystals (Figure 4). Figure 3 shows needles in a flux synthetic ruby, a gem with no boehmite infrared signal. The systematic infrared absorption approach did not always demonstrate the presence of boehmite absorptions when so-called boehmite needles are present. Over the years, this led the authors to believe that there was no systematic relation between the „needles“ inclusions and boehmite.

The SEM investigation turned out to be quite difficult, and often nothing was seen at the intersection of twin lamellae, even if visually there is the impression of a needle. Most of the time, there is a topographical depression at the intersection of twins. Sometimes, structures hard to explain are seen in the lamellae, which reveal an unexpected microstructure of what appears to be corundum, and not boehmite.

Discussion and conclusion

To reconcile observations and measurements, the view that needles are made of boehmite must be reconsidered. It is known in a small number of materials (some metals, calcite, diamond) that hollow channels may form at the intersection of twin lamellae (Seeger, 2007; Schoor et al., 2016), caused by deformation twinning. This was discovered by Rose (1868) in calcite, thus this feature is called “Rose channels”. This is one of the possibilities offered by migration of vacancies created during deformation.

We believe that “boehmite needles” are Rose channels. Even when very small, these channels would explain the optical relief observed, without a change in chemistry or infrared absorption. They fit the crystallographic nature of the structures observed. It explains also the quick propagation of diffusion, and even glass filling, along these features. It is possible that post deformation events created some dissolution or minor mineral transformation at the surface of these voids, reconciling this proposition with the variety of previous observations, including boehmite formation. This would account for the whitish appearance of this feature, created either by light scattering on a rough surface or mineral grains of a different index of refraction.

References

- Belyaev L.M. (Ed.), 1974. Ruby & Sapphire, Nauka publishers, Moscow, 443pp.
- Hughes, R. W, 1997. Ruby & Sapphire. RWH Publishing, Bangkok, Thailand. 511pp.
- Kan-Nyunt, H. P., Karpampelas, S., Link, K., Thu, K., Kiefert, L., Hardy, P., 2013. Blue sapphires from the Baw Mar Mine in Mogok. *Gems & Gemology*, 49(4), 223-232.
- Keller, P. C., Koivula, J. I., Jara, G., 1985. Sapphire from the Mercaderes–Rio Mayo area, Cauca, Colombia. *Gems & Gemology*, 21(1), 20-25.
- Rose, G., 1868. Über die im Kalkspath vorkommende hohle Canäle. *Abhandlungen der königlichen Akademie der Wissenschaften zu Berlin*, 57-79.
- Schoor, M., Boulliard, J.C., Gaillou, E., Hardouin-Duparc O., Estève, I., Baptiste, B., Rondeau, B., Fritsch, E., 2016. Plastic deformation in natural diamonds: Rose channels associated to mechanical twinning. *Diamond & Related Materials*, 66, 102-106.
- Seeger, A., 2007. Production of lattice vacancies in metals by deformation twinning, *Philosophical Magazine Letters*, 87, 95–102.
- Schmetzer, K., 1986. *Natürliche und synthetische Rubine: Eigenschaften und Bestimmung*. Schweizerbart'sche Verlagsbuchhandlung, Stuttgart, 131 pp.
- Stather, L. (ed.), 2008. *Foundation in Gemmology, Gem-A*, The Gemmological Association of Great Britain, London. pp. 250
- White, J. S., 1979. Boehmite exsolution in corundum. *American Mineralogist*, 64(11), 1300-1302.

Sapphire Mining in Montana

Shane F. McClure

GIA, Carlsbad, USA; smcclure@gia.edu

The sapphire mines of Montana have always been fascinating. Where else in the world do you see in such close proximity two completely different types of sapphire deposits? On the one hand you have a hugely prolific deposit that can produce many kilos of material, but it tends to be small and a large percentage of it needs to be heat treated to be useful (Emmett & Douthit, 1993).

On the other hand, not far away, you have a primary deposit that is not prolific and is hard to mine, but produces beautiful blue sapphires that do not need heat treatment. The one factor they share with the other deposit is that they too tend to be small (Mychaluk, 1995).

We are of course referring to the Gem Mountain and Missouri river secondary deposits versus the Yogo Gulch primary deposit (Kane, 2003).

In August of 2015 a team from GIA had the opportunity to visit some of these mines and with the help of colleagues were able to get what is probably unprecedented access to several of the mining operations. Unfortunately this did not include the legendary Yogo deposit, so that will have to wait for another time.

Gem Mountain

The first operation we visited was the Gem Mountain claim owned by Chris Cooney. His is primarily a tourist based operation where he hauls gravel down from his claim about four miles up the mountain which he then bags and sells to people who want to find their own sapphires. He has a facility set up where people can wash and shake their gravel on screens, concentrating the sapphires on the bottom much like panning for gold.

The interesting thing about Chris' operation is that if the client wishes he will have the stones they found cut for them and he will even heat treat them in a furnace he has set up onsite (Figure 1). We are not aware of another operation that will heat treat sapphires to order for the public. With his permission we were allowed to film his entire heating operation and interview him about it. According to Chris this is the first time he has allowed this.

We spoke to several people who come to screen for sapphires every year and have jewelry made with the stone they found, which are typically in a wide range of colors.



Figure 1. A group of heated Gem Mountain sapphires just after being removed from the furnace.



Figure 2. The four largest sapphires recovered from a day's run at Eldorado bar on the Missouri river. The largest weighs 16.77 carats.

Eldorado bar

The second location we visited was the Eldorado Bar on the Missouri river. There are a number of claims being mined along this bar but the one we went to belongs to Cass Thompson. Cass and his family have been operating in this area for about 65 years and his family has owned several other claims in the area.

Our purpose for doing expeditions such as this are usually twofold. One is to document the mines, miners and processes and other details to produce reports, articles and videos for education purposes. The other is to collect samples as close to the source as possible to add to our research reference collection. With this in mind, we made a deal with Cass to buy a whole day's production of the mine for a set fee. This means that they would run the typical number of square yards of gravel through the plant and whatever comes out of the jig at the end of the day would be ours. This kind of an agreement is obviously somewhat of a gamble for both parties. If by chance a spectacular stone was found that day it would belong to GIA. If on the other hand it was not a good day there might be a low yield or few good stones in the run.

As it turned out and as one would hope, everyone was happy in the end. They did not miss out on a spectacular stone but we acquired many good stones for our collection, the largest being a clean prismatic greenish blue crystal over 16 carats (Figure 2). By the time we finished sorting through all the gravel that came out of the jig the yield was more than 1000 carats of sapphire of various color, including a clean pink stone over 7 carats.

The overburden in the Eldorado bar area can vary extensively. It might only be one foot thick or could be 10 to 15 feet thick or more. The sapphire bearing gravel, or "pay" as they refer to it, is located just above the bedrock and could be 10 feet or more thick. One of the problems with some of the other claims in the area is the overburden is much deeper, making it much more difficult to get to the sapphires.

After recovering the gravel from the deposit the operation is similar to many recovery plants, first running the gravel through a "grizzly" to remove all the large rocks and then running what's left through a washing plant that feeds the gravel at a measured rate on to conveyor belts that lead to a large trammel. The trammel washes the material and removes dirt and sand as well as any larger rocks. The remaining gravel is fed through a large jig that traps the sapphires and is periodically vacuumed out and sorted by hand.

They operate this mine year round and produce on the average about 200,000 carats of sapphire per year. Just as with Chis Cooney's operation, most of this goes to the tourist trade. They have set up a shop outside Helena on Houser Lake that offers bags of gravel from the jig that the public can wash.

Rock Creek

The final site we visited on this trip was very different from the other two. The company is called Potentate Mining and is owned by Keith Barron. The site is at Rock Creek, which is actually the same deposit that is often referred to as Gem Mountain. Potentate has been steadily buying up the claims on this mountain and when we visited they were in control of almost the whole mountain except for a couple of claims (Boyd & Barron, 2015), including the one belonging to Chris Cooney.

Their intent is to control the whole deposit and through the use of modern recovery methods and surveying techniques recover large volumes of sapphires which they intend to offer for sale to the industry mostly as rough.

When we were there they were mining at the top of the mountain where they have a large screening plant that sorts the material into three sizes – 1/8 inch and smaller, 1/8 to 1.0 inch and larger than one inch. The 1/8 to 1.0 inch is what they truck down mountain to the washing plant at Eureka Gulch. At that time the gravel was producing 40 to 50 carats of sapphire per cubic yard. They were not yet in full operation but they planned to be for the 2016 season.



Figure 3. A sapphire as it was found in the gravel of the jig at Rock Creek.



Figure 4. A pan of material out of the sluice revealed a few small sapphires and a good amount of gold.

The biggest issue they have at this time is maintaining an adequate water supply for the washing plant through the summer. To this end they have built a large settling pond to try and recycle as much water as possible. In this way they also avoid contamination of local streams (Barron & Boyd, 2015)

We had the opportunity to stand next to the jig after it had been turned off and pull sapphires out of the gravel ourselves (Figure 3). In a matter of 15 to 20 minutes I was able to recover a whole handful of sapphires.

It is interesting to note that they have developed a secondary sluice system that the small material is fed through. The purpose of this is to collect gold, which is also present in these deposits (Figure 4). While not present in huge amounts, it is a useful secondary revenue source. We were allowed to keep a small handful of the sapphires we recovered that day from the jig to add to the research sample collection and upon our return home we cleaned off the small amounts of sand that were still attached to the stones. Close inspection in the microscope of this left over sand revealed a few tiny flakes of gold that were still present.

Potentate has done extensive surveys of the mountain and has identified a number of areas that should be rich in sapphires. In fact, in their opinion, this is certainly the richest gem deposit in the Americas by volume. In the 2016 season they recovered more than 40 kilos of sapphire and in that found a 32 carat stone that has been cut into 12.62 carat finished stone. They believe this now holds the record for the largest cut sapphire from Montana.

References

- Barron K.M., Boyd W.F., 2015. The Rock Creek Sapphire Mine of Montana – A New Era. In *Color*, 28, 2-13.
- Boyd W.F., Barron K.M., 2015. Update on Rock Creek Deposit. *Gems and Gemology*, 51(2), 215-216.
- Emmett J.L., Douthit T.R., 1993. Heat Treating the Sapphires of Rock Creek, Montana. *Gems and Gemology*. 29(4), 250-272.
- Kane R.E., (2003). The Sapphires of Montana: A Rainbow of Color. *Gem Market News*, 22(1), 1-8.
- Mychaluk K., 1995. The Yogo Sapphire Deposit. *Gems and Gemology*, 31(1), 28-41.

Acknowledgements

I would like to thank Chris Cooney, Cass Thompson, Keith Barron and Warren Boyd for their time and willingness to show us their operations and would especially like to thank Robert Kane of Fine Gems International for setting the excursion up.

Padparadscha Color Grading for Gem Trade

**W. Atichat, J. Jakkawanvibul, M. Maneekrajangsaeng, T. Sripoonjan, T. Leelawatanasuk,
V. Pisutha-Arnond, N. Narudeesombat, P. Chanthayod, B. Sriprasert**

The Gem and Jewelry Institute of Thailand, Bangkok, Thailand;
Email: awilawan@git.or.th, wilawan.atichat@gmail.com

Introduction

Padparadscha is a variety of corundum with colors ranging from orange-pink to pink-orange, comparable to a lotus' color or sunset sky. Its name, padparadscha, is derived from "padmaraga" in Sanskrit, which means a lotus' color ("padma" means lotus while "raga" means color) (Crowningshield, 1983). Color grading for padparadscha is a sensitive subject as there is no universally accepted standard.

GIT Laboratory had an initiative in 2007 to create master sets of major varieties of corundum including padparadscha that made up entirely of natural stones. In practical work, when a stone was graded with reference to a standard of the same material, it made the grading process simpler and more precise. Those natural padparadscha stones were acquired from the trade and the Munsell color system, a globally trusted system used in many industries, was used as a basis for the comparison of colors of those stones (Chandayot et al., 2007). However, this master stone set was still ambiguous to some traders and buyers because they did not cover all the colors of padparadscha known in the trade yet. Therefore, GIT has undertaken an ongoing research project to upgrade and standardize our 2007 master set. Our main objective is again to create a set of genuine master stones to cover the padparadscha color range that is acceptable by the trade for practical usage in the lab.

Samples and Procedures

In this research, we firstly made a literature survey of current references related to padparadscha. We have modified the color range of the GIT 2007 Master stones set compatible with those defined by LMHC Information Sheet #4. This color range is used because it is well accepted by the leading gemological laboratories and somewhat similar to those proposed by Hughes (2016), except the Hughes' version encompasses a wider range of hues and saturations. Both the LMHC's and Hughes', however, define their color ranges based on the color charts, which are 2-dimensional, and are not practical to be used in the lab for color grading of the stone--which is 3-dimensional. So we have to find the real stones that match the color chart of padparadscha.

For the samples themselves, we used our 2007 original padparadscha master stones (Figure 1), as the starting specimens. We started our work by scrutinizing the pros and cons of this original master set. Then, we acquired additional stones from a number of trusted traders with the following selection criteria: natural stones (untreated or conventional heat-treated, no Be-treatment or irradiation), weights from 0.50 to 1.00 ct for the ease of color observation; and the colors ranging from orange-pink to pink-orange of padparadscha in the trade.

After that, we compared the color of the stones to the Munsell color charts (Munsell Book of Color, 2014) under a specified viewing environment and a systematic comparison method to determine the color code of the stones by at least 2 experienced graders. We used a Macbeth standard light booth with two light sources having the color temperature of 5000K (i.e., 2 Gretag Macbeth 5000K F20T12/50 light bulbs) which provide color shades least affecting the gemstone colors. The results from both graders were considered and selected for the only color chip with the closest match to the stone. The hue, value and chroma of the final chosen color were recorded.

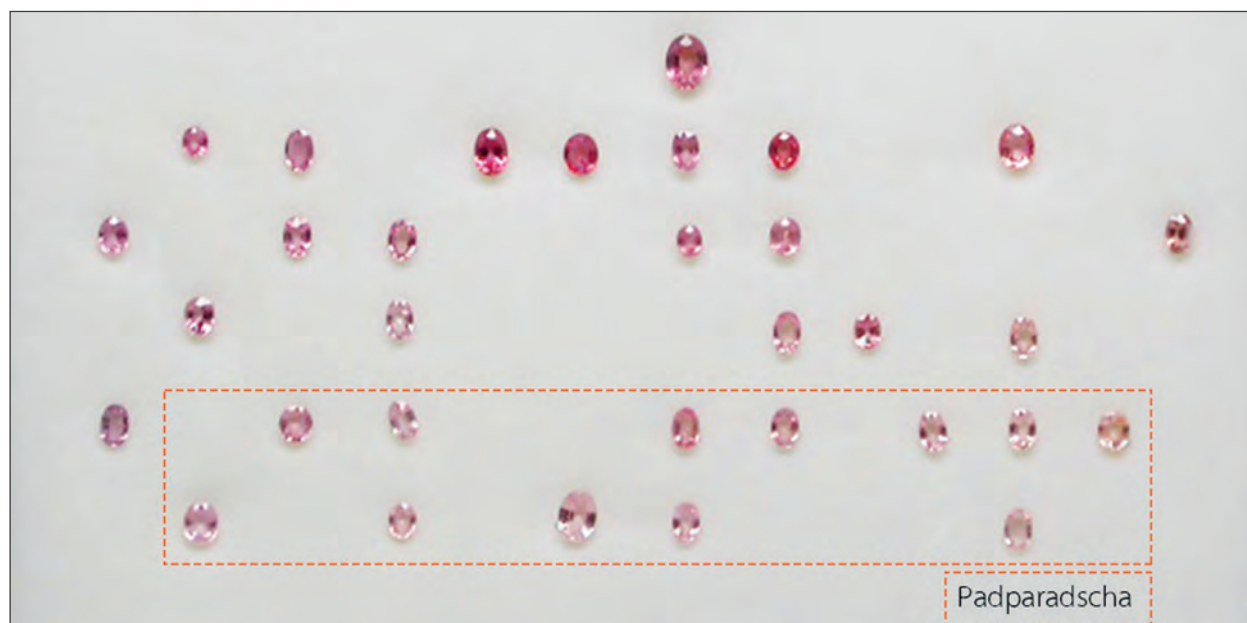


Figure 1. The original set of GIT's padparadscha master stones in 2007 (the lowest dashed rectangular).

After the final hue, value and chroma of each stone were compared to the LMHC's padparadscha color charts, a new set of genuine master stones was selected and formulated into our padparadscha standard. Finally, the research team conducted a survey to acquire opinions of connoisseurs and Thai, Sri Lankan, and Japanese entrepreneurs regarding the master stone set to specify color names and color ranges conforming to the ones known in the gem market.

Result and Conclusion

As shown in Table 1 and Figure 2, the result of hue, value and chroma of all stones are compared with 6 hue charts of the LMHC's padparadscha color, i.e., orangy pink 10RP to 2.5R, orange-pink 5R to 7.5R and pinkish orange 10R to 2.5YR (LMHC Information Sheet #4).

Altogether 21 stones that fell within the LMHC's padparadscha color range were selected and arranged into our new GIT's padparadscha master stone set (Figure 3). The color ranges of our current padparadscha master set are able to specify the border line colors more accurately. Furthermore, the survey results with traders in major padparadscha producing (Sri Lanka), trading (Thailand) and consuming (Japan) countries revealed that the range of color proposed by LMHC was acceptable but most of them advised that more colors should be added to cover the range of "Padparadscha" use in their markets. Finally, even though the true international acceptance of the color standard of our padparadscha sapphire master stones still need time, but, at least, this work should help color grading of padparadscha with better precision and accuracy. It could also reduce the difficulty in communication with business operators and promote padparadscha trading.

| LMHC Chart | Color | Stones match with the chart |
|------------|------------------------|--|
| 1 | Orangy pink (10RP) | Pad57-009, Pad57-069, Pad57-011, Pad57-006, Pad57-019 |
| 2 | Orangy pink (2,5R) | PAD57-031, PAD 57-024, PAD57-013 |
| 3 | Orange-Pink (5R) | PAD57-032, PAD57-025, PAD57-026, PAD57-042, PAD57-022, PAD57-027 |
| 4 | Orange-Pink (7,5R) | PAD57-070, PAD57-039, PAD57-041 |
| 5 | Pinkish orange (10R) | PAD57-036, PAD57-005 |
| 6 | Pinkish orange (2,5YR) | PAD57-005, PAD57-067, PAD57-037 |

Table 1. A list of the GIT's stones that match with the 6 color charts of LMHC's padparadscha

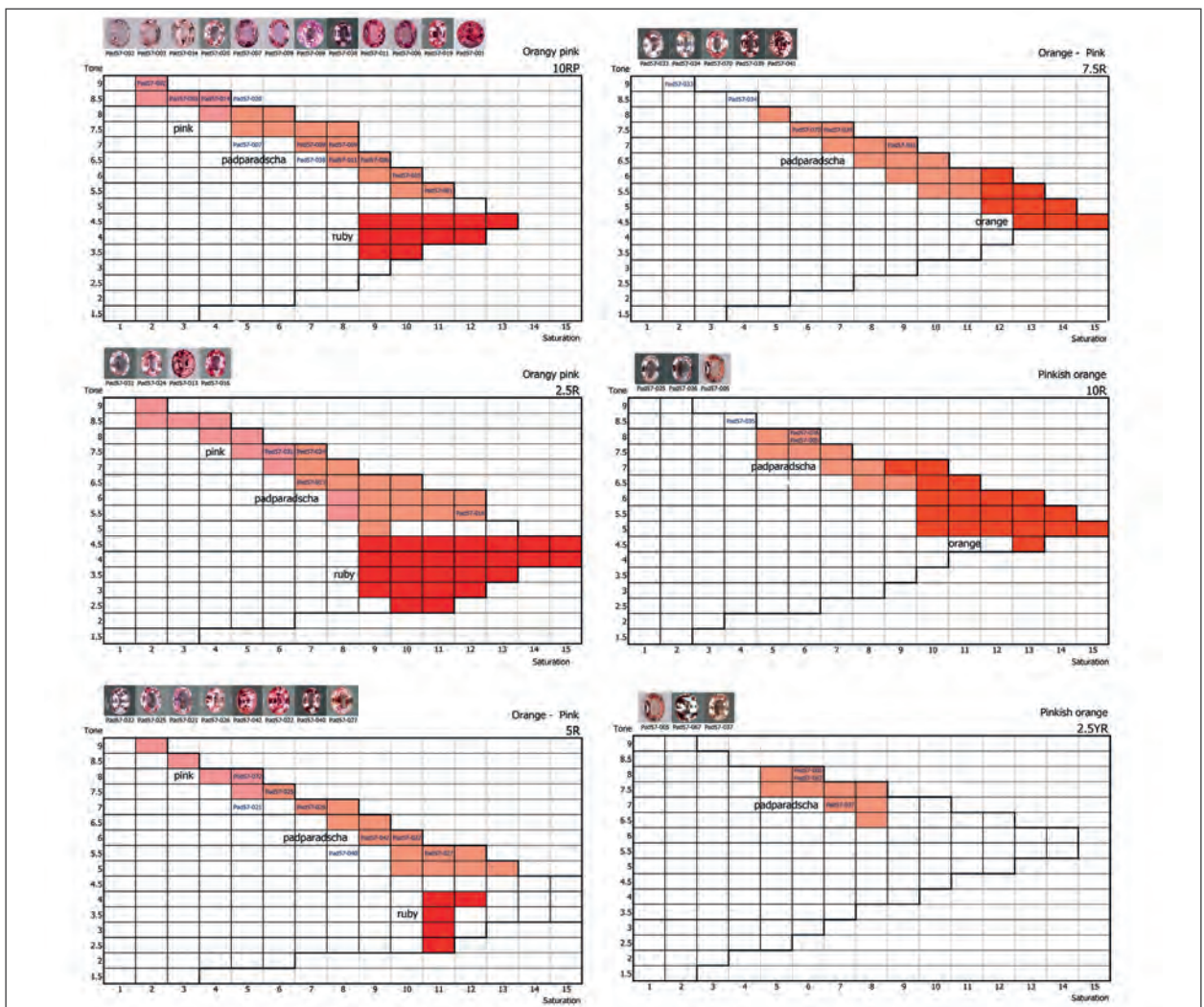


Figure 2. Matching of the GIT's stones with the 6 color charts of LMHC's padparadscha.

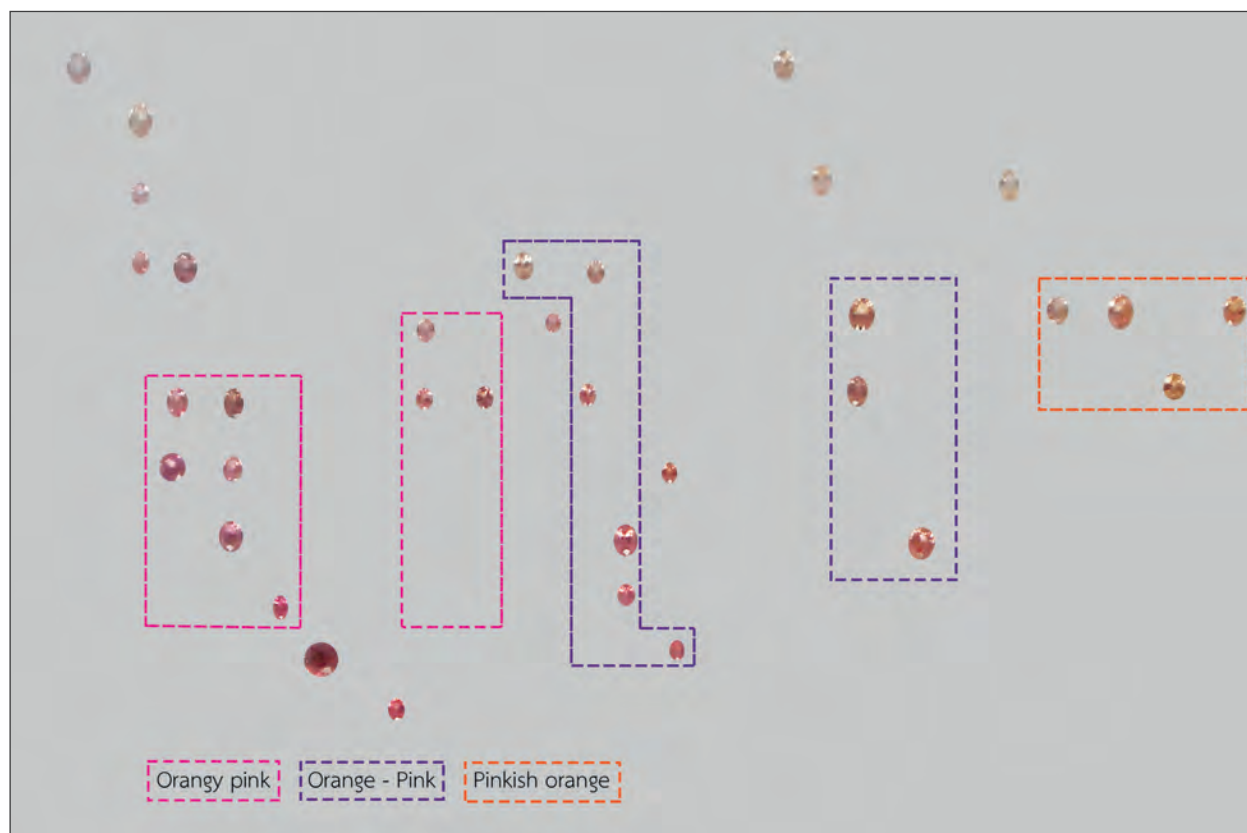


Figure 3. The current GIT's padparadscha master stone set showing three main hues (orangy pink, orange-pink and pinkish orange) along the X-axis, and the tone variation along the Y-axis.

References

Chandayot, P., Atichat, W., Suriyachot, J., Saejoo, S., Saengbuangamlam, S., 2007. Colour Communication of corundum. The Gem and Jewelry institute of Thailand, 103pp.

Crowningshield, R., 1983. Padparadscha: What's in a name?, *Gems & Gemology*, 19(1), 30-36.

Hughes, R.W., 2016, Pretty Padparadscha, In *Color Magazine*, winter, 30-40.

LMHC Information Sheet #4, http://www.lmhc-gemology.org/pdfs/IS4_18012010.pdf

Munsell Book of Color - Glossy Edition, PN: M40115B, 2014.

Two kinds of synthetic diamonds having features similar to natural diamonds

Hiroshi Kitawaki, Kentaro Emori, Mio Hisanaga, Masahiro Yamamoto

Central Gem Laboratory, Tokyo, Japan; kitawaki@cgl.co.jp

Identification of synthetic diamond requires advanced laboratory techniques such as FITR, photoluminescence (PL) analysis or DiamondView™ analysis as well as standard gemmological tests. In this report, two kinds of synthetic diamond which showing features that can be misidentified for natural, are presented.

Background

Synthetic diamonds have been growing in size and quality year after year, and those of over 10 ct (International Gemological Institute, 2015) and 5 ct (Law et al., 2016) produced by HPHT and CVD method respectively have been reported. Meanwhile, melee-sized colourless synthetic diamonds coming to be mixed in jewellery are becoming a major concern to the industry (e.g., Soonthorntantikul et. al., 2015; Lan et al., 2015).

Standard gem testing techniques such as magnification under the gemmological microscope, UV fluorescence test and observation of strain birefringence are essential for identification of synthetic diamond. In addition, advanced laboratory techniques such as PL analysis or observation using DiamondView™ are required in many cases.

In this report, we introduce: (1) a brown CVD synthetic diamond showing distinct linear colour zoning (brown graining) under magnification and (2) a yellow HPHT synthetic diamond showing B' centre (platelet) and a C-H related peak in FTIR analysis. As these features only by themselves can be misidentified as natural diamonds, it is critical to identify a stone comprehensively by combining them with other analytical techniques.

Materials and Methods

We examined two fancy coloured diamonds which were submitted to CGL in Tokyo for grading recently by different clients, both without being disclosed as the potential synthetic origin. One weighed 1.027 ct and was graded as Fancy Dark Brown with VS1 clarity, and identified as CVD synthetic after the tests (Figure 1). The other was 0.066 ct in weight and graded as Fancy Vivid Yellow, SI1 colour, and identified as HPHT synthetic (Figure 2). Analysis using laboratory techniques were performed on the samples. JASCO FT/IR 4200 was used for infrared spectroscopy in the range 7000–400 cm^{-1} , at 4.0 cm^{-1} and 1.0 cm^{-1} resolution with accumulation 512. For photoluminescence (PL) analysis, Renishaw inVia Raman Microscope and Renishaw Raman system-model 1000 were used with 633, 514, 488 and 325 nm lasers as exciting sources for the samples being immersed in liquid nitrogen. UV luminescence images were also observed using DiamondView™.



Figure 1. CVD synthetic diamond tested in this study (1.027ct, Fancy Dark Brown).

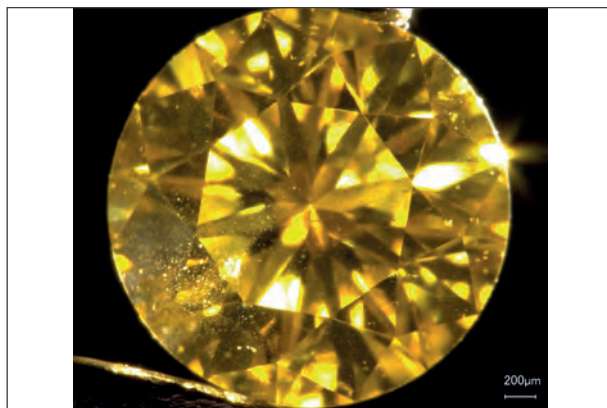


Figure 2. HPHT synthetic diamond tested in this study (0.066ct, Fancy Vivid Yellow).

Results and Discussions

(1) Brown CVD synthetic diamond showing distinct “brown graining”

Many natural brown diamonds contain “brown graining” that is formed due to plastic deformation. This graining runs in parallel with {111} planes and usually seen throughout a faceted stone, may be in one direction but often in two or three directions crossing each other (Kitawaki, 2007).

Contrary to this, the 1.027 ct Fancy Dark Brown diamond tested in this study showed several sets of distinct brown colour zoning only in one direction (Figure 3). The Fancy Dark Brown body colour and the presence of the brown graining were suggestive of natural diamond in our preliminary tests. Natural brown diamonds generally show anomalous birefringence with high-order interference colours along the brown graining under crossed polarised lights, but this stone showed strain with first-order interference colours along the graining accompanied by strain birefringence stretching perpendicular to it. Infrared absorption spectroscopy revealed that this sample was type II.



Figure 3. Fancy Dark Brown CVD synthetic diamond showed several sets of distinct brown colour zoning only in one direction.

A series of peaks at 7352, 6854, 6425 and 5564 cm^{-1} were detected. These peaks are characteristic to CVD synthetic diamonds and supposed to be related to interstitial hydrogen atoms or hydrogen atoms trapped in the vacancies (Wang et al., 2003, 2007; Martineau et al., 2004). The 3123 cm^{-1} peak derived from NVH⁰ (Khan et al., 2009) together with many peaks related to C-H were also detected between 3400 and 2700 cm^{-1} .

From the PL analysis using a 488 nm laser excitation, rather distinct peak at 503.2 nm (H3) and weaker peaks at 493, 501.7, 512.1, 523.6, 524.4 and 523.2 nm were observed.

Likewise, using a 514 nm laser, very strong peaks were detected at 574.9 nm (NV⁰) and 637.0 nm (NV⁻) as well as a weaker doublet at 596.4 and 597.0 nm. Also detected was a peak at 595.3 nm.

The 737 nm (SiV⁻) peak that is characteristic to CVD synthetic diamond (e.g., Wang et al., 2003; Martineau et al., 2004) was not detected either by 514 or 633 nm laser sources. With a 833 nm excitation laser, a series of peaks at 853.2, 855.1, 861.4, 863.9, 865.8 and 866.8 nm, 878.3 nm peak and a series of 884.4, 885.9, 886.9 and 887.9 nm peaks, together with 917.4, 938.5, 945.7 and 949.8 nm peaks, were recognised.

DiamondView observation revealed orange luminescence colour throughout the stone that originates in NV centre, and curved stripes characteristic to CVD synthetic diamond (e.g., Martineau et al., 2004) were also observed.

From the results obtained above, this stone was concluded as an CVD synthetic diamond without post growth HPHT treatment. The brown linear colour zoning assumedly originates from imperfection of crystal growth parallel with {100} orientation of a seed crystal caused by variable accumulation of non-diamond carbon or vacancy clusters but not in plastic deformation similarly to natural diamond.

(2) Yellow HPHT synthetic diamond showing B' centre in Infrared absorption spectra

In most of commercially produced yellow HPHT synthetic diamonds are type Ib and contain isolated substitutional nitrogen approximately 200 ppm (Collins et al., 2000). It is well known that the higher temperature involved in their synthesis or succeeding HPHT treatment will turn the stones into a mixed type Ib + IaA (e.g., Shigley et al., 1993).

The 0.066 ct Fancy Vivid Yellow diamond tested here showed B centre and B' centre (platelets) in addition to C and A centres in FTIR analysis. The nitrogen concentration reached to 700 ppm in total, and a C-H related peak was detected at 3107 cm⁻¹ (Figure 4). From the presence of the B' centre and the 3107 cm⁻¹ peak, this yellow stone implied natural origin. However, this diamond also shows a C centre together and this is suspicious for a HPHT treatment applied either on a natural diamond or on a synthetic diamond.

In PL analysis with a 325 nm laser excitation, a distinct peak at 415.2 nm (H3) was detected. Weaker peaks were also detected at 361, 379 and 389 nm. With a 488 nm excitation source a relatively distinct peak was detected at 503.2 nm (H3), and with a 514 nm laser excitation, a series of Co-related centres were detected at 523.8, 542.9, 544.5, 560.9, 561.7, 579.3 and 580.7 nm (Lawson et al., 1996). With a 633 nm laser, a very clear peak at 992.6 nm (Co-related) (Kiflawi et al., 2002) was detected in addition to many other peaks at 728.9, 735.3, 736.7, 793.4, 815.4, 816.8, 834.7, 852.2 and 869.1 nm.

Minute pinpoint inclusions and metallic inclusions were recognised under magnification observation, and sector zoning characteristic to HPHT synthetic diamond was observed under DiamondViewTM imaging.

These results above lead us to the conclusion that the stone is a HPHT synthetic diamond produced using a Co solvent and then irradiated and HPHT treated after the growth, i.e., a HIH (HPHT growth/ Irradiation/ HPHT treatment) synthetic diamond (Hainschwang et al., 2011).

Conclusion

Synthetic diamonds for gem use have been growing in their size and quality, and they now cover a wide range. The characteristics, such as a linear colour zoning only in one direction is not indicative for a natural brown diamond only by themselves, and the presence of platelets is not indicative for a natural yellow diamond (although it is still characteristic for colourless natural diamonds). Since there are now various types of synthetic diamonds, it is important to distinguish with comprehensive methods including standard gemmological test and laboratory techniques.

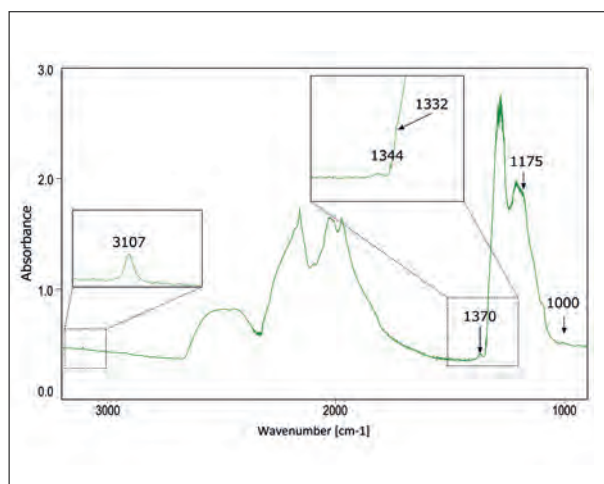


Figure 4. Fancy Vivid Yellow HPHT synthetic diamond showed B and B' centre (platelets) in FTIR analysis. C-H related peak was also detected at 3107 cm⁻¹.

References

- Collins A.T., Kanda H and Kitawaki H., 2000. Colour changes produced in natural brown diamonds by high-pressure, high-temperature treatment. *Diamond and Related Materials* 9, 113-122
- Hainschwang T and Notari F., 2011. HH: Multi-treated HPHT-grown synthetic diamonds showing some characteristics of natural diamonds. *GGTL Laboratories Gemmological Newsletter* 1, Sept
- International Gemological Institute, 2015. International Gemological Institute (IGI) Hong Kong certifies record-breaking, world's largest colorless grown diamond, May 26, <http://www.igiworldwide.com/igi-certifies-worlds-largest-colorless-grown-diamond.html>
- Khan R.U.A., Martineau P.M., Cann B.L., Newton M.E and Twitchen D.J., 2009. Charge-transfer effects, thermo and photochromism in single crystal CVD synthetic diamond. *Journal of Physics: Condensed Matter*, 21(36), article no.36214.
- Kiflawi I., Kanda H and Lawson S.C., 2002. The effect of the growth rate on the concentration of nitrogen and transition metal impurities in HPHT synthetic diamonds. *Diamond and Related Materials* 11, 204-211.
- Kitawaki H., 2007. Gem diamonds: Causes of colors. *New Diamond and Frontier Carbon Technology*, 17(3), 119-126.
- Lan Y., Liang R., Lu T., Zhang T., Song Z., Ma H and Ma Y., 2015. Identification characteristic of near-colourless melee-sized HPHT synthetic diamond in Chinese jewelry market. *Journal of Gems & Gemmology*, 17(5), 12-17.
- Law B., Wang W., 2016. CVD Synthetic diamond over 5 carats identified. *Gems & Gemology*, 52(4), 414-416.
- Lawson S.C., Kanda H., Watanabe K., Kiflawi I and Sato Y., 1996. Spectroscopic study of cobalt-related optical centers in synthetic diamond. *Journal of Applied Physics*, 79(8), 4348-4357.
- Martineau P.M., Lawson S.C., Taylor A.J., Quinn S.J., Evans D.J.F and Crowder M.J., 2004. Identification of synthetic diamond grown using chemical vapor deposition(CVD). *Gems& Gemology*, 40(1), 2-25.
- Shigley J.E., Fritsch E., Koivula J.I., Sobolev N.V., Malinovsky I.Y and Pal'yanov Y.N., 1993. The gemological properties of Russian gem-quality synthetic yellow diamonds. *Gems& Gemology*, 29(4), 228-248.
- Soonthorntantikul W and Siritheerakul P., 2015. Near-colorless melee-sized HPHT synthetic diamonds identified in GIA laboratory. *Gems& Gemology*, 51(2), 183-185.
- Wang W., Moses T., Linares R.C., Shigley J.E., Hall M and Butler J., 2003. Gem-quality synthetic diamonds grown by a chemical vapor deposition (CVD) method. *Gems& Gemology*, 39(4), 268-283.
- Wang W., Hall M.S., Moe K.S., Tower J and Moses T.M., 2007. Latest-generation CVD-grown synthetic diamonds from Apollo Diamond Inc. *Gems & Gemology*, 43(4), 294-312.

Acknowledgement

We express our gratitude to Dr. Kenji Watanabe of the National Institute for Materials Science for his cooperation on the PL analyses with UV lasers, and to Dr. Hisao Kanda of the Tsukuba Expo Center for his discussion with us on the optic centres.

Hybrid diamonds: Natural Diamonds overgrown with CVD Synthetic

R. Serov, Y. Shelementiev, A. Serova

Gemological Center, Lomonosov Moscow State University, Moscow, Russia, potomskajy@gmail.com

Introduction

Deposition of CVD synthetic diamond films on natural diamond substrates have been described in literature since the early 1960s. In the late 1980 - early 1990s CVD synthetic type IIb and IIa diamond films were successfully grown on natural type IIa and Ia diamonds (Yacobi et al., 1993; Fritsch&Phelps, 1993). Since then in gemological literature the reports concerning natural diamonds with CVD synthetic IIb diamond films had been published (Eaton-Magaña, 2014; Moe et al., 2017). This thin synthetic layer in some cases effectively enhanced the color of the stone.

The CVD are now being applied to natural diamonds not only for color treatment purpose, but in an attempt to gain a bigger polished diamond weight. Thus, such hybrid diamonds can enter the jewelry market and the gemological community must be ready to propose their proper description and disclosure.

We report the gemological and spectroscopic properties of natural diamonds overgrown with CVD diamond manufactured in Russia.

Samples and Methods

Five hybrid diamonds produced by Ltd. Koh-i-noor company, Moscow, Russia were investigated. The samples were presented as natural diamonds overgrown with diamond material by a CVD process. A thick layer about 400 μm thick of synthetic CVD diamond was deposited on the (001) faces of natural rough diamonds. All samples were subjected to subsequent polishing. These faceted hybrid diamonds had a weight range of 0.08 to 0.29 ct.

FTIR spectra were recorded on Bruker ALPHA in the range of 400-7000 cm^{-1} , at 2 cm^{-1} resolution, averaging 120 scans. VIS-NIR spectra were obtained using Ocean Optics QE65000 spectrometer in the range of 400-1100 nm, accumulating 30 scans. Photoluminescence (PL) spectra were performed on EnSpectr R532 (M532) spectrometer. VIS-NIR and PL spectra were collected at room and liquid-nitrogen temperature. Color cathodoluminescence images for this study were collected using a Gatan ChromaCL2 system.

Results

Microscopic examination revealed sporadic black inclusions within the crown (i.e. inside the CVD part of the samples) and fractures along the girdle. Needle-like inclusions were observed within CVD layer in one sample. Black inclusion approximately 60 μm (fig. 1, right) were graphite according to their Raman spectra.

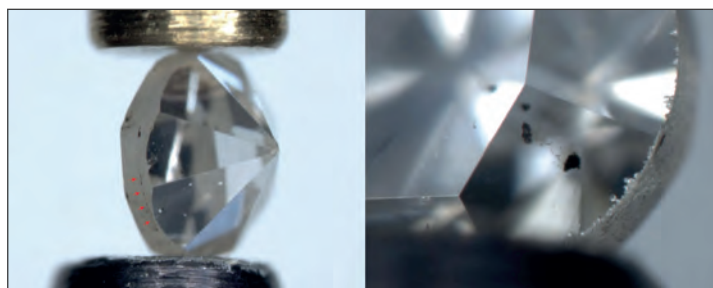


Figure 1. 0.03 ct natural diamond with a CVD synthetic diamond layer on the crown. Field of view 3 mm (left), 1 mm (right). Both inclusions are in the CVD part of the stone.

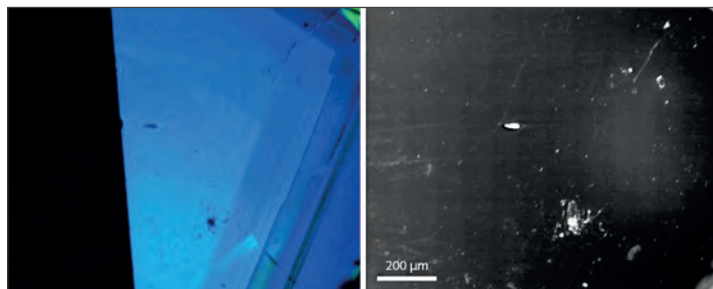


Figure 2. Left - Color cathodoluminescence image of hybrid diamond revealed a clearly visible boundary between CVD synthetic (inert) and natural (blue and green) parts. Right – Back-scattered electron image.

Even under high magnification the boundary between natural and synthetic parts was not visible, aside for the smallest 0,08ct stone of poor CVD layer quality. This evidences that there is no lattice mismatch in the crystal structure between the CVD synthetic film and the natural diamond (Eaton-Magaña, 2014). But some marks of the boundary were found on the girdle of the stones (fig. 1, left).

The samples were inert to long-wave and short-wave UV radiation.

Color cathodoluminescence images revealed a clearly visible boundary between natural and synthetic parts of the examined samples. The pavilion part of the samples exhibited concentric bands of octahedral growth patterns distinctive for natural diamonds. CL reaction colors of natural parts were blue and green resulted from so-called band A emission together with some fluorescence from the 415 nm system and H3, respectively. The crown parts of the hybrid diamonds consisted of CVD synthetic showed no reaction under electron beam, as illustrated in figure 2.

Infrared absorption spectroscopy obtained from the whole volume of the samples showed nitrogen-related absorption in the one-phonon region, which classified the diamonds as type IaAB; platelets absorption bands were also observed. No CVD-specific 3123 cm^{-1} peak was detected.

Vis-NIR absorption spectra revealed a major feature at 737 nm (unresolved doublet of $[\text{SiV}]^-$ defects) and a small absorption peak at 596 nm in some samples.

Photoluminescence (PL) spectra acquired with 532 nm laser excitation at liquid-nitrogen temperature revealed a doublet at 596/597 nm of unknown origin (in some samples), nitrogen-vacancy centers at 575 $[\text{NV}]_0$, 637 $[\text{NV}]^-$ nm, and dominating $[\text{SiV}]^-$ luminescence with ZPL at 736.6/736.9 and a broad band at 766 nm (fig. 3). These PL characteristics are common for CVD samples (Wang et al., 2012; Eaton-Magaña&Shigley, 2016). This band is part of the vibronic structure of $[\text{Si-V}]^-$, and thus the feature's intensity correlated with that of the $[\text{Si-V}]^-$ ZPL (Clark and Dickerson, 1991; Wang et al., 2012).

Conclusions

Although hybrid diamonds are not entering the diamond trade any time soon nevertheless each new prospective material raises questions about its identification and disclosure.

The identification of the CVD overgrowth on natural diamond can be done in gemological laboratory. The best evidence of overgrowth on the natural diamond was from cathodoluminescence imaging (Diamond View also can be used), VIS-NIR and PL spectroscopic analyzes.

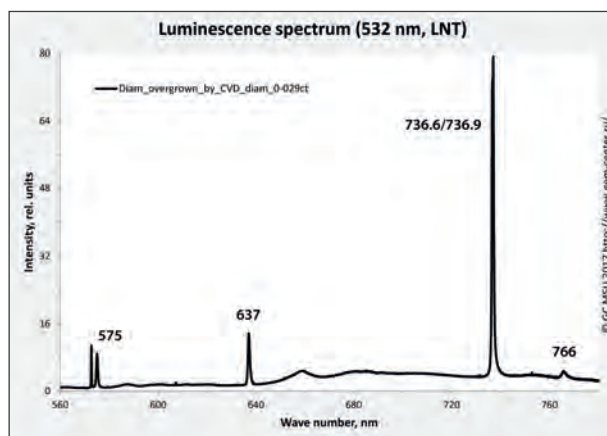


Figure 3. Photoluminescence spectra of CVD part of the diamond (532 nm laser excitation). The thickness of the CVD layer in our samples is about 1000 nm.

However the screening procedure for such hybrid diamonds can be challenging since basic gemological methods such as microscopy or D-screen check do not reveal overgrowth features. Also it was not possible to detect the presence of the CVD layer on natural diamonds using FTIR spectroscopy which provides data from the bulk of the diamond. And if identification of colored diamonds always requires careful examination, colorless and nearcolorless type Ia diamonds are usually not subjected to accurate investigation. This approach should be changed from now.

Literature

Eaton-Magaña S., 2014. Long-term durability of CVD synthetic film on natural diamond. *Gems & Gemology*, 50 (2), 152

Eaton-Magaña S., Shigley J. E., 2016. Observations on CVD-Grown Synthetic Diamonds: A Review. *Gems & Gemology*, 52 (3), 222-245

Fritsch E., Phelps A.W., 1993. Type IIb diamond thin films deposited onto near-colorless natural gem diamonds. *Diamond and Related Materials*, 2 (2-4), 70-74

Moe K. S., Johnson P., D'Haenens-Johansson U., Wang W., 2017. A synthetic diamond overgrowth on a natural diamond. *Gems & Gemology, Research News*

Wang W., D'Haenens-Johansson U. F. S., Johnson P., Moe K. S., Emerson E., Newton M. E., Moses T. M., 2012. CVD synthetic diamonds from Gemesis Corp. *Gems & Gemology*, 48 (2), 80–97

Yacobi B.G., Lebens J., Vahala K.J., Badzian A.R., Badzian T., 1993. Preferential incorporation of defects in monocrystalline diamond films. *Diamond and Related Materials*, 2 (2-4), 92–99

Skins, stains, spots and ruts: Green diamonds from Brazil

Rainer Schultz Guttler,

Gemlab-USP, Geological Institute of University of São Paulo, Brazil, rainersgut@gmail.com
in memory of N.Haralyi, one of the few diamond specialists of Brazil

Abstract

A photographic documentation of green and brown stains, their origin and their position at specific growth and dissolution defects in small rough diamonds mainly from the Chapada Diamantina, Bahia, Brazil has been prepared. It could be shown that the green stain may be produced by 3 processes:

1. Presence of minute radioactive minerals, located at crevices of the imperfect growth and/or dissolution features of the diamond crystals forming radio halos of circular shape.
2. Products of radiation damage from external solid radioactive material nearby of the diamonds or in gaseous form producing generally roundish or irregular shaped spots or even continuous green skins.
3. Infiltration of radioactive material in form of solutions carrying minute radioactive grains or ions in dissolved form in ruts, voids or along etch channels outlining those with irregular stains.

The diamonds suffered a prolonged period of residence as shown additionally by the presence of brown stains, indicative of metamorphic processes. Photographic documentation of each process is provided in the text.

Introduction

Although the majority of rough mined diamonds is grey, white, yellowish or brown, the appearance of fancy colors, blue, pink, canary yellow and green aroused great interest in the trade and science. A compilation by Zaitsev (2000) showed diamond has numerous defects, some formed by imperfect growth, twinning and structural damage and others produced by external factors like impurities, mainly Nitrogen and Boron, pressure, heat, deformation and irradiation, and the interaction of these contribute to the observed colors. Much research has been undertaken to unravel the detailed causes of color as shown by work of Orlov (1977), Collins (1982), Harlow (1998), Breeding & Shigley (2009) and Nasdala et al. (2013), the latter investigating the effect of alpha particle irradiation, to cite only a very few here.

Diamonds with a green or greenish hue gained great interest mainly to the famous diamond "Dresden Green" investigated by Bosshart (1989). This diamond acquired a green body color by natural irradiation and belongs since the 18th Century to the Emperor of Saxe. The green body color is a rare feature, in stark contrast to most green diamonds, obtained by artificial irradiation, or found in nature with green hues confined to shallow stains (Raal, 1969, Shigley & Fritsch, 1990). Brazil, for instance, has alluvial diamond occurrences with up to 80% of diamonds showing greenish hues as shown by Chaves (1997), Haralyi (1991) and by Figure 1, a collection of colored diamonds from Minas Gerais. One notes the green colors of many of those small sized diamonds. Since very limited photographic documentation exists, (Koivula 2000, Nasdala et al., 2013, Tapper & Tapper, 20012) especially from rough natural crystals, it has been decided to show in the present communication the results of a preliminary study of the features of diamonds with green color confined to skins, spots, stains and ruts or etch channels.

Material and Methods

A collection of 92 diamonds with weights of 0.02 to 1.2 carats and sizes of 1.5 to 6 mm could be used for this study. 26 crystals, mostly chips, have continuous green skin and are from Minas Gerais and 66 smaller diamonds with patchy green stains are from Andaraí, a small town near the hills of spectacular Chapada Diamantina, Bahia, famous for alluvial diamonds and carbonado, the microcrystalline form of diamond. The occurrence of the diamonds is thought to be the Tombatur conglomerate of pre-Cambrian age. Although most of the area today is protected as natural parks, artisanal miners still dig for diamonds leading to a small production (Carvalho et al., 2016). The collection is by no means representative of diamonds of this area, but all surface features shown and mentioned by Tappert & Tappert 2000 could be observed in the samples analysed. The diamonds are on loan for studies.

A Standard Gemological Microscope, Olympus JM and a Standard Petrological Microscope Nikon. By its higher magnification power the latter microscope permitted the analysis of more details and of the tiny radio halos observed in some samples.

Results

As a result of this optical study it can be stated that the green stain observed on and in those diamonds is produced by three different causes:

1. Entrapment of mineral particles containing radioactive elements in growth defects of the partly imperfect grown or strongly corroded crystals (serrate laminae, cracks, fractures and ruts) and in the interstices of blocky mosaic type growth giving rise to perfectly round radio halos (Armitage & Snelling 2008). They are very small (about 25 micrometers in diameter) and observable only with high magnification 200 to 400X, normally not used by gemological examination. These crystal defects are produced under diamond stable conditions but the formation of halo is epigenetic since it cannot form at high temperature. Figure 2 shows small radio halos with very small nuclei attached to laminar features.

2. Infiltration of radioactive material in form of ionic solutions or fluids carrying minute crystallites and seeping into surface fractures like ruts or cleavage planes or fractures and decorating those with green stains (Figure 3).

3. Stains produced by irradiation from external radioactive material in form of mineral grains or scavenged by hydroxides as proposed by Bosshart (2007) in Surbeck (2013), or by percolation of radioactive gas dissolved in fluids and producing irregular or meshlike stains (the one shown here has been heated by metamorphism) at the one hand or continuous skin deep coloring at the other. (Figure 4 and 5).



Figure 1.

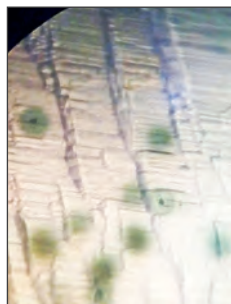


Figure 2.

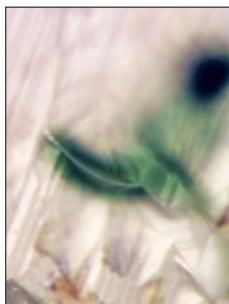


Figure 3.



Figure 4.



Figure 5.

Figure 1. A selection of colored diamonds from Chapada Diamantina, Bahia state, Brazil. The weights are from 0.2 to 1.5 carats. Picture provided by Mr. Alves, Andarai.

Figure 2. Radio Halos at surface of a small diamond (2 mm). Diameter of each one is about 25 micrometers. One notes the central inclusion and the variable green hues, result of differences in content of radioactive elements.

Figure 3. Green stain on fissure, produced by infiltrating fluids carrying radioactive material. Size of upper green oval spot 35 micrometers. Brown stain visible lower left side of picture.

Figure 4. Network like brown stain, indicating previous irradiation (green stain) and a following heating up by a metamorphic event, changing the original green to brown stains. Field of lateral view 400 micrometers.

Figure 5. Collection of surface green colored diamonds, chip forms, from Minas Gerais State, weights from 0.3 to 1.4 cts. Color produced by radioactive solutions circulating in the conglomerate hosting the diamonds.

References

- Armitage, M.H, Snelling, A.A., 2008. Radiohalos and Diamonds: Are diamonds really forever? Proceedings of the sixth International Conference on Creationism, Pittsburgh (323-334).
- Bosshart, G., 1989. The Dresden Green. *Journal of Gemmology* 21, 351-356.
- Breeding, Ch. M., Shigley, J., 2009. The type classification system of diamond and its importance in gemology. *Gems and Gemology* 45(2) 96-111.
- Carvalho, D.V.L., Schnellrath, J., Medeiros, S.R., Vieira F. F., 2016. Aspectos mineralógicos dos diamantes de Andaraí, Chapada Diamantina - Bahia. IV Simposio de Minerais Industriais do Nordeste, João Pessoa, (116-124).
- Chaves, M.L.S.C., 1997. Geologia e Mineralogia do diamante da Serra do Espinhaço em Minas Gerais, USP, São Paulo, Instituto de Geociências, PhD thesis 289p.
- Haralyi, N.E., Hasui, Y., Morales, N., 1991. O diamante Pré-cambriano da Serra do Espinhaço, Minas Gerais. In: Principais depósitos minerais do Brasil. DNPM, V.4A, 209-222.
- Koivula, J.I., 2000. The Micro World of Diamonds, *Gemworld Int.* IL, USA 156 p.
- Nasdala, L., Grambole, D., Wildner, M., Gigler, A.M., Hainschwang, Th., Zaitsev, A.M., Harris, J.W., Milledge, J., Schulze, D.J., Hofmeister, W., Balmer, W.A., 2013. Radio-coloration of diamond: a spectroscopic study. *Contrib. Mineral. Petrol.* 165, 843-861.
- Raal, F.A., 1969. A study of some gold mine diamonds. *The Amer. Min.* 54, 292-296.
- Shigley, J.E., Fritsch, E., 1990. Optical properties of some greenish blue-to-green diamonds. *SPIE Vol. 1325 Diamond Optics III*, 315-324.
- Tapper, R., Tapper, M., 2011. *Diamonds in Nature*, Springer Verlag Heidelberg, 135p.
- Vizenzi, E.P., Heaney, P.J., Snyder, K., Armstrong, L., 2002. Radiation Halos, a rare microstructure in diamonds from the Central African Republic. *American Geophysical Union, Spring Meeting 2002, Abstr.* V31A-10.
- Zaitsev, A.M., 2001. *Optical Properties of Diamond*, Springer Verlag, Heidelberg 502 p.

Kalimantan diamonds from Landak: gemmological characteristics, FTIR and photoluminescence spectroscopy

Andy H. Shen¹, Tay Thye Sun², Ye Luo¹, J.T. van Gorsel³, Mega Rosana Fatimah⁴, Tay Kunming², Wilyanto Deng⁵

¹ Gemmological Institute, China University of Geosciences, Wuhan, China

² Far East Gemological Laboratory, Singapore 409958; tay@gem.com.sg

³ 6516 Minola St., Houston, Tx 77007, U.S.A

⁴ Research Center of Geopark & Geological Hazard, Universitas Padjadjaran, Bandung, Indonesia

⁵ Ngabang, Kalimantan, Indonesia

Diamonds has been found in Kalimantan for about 3,000 years (Hershey, 1940) and only second to India. The mining of diamonds was carried out by Malay and Chinese around 600 AD (Webster, 1983). The Kalimantan Sultanah used diamonds as tribute to the Sung Emperor 960-1279 AD (Schnubel, 1980). The diamond resource was first exploited by Hindus with the help of Malays and the Chinese, then Portuguese and later by Dutch colonists. As a result, the Dutch was able to establish diamond cutting centre in Amsterdam thus enable to supplement diamonds, besides Indian diamonds, to the European market in the 17th century (van Leeuwen, 2014).

Kalimantan diamonds could be found at four locations i.e. Landak, Puruk Cahu, Martapura, and Kelian region (Figure 1). Most of the alluvial diamonds were mined from Quaternary to recent alluvial, while some could be found in Cretaceous and Eocene conglomerates. Various researchers have tried to locate the primary source of diamond either kimberlite or lamproite, so far none could be found (Krol, 1922; Koolhoven, 1935; van Bemmelen, 1949; Sigit et al, 1969; Bergman et al, 1987; Tay et al, 2005; Smith et al, 2009; van Leeuwen, 2014; White et al, 2016; Kueter et al, 2016).

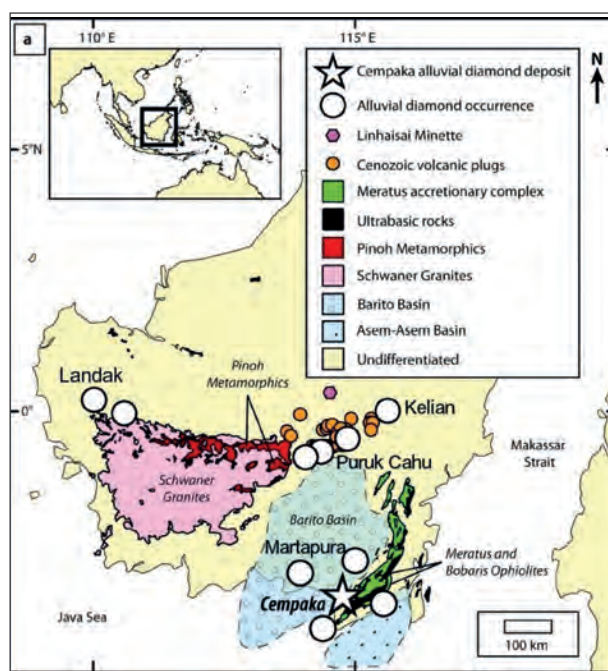


Figure 1. Map of Borneo showing the location of Cempaka and other alluvial diamond deposits across Kalimantan (modified from Smith et al, 2009, White et al, 2016).

Varieties of colours of diamond from fine white to yellow, fancy intense yellow, brown, green, orange and canary-yellow (Figure 2) and some black ballas, were recovered. Rare one like pink and blue has been reported (Spencer et al, 1988).



Figure 2. Various colour of diamonds from western Kalimantan with size from 0.10 carat to 0.78 carat (photo by Tay, 2016).

This paper focus on diamond morphology, surface features, infrared and photoluminescence analysis on diamonds from Western Kalimantan especially around Kuala Behe and Temayo, along the river Landak (Figure 2). The geology of Landak river is made up of Pedawan formation, Gunungapi Raya Volcanic, Granodiorite Mensibau, Landak Sandstone, Sintang Intrusion, and alluvium (Supriatna, et al, 1993; Aziz, 2007). The diamond deposits are found along the lower terrace of Landak river and also the geology belongs to Landak sandstone of Oligocene (Aziz, 2007).

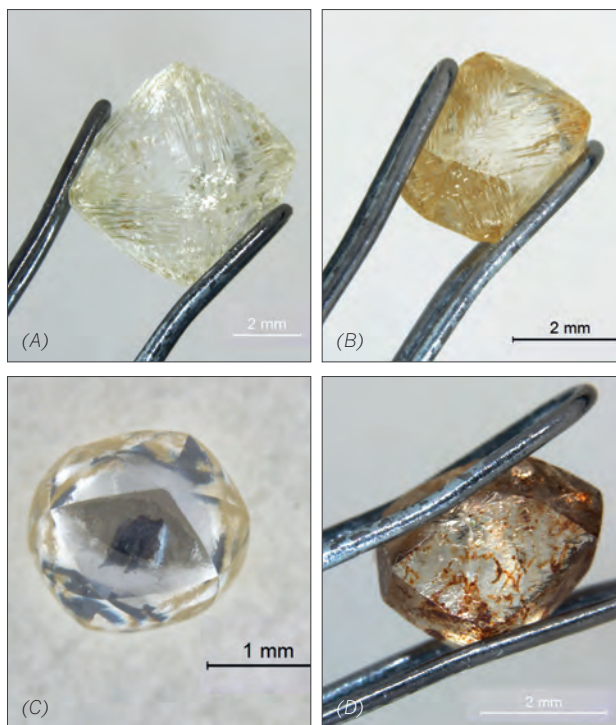


Figure3. Samples of the Kalimantan diamonds. A. colorless, octahedron with trigons. B. yellow, rhombic dodecahedron with growth lines along the long diagonal on rhombic surfaces. C. a black shapeless unknown inclusion. D. brown radiation stains. (photo by Ye Luo).

A total of 40 rough diamonds were collected from Kuala Behe and Temoyo, West Kalimantan, Indonesia. The size ranges from 0.018 ct to 0.790 ct with range of colour from colourless to light to deep yellow, light to dark brown, green and near black.

Among the 40 diamonds, 4 are near round, 2 are octahedral, 29 are rhombic dodecahedral while 5 cannot be identified in shape. Surface features like trigons are found on many octahedral surfaces and growth lines can be seen along the long diagonal on rhombic surfaces of 4 diamonds (Tappert & Tappert, 2011). Most diamonds are near colourless with light yellow or light brown colour. Five stones are deep brown and even near black. Only 3 samples show strong yellow and one is in green. A dark shapeless unknown inclusion was seen in a diamond and is way too deep to be identified by Raman spectroscopy. Some diamonds also show green or brown radiation stains. (Figure 3). All diamonds showed none to strong LWUV and none to weak SWUV.

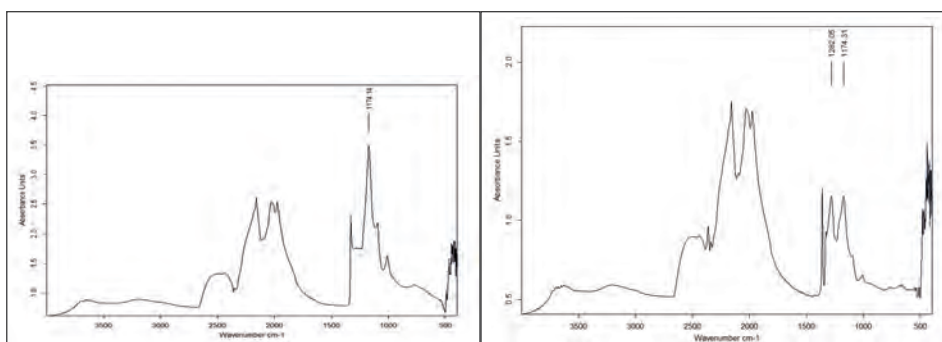


Figure 4. The FTIR spectra of diamond No.8 (left) is identified as type IaB and diamond No.26 (right) is identified as type IaA and IaB.

The FTIR spectra was recorded with transmitted light in the range from 400cm^{-1} to 4000cm^{-1} at 4cm^{-1} resolution, using a Bruker Vertex 80 FTIR spectrometer coupled with a Bruker HYPERION 3000 IR microscope. Among 40 samples, 14 of them were identified as type IaA+IaB. Fifteen (15) were identified as pure type IaA. Two crystals were identified as pure type IaB (Breeding et al., 2009) (Figure 4). In the remaining 9 samples. Eight of them have saturated signals between 1300cm^{-1} - 1100cm^{-1} spectral range and are thus attributed to type Ia. There is only one sample without any peaks related to nitrogen and boron, which is assigned as type IIa. Among 40 samples, 26 of them have clear peak at 3107cm^{-1} , which is related to hydrogen. (Fritsch et al., 2007).

We conducted photoluminescence study on all diamonds at liquid nitrogen temperature (-196°C), using a HORIBA Jobin Yvon LabRAM HR800 Raman spectrometer and a solid state 532.1nm laser as the light source. All spectra were collected at 0.1nm resolution. The most common peaks are 575nm (20 of 40 samples) related to NV0 center, 637nm (36 of 40 samples) related to NV⁻ center and 741nm (30 of 40 samples) related to GR1 center (Breeding et al., 2009). We also find that 21 samples have sharp peak at 588.0nm , which is related to hydrogen defect (Fritsch et al., 2007). 662.4nm (19 of 40 samples), 680.1nm (10 of 40 samples), 700.4nm (13 of 40 samples) peaks are also commonly seen in the photoluminescence spectra. (Figure 5 - left). In some samples, we also see sharp peaks at 612.4nm with a band at 625.9nm , and the combination make the PL spectrum looks like a step. (Figure 5 right). Using 532.1nm laser, 612.4nm is the right position of 2467cm^{-1} Raman shift, which is the second order Raman shift of diamond (Praver, et al., 2004). However, the shape of this 612.4nm is totally different from previously reported and the intensity is also very high – thus the sharp peak at 612.4nm is most likely due to a new center.

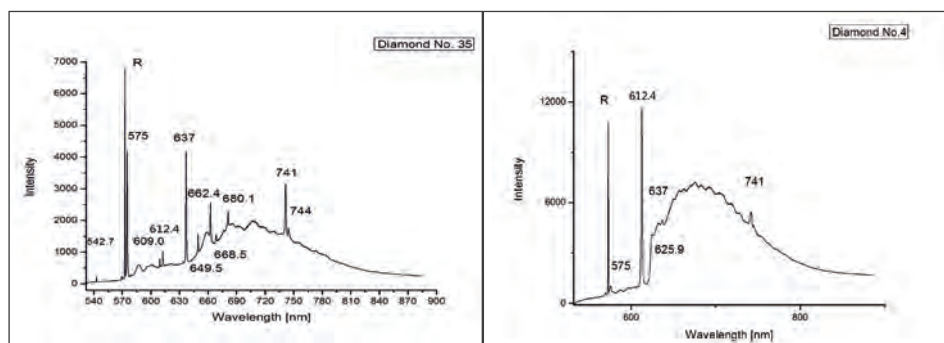


Figure 5. The photoluminescence spectra of two samples. Sample 35. 575nm NV⁰ center, 637nm NV⁻ center, 741nm and 744nm GR1 center are seen in the spectrum. 542.7nm, 609nm, 612.4nm, 649.5nm, 662.4nm, 680.1nm peaks are also seen in the spectrum. Sample 4. Sharp, high-intensity 612.4nm peak with 625.9nm sideband is seen in the spectrum. 612.4nm is the position of 2467cm⁻¹ Raman shift, which is the place of 2nd order Raman shift. But the shape and intensity are different.

Conclusions

Forty samples of Kalimantan diamond from Landak were collected from Kuala Behe and Temoya. The geology of Landak region is mostly Oligocene Landak sandstone. The shapes of diamond crystals are rounded, octahedral, rhombic dodecahedral and five were unidentifiable. Their colours range from near colourless to light yellow and some are light brown, green and some were near black. Several has brown and green radiation stains. FTIR identified the diamonds are Type Ia (8), IaA (15), IaB (2) and IIa (1). Twenty-six (26) out of forty (40) showed the 3107cm⁻¹ peak, which is related to hydrogen. Photoluminescence were performed at cryogenic temperature at -196°C. We found twenty-one samples with sharp peak at 588.0nm, which is probably related to radiation. Some samples have a sharp peak at 612.4 nm accompanied with a band at 625.9 nm, such combination make the spectrum appeared with a sharp rise around 623 nm. The exact defects for producing such features is not clear and requires further research.

References

- Aziz, S., 2007. Keterdapatan intan sekunder di sepanjang sungai Landak, Kalimantan Barat. Pusat Survei Geologi, JSDG, Vol.XVII, No.5 Oktober, 2007.
- Bergman, S.C., Turner, W.S., Krol, I.G., 1987. A reassessment of the diamondiferous Pamali Breccia, Southeast Kalimantan, Indonesia: intrusive kimberlite breccia or sedimentary conglomerate? Geological Society of America, Special Papers 215, 183-196.
- Breeding C.M., Shigley J.E., (2009) The "type" classification system of diamonds and its importance in gemology. *Gems & Gemology*, 45(2), 96–111.
- Fritsch E., Hainschwang T., Massi L., Rondeau B., (2007) Hydrogen-related optical centers in natural diamond: an update. *New Diamond and Frontier Carbon Technology*, 17(2), 66-87.
- Hersey, W., 1940. *The Book of Diamonds*. New York, Heartside Press.
- Koolhoven, W.C.B., 1935. The primary occurrence of South Borneo diamonds: *Geologisch-Mijnbouwkundig Genootschap voor Nederland en Kolonien, verhandelingen, Geologische serie 9*, 189-232 (in Dutch).
- Krol, L.H. 1922. Bijdrage tot de kennis van de oorsprong en de verspreiding der diamanthoudende afzettingen in ZO. Borneo. *Jaarboek van het Mijnwezen* 49, 250-304 (in Dutch).
- Kueter, N., Soesilo, J., Fedortchouk, Y., Nestola, F., Belluco, L., Troch, J., Wälle, M., Guillong, M., Von Quadt, A., Driesner, T., 2016. Tracing the depositional history of Kalimantan diamonds by zircon provenance and diamond morphology studies, *Lithos* 265 (2016) 159-176.
- Praver S., Nemanich R.J., (2004) Raman spectroscopy of diamond and doped diamond. *Mathematical, Physical and Engineering Sciences*, 362, issue 1824.
- Smith, C.B., Bulanova, G.P., Kohn, S.C., Milledge, H.J., Hall, A.E., Griffin, B.J., Pearson, D.G., 2009. Nature and genesis of

- Kalimantan diamonds. *Lithos* 112, 822-832. <http://dx.doi.org/10.1016/j.lithos.2009.05.014>.
- Spencer, L.K., Dikinis, D.S., Keller, P.C., Kane, R.E., 1988. The Diamond Deposits of Kalimantan, Borneo. *Gems & Gemology*, Summer 1988, 67-80.
- Schnuberl, H-J, 1980. Other producers. In: Legrand, I. (Ed), *Diamonds: Myth, Magic, and Reality*. Crown Publishers, New York, 180-187.
- Sigit, S., Purbo-Hadiwidjojo, M.M., Sulasumoro, B., Wirjosudjon, S., 1969. Minerals and mining in Indonesia. *Geologi Indoensia: Journal of the Indonesian Association of Geologists* 13, 1-31.
- Supriatna S., Margono U., Sutrisno, Pieters P.E. dan Langford R.P., 1993. Peta Geologi Lembar Sanggau, Kalimantan, skala 1:250,000. Pusat Penelitian dan Pengembangan Geologi, Bandung.
- Tappert R., Tappert M.C., (2011). *Diamonds in Nature: A Guide to Rough Diamonds*. Springer, pp 142.
- Tay, T.S., Wathanakul, P., Atichat, W., Lim, H.M., Lee, K.K., Hermanto, R., 2005. Kalimantan diamond, *The Australian Gemologist*, 22, 186-195.
- Webster, R., 1983. *Gems, Their Sources, Description, and Identification*. 4th edition Butterworths, London, England.
- White, L.T., Graham, I., Tanner, D., Hall, R., Armstrong, R.A., Yaxley, G., Barron, L., Spencer, L., van Leeuwen, T.M., 2016. The provenance of Boreno's enigmatic alluvial diamonds: A case study from Cempaka, SE Kalimantan. *Gondwana Research*, 38, 251-272.
- Van Bemmelen, R.W., 1949. *The Geology of Indonesia, Volume II Economic Geology*. Government Printing Office, The Hague, 265pp.
- Van Leeuwen, T., 2014. The Enigmatic Sundaland Diamonds – a Review, *Proceeding of Sundaland Resources 2014 MGEI Annual Convention*, Palembang, South Sumatra, Indonesia.
- Yang, J.S., Robinson, P.T., Dilek, Y., 2014. Diamonds in ophiolites. *Elements* 10, 127-130. <http://dx.doi.org/10.2113/gselements.10.2.127>.

Acknowledgements

We are grateful to Wanjun Lv, Qian Zhou for the using of LabRAM HR800. We also wish to thank Jia Liu for her support and understanding.

Study and investigation of spinel from Kermunda in Odisha, India

Jayshree Panjekar^{1,2} and Aatish Panjekar^{1,2}

¹Pangem Testing Laboratory, Pune, India

²PANGEMTECH – Panjekar Gem Research & Tech Institute, Pune, India
jayshreepanjekar@gmail.com

Abstract

Spinel found in the Kermunda village (19.9671° N, 82.7913° E) located in Golamunda Tehsil of Kalahandi district of Odisha state of India were investigated. Odisha was formerly known as Orissa state and has been known for gemstone deposits. In Kermunda, in Kalahandi (Fig1) the area constitutes a part of the Precambrian khondalite-charnockite-granite gneiss terrain of Eastern Ghats having thick soil horizon. It is common to find spinel along with corundum and other minerals in this soil. Locals collect red coloured broken spinel crystals, calling them “naram” meaning low grade “ruby”, to make beads. Gemmological properties, values for refractive indices, specific gravity, as well as FTIR and UV-Vis data have been determined for the Kermunda spinel. Semi-quantitative analyses carried out using EDXRF show considerable presence of titanium and iron oxides in the spinel. Inclusion studies by Raman microspectroscopy identified mineral inclusions as apatite, ilmenite, rutile, spinel and zircon. It is for the first time that högbomite has been reported as an inclusion in gem-quality Indian spinel.

Keywords: Spinel, inclusions, högbomite, analyses, Kermunda, Odisha

Materials and methods:

Forty cabochon spinel pieces (Fig 2) ranging from 8.20carats to 1.03carats with prominent inclusions were selected and with gemmological methods their optical properties, specific gravity, UV fluorescence were determined. In depth study of the internal features was done using gemmological microscopes. Raman micro-spectroscopy, using Renishaw 2000 with Ar 514 laser, was used to determine the identity of the microscopic inclusions crystallizing near the surface. Non-polarized UV-Vis spectra for all samples were collected using JASCO F660 spectrophotometer over the 350nm - 800nm range. Mid Infrared spectra of 4 samples were collected in transmission mode by JASCO FT/IR-6600 with a resolution of 4cm⁻¹. Semi-quantitative analyses were carried out using EDXRF of Oxford Instruments LabX3500 with extra accessory for micro analyses.

Results

Visual Appearance

Spinel cabochons from Kermunda village occur in shades of pale purplish red to dark orange red colour with plenty of visible inclusions. Most of the material was transparent to semi transparent.

Gemmological Properties

Specific Gravity was found to be in the range of 3.59 to 3.61, refractive indices fell in the range of 1.718 to 1.723 determined by spot method. All samples showed strong to medium red fluorescence under LWUV and moderate to weak red fluorescence under SWUV.

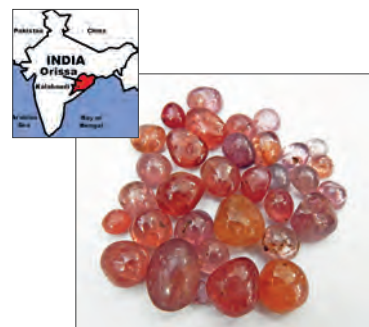


Figure 1. Location of Kalahandi in Odisha.

Figure 2. Spinel from Kermunda in Kalahandi, Odisha.

Microscopic Observations

Generally spinel has small syngenetic spinel crystals as the most common inclusion. In the case of Kermunda spinel, such small octahedral inclusions of spinel were a common sight in all the investigated samples. Prismatic crystals of zircon (Fig 3) and octahedral crystals of spinel shape (Fig 4) were observed as inclusions. In many of the specimen phlogopite (Fig 5) and ilmenite crystals were found to be prominent. Titanium oxide as rutile crystals were identified by Raman micro-spectroscopy spectroscopy in majority of specimen. In one sample there were tiny octahedral crystals surrounded by haloes (Fig 6). These octahedral crystals could be hollow negative crystals. Among the other commonly found inclusion was that of transparent colourless apatite crystals (Fig 7). The Kermunda spinels show the presence of large crystal what appear to be crystal of högbomite (Fig 8).

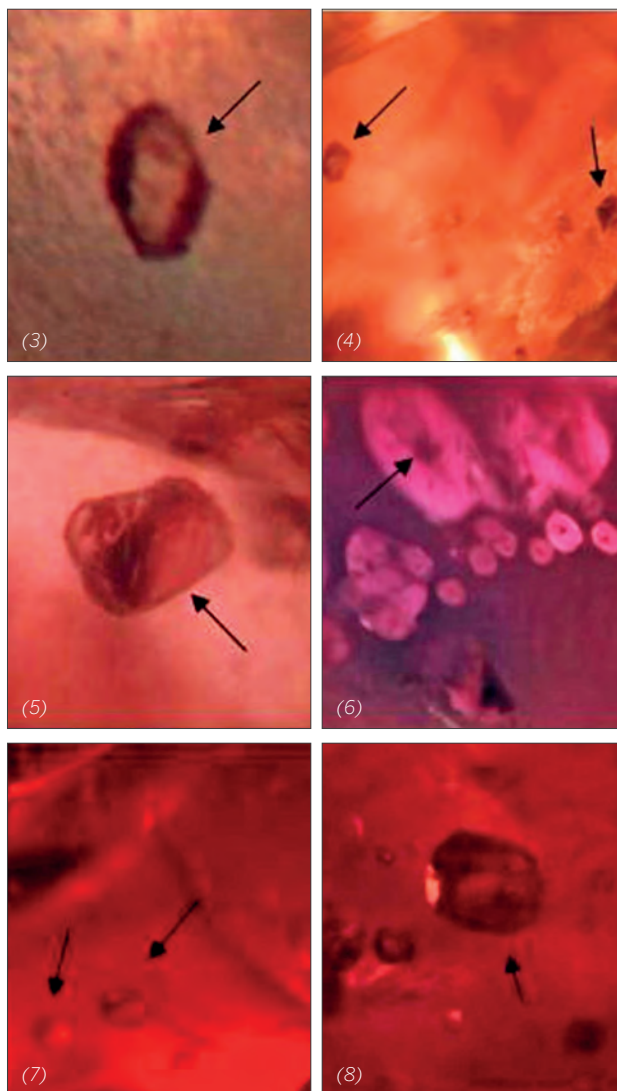


Figure 3. Zircon Crystal - Figure 4. Octahedral Spinel Crystal -
Figure 5. Phlogopite inclusion Figure 6. Octahedral negative crystals
with halo - Figure 7. Apatite crystals - Figure 8. Högbomite crystal

Tsunogae and Santosh (2005) had reported Ti-free h ogbomite in spinel bearing rock in southern India. It is for the first time that Ti bearing h ogbomite crystals have been reported in gem spinel from Kermunda. Although h ogbomite is not unknown to this region (Mohanty et al 2000, & Beura et al 2009) it is an indication of very high grade metamorphism.

Raman Spectra:

Raman micro-spectroscopy was used to ascertain the identity of inclusions. Typical Raman peaks obtained at 1008 cm^{-1} , 975 cm^{-1} , 441 cm^{-1} , 357 cm^{-1} , 225 cm^{-1} confirmed the identity of the prismatic crystal to be zircon (Fig 3). The dark coloured octahedral crystals (Fig 4) showed the characteristic peaks of spinel (MgAl_2O_4) at 409 cm^{-1} , 660 cm^{-1} and 767 cm^{-1} . The reddish brown crystal (Fig 5) gave the prominent Raman peaks at 704 cm^{-1} , 266 cm^{-1} and 410 cm^{-1} apart from small ones at 750 cm^{-1} , 915 cm^{-1} , 959 cm^{-1} and 1119 cm^{-1} proving it be a mica crystal of phlogopite. Apatite crystals (Fig 7) were confirmed by the Raman shift prominently obtained at 968 cm^{-1} along with minor peaks at 450 cm^{-1} , 584 cm^{-1} , 1015 cm^{-1} , 1036 cm^{-1} and 1063 cm^{-1} . Apart from these inclusions two other inclusions were observed and confirmed by their Raman shifts. One inclusion was of ilmenite which gave peaks at 159 cm^{-1} , 225 cm^{-1} , 400 cm^{-1} , 516 cm^{-1} and a prominent peak at 643 cm^{-1} and a minor one at 1311 cm^{-1} and the other inclusion was that of rutile with the typical peaks at 614 cm^{-1} , 450 cm^{-1} , 248 cm^{-1} and minor one at 802 cm^{-1} .

The Raman spectra for h ogbomite (Fig 8) with peaks at 264 cm^{-1} , 421 cm^{-1} , 844 cm^{-1} with main peaks at 869 cm^{-1} , 709 cm^{-1} and 508 cm^{-1} are similar to those obtained by Tsunogae & Santosh 2005 (261 cm^{-1} , 421 cm^{-1} , 529 cm^{-1} , 723 cm^{-1} , 782 cm^{-1} and 846 cm^{-1}). As the Manavadi h ogbomite reported by Tsunogae & Santosh (2005) are supposed to be Ti free, it may be inferred that the peak at 709 cm^{-1} is related to Ti-O vibration as there is TiO_2 obtained in the chemical analyses. The slight differences in wavenumber (within < 16 cm^{-1}) may be due to compositional variations.

UV-Vis Spectra:

The UV-Vis spectroscopy of Kermunda spinel revealed the typical small Cr^{3+} absorption peaks at 701 nm, 665 nm and 641 nm (Fig 9). In addition the spectra generally exhibited a strong general increase of absorption starting from 600 nm increasing towards the UV absorption edge due to the presence of iron. Other peaks 750 nm and 542 nm are the main chromium absorption bands. They are responsible for the reddish colour of these spinel. The minor band at 386 nm is presumably due to Fe^{2+} (Malsy & Klemm, 2010).

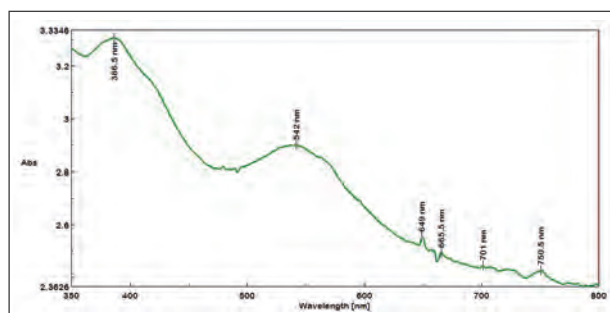


Figure 9. UV-Vis spectrum of Kermunda Spinel.

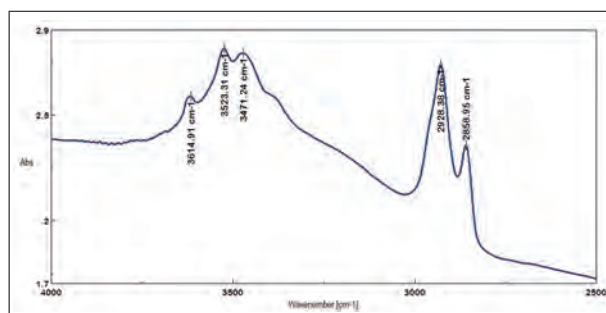


Figure 10. FTIR spectrum of Kermunda Spinel.

FTIR Spectra

The FTIR spectra in the mid infrared region between 4000 and 2000 cm^{-1} region for the Kermunda spinel showed certain distinct features (Fig 10). The absorption peaks at 3471 cm^{-1} , 3523 cm^{-1} and 3614 cm^{-1} are due to O-H stretching bands of gibbsite $\text{Al}(\text{OH})_3$, an aluminium hydroxide. Gibbsite is commonly found in soils and may be a secondary filler of fissures in the Kermunda spinel whereas the peaks at 2928 cm^{-1} and 2858 cm^{-1} are probably due to CH stretching modes, and may be the result some organic matter in the fissures.

Chemical Analyses:

Semi-quantitative chemical analyses by EDXRF for spinel from Kermunda gave oxide wt % for $\text{Cr}_2\text{O}_3 = 0.2\text{-}2.0$, $\text{TiO}_2 = 0.9\text{-}1.6$ and for $\text{Fe}_2\text{O}_3 = 0.01\text{-}0.14$ apart from the standard the oxide wt % for Al_2O_3 and MgO. Högbomite is a complex group of minerals having Fe, Mg, Al and Ti (Armbruster, 2002). Chemical analyses carried out on the surface reaching crystal gave the average oxide wt % for $\text{Al}_2\text{O}_3 = 58.22$, $\text{Fe}_2\text{O}_3 = 26.86$, $\text{MgO} = 9.31$, $\text{TiO}_2 = 4.56$, $\text{ZnO} = 1.68$ and the oxide wt % for $\text{Cr}_2\text{O}_3 = 0.20$ which are in coordination for högbomite (Orozbaev et al, 2011) and is confirmed by the Raman spectra similar to that reported by Tsunogae & Santosh 2005.

Discussion:

Kermunda spinel found along with corundum in the soil horizon of the khondalite-charnockite-granite gneiss show a variety of inclusions. Malsy & Klemm (2010) have given a detailed report on the distinction of gem spinel from the Himalayan Belt wherein spinel from Mogok in Myanmar, Luc Yen in Vietnam and Kuh-i-Lal in Tajikistan are considered. If one considers the Kermunda spinel they appear to have properties which have some similarities with those of the Mogok spinel and to some extent to those of Luc-Yen spinel. Inclusions of apatite and negative octahedral crystal in Kermunda spinel are similar to those in Mogok spinel and the zircon crystal and apatite inclusions makes Kermunda spinel more towards the Luc Yen spinel. In Kermunda spinel there is also presence of phlogopite crystals along with ilmenite, rutile and högbomite. The UV spectra of Kermunda spinel represent predominantly the Cr^{3+} and Fe^{2+} peaks and falls into the category of Cr ~ Fe as discussed by Malsy & Klemm (2010).

Conclusion

Spinel cabochons from Kermunda village have been investigated. They display a wide range of inclusions. Crystalline inclusions observed and identified were apatite, högbomite, ilmenite, rutile, spinel and zircon. It is for the first time that högbomite has been found as an inclusion in spinel from Odisha and more research needs to be done to get a better understanding of the crystallization of this mineral. The spinel from Kermunda in Kalahandi, Odisha, had crystallized during high grade metamorphic activity which is corroborated by the presence högbomite which forms under very intense grade of metamorphism (Petersen et al 1989).

Acknowledgements:

Authors thank Mr. A. Sharma of Kalahandi Gems for his invaluable help to procure the samples. Authors express their gratitude to Dr. Michael Krzemnicki for valuable suggestions and literature, to the National Chemical Laboratory, to the Dept. of Geology, University of Pune and their scientists for carrying out the analyses.

References

- Armbruster T. 2002: Revised nomenclature of högbomite, nigerite and taaffeite minerals. *Eur. J. Mineralogy* Vol. 14, 389-395.
- Balan E., Lazzeri M., Morin G. And Mauri M. 2006: First-principles study of the OH-stretching modes of gibbsite. *American Mineralogist*, Vol.91, pp115-119
- Beura D., Acharya D., Singh P and Acharya S., 2009: Högbomite associated with vanadium bearing titaniferous magnetite of mafic-ultramafic suite of Moulabhanj Igneous Complex, Orissa, India. *Journal of Minerals & Materials Characterization & Engineering*, Vol. 8, No. 9, pp 745-753.
- Das S. K. and Mohanty J. K., 2014: Characterisation of Eluvial Corundum (Ruby) from Kermunda, Kalahandi district, Odisha, India. *J Geol Geosci* Vol.3, Issue 6 pp1- 6
- Malsy A. and Klemm L., 2010: Distinction of Gem Spinel from the Himalayan Mountain Belt. *Chimia (Schweizerische Chemische Gesellschaft)*, Vol. 64, pp 741-746.
- Mohanty, J.K., Sahoo, R.K. and Paul, A.K., 1995: Research note on Högbomite from Fe-Ti Oxide deposit, Boula-Nausahi Igneous Complex. *Ind. Miner.* Vol. 49 (4), pp. 293-294.
- Orozbaev R.t., Yoshida K., Bakirov A.B., Hirajima T., Takasu A., Sakiev K.S. and Tagiri M. 2011: Preiswerkite and högbomite within garnets of Aktyuz eclogite, Northern Tien Shan, Kyrgyzstan. *Journal of Mineralogical and Petrological Sciences*, Vol.106, pp 320-325.
- Petersen E.U., Essene E.J., Peacor D.R. and Marcotty L.A., 1989: The occurrence of högbomite in high-grade metamorphic rocks. *Contributions to Mineralogy and Petrology* Vol. 101, Issue 3 pp 350-360.
- Prakash D., Singh P.C. and Hokada T., 2013: A new occurrence of sapphirine-spinel-corundum bearing granulite from NE of Jagtial, Eastern Dharwar Craton, Andhra Pradesh. *Jour Geol Soc India* Vol.82, pp 5-8.
- Tsunogae, T. and Santosh, M. 2005: Ti-free högbomite in spinel- and sapphirine-bearing Mg-Al rock from the Palghat-Cauvery shear zone system, southern India. *Mineralogical Magazine*, Vol.69, No.6, pp. 937-949.

Reversibility of Photoluminescence Spectra of Spinel with heat treatment

Cheng-Si WANG, Andy H. Shen

Gemmological Institute, China University of Geosciences, Wuhan, China; ahshen1@live.com

The photoluminescence (PL) has been studied extensively and applied widely in diamond identification, but not as intensively used for the other gem materials (Eaton-Magana & Breeding, 2016). This may be attributed to the limited PL research and understanding of such phenomenon in other gemstones. Spinel is gaining popularity in the gems and jewelry market; it has been shown that photoluminescence is an efficient method to identify heat-treated and synthetic spinels (Peretti et al., 2012b, Peretti et al., 2012a, Saeseaw et al., 2009).

The basis of the PL testing criterion used in above references is due to effect of spinel's order-disorder phase transition when heated above the transition temperature. The PL spectra due to Cr^{3+} in an ordered or disordered spinel structure have dramatic differences. The main issue in applying PL spectra in real-life spinel heat treatment identification is whether the PL spectra can be reversed within a feasible time frame when the heat-treated spinel has been annealed below the phase transition temperature.

A typical PL spectrum of an unheated Cr-containing natural spinel at liquid nitrogen temperature (77K) is illustrated on the righthand side of Figure 1. The zero phonon lines of Cr^{3+} ion in a completely ordered site are named R lines (684.5nm and 684.8nm) and those of Cr^{3+} ion in a disordered site, N-lines (685.5nm-690nm) (Mikenda & Preisinger, 1981, Mikenda, 1981). The spectral features in 690-730 nm are the phonon sidebands.

The phase transition temperature is reported to be around 650 – 700 °C (Peterson et al., 1991, Slotznick & Shim, 2008, Redfern et al., 1999). We have heated spinel samples in a tube furnace to temperatures up to 1600 °C, and maintained the structure by rapid quenching. We subsequently explore the possibilities of reversing the transition by annealing the samples below the transition temperature.

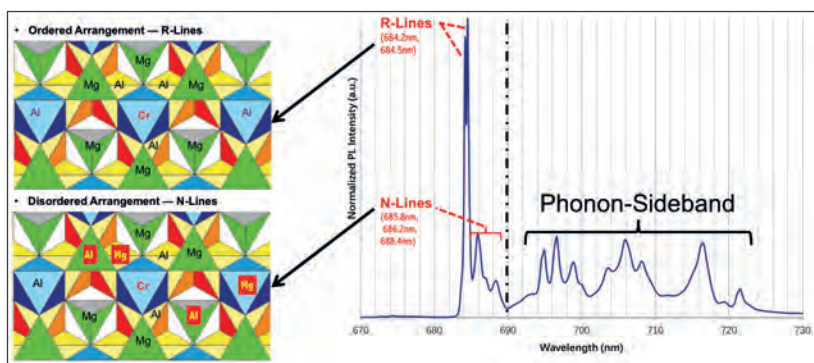


Figure 1. Typical PL spectra of natural unheated spinel and the cause of the zero phonon lines in terms of the ordering of Cr^{3+} surroundings.

The crystal structure images are observed down the three-fold axis.

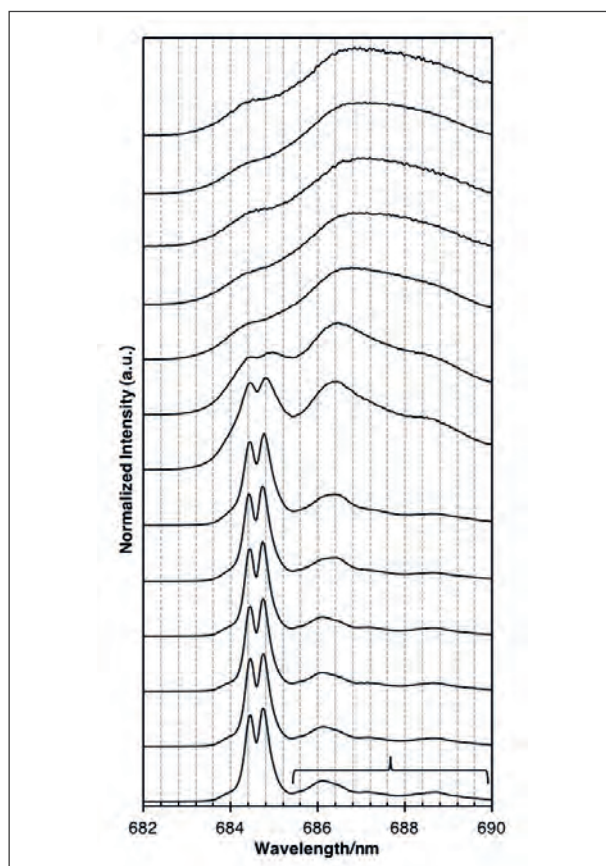


Figure 2. PL zero-phonon peaks (682nm - 690nm) variation during the heating and quenching process. The peaks become broader and the intensities of R-lines decrease but those of N-lines increase.

After analyzing the spectral parameters of quenched samples, we know that when treatment temperature rises, the FWHM of PL peaks increases, and the peak heights of the R line reduce dramatically, whereas the peak heights of the N lines increase. (Figure 2). This is what happens when the spinel structure becomes disordered, with Mg and Al occupying both octahedral and tetrahedral sites. Such spectral changes are the basis of the previously reported testing criterion for distinguishing treated and synthetic spinels from their natural equivalents.

Since the order-disorder phase transitions are reversible, so what requires more attention is the degree of reversibility of such transition and the kinetics of such reversion under annealing. To answer this question, we annealed our samples at 700°C up to several days, and then measured their PL spectra after each annealing experiment as a function of the annealing time. Through this research, we discovered that the PL spectra can only be partially restored to a more ordered state (Figure 3), however, we were not able to completely restore to a fully ordered state. The UV-Vis absorption spectra also have been taken before the initial heat treatment and after the annealing experiments. The peaks underwent a redshift after being quenched from high temperature, and a partial blue-shift after annealing process (Figure 4). According to this result, the reorder indeed caused a partial color reversing. Therefore, the current PL spectral criterion in identifying synthetic or heated spinel still seems to be very robust.

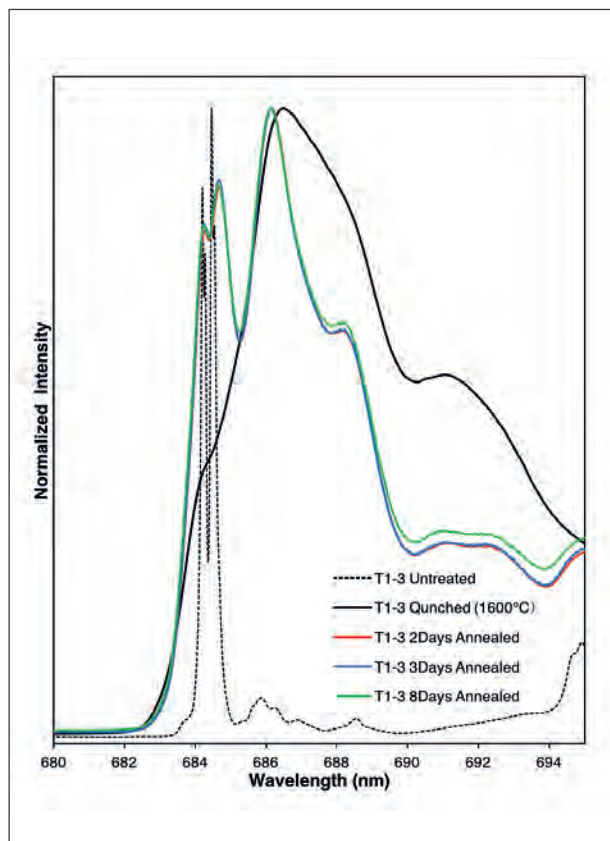


Figure 3. PL spectra of natural spinel samples that was annealed several days in 3 steps, the annealing process stopped but did not revert to the initial spectrum. The 2Days annealed spectrum and 3Days annealed spectrum almost totally overlap with each other.

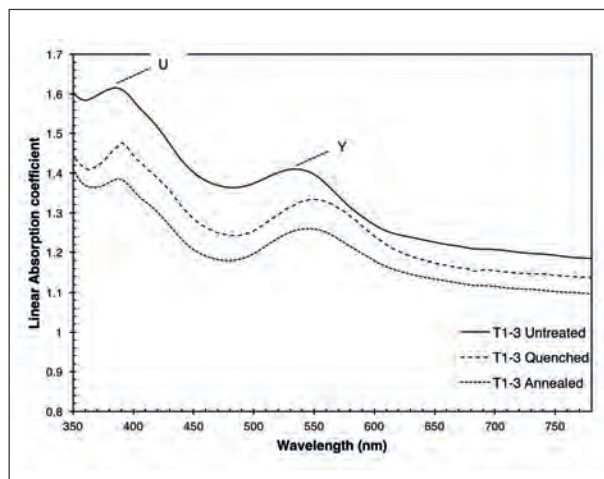


Figure 4. UV-Vis spectra of T1-3 sample during the treatment process. The U and Y bands represents the 2 main absorption bands in the spectra. The absorption bands underwent a redshift when sample was heated to high temperature and quenched. Annealing the treated sample caused a partial blue-shift of the absorption bands.

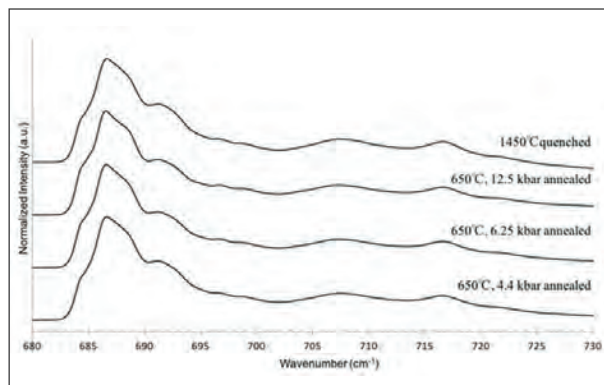


Figure 5. After being annealed under 3 HPHT conditions, the PL spectra of the quenched samples show no obvious difference. Treatment conditions are labeled next to their corresponding spectrum.

A further high pressure-high temperature annealing experiment also was carried out at about 650°C and at the pressure of 12.5 kbar, 6.25 kbar and 4.4 kbar respectively to anneal the treated samples, but no obvious spectra variation has been observed (Figure 5). These results indicate that pressure may have very little influence in the order-disorder transition and made the current PL spectral criterion quite safe to use.

References

- Eaton-Magana, S., Breeding, C. M. 2016. An Introduction to Photoluminescence Spectroscopy for Diamond and Its Applications in Gemology. *Gems & Gemology*, 52, 2-17.
- Mikenda, W., 1981. N-lines in the luminescence spectra of Cr³⁺-doped spinels (II) origin of N-lines. *Journal of Luminescence*, 26, 67-83.
- Mikenda, W., Preisinger, A. 1981. N-lines in the luminescence spectra of Cr³⁺-doped spinels (I) identification of N-lines. *Journal of Luminescence*, 26, 53-66.
- Peretti, A., Bieri, W., Alessandri, M., Huber, A., Meier, M. 2012a. New generation of pulled synthetic spinel from Russia imitating natural "lavender"-colored and natural "cobalt"-spinel from Vietnam. *Contributions to Gemology*, 11, 285-296.
- Peretti, A., Tun, N. L., Armbruster, T. 2012b. Heat-treatment of spinel. *Contributions to Gemology*, 11, 269-278.
- Peterson, R. C., Lager, G. A., Herterman, R. L. 1991. A time-of-flight neutron powder diffraction study of MgAl₂O₄ at temperatures up to 1273K. *American Mineralogist*, 76, 1455-1458.
- Redfern, S. A. T., Harrison, R. J., O'Neill, H. S. C., Wood, D. R. R. 1999. Thermodynamics and kinetics of cation ordering in MgAl₂O₄ spinel up to 1600°C from in situ neutron diffraction. *American Mineralogist*, 84, 299-310.
- Shen, A.H., Breeding, C.M., Deghionno, D. 2004. Natural, Identified with Photoluminescence, *Gems and Gemology*, 40, 168-169.
- Saeseaw, S., Wang, W., Scarratt, K., Emmett, J.L., Douthit, T.R., 2009. Distinguishing Heated Spinel from Unheated Natural Spinel and from Synthetic Spinel: A Short Review of on Going Research. *News From Research Online Article*, GIA.
- Slotznick, S. P. & Shim, S. H. 2008. In situ Raman spectroscopy measurements of MgAl₂O₄ spinel up to 1400 C. *American Mineralogist*, 93, 470-476.

REE photoluminescence in Paraíba type tourmaline from Mozambique

Claudio C. Milisenda, Stefan Müller

DSEF German Gem Lab, Prof.-Schlossmacher-Str. 1, D-55743 Idar-Oberstein, Germany, gemlab@dgemg.com

During our continuing effort in origin determination of Paraíba type tourmalines it became obvious that a number of cuprian specimens from Mozambique showed a distinct greenish fluorescence that was particularly visible under long-wave UV exposure. The fluorescence was not homogeneously distributed throughout the stone but rather confined to distinct growth structures (Figure 1). These tourmalines are reportedly from Maraca, located some 20 km away from the well known Mavuco deposit in the Nampula area of north eastern Mozambique.

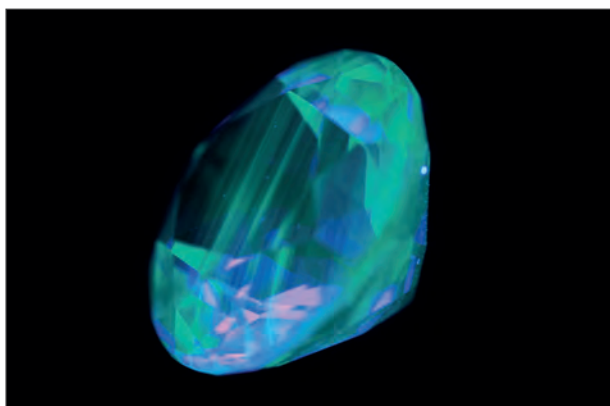


Figure 1. LUV fluorescence in a Paraíba-type tourmalines from Maraca (weight 9 ct.).

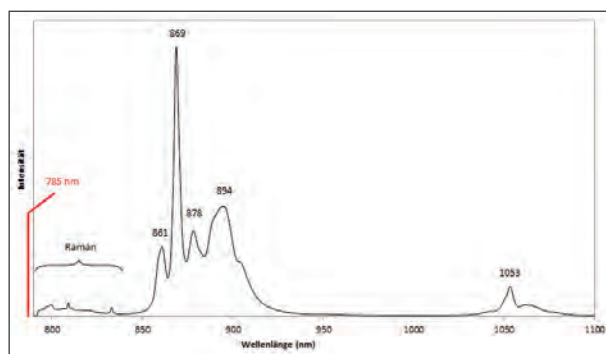


Figure 2. PL spectrum of a cuprian tourmaline from Maraca, Mozambique.

These tourmalines show distinct photoluminescence peaks when excited by a 785 nm laser (Milisenda et al., 2016). The bands with maxima at 861, 869, 878, 894 und 1053 nm (Figure 2) are consistent with PL spectra observed in titanite (Gaft et al. 2003), tsavolites (Hänni, 2013) and in a number of other calcium-rich minerals (Chen & Stimets, 2014). The authors attributed the presence of these multiple luminescence centres to the trivalent rare earth element neodymium. Jasinevicius (2009) observed similar bands in elbaite and liddicoatite and also attributed those to Nd^{3+} . LA-ICP-MS analyses have been performed on three fluorescent tourmalines from the Maraca area and compared to two non-fluorescent cuprian tourmalines from the Mavuco deposit.

All specimens represent lithium-rich tourmalines, however, the former contain more calcium than alkalis (Table 1) and, as such, represent liddicoatite-rich solid solutions. This finding is consistent with the measured birefringence of 0.015 to 0.018, which is lower when compared to the birefringence of elbaite tourmaline (average $\Delta n = 0.020$). In addition, the calcium-rich stones are also enriched in lead and bismuth and depleted in manganese when compared to the elbaite counterparts.

A few specimens of cuprian liddicoatite tourmaline have been reported in the literature (e.g. Katsurata & Sun, 2017), however, the vast majority of cuprian tourmalines from the deposits in Brazil, Nigeria and Mozambique represent elbaite tourmalines.

Table 1 shows, that the REE concentrations of the measured elbaïtes were below detection limit whereas the fluorescent samples were enriched in REE with Ce and Nd being the most abundant elements. It is known that the total concentration of REE in tourmalines may reach several hundreds of ppm (e.g. Jiang et al., 2004, Bortnikov et al., 2008). The positive correlation of REE with calcium is consistent with REE being one of the main substituting luminescence centres in Ca²⁺-bearing minerals (Gaft et al., 2005).

Among the cuprian tourmalines, we have only observed these centres in samples from Mozambique. Further studies on tourmalines from Brazil and Nigeria may show of whether luminescence is a further criteria for origin determination of Paraíba-type tourmalines.

| | La | Ce | Pr | Nd | Sm | Eu | Gd | Tb | Dy |
|---|--------|--------|-------|--------|-------|------|-------|------|------|
| 1 | 111,46 | 313,51 | 45,54 | 155,00 | 39,81 | 0,92 | 11,34 | 0,66 | 1,29 |
| 2 | 72,31 | 209,67 | 31,86 | 113,04 | 35,45 | 0,85 | 9,39 | 0,54 | 1,01 |
| 3 | 13,61 | 42,80 | 9,17 | 50,61 | 44,50 | 1,23 | 14,49 | 0,91 | 1,76 |
| 4 | bdl | bdl | bdl | bdl | bdl | bdl | bdl | bdl | bdl |
| 5 | bdl | bdl | bdl | bdl | bdl | bdl | bdl | bdl | bdl |

| | Ho | Er-Lu | Li | B | Na | Ca | Mn | Pb | Bi |
|---|------|-------|-------|-------|-------|-------|-------|-------|-------|
| 1 | 0,08 | bdl | 12613 | 34288 | 8261 | 28457 | 6497 | 675 | 1144 |
| 2 | 0,06 | bdl | 12735 | 34232 | 8105 | 26398 | 4415 | 793 | 1500 |
| 3 | bdl | bdl | 12676 | 34931 | 9253 | 24752 | 2974 | 811 | 2899 |
| 4 | bdl | bdl | 8779 | 33326 | 17114 | 1899 | 19256 | 10,49 | 52,65 |
| 5 | bdl | bdl | 8746 | 33254 | 17459 | 1805 | 19640 | 10,12 | 48,21 |

Table 1: REE and other selective element concentrations (in ppm) in cuprian tourmalines from Mozambique (LA- ICP-MS analyses). 1-3: Maraca, 5-6: Mavuco, bdl: below detection limit

References

- Bortnikov, N. S., Gorelikova, N. V., Korostelev, P. G., Gonevchuk, V. G., 2008. Rare earth elements in tourmaline and chlorite from tin-bearing assemblages: Factors controlling fractionation of REE in hydrothermal systems. *Geology of ore deposits*, 50(6), 445-461.
- Chen, H., Stimets, R.W., 2017. Fluorescence of trivalent neodymium in various materials excited by a 785 nm laser. *Am. Min.*, 99(2-3), 332-342.
- Gaft, M., Nagli, L., Reinfeld, R., Panczer, G., 2003. Laser-induced time-resolved luminescence of natural titanite CaTiO_3 . *Optical Materials*, 24 (1), 231-241.
- Gaft, M., Reinfeld, R., Panczer, G., 2005. *Modern luminescence spectroscopy of minerals and materials*. 2nd edition, Springer, Heidelberg, 606 pp.
- Hänni, H.A., 2013. Rare earth elements in mint green grossular garnet from Merelani, Tanzania. *Abstract Proceedings, 33rd IGC, Hanoi, Vietnam*, 92-94.
- Jasinevicius, R., 2009. Characterization of vibrational and electronic features in the Raman spectra of gem minerals. *Master Thesis, University of Arizona*.
- Jiang, S. Y., Yu, J. M., Lu, J. J., 2004. Trace and rare-earth element geochemistry in tourmaline and cassiterite from the Yunlong tin deposit, Yunnan, China: implication for migmatitic–hydrothermal fluid evolution and ore genesis. *Chemical Geology*, 209(3), 193-213.
- Katsurata, Y., Sun, S., 2017. Cuprian liddicoatite tourmaline. *Gems & Gemology*, 53(1), 1-8.
- Milisenda, C., Müller, S., Koch, S., Guo J., Stoffel, C. 2016. Paraíba-Tourmaline. *Zt. Dt. Gemmol. Ges.*, 65(3/4), 41-56.

Acknowledgements

The authors would like to thank Dr. Regina Mertz and Dr. Tobias Häger, Institute of Geosciences, University of Mainz, Germany for LA-ICP-MS analyses.

Origin determination of garnets: search for historical trade routes

Karl Schmetzer¹, H. Albert Gilg², Ulrich Schüssler³, Jayshree Panjekar⁴

¹ 85238 Petershausen, Germany, SchmetzerKarl@hotmail.com

² Lehrstuhl für Ingenieurgeologie, Technische Universität München, 80333 Munich, Germany

³ Institut für Geographie und Geologie, Universität Würzburg, 97074 Würzburg, Germany

⁴ Panjekar Gem Research & Tech Institute, Pune 411001, India

During the Hellenistic and Roman eras, garnets in the red to purple colour varieties were one of the most appreciated and expensive gem minerals. Usage continued in the Early Middle Ages, with garnet becoming the dominant gem mineral employed in producing so-called cloisonné jewellery. The origin of the primary garnet material used in the Antique world and the Early Middle Ages, and correlation with information found in historical texts was a matter of speculation for decades. Based upon non-destructive analyses (electron microprobe, PIXE) and microscopic examination of inclusions, garnet samples found in Early Medieval jewellery or excavated at historical sites were subdivided in different types, clusters or groups, and suggestions for possible origins were given, e.g. India or Sri Lanka (Quast & Schüssler, 2000; Calligaro et al., 2002; Gilg et al., 2010). However, the real origins of most types with the exception of Bohemian, chromium-rich pyropes remain unresolved. This applies also for engraved garnets from the Greek and Roman eras (Thoresen & Schmetzer, 2013).

Excavations at the historical site of Arikamedu, located in the Tamil Nadu State on the Indian east coast (Figure 1), supplied numerous glass and stone beads, including garnets, but the source of the garnet material has remained an open question, too. In addition to its role as bead-producing center, Arikamedu is considered as an important Indian trading place and harbour, connecting the Indian east coast with the Western world from the 1st century B.C. to the 7th century A.D. Furthermore, it has been speculated that a text by Cosmas Indicopleustes, written in the mid 6th century A.D. refers to the export of almandine from Kaveripattinam, a port located close to Arikamedu on the Indian East coast (Roth, 1980).

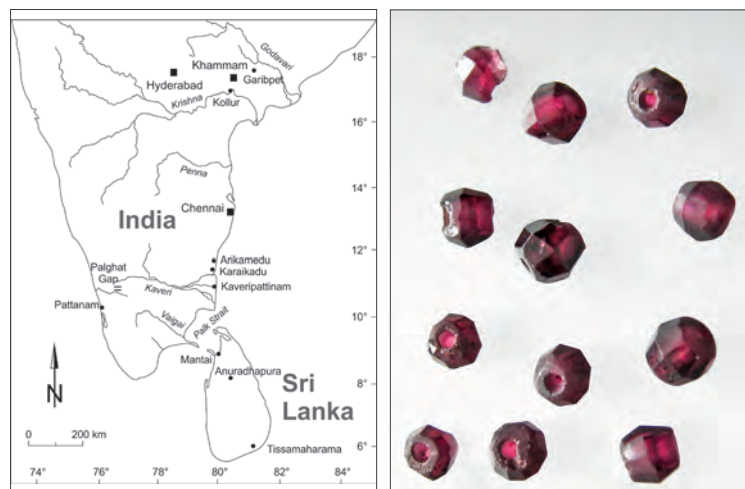


Figure 1. (left) Map showing the locations of Arikamedu and Garibpet on the Indian subcontinent.

Figure 2. (right) Transparent garnet beads (faceted bicones) from Arikamedu, measuring about 4.5 - 5.5 mm in diameter.

The present study started with the examination of garnet beads found at Arikamedu (Figure 2). In due course we were able to identify the secondary deposit of Garibpet, located in the Telangana State, east of the city of Hyderabad, India (see again Figure 1), as source of the garnets used for bead production and found in Arikamedu. Six criteria that can be key features in any endeavor to establish a common source for groups of gem samples, including historical material, were considered and found to be consistent for garnets from Arikamedu and Garibpet:

- chemical composition, namely in terms of the percentage of garnet end members;
- chemical zoning for major and minor elements within the crystals from core to rim;
- trace element contents;
- zoning of trace elements from core to rim;
- general inclusion assemblage and appearance of individual inclusions; and
- distribution and zoning of inclusions.

Chemically, the stones reflected high almandine levels (averaging almandine 81.0%, pyrope 11.5%, spessartine 3.3%, and grossular 1.5%), with especially pronounced zoning for manganese and magnesium (Figure 3).

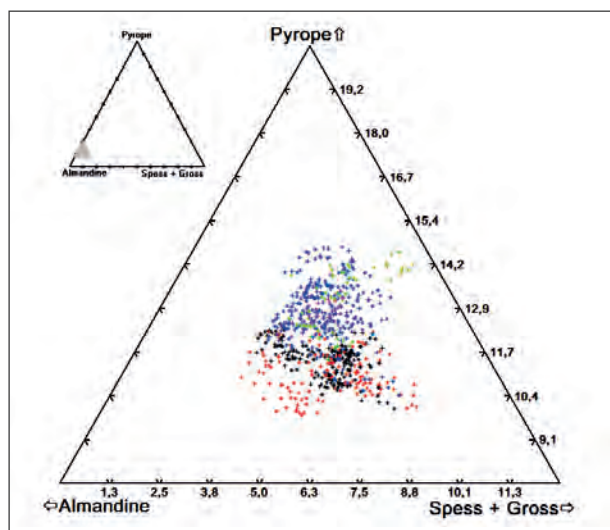


Figure 3. Triangular diagram of the chemical composition for garnets from Arikamedu and Garibpet calculated to the molecular end members pyrope, almandine, and spessartine + grossular; an enlarged detail of the main compositional field is shown, the position of which within the complete ternary plot is shown by the grey triangle in the full diagram at the upper left. Blue crosses represent transparent bicones and spheres from Arikamedu, green crosses represent translucent spheres from Arikamedu, violet crosses represent irregularly shaped fragments from Arikamedu, black crosses represent transparent pebbles from Garibpet, and red crosses represent translucent pebbles from Garibpet.

The most characteristic aspects of the inclusion pattern were sillimanite fibres and their particular concentration in a zone between an inclusion-rich core and an inclusion-poor rim (Figure 4). Inclusions in the cores comprised with decreasing abundance apatite with graphite inclusions, quartz (Figure 5), ilmenite, rutile, monazite, zircon, graphite, and fluid inclusions. Isolated zircon, monazite, and quartz crystals were also found occasionally in the rims.

Recently, the same characteristic chemical composition and chemical zoning combined with a typical inclusion assemblage and zoning of inclusions as established now for garnets from the historical site of Arikamedu and the secondary garnet occurrence of Garibpet was also observed in an engraved Byzantine almandine. This sample was dated by Spier (2011) to the late 6th, early 7th century. This observation suggests the use of Garibpet garnets for engraving in the Early Byzantine era and might support the historical text from mid 6th century A.D.

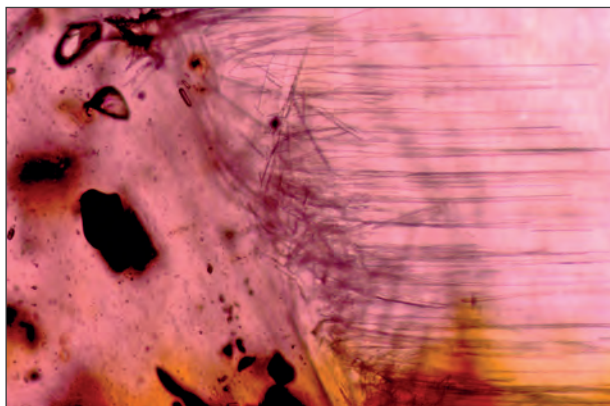


Figure 4. (left) Zoning of inclusions in a garnet pebble from Garibpet. The heavily included core is separated from the transparent rim by a zone enriched with a high concentration of sillimanite fibres.

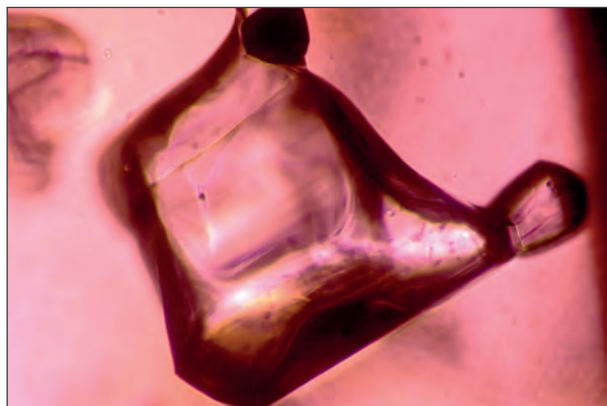


Figure 5. (right) Irregularly shaped quartz grains were commonly seen in garnets from Garibpet and Arikamedu.

References

- Calligaro, T., Colinart, S., Poirot, J.-P., Sudres, C., 2002. Combined external-beam PIXE and μ -Raman characterisation of garnets used in Merovingian jewellery. *Nuclear Instruments and Methods in Physics Research B*, 189(1-4), 320-327.
- Gilg, H.A., Gast, N., Calligaro, T., 2010. Vom Karfunkelstein. In: Wamser, L. (ed.), *Karfunkelstein und Seide. Ausstellungskataloge der Archäologischen Staatssammlung, München, Band 37*, 87-100.
- Quast, D., Schüssler, U., 2000. Mineralogische Untersuchungen zur Herkunft der Granate merowingerzeitlicher Clouonnearbeiten. *Germania*, 78(1), 75-96.
- Roth, H., 1980. Almandinhandel und -verarbeitung im Bereich des Mittelmeeres. *Allgemeine und vergleichende Archäologie*, 2, 309-333.
- Spier, J., 2011. Late antique and early Christian gems. In: Entwistle, C., and Adams, N. (eds.), 'Gems of Heaven': Recent Research on Engraved Gemstones in Late Antiquity c. AD 200-600. *British Museum Research Publication 177*, The British Museum, London, pp. 193-207.
- Thoresen, L., Schmetzer, K., 2013. Greek, Etruscan and Roman garnets in the antiquities collection of the J. Paul Getty Museum. *Journal of Gemmology*, 33(7-8), 201-222.

Characterisation and formation of ‘metamorphic’ sapphires – examples from Sri Lanka

**J.C. (Hanco) Zwaan¹, Leo M. Kriegsman^{1,2}, Jorien L.N. van der Wal², Richard J.M. Taylor³,
E. Gamini Zoysa⁴**

¹ Netherlands Gemmological Laboratory - Naturalis Biodiversity Center, Darwinweg 2, 2333 CR Leiden, the Netherlands; Hanco.Zwaan@naturalis.nl; ² Dept. Earth Sciences, University of Utrecht, Utrecht, the Netherlands; ³ Department of Applied Geology, Curtin University, Perth, WA, Australia;

⁴ Mincraft Co., Colombo, Sri Lanka

Optical properties, inclusions and geochemistry are commonly measured and interpreted meticulously to form an opinion on the provenance and origination of sapphires. The origin of sapphires is often simply referred to as basalt-related or non-basalt related or linked to the mode of formation, e.g., syenitic, plumasitic, metamorphic and metasomatic (e.g., Simonet et al., 2008). While the geology of basalt-related sapphires is often well known, the formation of sapphires related to a metamorphic origin is less understood, because these sapphires are often found in alluvial deposits and primary rocks are not well known or were not even found.

A recently discovered locality of rare *in situ* sapphire (Liu Shang-I & Zoysa, 2011) has been studied in SE Sri Lanka, at Mirisatahela, 5 km NE of Wellawaya. This locality shows small-scale mining activity and fair outcrops, with large corundum crystals, up to 15 cm. The samples from Wellawaya generally consist of approximately 20-30% large corundum crystals, surrounded by plagioclase, K-feldspar and biotite, interpreted as crystallised, silica-undersaturated melt. The large corundum crystals are commonly colourless, with locally a faint blue hue, but may also be very light blue or light purple. These crystals are found at the contact between restitic metapelites (khondalites) and a late- to post-tectonic, coarse-grained (pegmatitic) melt of external origin that seems to have acted as a trigger and catalyst for local reactions. The field relations suggest open-system, metasomatic processes at the contact between contrasting lithologies, aided by melts. The most likely mineral reaction that produced the large corundum crystals is a partial melting reaction of the dry khondalites:



Pressure-temperature diagrams for specific bulk rock compositions (P-T pseudosections) were calculated with *Perple_X* software, and gave broad ranges for these high-variance samples, that overlap in a P-T window from 6-9 kbar and 690-830 °C. When compared to the well-established regional P-T path for the Highland Complex (e.g., Dharmapriya et al., 2015), these results show that large-sized corundum (sapphire) was produced after the metamorphic peak (with locally ultra-high temperature (UHT) conditions - 775-925 °C, 9.5-11 kbar) and after a subsequent cooling and decompression phase. This fits the overall post-tectonic timing of related pegmatitic dykes. The regional distribution of *in situ* sapphire, suggests a causal link with thrusting of the Highland Complex over the Vijayan Complex.

SHRIMP U-Pb zircon geochronology for four corundum-bearing samples gives three data clusters: 1.8-2.1 Ga, probably representing igneous activity in the provenance area of the sediments; 610 and 550 Ma, both interpreted as metamorphic ages. The older of these is interpreted as the regional peak metamorphism, and the younger is interpreted as the time of sapphire growth. Large sapphire is restricted to samples showing both metamorphic ages. Hence, we postulate that during peak metamorphism at 600-620 Ma, by melting out silica, rocks obtained the right, high-Al, silica-poor chemistry for corundum growth, and that the later, fluid-rich event at 550 Ma triggered the growth of large crystals of commercial interest.

In Sri Lanka, large quantities of gem-quality sapphires are found in secondary alluvial and eluvial deposits. The major gem area is located within the Highland complex, in the Ratnapura-Balangoda region, relatively close to Wellawaya. For long, the whereabouts of primary sources and the growth mechanism that could produce such large quantities, were enigmatic (e.g., Kumaratilake & Ranasinghe, 1992; Zwaan, 1982, 1986; Pardieu et al., 2012). However, the proposed mechanism for large corundum growth, with a precursor regional peak-metamorphic event of melting out silica, indicates the possibility of corundum growth on a larger scale, producing larger quantities. The chemistry of the Wellawaya crystals corresponds to the chemistry of (very) light blue to blue sapphires found in alluvial deposits around Ratnapura (including Balangoda; e.g., Abduriyim & Kitawaki, 2006; Peucat et al., 2007), which would support the likelihood of similar origin (Figure 1). Ga/Mg versus Fe and Fe/Ti versus Cr/Ga diagrams show compositions of Wellawaya corundum plotting largely within the compositional ranges of sapphires found in the Ratnapura-Balangoda region, which correspond to the compositional range of metamorphic sapphires in general, differing greatly with those of sapphires with a basalt-related origin.

We conclude that gem-quality sapphire growth in Sri Lanka was essentially metasomatic, promoted by a sequence of events including UHT metamorphism priming the rocks, a tectonic contact creating space, and fluid/pegmatitic melt transfer from underthrust gneisses.

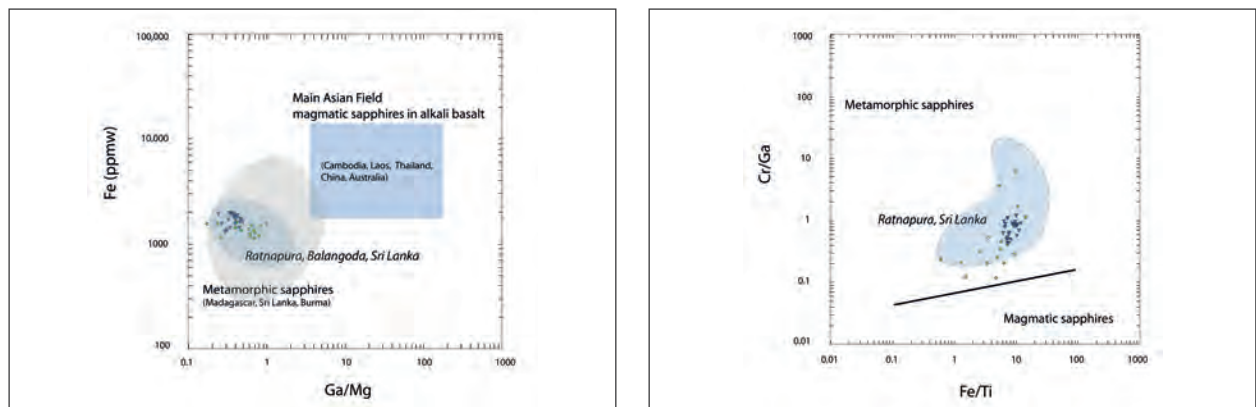


Figure 1. Compositions of large corundum crystals from Wellawaya, respectively 8 cm across (Wella 63 - green lozenge shapes) and 4 cm (13HZ30 - blue triangles), in relation to metamorphic and magmatic sapphires, and in particular to sapphires from the Ratnapura-Balangoda gem gravels (shaded compositional ranges), as shown by Peucat et al., 2007 (left) and Abduriyim & Kitawaki, 2006 (right).

References

- Abduriyim, A. & Kitawaki, H., 2006. Determination of the origin of blue sapphire using laser Ablation Inductively Coupled Plasma mass Spectrometry (LA-ICP-MS). *J. Gemmology*, 30, 1/2, 23-36.
- Dharmapriya, P.L, Malaviarachchi, S.P.K., Galli, A., Ben-Xun Su, Subasinghe, N.D. Dissanayake, C.B., 2015. Rare evidence for formation of garnet + corundum during isobaric cooling of UHT meta-pelites: New insights for retrograde P-T trajectory of the Highland Complex, Sri Lanka. *Lithos*, 220, 300-317.
- Kumaratilake, W. L. D. R. A., and U. N. Ranasinghe (1992). Unusual corundum-bearing gem pockets at Avissawella and Getahetta, Sri Lanka. *Zeitschrift der Deutschen Gemmologischen Gesellschaft*, 41, 1, 7–16.
- Liu Shang-I, E. and Zoysa, E.G., 2011. The Mirisatahela primary sapphire deposit in Sri Lanka. *Incolor*, winter, 34-39.
- Pardieu, V., Dubinsky, E.V., Sangsawong, S. Chauviré, B., 2012. Sapphire rush near Kataragama, Sri Lanka (February-March 2012). *GIA News from Research*, May 2012, <http://www.giathai.net>.
- Peucat J.J., Ruffault P., Fritsch E., Bouhnick-le Coz M., Simonet C., Lasnier B., 2007. Ga/Mg ratio as a new geochemical tool to differentiate magmatic from metamorphic blue sapphires. *Lithos*, 98: 261 – 274.
- Simonet, C., Fritsch, E., & Lasnier, B. (2008). A classification of gem corundum deposits aimed towards gem exploration. *Ore Geology Reviews*, 34(1-2), 127–133.
- Zwaan P. C. (1982). Sri Lanka: The gem island. *Gems & Gemology*, 18, 2, 62–71.
- Zwaan P. C. (1986). Gem minerals from the Embilipitya and Kataragama areas in Sri Lanka, *Australian Gemmologist*, 16, 2, 35–40.

Preliminary Report on New Corundum Deposits of Sri Lanka

E. Zoysa Gamini¹, Liu Shang I, Edward², Arūnas Kleišmantas³

¹ Ceylon Gemmological Sciences, Sri Lanka; gaminigz@hotmail.com

² The Gemmological Association of Hong Kong, Hong Kong; gemedward@hotmail.com

³ Department of Geology and Mineralogy, Vilnius University, Lithuania; arunas@kleismantas.eu

Introduction

Sri Lanka has long been one of the world important corundum production countries. Many new and important corundum deposits have been discovered in recent years. This report is focused on four of them, namely the sapphire deposits at Hatton (found Mid-2016), Kataragama (new area, December 2016) and Rakwana (end of March 2017) and a padparadsha deposit at Pohorabawa (in March 2017) (Figure1 and 2).



Figure 1. Sapphire deposits in Sri Lanka



Figure 2. Gem Mining in the paddy fields of Rakwana.

Geology and Production

Geologically, Sri Lanka is dominated by Precambrian high-grade metamorphic rocks which can be divided into four major lithotectonic units, namely the Highland Complex (HC), Vijayan Complex (VC), Wannu Complex (WC) and Kadugannawa Complex (KC) (Milisenda et al. 1988; Cooray 1994). The new mines at Hatton, Rakwana and Pohorabawa are located in the Highland Complex, which is metamorphosed at granulite-facies conditions during the Pan-African orogeny and consists of a variety of metasediments (including metapelites, quartzite, calc-silicates, garnet sillimanite gneisses and marbles) and metamorphosed igneous rocks (metabasites to meta-acidites). The Kataragama sapphire mine is located on the Kataragama Klippe, which is mainly constituted by garnetiferous charnockite, granulite quartzite and marble.

Kataragama mine - This new sapphire deposit is an eluvial deposit which is located near the old mining site in Tammanawa village ("road construction" site discovered in 2012) (Zoysa & Rahuman, 2012, Pardieu et al. 2012, Zoysa & Zwaan, 2012). Kataragama sapphires are notable for their size (up to 40mm, the largest weighing close to 12g) and intense blue colour. Euhedral crystals are common and usually appear in the form of a long hexagonal bipyramid with a length/ width ratio of 3:1-4:1 (Figure 3a). The production is about 60g per week.

Rakwana mine - It was a famous old mining area of producing sharp and electric blue sapphires in the south of Sri Lanka. Mines had been exhausted for long. This new deposit is an alluvial deposit with gem pits that are rather deep (about 80-120 feet), compared to those in Ratnapura. Only 5 shafts were found by one of the authors (GZ) during the first visit (Figure 2). The production is small, about 150g per week, of which around 15% are good quality materials (mostly in intense blue with a dark surface and sizes varying up to 30mm) (Figure 3b).

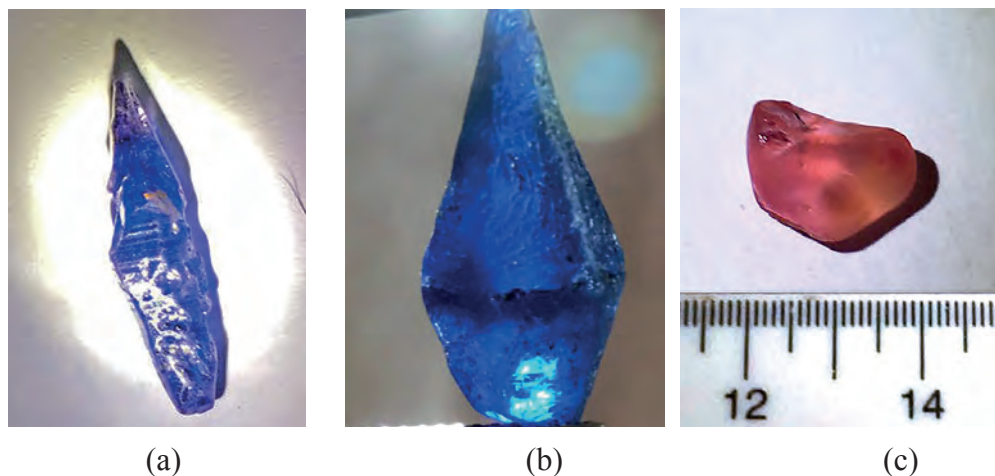


Figure 3. (a) A 11.07ct hexagonal bipyramidal Kataragama sapphire crystal; (b) A 13.29ct Rakwana sapphire crystal; (c) A 3.24 ct Pohorabawa padparadsha rough.

Hatton mine – An eluvial deposit found in a valley in the central highland of Sri Lanka. Small open pit mines of 5-10 feet in depth are being operated. The quality of Hatton sapphire rough is average and weighs between 1 and 5cts. The mine also produces large quantities of Geuda sapphire. Most of the sapphires are largely transparent. Associated gem minerals such as andalusite, sinhalite, garnet, blue spinel and chrysoberyl were common. The production of sapphire and Geuda is around 5-6 kg a week.

Pohorabawa mine – It is an old existing alluvial gem pit which mainly produced scapolite, geuda and fancy sapphires before. The mine is small and shallow. Good quality padparadsha sapphires (up to 6ct) were being discovered in this mine recently (Fig. 3c).

Experimental

UV-Vis-NIR spectra were collected using a PerkinElmer Lambda900 spectrophotometer for polarized ordinary and extraordinary rays. FTIR spectroscopy was performed using a Thermo Scientific Nicolet 6700 FTIR spectrometer. Raman spectroscopy was performed using a Renishaw InVia Raman Microscope for inclusion identification. Chemistry was determined using the EDAX EAGLE III EDXRF Analyzer and Thermo Scientific iCAP RQ ICP-Ms (laser ablation using ESI UP 213 & YAG laser).

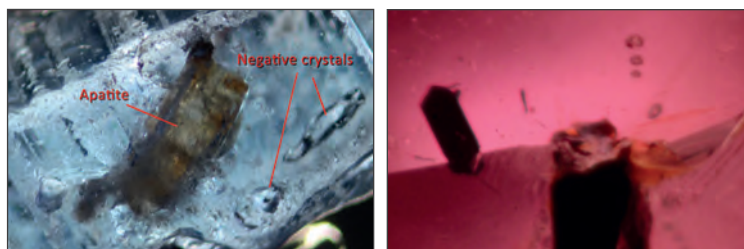


Figure 4. (left) Apatite inclusions and negative crystals in Kataragama sapphire - Figure 5. (right) Black opaque crystal inclusions and negative crystals in Pohorabawa padparadsha.

Results

All sapphire samples showed clouds of rutile needles and colour zoning. Samples from Kataragama display typical blue (or greenish blue) and pink colour zoning associated with twinning planes, which can be observed under crossed polarizing filters. Partial healed fissures, biotite flakes and high relief negative crystal inclusions were common (cf., Pannipiyiye et al. 2012). Yellow apatites and black opaque graphite platelets were identified in Kataragama sapphires and Pohorabawa padparadsha respectively by using Raman spectroscopy (Figure 4 and 5).

The UV-Vis-NIR spectra of sapphire samples are dominated by iron absorptions with a broad absorption band around 570nm (intervalence charge transfer of $\text{Fe}^{2+}/\text{Ti}^{4+}$) when $E \perp c$ and two strong and sharp Fe^{3+} absorption bands at about 377 and 388nm, and an absorption shoulder at 450nm (Schmetzer & Schwarz, 2004). Samples from Kataragama and Pohorabawa respectively showed extra or dominating Cr^{3+} absorption bands at about 405-410nm and 560nm (may overlap the $\text{Fe}^{2+}/\text{Ti}^{4+}$ IVCT absorption at 570nm) respectively.

All sapphire samples from Kataragama, Hatton and Rakawana showed IR absorption peaks of kaolinite-group minerals at 3697, 3669, 3654 and 3622 cm^{-1} (Beran & Rossman 2006, Zoysa & Zwaan, 2012). Distinct absorption peaks at 2359 and 2339 cm^{-1} indicate the presence of CO_2 in negative crystals. Peaks near 2855, 2920 and 2955 cm^{-1} indicate the presence of trace of oil. A broad absorption band around 3200-3600 cm^{-1} (center at 3450 cm^{-1}) is associated with the presence of molecular water. A very weak to insignificant absorption peak can be observed at 3309 cm^{-1} .

Chemical compositions are summarized in table 1. All sapphire samples in this study showed a rather consistent composition. They are characterized of having low Fe and Ga (52 to 246ppmw and 13 to 42ppmw, respectively) and medium Mg contents (10 to 37ppmw). Sapphires from Kataragama have higher mean Fe, Ti and Cr contents than sapphires from other localities. Padparadshas from Pohorabawa showed a relatively high Cr (around 171ppmw) and low Fe and Ti (around 52 and 21ppmw, respectively) contents.

The Fe concentration versus Ga/Mg ratio has been used to show the "metamorphic" origin of those sapphires samples (Peucat et al, 2007). Other geochemical plots of trace-element concentrations and ratios have been used to distinguish between sapphires of different localities (Sutherland et al., 1998; Zwaan et al., 2015). Samples from Rakwana, Hatton and Pohorabawa are high in Mg contents (40 to 80 ppmw), low in Ga (45 to 70 ppmw) and have low Ga/Mg ratios (0.81-1.69). However, the measured Ga/Mg ratios of Kataragama sapphires are higher (varied between 2.44 and 6.56).

References

Beran, A., Rossman G.R., 2006. OH in naturally occurring corundum. *European Journal of Mineralogy*, 18, 441-447.

Cooray, P.G. 1994. Precambrian of Sri Lanka: A historical review. *Precambrian Research*, 66, 3-20.

| Locality | Kataragama | | Rakwana | | | Hatton | Pohorabawa |
|-----------------|----------------|--------|-----------|--------|------------|------------|-------------|
| Variety | Sapphire | | Sapphire | | | Sapphire | Padparadsha |
| Colour (zone) | Blue with pink | Pink | Deep blue | Blue | Light blue | Light blue | Pink orange |
| No. of analyses | 3 | 3 | 1 | 3 | 2 | 3 | 3 |
| Be | 0.05 | bdl | 0.02 | 0.04 | 0.02 | 0.03 | 0.013 |
| Mg | 15.40 | 5.34 | 26.34 | 26.14 | 17.87 | 36.66 | 9.72 |
| Ti | 366.39 | 19.88 | 196.28 | 151.27 | 103.24 | 68.79 | 21.12 |
| V | 7.02 | 11.31 | 4.89 | 5.24 | 4.11 | 14.92 | 0.68 |
| Cr | 64.38 | 107.09 | 0.81 | 1.15 | 0.59 | 6.71 | 170.85 |
| Mn | 0.12 | 0.13 | 0.21 | 0.14 | 0.11 | 0.12 | 0.12 |
| Fe | 245.84 | 227.13 | 145.76 | 159.66 | 140.77 | 142.43 | 52.33 |
| Ga | 42.33 | 32.44 | 24.79 | 28.18 | 26.76 | 32.21 | 12.62 |

Table 1. Trace-element concentrations of 4 samples (3 sapphires and 1 padparadsha) by LA-ICP-MS analyses in average ppmw from new deposits of Sri Lanka.

Milisenda, C.C., Liew, T.C., Hofmann, A.W., Köhler, H., 1994. Nd isotopic mapping of the Sri Lanka basement; update and additional constraints from Sr isotopes. *Precambrian Research*, 66, 95- 110.

Pannipitiye G. R., Dharmaratne, H., Ranjith Premasiri, H. M., Dillimuni, D., 2012. Sapphires from Thammannawa, Kataragama Area, Sri Lanka. *Gems & Gemology*, 48(2), 98-107.

Pardieu V., Dubinsky, E.V., Sangsawong S., Chauviré, B., 2012. Sapphire Rush near Kataragama, Sri Lanka. *GIA News from Research*, May 2012, <http://www.giathai.net>.

Peucat, J.J., Ruffault, P., Fritsch, E., Bouhnik-Le Coz, M., Simonet, C., Lasnier, B., 2007. Ga/Mg ratio as new geochemical tool to differentiate magmatic from metamorphic blue sapphires. *Lithos, Elsevier*, 98 (1-4), 261-274.

Schmetzer, K., Schwarz, D., 2004. The causes of colour in untreated, heat treated and diffusion treated orange and pinkish orange sapphires- a review. *Journal of Gemmology*, 29(3), 149–82.

Sutherland F.L., Schwarz D., Jobbins E.A., Coenraads R.R., Webb G., 1998. Distinctive gem corundum suites from discrete basalt fields: a comparative study of Barrington, Australia, and West Pailin, Cambodia, gemfields. *Journal of Gemmology*, 2(2), 65–85.

Zoysa, E.G., Rahuman, S., 2012. Sapphire Rush in Kataragama, *InColor*, 19, 56-62.

Zoysa, E.G., Zwaan, J.C., 2012. A gemmological update on the Sapphire Deposit from Tammannawa, Kataragama, Sri Lanka. *Proceedings 3rd International Gem & Jewelry Conference (GIT 2012)*, Bangkok, Thailand, 52-59.

Zwaan, J.C., Buter, E., Mertz-Kraus, R., Kane, R.E., 2015. Alluvial sapphires from Montana – inclusions, geochemistry, and indications for a metasomatic origin. *Gems & Gemology*, 51, 370-391.

Acknowledgements

Special thanks to Mr. Thanong Leelawatanasuk of GIT Lab for providing UV-Vis-NIR, FTIR and Raman spectroscopy and EDXRF experiments and Dr. Ahmanjan Abduriyim of Tokyo Gem Science for LA-ICP-MS experiments.

Lead Glass-Filled Padparadscha

Sutas Singbamroong, Aisha Rashid Almazrooei, Nazar Ahmed

Gemstone and Precious Metal Laboratory, Dubai Central Laboratory Department,
Dubai Municipality, Dubai, United Arab Emirates, P.O. Box:67, sssutas@dm.gov

In recent years, fracture and cavity filling treatment has become more sophisticated and widespread, especially with the use of a high-lead-content glass, which is most commonly seen in rubies introduced to the gem market since 2004 (Rockwell & Breeding, 2004; Smith et al., 2005). This treatment was also applied for various other colors of corundum such as lead glass-filled color-change sapphire (Choudhary, 2008), blue cobalt-doped lead glass-filled corundum (Leelawatanasuk et al., 2013), green glass-filled sapphires (Henn et al., 2014; Leelawatanasuk et al., 2015), lead glass-filled yellow sapphire (Choudhary, 2014), beryllium-diffused and lead glass filled orange sapphire (Sun, 2015), and lead glass-filled black star sapphire (Sehgal, 2016).

In February 2017, the gemstone and precious metal laboratory of Dubai central laboratory department had the opportunity to examine eight orange-pink sapphires so called padparadscha that proved to be filled with lead glass (Figure 1). The samples weighed from 1.02 to 1.73 carats with color ranging from orangy pink to orange-pink. Standard gemological testing gave RI of 1.762-1.770, hydrostatic specific gravity of 4.00-4.02 and orangy red fluorescence in both long and short wave ultraviolet radiation. These properties are consistent with natural corundum.

Microscopic examination revealed numerous low-relief fractures throughout the stone with a distinct blue and orange flash effect, consistent with a lead-glass filling, as well as flattened gas bubbles trapped within the filler. Also observed were reflective rutile needles in milky zones, whitish melted crystals associated with liquid films or discoids (Figure 2).



Figure 1. Orange-pink sapphires so called padparadscha that proved to be filled with lead glass.



Figure 2. Numerous low-relief fractures with a distinct blue and orange flash effect, as well as flattened gas bubbles trapped within the filler.

Energy-dispersive X-ray fluorescence (EDXRF) analysis confirmed the presence of lead. X-ray imaging analysis also confirmed that the fractures had been filled with lead glass and revealed with quantifying of minor to moderate extents (Figure 3).

UV-visible spectroscopy was used to confirm whether the color was intrinsic to the corundum or intrinsic to the filler glass as in sapphire filled with a lead glass colored by other elements. The UV-Vis spectrum revealed Cr absorption bands with a prominent 450 nm series related to Fe³⁺ pairs responsible for the yellow component of the orange color which was consistent with the overall orange-pink bodycolor of the stone (Figure 4). Moreover, laser induced breakdown spectroscopy (LIBS) was used to detect the beryllium-diffusion treatment. Beryllium was not present in all the samples.

These were the first group of lead glass-filled padparadscha sapphires examined at the gemstone and precious metal laboratory of Dubai Central Laboratory Department.

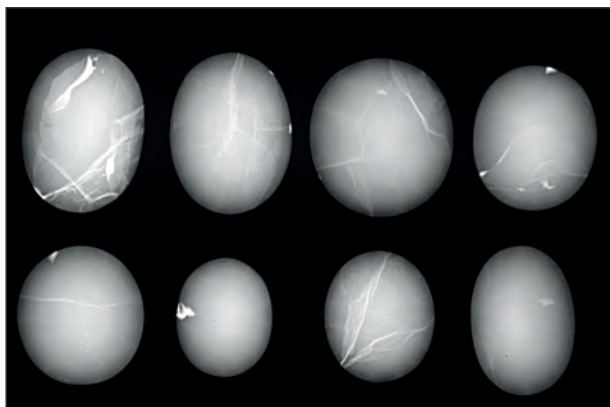


Figure 3. Real-time X-ray images of the orange-pink sapphires. The white areas indicate higher opacity in fractures and cavities, evidence of lead glass filling.

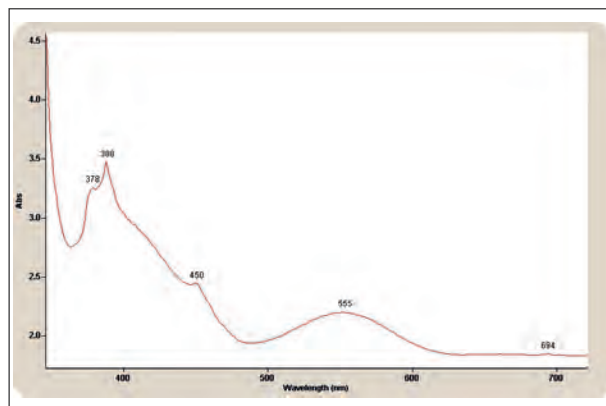


Figure 4. UV-Vis spectrum showed Cr absorption bands with a prominent 450 nm series related to Fe³⁺ pairs responsible for the yellow component of the orange color.

References

- Choudhary, G., 2014. Gem News International: Yellow sapphire filled with lead glass. *Gems & Gemology*, 50(1), 92-93.
- Choudhary, G., 2008. Gem News International: Lead glass-filled color-change sapphire. *Gems & Gemology*, 44(1), 88-89.
- Henn, U., Schollenbruch, K., Koch, S., 2014. Gem Notes: Corundum with coloured lead-glass fillings. *Journal of Gemology*, 34(2), 111–112.
- Leelawatanasuk, T., Atichat, W., Pisutha-Arnond, V., Wattanakul, P., Ounorn, P., Manorotkul, W., Hughes, R.W., 2013. Cobalt-doped glass-filled sapphires: An update. *Australian Gemmologist*, 25(1), 14–20, www.git.or.th/2014/eng/testing_center_en/lab_notes_en/glab_en/2013/cobalt_doped_glass_filled_sapphires.pdf.
- Leelawatanasuk, T., Susawee, N., Promwongnan, S., Atsawatanapirom, N., 2015. Green Lead Glass-filled Sapphires. *The Journal of Gemmology*, 34(5), 2015, 420-427.
- Rockwell, K.M., Breeding, C.M., 2004. Lab Notes: Rubies, clarity enhanced with a lead glass filler. *Gems & Gemology*, 40(3), 247–249.
- Sehgal, A., 2016. Lab Notes: Lead glass-filled black star sapphire. *Gems & Gemology*, 52(3), 304-305.
- Smith, C.P., McClure, S.F., Wang, W., Hall, M., 2005. Some characteristics of lead-glass-filled corundum. *Jewellery News Asia*, 255.
- Sun, Z., 2015. Lab Notes: Beryllium-diffused and lead glass-filled orange sapphire. *Gems & Gemology*, 51(2), 181-182.

Acknowledgements

The authors would like to express their thanks to the Gem and Jewelry Institute of Thailand's Gem Testing Laboratory (GIT-GTL) for help LIBS analysis.

Raman study for heat-treated sapphires based on the structural relaxation by impurities and thermal energy

Seung Kwon Lee, Kiran Kwon

Woosin Gemological Institute of Korea, 06022, Seoul, South Korea,
sklee1201@korea.ac.kr

Introduction

Heat-treated sapphires including Be-diffusion treated sapphires were investigated with Raman spectroscopy under 785 nm Laser excitation and with chemical analysis. Broadening of a Raman peak for heated sapphires reveals alteration of their crystallinity. Heat-treated sapphires show the increased value of full width at half maximum (FWHM) around 417 cm^{-1} (A_{1g} phonon mode). From chemical analyses and Raman study, we suggest that the structural relaxation of heat-treated sapphire might be correlated with Fe concentration and treatment temperature.

Materials and experimental methods

46 sapphire samples were examined using microscopy, FTIR and UV-Vis spectroscopy to determine their heat treatment. Some of samples were also cross-checked by GIA Japan, GIA Thailand and BGL (Burapha Gemological Laboratory) Thailand. Through this process, the samples were identified as 14 unheated and 32 heat-treated sapphires. Raman spectra were collected over the $100\sim 1000\text{ cm}^{-1}$ Raman shift range using a Renishaw InVia Raman microscope (excitation produced by 785 nm Diode laser). A 100x microscope objective was used for focusing of the laser beam and collection of the scattered light. Typical integration times were in the order of 10 s and total laser power was 250 mW. Analysis was carried out using a focused beam on the table facet of the sapphire sample except for rough stones. Chemical analysis by energy-dispersive X-ray fluorescence (EDXRF) spectroscopy was performed on all samples with a Shimadzu EDX-8000 instrument using a Rh X-ray tube, an accelerating voltage of 50 kV and a beam current of 1000 μA . The diameter of the X-ray beam was 3000 μm .

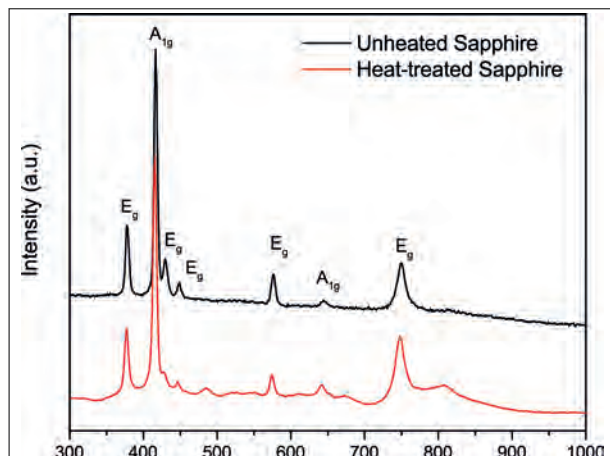


Figure 1. The Raman spectra of unheated and heat-treated sapphires with 7 phonon mode assignment. Heated sapphire shows a broad band around 802 cm^{-1} .

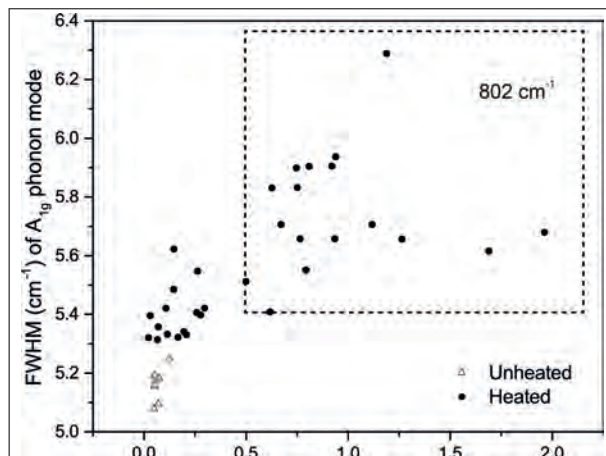


Figure 2. Fe concentration and FWHM values around 417 cm^{-1} from Raman spectra.

46 sapphire samples were measured by Raman spectroscopy. 7 samples had strong fluorescence around 417 cm^{-1} and only 39 samples were analyzed.

Results and discussion

Figure 1 shows representative Raman spectra of unheated and heat-treated sapphires in this study. Sapphire belonging to corundum group has seven phonon modes as predicted by group theory (Cotton, 1971). The most intensive phonon mode of all samples is A_{1g} ($\sim 417\text{ cm}^{-1}$) and 17 heated samples exhibit an extra broad band around 802 cm^{-1} . Fe_2O_3 concentration and FWHM value of A_{1g} phonon mode from Raman spectra are presented in Figure 2. The FWHM value is proportional to the Fe_2O_3 concentration. This correlation could be explained by the larger ionic radius of

Fe^{3+} compared to Al^{3+} ($r_{\text{Fe}^{3+}} = 0.645\text{ \AA}$ and $r_{\text{Al}^{3+}} = 0.535\text{ \AA}$ in an octahedral site, Shannon, 1976) and the electrostatic energy based on the Coulomb interaction between two charges which influences the lattice energy. As a result, the Fe-O bond is weaker than Al-O bond in $\alpha\text{-Al}_2\text{O}_3$. Previous study using EXAFS measurement and *ab initio* calculations of $\alpha\text{-Al}_2\text{O}_3\text{:Fe}^{3+}$ shows that a displacement of Fe^{3+} in $\alpha\text{-Al}_2\text{O}_3$ could affect the local symmetry of sapphire (Gaudry E., 2003). During the heat treatment of natural sapphire, iron atoms in the octahedral site could move to slightly different position from original site and some of Fe atoms contained in solid inclusions such as hematite, and ilmenite might substitute Al^{3+} atoms. Consequently, the introduction of iron impurities leads to structural relaxation around itself, increasing the FWHM value around 417 cm^{-1} . The FWHM values of unheated sapphire are below 5.3 cm^{-1} , whereas those of heat-treated sapphire are over 5.3 cm^{-1} . It is also observed that heat-treated sapphire has a broad band around 802 cm^{-1} , if the sapphire has Fe_2O_3 content higher than 0.5%.

Conclusion

In this study, Micro-Raman analyses were applied in order to identify heat-treated sapphires. During the heat treatment of a sapphire, impurities within the sapphire host lattice absorbed thermal energy. As a result, impurity atoms experiencing general heating treatment temperature could affect the local structure of the sapphire. We suggest that the local arrangement of atoms surrounding a substitutional Fe^{3+} ion in $\alpha\text{-Al}_2\text{O}_3$ was mainly governed by kinetics rather than thermodynamics while heat treated, because the heat treatment process of the sapphire was relatively shorter than the creation process by nature.

The Raman spectroscopy and EDXRF chemical analysis suggest that the displacement of iron ions in heated sapphire changes the local geometry and reduces crystallinity. This result is reflected in the increase of the FWHM of A_{1g} (417 cm^{-1}) Raman shift after heat treatment. The untreated sapphire samples have the value of FWHM at 417 cm^{-1} below 5.3 cm^{-1} , while heat-treated sapphire samples have the value of over 5.3 cm^{-1} . Raman shift around 802 cm^{-1} was observed for some heat-treated sapphires. This broad band might come from the split of E_g mode (751 cm^{-1}) due to the iron impurities. In addition, the variation in crystallinity of heat-treated sapphire may relate with concentration of iron ions.

However, some of sapphire samples displayed strong fluorescence while measuring Raman spectra, which strongly limited Raman method in this case. In addition, the structural relaxation of heated sapphire is not yet fully understood. Further investigation is needed for structural analysis, e.g. using XANES, EXAFS, or theoretical study for the heated sapphire.

Despite that, Raman study on the structural relaxation by impurities might open the opportunity to identify heat-treated sapphires.

Reference

- Cotton F.A., 1971. "Chemical Applications of Group Theory", Wiley-Interscience, 3rd edition.
 Gaudry E., et al., 2003. Structural and electronic relaxations around substitutional Cr^{3+} and Fe^{3+} ions in corundum. Phys. Rev. B, 67, 094108-1 – 094108-10.
 Shannon, R. D., 1976. Revised effective ionic radii and systematic studies of interatomic distances in Halides and Chalcogenides. Acta Crystallographica A, 32, 751-767.

Acknowledgements

We thank Miran Heo for supplying the corundum samples and Dr. Kook-Whee Kwak for help improving this manuscript.

GemTOF: A new and highly versatile method to analyse trace elements and isotopes of gemstones and pearls

Michael. S. Krzemnicki¹, Hao A. O. Wang¹, Walter A. Balmer², Jean-Pierre Chalain¹, Pierre Lefèvre¹, Wei Zhou¹, and Laurent Cartier¹, Henry A. Hänni³

Swiss Gemmological Institute SSEF¹, Chulalongkorn University (Bangkok)², GemExpert (Switzerland)³
michael.krzemnicki@ssef.ch

Introduction

Since decades, the chemical characterisation of gem materials is considered very important as it provides data not only for material identification (e.g. to identify turquoise against its imitations or to identify species within the garnet-group solid solution), but also for detecting synthetics and treatments (e.g. diffusion treatment or inorganic dyes in fissures). The main driving force for detailed trace-element analysis of gem materials, however, has been the demand from the trade for laboratories to deliver a scientifically based opinion of geographic origin for coloured gemstones such as rubies, sapphires, and emeralds, to name a few. This has resulted from value factors attributed to certain origins (e.g. sapphires from Kashmir), but also from the growing need for traceability of gems due to political (trade bans) or ethical (fair trade) reasons.

Since more than a decade, laser ablation inductively coupled mass spectrometry (LAICPMS) has become more and more important for trace element analysis of gem materials with a special emphasis on the chemical characterization of gems from different origins (Guillong & Günther 2001; Rankin et al., 2003; Abduriyim & Kitawaki, 2006). So far, most research was carried out with a so-called quadrupole mass spectrometer system (LA-ICP-Q-MS), by which mass per mass of a pre-defined list of elements (isotopes) (up to about 50 elements per 'sweep') are analysed sequentially, before starting the next circle of mass-hopping with the next 'sweep' of the pre-defined elements.

In the following, the authors will provide insight into a novel and highly versatile and sensitive method to analyse chemical composition (and isotopes) using a Time-Of-Flight mass spectrometer (LA-ICP-TOF-MS) (Wang et al. 2016) and discuss advantages of the so-called GemTOF system (in operation at SSEF since July 2016) compared to quadrupole based systems.

Principle of LA-ICP-TOF-MS and the GemTOF setup at SSEF

Similar to any LA-ICP-MS system, a time-of-flight setup consist of three units: 1) a *laser* for sample ablation, 2) an *ICP unit* for ionisation of the ablated material into (mostly singly) charged ions, and 3) a *mass spectrometer*. Specifically for our GemTOF setup, we use a nanosecond-pulsed deep-ultraviolet laser at 193 nm (NWR193UC ArF excimer laser from ESI, UK), an iCAP Qc from ThermoFisher Scientific, and an icpTOF time-of-flight mass spectrometer from ToFwerk, Switzerland).

The principle of a 'time-of-flight' (TOF) system is based on the fact that the 'flight' duration for a specific ion passing through a fixed flight tube is related to its mass to charge ratio (m/Q). As a consequence, light ions will travel faster through the system than their heavier counterparts with the same charge, provided they have identical kinetic energy; hence mass separation is achieved. The flight time difference between the lightest and the heaviest ions traveling to the detector is so minimal that one may even consider them to arrive almost at the same time (i.e. simultaneously) at the detector. Benefiting from recent developments in ultra-fast electronics and optimized ion optics, ICP-TOF-MS acquires simultaneous full mass-spectra from the lightest (${}^7\text{Li}$) to the heaviest isotopes (${}^{238}\text{U}$) at a high speed and high

spectral resolving power. Routinely, it provides limits of detection of about 1 ppm for light elements to ultra-trace levels of less than 10 ppb for heavy elements.

What is the advantage of time-of-flight (TOF-MS) compared to quadrupole mass spectrometry (Q-MS)

The key difference between quadrupole (Q-MS) and time-of-flight (TOF-MS) is their mass-separation scheme. Whereas the Q-MS instrument sequentially measures one isotope/mass after another (i.e. peak hopping) over a period of time (commonly about 0.5-1 seconds for a set of about 50 elements), the TOF-MS simultaneously analyses the full mass spectrum at high speed (about 0.001 sec per full mass analysis). This basic difference has a number of important advantages, greatly boosting its analytical and application capabilities.

In TOF-MS, there is no need to choose/pre-define a list of elements (isotopes) to be analysed. All masses present in the gem material between ⁷Li and ²³⁸U are immediately and simultaneously analysed (Figure 1a). Our research has revealed that this offers great advantages, as we are able to detect a number of (exotic) trace elements in gem materials. They have never been documented before with Q-MS, as they were just not included in the list of elements to be analysed. Additionally, with TOF-MS the full spectral data is stored and can be re-evaluated at any time. This allows us to look for hitherto unconsidered mass peaks even at a later time. This is especially important when analysing samples which are only temporarily at the laboratory. With Q-MS, there is no such option, as only the pre-defined list of elements is analysed, and furthermore as the ablated and analysed volume from the sample is gone.

A drawback of sequential acquisition in Q-MS is, that any ions of other masses are lost for analysis, if they enter the quadrupole during the short period when one mass is being analysed, as the Q-MS system can handle only one mass per moment. So consider the Q-MS system is accumulating the iron signal from a sapphire, it will not measure beryllium, which was ablated at the same time from the sapphire and ejected at the same time into the Q-MS system. With the simultaneous full mass-spectral range of the TOF-MS, there are no such drawbacks, which has an impact on quality of the analysis and the limit of detection (LOD), but also allows us to considerably reduce the amount of ablated material required from the sample, thus creating less impact, i.e. a smaller pit on the analysed gemstone (usually between 10-100 µm pit diameter).

The high speed of TOF-MS analysis can capture short transient signal at much greater detail than with the peak-hopping mode of the quadrupole setup. It is thus ideal to analyse small-scale chemical zoning in gems, or tiny inclusions encountered during laser ablation of a gemstone.

And finally, the TOF-MS setup offers a much higher mass-resolving power than Q-MS. It thus reduces misinterpretation (and wrong quantifications) due to peak interferences (Figure 1b). As we have access to all isotopic masses of an element (full mass spectrum), it is even possible to mathematically correct certain isobaric mass interferences, relying on the constant ratio of natural abundance of the isotopes of the involved chemical elements.

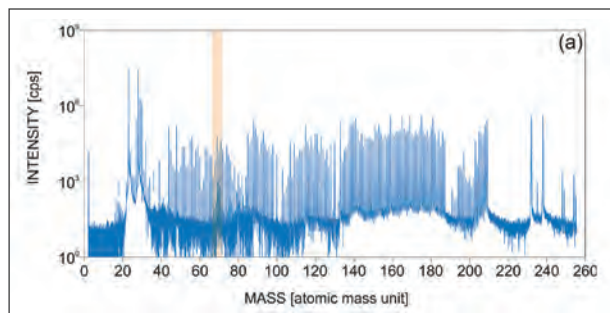


Figure 1a. Full mass spectrum (‘snap picture’) acquired by LA-ICP-TOF-MS (average of 20 s ablation)

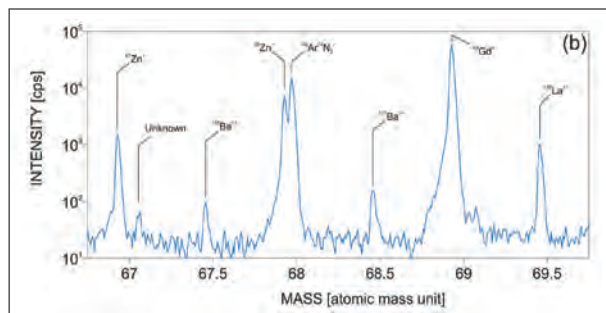


Figure 1b. Mass resolving power of this method exemplified by the $^{68}\text{Zn}^+ / ^{40}\text{Ar}^{14}\text{N}_2^+$ interference.

Application of GemTOF analyses on gem materials for research and in daily routine analysis

In the past months, we have analysed with our GemTOF instrument a large number of gem materials from our reference collections (SSEF collection and Henry A. Hänni collection) but also numerous client stones.

At SSEF, a major focus of research is the chemical characterisation of gemstones and their inclusions from different geological settings and geographic origin, given our expertise in this field. The authors will present GemTOF data on a number of gemstones, including sapphires, rubies, spinels, and Paraiba tourmaline, to name a few. We also will present our preliminary age dating results on zircon inclusions in various gemstones based on the widely used U-Pb system (Coenraads et al., 1990; Sutherland et al. 2002; Link 2015).

And finally, we will also discuss analytical limitations due to the GemTOF instrument itself and due to overlapping chemical compositions of gemstones from different geographic origin but similar geological setting.

Conclusions

GemTOF is a new and highly versatile method in mass spectrometry to analyse the full mass-spectrum of gemstones at high speed and high sensitivity. It is based on the 'time-of-flight' principle (TOF-MS) and is characterised by a number of important advantages compared to the more commonly applied quadrupole setup (Q-MS). Although this new method provides a wide range of chemical data, we would like to remind the reader of the fact, that in our opinion any conclusion (e.g. about a probable origin of a gemstone) has to rely on an approach, which combines advanced analytical methods (such as GemTOF, Raman, etc.) with traditional gemmological methods (such as meticulous microscopic observation).

References

- Abduriyim A. and Kitawaki H., 2006. Determination of the origin of blue sapphire using laser ablation inductively coupled plasma mass spectrometry (LA-ICP-MS). *Journal of Gemmology*, 30(1), 23–36, <http://dx.doi.org/10.15506/JoG.2006.30.1.23>
- Coenraads R.R., Sutherland F.L. and Kinny P.D., 1990. The origin of sapphires: U-Pb dating of zircon inclusions sheds new light. *Mineralogical Magazine*, 54(374), 113–122, <http://dx.doi.org/10.1180/minmag.1990.054.374.13>
- Guillong M. and Günther D., 2001. Quasi 'non-destructive' laser ablation-inductively coupled plasma mass spectrometry fingerprinting of sapphires. *Spectrochimica Acta Part B: Atomic Spectroscopy*, 56(7), 1219–1231, [http://dx.doi.org/10.1016/s0584-8547\(01\)00185-9](http://dx.doi.org/10.1016/s0584-8547(01)00185-9)
- Link K., 2015. Age determination of zircon inclusions in faceted sapphires. *Journal of Gemmology*, 34(8), 692–700, <http://dx.doi.org/10.15506/JoG.2015.34.8.692>
- Rankin A.H., Greenwood J. and Hargreaves D., 2003. Chemical fingerprinting of some East African gem rubies by laser ablation ICP-MS. *Journal of Gemmology*, 28(8), 473–482, <http://dx.doi.org/10.15506/JoG.2003.28.8.473>
- Sutherland F.L., Bosshart G., Fanning C.M., Hoskin P.W.O. and Coenraads R.R., 2002. Sapphire crystallization, age and origin, Ban Huai Sai, Laos: Age based on zircon inclusions. *Journal of Asian Earth Sciences*, 20(7), 841–849, [http://dx.doi.org/10.1016/s1367-9120\(01\)00067-0](http://dx.doi.org/10.1016/s1367-9120(01)00067-0)
- Wang H.A.O., Krzemnicki M.S., Chalain J.P., Lefèvre P., Zhou W. and Cartier L.E., (2016) Simultaneous high sensitivity trace-element and isotopic analysis of gemstones using laser ablation inductively coupled plasma time-of-flight mass spectrometry. *Journal of Gemmology*, 35(3), 212–223, <http://dx.doi.org/10.15506/JoG.2016.35.3.212>

Identification of natural and synthetic amethyst using multivariate analysis

Kentaro Emori, Hiroshi Kitawaki

Central Gem Laboratory, Tokyo, Japan; emori@cgl.co.jp

Abstract

The possibility of the identification of natural and synthetic amethyst by multivariate analysis using the data of LA-ICP-MS trace element analysis was examined. The samples used for the analysis consist of 50 natural amethysts from Brazil, Zambia and Japan and 49 synthetic amethysts obtained from the countries of their origin as well as from the gem market in Japan. The discriminant analysis and logistic regression analysis revealed that the elements ${}^7\text{Li}$, ${}^9\text{Be}$, ${}^{11}\text{B}$, ${}^{23}\text{Na}$, ${}^{27}\text{Al}$, ${}^{39}\text{K}$, ${}^{45}\text{Sc}$, ${}^{47}\text{Ti}$, ${}^{66}\text{Zn}$, ${}^{69}\text{Ga}$, ${}^{72}\text{Ge}$, ${}^{90}\text{Zr}$ and ${}^{208}\text{Pb}$ are a good indication to distinguish between natural and synthetic amethyst.

Introduction

Synthetic amethyst has been commercially supplied since the 1970s, and is mass-produced in Russia and China by the hydrothermal method using autoclaves. The gem industry members have been concerned by the risk of the synthetic amethyst getting mixed in natural amethyst at the source and being distributed in the market without being identified. According to JCK Magazine 1998, for example, half of the amethysts on the market were synthetic, and Borenstein (2010) said 25 % of the amethysts traded in East Asia were synthetic. Also, a gemmological laboratory in Europe reported that 70 % of quartz items submitted during the year were synthetic (Hainschwang, 2009).

As is the case for amethyst “that is synthetic but sold as natural without being noticed”, identification of natural and synthetic amethyst is important from a recent viewpoint of information disclosure and consumer benefit.

In gemmological laboratories routine distinction between natural and synthetic amethyst is due to microscopic investigations and infrared spectroscopy.

Chemical analyses for the separation of natural and synthetic amethyst and citrine by using LA-ICP-MS was introduced by Breeding & Shen (2010).

In this study, we have attempted multivariate analysis of LA-ICP-MS data for the identification (Fisher 1936 and Cox, 1958).

Material and Method

50 natural amethysts (10 from Brazil, 6 from Zambia, 2 from Japan, 1 from New Zealand and the others of unknown origin) and 49 synthetic amethysts (5 made in Japan, 4 made in Russia and the others of unknown origin) were analyzed (Figure 1). All samples are facet cut. We analyzed 5 points in each of the 5 Brazilian and 6 of the Zambian samples and 2 points at the other samples by LA-ICP-MS.



Figure 1. Some of the natural (0.54-1.86 ct, left) and synthetic (1.65-3.65 ct, right) amethysts analyzed in this study (Photo by Kentaro Emori).

We used New Wave Research UP-213 for laser ablation system and Agilent 7500a for ICP-MS. Analysis conditions were as follows; Laser ablation setting: laser wavelength 213nm, crater size 80mm, laser power 0.750 mJ, laser frequency 20Hz, ICP-setting: ICP 27.15MHz, RF power 1200W, Plasma gas(Ar) 14.93 l/min, Auxiliary gas(Ar) 0.89l/min, Carrier gas(Ar) 1.44l/min. At first, we performed qualitative analysis preliminarily and then for the elements detected (⁷Li, ⁹Be, ¹¹B, ²³Na, ²⁷Al, ³⁹K, ⁴⁵Sc, ⁴⁷Ti, ⁶⁶Zn, ⁶⁹Ga, ⁷²Ge, ⁹⁰Zr and ²⁰⁸Pb), we performed quantitative analysis. We used NIST612 as a standard material and ²⁹Si as internal standard and R language for the calculation of statics.

Result and Discussion

Discriminant analysis were performed using data of the trace elements that had been detected in the natural and synthetic amethysts. 133 points of natural amethyst and 98 points of synthetic amethyst were used for "training group". The parameters of discriminant analysis are the concentrations of these trace elements (⁷Li, ⁹Be, ¹¹B, ²³Na, ²⁷Al, ³⁹K, ⁴⁵Sc, ⁴⁷Ti, ⁶⁶Zn, ⁶⁹Ga, ⁷²Ge, ⁹⁰Zr and ²⁰⁸Pb), and calculation was performed by MASS package in R language. Fe, which causes the colour of amethyst, is inappropriate as the parameter used in discriminant analysis, because the Fe-concentrations are inhomogeneous in a stone according to its colour intensity. One discriminant score would be sufficient for separation into two groups (natural and synthetic), but we extended into two dimensions and calculated. The obtained functions are:

$$\text{LD1} = -0.0068[\text{Li}] + 0.0013[\text{Be}] + 0.2208[\text{B}] - 0.0354[\text{Na}] + 0.0051[\text{Al}] + 0.0075[\text{K}] + 0.0224[\text{Sc}] \\ - 0.0074[\text{Ti}] - 0.0368[\text{Zn}] - 0.0904[\text{Ga}] - 1.1317[\text{Ge}] - 0.0338[\text{Zr}] - 0.0007[\text{Pb}]$$

$$\text{LD2} = -0.0930[\text{Li}] + 0.1645[\text{Be}] - 0.1744[\text{B}] + 0.0052[\text{Na}] + 0.0195[\text{Al}] - 0.0003[\text{K}] - 0.1368[\text{Sc}] \\ + 0.0119[\text{Ti}] + 0.0095[\text{Zn}] + 0.0470[\text{Ga}] - 1.1722[\text{Ge}] - 0.0756[\text{Zr}] + 0.0021[\text{Pb}]$$

The elements are indicated in brackets directly after their concentration values (ppmw). The result is shown in Figure 2. Cross validation (CV) was used to see the performance of this discriminant analysis. On the CV, we got an error rate of 0.12. Compared to the simple plot of the concentrations of the trace elements, the graph obtained from the discriminant analysis has less overlap of the two groups, which shows good separation.

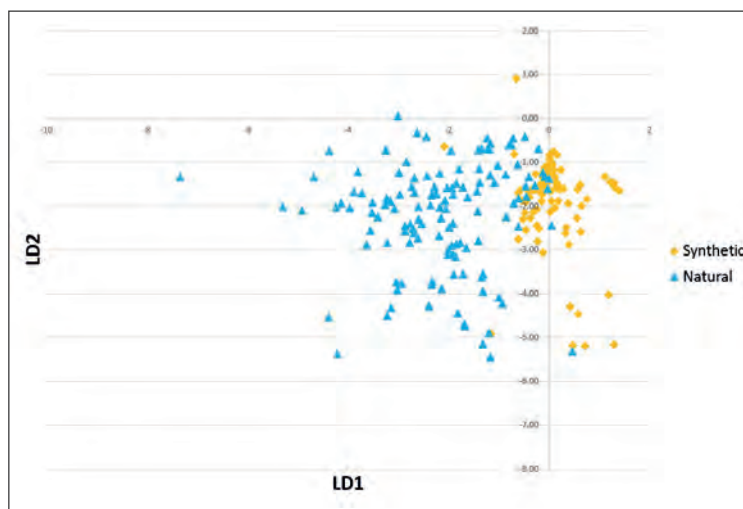


Figure 2. Graph of discriminant analysis of natural and synthetic amethyst.

Identification of natural and synthetic amethyst using Logistic regression

Performed logistic regression based on the data obtained in (1) was used. The probability that the stone was judged to be 1 for natural and 0 for synthetic amethyst was calculated. The parameters of logistic regression are the concentrations of trace elements (⁷Li, ⁹Be, ¹¹B, ²³Na, ²⁷Al, ³⁹K, ⁴⁵Sc, ⁴⁷Ti, ⁶⁶Zn, ⁶⁹Ga, ⁷²Ge, ⁹⁰Zr and ²⁰⁸Pb), and calculation was performed by 'glm' function in R language. The obtained functions are;

$$\text{logit}(p) = -0.38475[\text{Li}] + 55.56693[\text{Be}] - 13.2438[\text{B}] + 0.21611[\text{Na}] - 0.18751[\text{Al}] - 0.93194[\text{K}] + 0.89311[\text{Sc}] - 1.51653[\text{Ti}] \\ + 0.42607[\text{Zn}] + 16.56753[\text{Ga}] + 5.61131[\text{Ge}] + 60.20579[\text{Zr}] - 0.05453[\text{Pb}] + 2.81222$$

The elements are indicated in brackets directly after their concentration values (ppmw). $\text{logit}(p)$ is an inverse function of the logistic function, $\text{logit}(p) = \log(p/p-1)$, where p is the predicted value for natural amethyst. The result is shown in Figure 3.

Cross validation (CV) was used to see the performance of this logistic regression. On the CV, we got error rate of 0.02 when we judge that natural amethyst has values larger than 0.5. The logistic regression shows an error rate smaller than the discriminant analysis,

Conclusion

Trace elements in natural and synthetic amethyst were studied using LA-ICP-MS aiming to establish an identification method to distinguish them, and found that multivariate analysis was more efficient than the conventional comparison of concentrations of the trace elements. In this study we applied discriminant analysis and logistic regression for multivariate analysis, logistic regression shows an error rate smaller than the discriminant analysis in the identification of natural and synthetic amethyst.

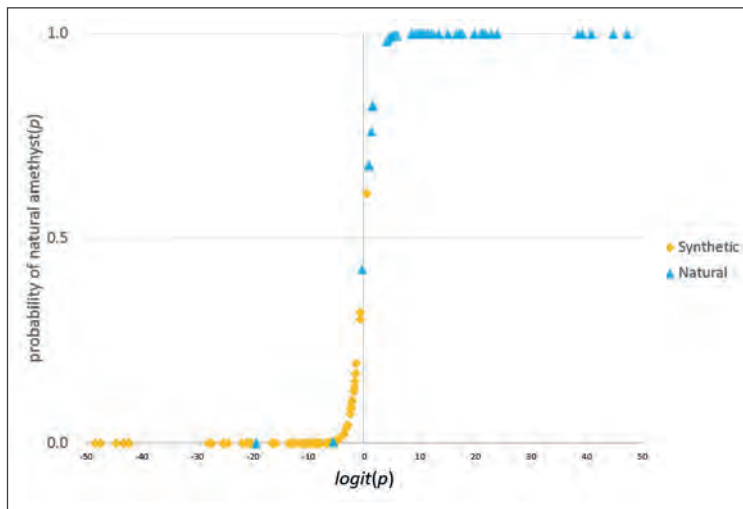


Figure 3. Graph of logistic regression of natural and synthetic amethyst.

References

- Borenstein G., 2010. Visual Characteristics of synthetic quartz, THE VALUER, April - June 2010, 2-6.
- Breeding, C.M., Shen, A.H., 2010. Separation of natural and synthetic gemstones using LA-ICP-MS: Amethyst, citrine, and malachite. Goldschmidt 2010, Knoxville, TN, June 13-18, A120.
- Cox, D.R., 1958. The Regression Analysis of Binary Sequences. Journal of the Royal Statistical Society Series B (Methodological), 20(2), 215-242.
- Fisher, R.A., 1936. The use of multiple measurements in taxonomic problems. Annals of Eugenics, 7, 179-188.
- Hainschwang T., 2009, The synthetic quartz problem, Gem Market News, January/February 2009, 1-5.
- JCK Magazine, 1998. Buying Amethyst Today, JCK Magazine, 1998, January 1.

The efficiency and limitation of phosphorescence imaging for screening current melee sized synthetic diamonds

Masaki Furuya

Japan Germany Gemmological Laboratory, Kofu, Japan E-mail:jgggl@sapphire.co.jp

In recent times melee sized synthetic diamonds have been an important issue in the international market (National Jeweler website, 2017 and Diamonds.net website, 2017). Due to the high volume distribution of melee sized diamonds, a speedy testing method to screen them is required from an industrial point of view.

Already in March 2014 SSEF Swiss Gemmological Institute made different announcements that they have developed a system that analyses 4000 melee size small diamonds per hour automatically with different spectral techniques. This automated diamond spectral inspection machine ASDI was presented to the press and during the CIBJO Congress in Moscow (CIBJO, 2014; Pia Grund Ludwig, 2014; SSEF, 2014).

In 2015, National Gemstone Testing Center (NGTC) announced “Multi-spectral induced luminescence imaging system (GV5000)” which takes the video of the phosphorescence of diamond and identifies the HPHT synthetics showing the strong greenish blue phosphorescence. It is feasible to be run in a batch, and so each testing can be conducted in a very short time like a photo-shooting (Liu, 2016). Since then, a large number of similar instruments have showed up in the market in order to check the phosphorescence of synthetic diamond made by HPHT method. HPHT synthetic diamonds can be easily detected under this method; however, there are some CVD synthetic diamonds without phosphorescence. However, with comparison of fluorescence colour some more of them are detectable and from the amount of distributions, this testing using phosphorescence imaging is still effective enough for screening synthetic.

In this research, I have utilized a phosphorescence device which is GLIS-3000 by Biaoqi Scientific Co., Ltd. The fluorescence and phosphorescence photos can be obtained from excited by UV light (the Deuterium arc lamp). The UV light covers the wide wavelength range between 180 and 250 nm. Moreover, the scanning is quite fast that is possible to scan the testing area 10 x 6 cm within 10 seconds.

With phosphorescence imaging, almost all melee sized HPHT synthetic diamonds of melee size can be clearly detected with its strong blue white phosphorescence as shown in Figure 1 & 2. As far as I see the distributed stones in Japanese market when it emerged in a large amount, most synthetic HPHT diamonds are from 1/180 to 1/100 ct size in 2016, but it becomes larger up to 1/30 ct at the middle of 2017. Its clarity is mostly VS and up. The colour is generally colourless to near-colourless, But some of them have brownish tint which are sorted as “top top light brown (TTLB)”.

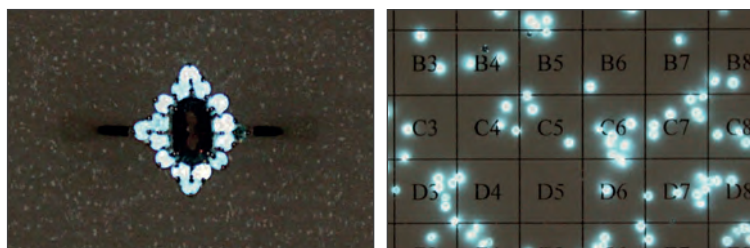


Figure 1. Phosphorescence image of many HPHT synthetic set in jewelry (with combined background) - Figure 2. A rot of melee sized HPHT synthetics showing phosphorescence (some dark stones: natural).

Almost all HPHT synthetic diamonds of above specifications show the blue white phosphorescence. This phosphorescence is due to the boron additives to keep the synthetic stone colourless. This phosphorescence is eminent with phosphorescence imaging instruments and highly accurate for screening HPHT synthetic from natural ones. In natural stones, it is quite rare (about 0.1%) to show the same kind of phosphorescence, and most of them are type IIb. When it is confirmed with photoluminescence, it often exhibits nickel related peaks of 883.2 and 884.9 nm associated with 483.9 nm in Figure 3. At stones with brownish tint, they often show the strong boron related absorption peaks with FT-IR spectroscopy (Figure 4).

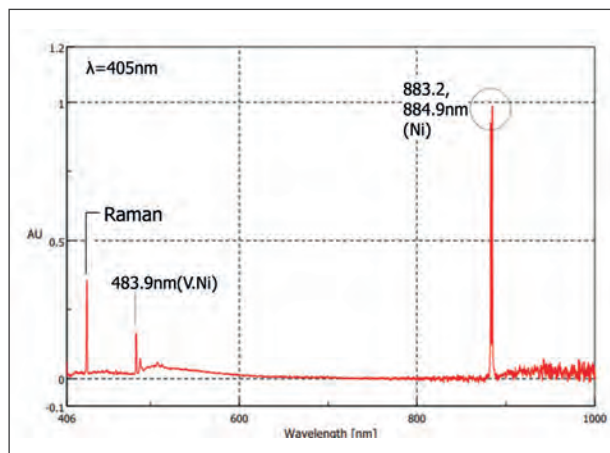


Figure 3. Typical photoluminescence spectrum of melee sized HPHT synthetic diamond.

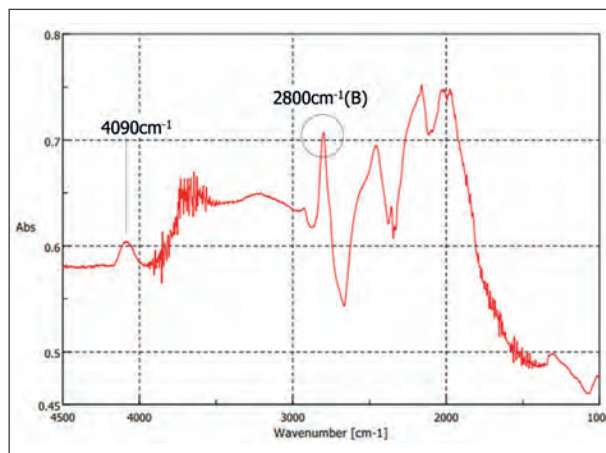


Figure 4. FT-IR spectrum of melee sized HPHT synthetic diamond with boron related peaks.

Actually in melee sized round synthetic diamond, HPHT method, especially Seed gradient temperature HPHT method has been applied much more than CVD method (Yuan, 2015 and Liu, 2016). Nevertheless, some melee sized round synthetic diamonds by CVD method have started to be sold in public since the Hong Kong show in 2016 (November) as well. Some of these CVD synthetic diamonds can be detected with its yellow green phosphorescence under phosphorescence imaging. We tested 85 pcs of melee sized (1/250-1/30 ct), round shaped CVD synthetic diamonds sold at the Hong Kong show. 67 pcs (79%) of them showed weak to moderate yellowish green to bluish green phosphorescence in Figure 5. And checking its fluorescence too can be helpful to identify CVD synthetics ones even though without showing any phosphorescence. 8 pcs (9%) of them do not show any phosphorescence but exhibit red to orange fluorescence (Figure 6). 4 pcs (5%) of them also show yellow and green fluorescence but no phosphorescence (Figure 7). Furthermore, 2 pcs (2%) of them show only weak violet fluorescence which is extremely faint. Moreover the rest of 2 pcs (2%) show even no fluorescence with broad band UV excitation, though they are not colourless enough and light gray or light brown which may self-absorb the fluorescence. Those could not be detected with this type of phosphorescence imaging. Thus, although there are some CVD synthetic diamonds which are not detectable with the phosphorescence imaging, it is possible to detect more with checking their fluorescence characteristics too.

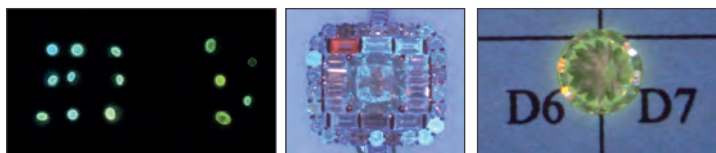


Figure 5. Yellow green to greenish yellow phosphorescence image of melee sized CVD synthetic -
 Figure 6. Baguette cut CVD synthetic showing red fluorescence (Only top left one is CVD synthetic.) -
 Figure 7. Yellow and green fluorescence seen in CVD synthetic

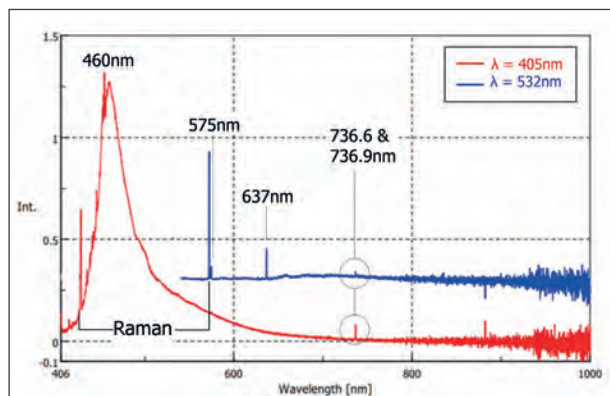


Figure 8. Photoluminescence spectra of CVD synthetic diamond with yellow green phosphorescence.

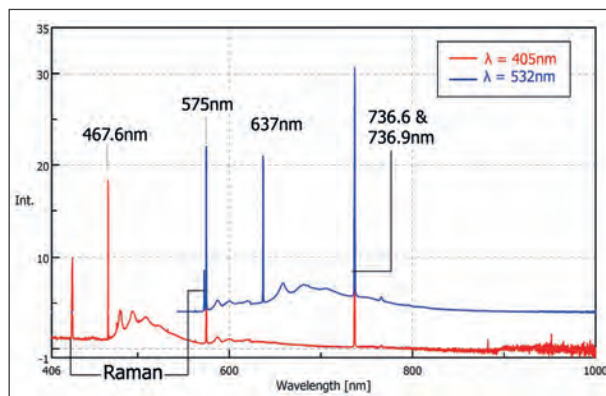


Figure 9. Photoluminescence spectra of CVD synthetic diamond without any phosphorescence but with red fluorescence.

Most of the CVD synthetic diamonds with above phosphorescence show the photoluminescence spectra as CVD synthetic with HPHT treatment (Figure 8). However, the CVD synthetics without phosphorescence show the photoluminescence spectra of As-grown CVD synthetic without or less HPHT treatment which exhibits the strong emission of silicon related peaks (Figure 9). It is not straightforward and take more time to grow the CVD diamond which is highly colourless as grown (Sonani, 2016) It will cost more to grow the As-grown CVD synthetic for reasonable me-lee-sized diamond which are not proper for commercial synthesis. Also, the CVD synthetic which does not even show any phosphorescence and fluorescence are light gray or light brown which are less expensive. Thus, it may imply that from the viewpoint of the synthesis cost, they are not many in the volume.

As mentioned above, with phosphorescence imaging for me-lee sized colourless to near colourless diamond, HPHT synthetic can be detected well and high percentage of CVD synthetic are also detectable. And the screening with phosphorescence imaging is quite speedy. Though there are little CVD synthetic which are not detectable with it, for industrial usage which need to screen a big amount of stones, it is still very effective.

Acknowledgments

Dialuster Co.,Ltd. - PDC Co., Ltd. - Diamond Elements PVT.LTD.

References

CIBJO, 2014. http://www.cibjo.org/index.php?option=com_content&view=article&id=682:cibjoconference-on-synthetic-diamonds-sparks-vigorous-debate&catid=7:news&Itemid=251

Diamonds.net News , 7th May 2017, "GIA Finds Significant Undisclosed Synthetics" Diamonds.net website. <http://www.diamonds.net/News/NewsItem.aspx?ArticleID=58658>

Fine Jewelry Industry News, 18th April 2017, "GIA Debuts Screening Device for Mounted Gems" National jeweler website. <http://www.nationaljeweler.com/diamonds-gems/grading/5351-gia-debuts-screening-device-for-mounted-gems>

Grund-Ludwig, Pia, 2014 Basel World Daily News, Friday March 28.

Hainschwang T., Notari F., 2013, "The Challenge of Identifying Recent Generations of Melee-Sized Synthetic Diamonds" Presentation in Kofu, Yamanashi.

Lu. T., Lan Y., Liang R., Zhang C., 2016 "Testing and screening of melee-sized near-colourless HPHT synthetic diamonds using a multi-spectral induced luminescence imaging system (GV5000) in China", ICGI newsletter winter 2015: 1-3

SSEF , 2014. Press Release, March 29. SSEF introduces the Automated Diamond Spectral Inspection (ASDI) System offers solution for authenticating large quantities of colourless melee

Sonani J., 2016, "Growth rate of CVD synthetic diamond with and without silicon contamination" Personal communication.

Yuan, J., 2015, "Identification and influence to the future market of synthetic diamond" 34th IGC2015 Abstracts: 36-39.

Origin determination of Iran Excellent-quality Turquoise based on trace element analysis using ICP-MS and Micro XRF

Bahareh Shirdam, Soheila Aslani

Gemological research laboratory, School of Mining engineering, College of engineering,
University of Tehran, Tehran, Iran; shirdam@ut.ac.ir

Abstract

Turquoise is one of the most important gems in ancient Persian history, holding a strong value for Iranian, not only in the past but also today. This gemstone's modern world market is very large, comprised of turquoises from China, US and Iran. But what separates Persian turquoise from the others, is the combination of its unique color and quality. Among all turquoise deposits in Iran, only Neyshabur area from Khorasan Province have enjoyed higher market price and popularity. However, the mine is at the verge of closure. In the interim a relatively new source of excellent-quality turquoise is discovered within slates in the western zone of Kerman Province, Meiduk, which separating it from Neyshabur's turquoise in matrix-less samples can be very confusing. There is a real need to study the trace elements and origin of these turquoises.



Figure 1. Geographical map of the locations of the two excellent quality Turquoise deposits in Iran.

52 Rough and polished samples, directly collected from Meiduk and Neyshabur mines, were studied using ICP-MS and Micro-XRF. The main color of samples ranged from very slightly greenish blue (vslgB) to light greenish blue (gB).



Figure 2. Turquoise samples from Neyshabur and Meyduk.

Trace elements concentrations of these 52 turquoise samples were measured by using both Micro-XRF and ICP-MS system. In first place 6 samples with equal quality and color from both Neyshabur and Meyduk had been selected to be analyzed by ICP-MS (Agilent 7900 ICP-MS) due to its high sensitivity to detect and select the trace elements. In the next step, all 52 samples were analyzed by Micro-XRF (Horiba XGT-7200 X-ray Analytical Microscope) to nondestructively reach the results. (Analysis full condition and software will be mentioned in the full paper.)

Cr, Fe, Zn, As and Sr were selected by the results of ICP-MS as reliable trace elements to separate Neyshabur and Meyduk origin. The presence and percentage of Cr in Meyduk samples (which varies from 0.02-0.04) could be an easy way to separate it from Neyshabur (which hardly reached 0.01), but due to the presence of a few exceptions, more caution is necessary. Higher Fe and the absence or low percentage (less than 0.01) of Cr in Neyshabur turquoise are key factors. Zn, As and Sr have different ranges but their combination created another factor to detect the origin.

It's important to remember origin determination in trace element analysis by ICP-MS and Micro-XRF does not always bring reliable information because the data obtained from different locations are sometimes the same. It must be used complementary with an observation of inclusions and gemmological characteristics.

References

Abduriyim A., Kitawaki H., 2006. Applications of Laser Ablation-Inductively Coupled Plasma-Mass Spectrometry (LA-ICP-MS) to Gemology. *Gems & Gemology*, 42(2), 98-118.

Mulhmeister S., Fritsch E., Shigley J., Devouard B., Laurs B., 1998. Separating Natural and Synthetic Rubies on the Basis of Trace-Element Chemistry. *Gems & Gemology*, 34(2), 80-101.

Shirdam B., Aslani S., 2016. A Microscopic and Micro-XRF spectroscopy study on Kerman Turquoise and introducing it as a gem-quality Turquoise. *Proceeding of the 3rd national symposium of Gemology and Crystallography, Shahid Beheshti University*, 137-143 (Persian).

“Golden” *Pinctada maxima* Non-bead Cultured Pearls with an Emphasis on their Internal Structures

Nick Sturman, Areeya Manustrong, Kwanruen Lawanwong, Promlikit Kessrapong, Nanthaporn Somsa-ard, Artitaya Homkrajae

GIA Laboratory, Bangkok, Thailand, nsturman@gia.edu

Introduction

The identification of pearls by gemologists in laboratories globally depends on many factors. The type of pearl under test, producing mollusc, sample size, type and quality of equipment, and experience of the gemologists employed are all part of the equation. However, one of the most critically important factors in addition to a gemologist's experience and quality of equipment available is that of access to known reference samples. By studying known samples, or at least ones with a very sound provenance, data may be collected to assist gemologists of all experiences when pearls of an unknown provenance are submitted by a laboratory's clients. This study focuses on a group of loose pearls collected from the farms of Jeweler Joaillerie (figure 1) in the Philippines with the purpose of seeing whether any would reveal structures that may pass as being characteristic of natural pearls. Only one pearl was found to possess such structure, while the rest revealed structures expected for non-bead cultured pearls and bead-cultured pearls. Some of the more characteristic structures expected for non-bead cultured pearls, together with a few uncharacteristic structures are discussed. The results add further information to that already in the public domain (Hänni 2006; Sturman 2009) on the types of non-bead cultured pearl structures expected when such pearls are submitted to microradiographic analysis.

Sample Details

Seven hundred and ninety-two loose pearls were kindly lent to GIA by Jeweler Joaillerie for examination and data collection after being hand selected by both Jeweler staff and two representatives from GIA who visited the farms to sort them. The pearls varied widely in their size, shape, and color and reportedly originated from *Pinctada maxima* shells on Jeweler's farms. While there was little doubt that the majority would reveal cultured structures, non-bead as well as bead, the work was necessary to make sure that no potential “natural” pearls existed among the samples. This was a particular point that Jeweler were interested in ascertaining from the outset although they obviously realized the chances of finding any natural pearls were very slim.



Figure 1. Ten loose pearls examined as part of this study. The majority of the samples varied from cream to strong yellow («golden»).

Gemological Analysis

All the pearls were examined using real-time microradiography (RTX) and pearls with structures of particular interest were subsequently examined in greater detail using X-ray computed microtomography (μ CT). While the structures of the majority showed the expected and characteristic void type features (figure 2) routinely observed in saltwater non-bead cultured pearls, other types of structure were also observed. As a result it was possible to group the structures into four main overall types; voids, voids with associated organic rich (“meaty”) areas (figure 3), linear (figure 4), and “atypical-like” (figure 5). Sometimes a combination of two forms was also apparent such as linear with meaty areas, or voids with meaty areas. Only one pearl showed clear structure that could be associated with a natural identity, yet the hatchery produced mollusc that created the sample and the fact that it originated from a farming environment open up a whole series of dilemmas pertaining to its correct nomenclature. The fact is that such a pearl, when submitted to a laboratory without any provenance, would have to be classified as natural based on the internal structure observed via RTX and/or μ CT analysis.

The nomenclature issues surrounding the remaining pearls were not so challenging, however it was very interesting to note that some pearls exhibited structures that may perhaps be considered more “atypical” in nature. These usually took the form of a concentrically structured inner pearl within a void feature, and while they may prove challenging to positively identify under laboratory conditions GIA was assured by Jewelmert that no such “atypical” culturing methods were employed on any of their farms.

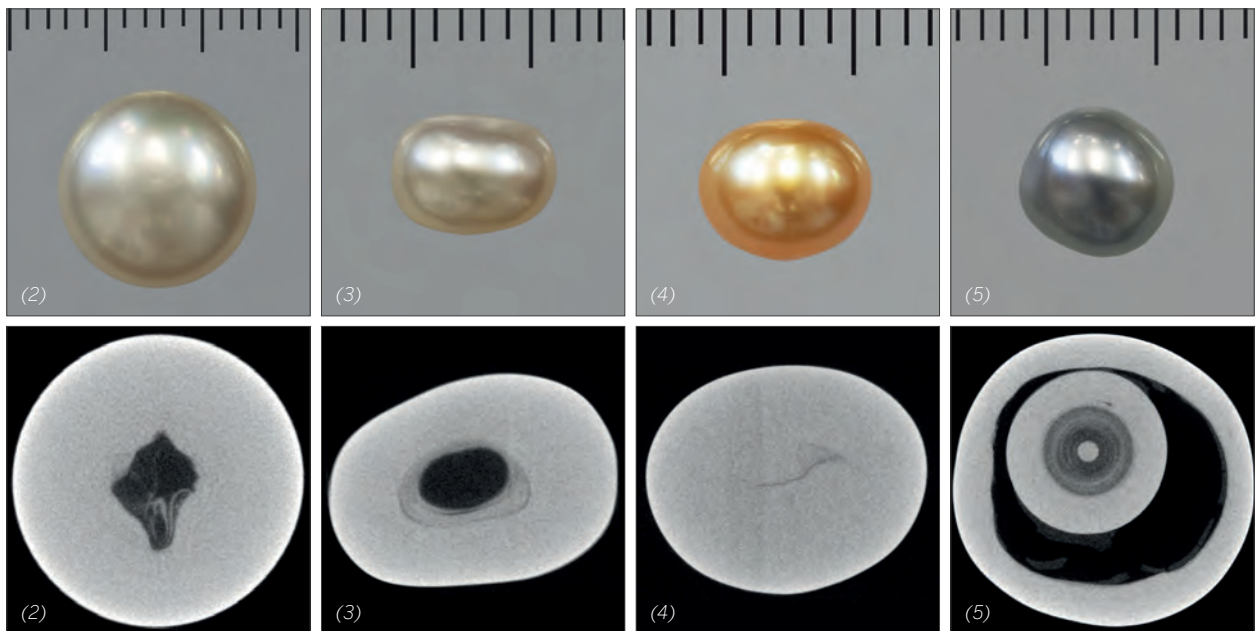


Figure 2. A μ -CT slice showing a void feature characteristic of such saltwater non-bead cultured pearls.

The pearl weighs 6.86 carats. Photomacrograph: Sasithorn Engniwat.

Figure 3. A μ -CT slice showing a void feature together with an organic or “meaty” area characteristic of some saltwater non-bead cultured pearls. The pearl weighs 1.56 carats. Photomacrograph: Sasithorn Engniwat.

Figure 4. A μ -CT slice showing a linear feature characteristic of some saltwater non-bead cultured pearls.

The pearl weighs 1.66 carats. Photomacrograph: Sasithorn Engniwat.

Figure 5. A μ -CT slice showing an “atypical-looking” structure.

This type of structure was encountered the least in the saltwater non-bead cultured pearls examined in this study.

The pearl weighs 1.40 carats. Photomacrograph: Sasithorn Engniwat.

Other analytical techniques including UV-Visible, Raman, and photoluminescence spectroscopy were carried out on a few of the samples to confirm the natural colour origin of the more saturated pearls and their long-wave and short-wave ultra-violet radiation reactions as well as DiamondView responses were also recorded.

Conclusion

The work undertaken on the samples described here builds on the data already obtained by GIA from known samples of natural, non-bead cultured and bead-cultured pearls obtained from Broome & Darwin, Australia (Scarratt et al., 2012; Sturman et al., 2015), Lombok, Indonesia (Sturman et al., 2016) and The Mergui Archipelago, Myanmar (Sturman et al., 2016). Such work is vital in compiling a useful database to assist in the identification of more challenging pearls (Sturman, 2009) lacking provenance that are often submitted to laboratories by their clients.

The analytical tests applied to determine the colour origin of a random sampling proved that they were not treated to modify their appearance in any way and this tallied with the information provided by Jeweler.

The majority of the samples in this study revealed microradiographic and computed microtomography structures expected for saltwater non-bead cultured pearls produced by the *Pinctada maxima* mollusc, yet a few revealed structures that have the potential to create inconsistent results between laboratories. This shows why such work and the creation of a known database of reference structures are of great importance to gemological laboratories. The discussions that result from such studies and the subsequent sharing of the results also assist the gemological community in the long run as they help resolve differences in opinion that may exist.

References

- Hänni, H.A., 2006. A short review of the use of "keshi" as a term to describe pearls. *Journal of Gemmology*, 30(1/2), 51-58.
- Scarratt, K., Bracher, P., Bracher, M., Attawi, A., Safar, A., Saeseaw, S., Homkrajae, A., Sturman, N., 2012. Natural pearls from Australian *Pinctada maxima*. *Gems & Gemology*, 48 (4), 236-261.
- Sturman, N., 2009. The microradiographic structures of non-bead cultured pearls. GIA Thailand, Bangkok, November 21, www.giathai.net/pdf/The_microradiographic_structures_of_NBCP.pdf
- Sturman, N., Homkrajae, A., Manustrong, A., Somsa-ard, N., 2015. X-ray Computed Microtomography (μ CT) Structures of known Natural and Non-bead Cultured *Pinctada maxima* Pearls. Proceedings of the 34th International Gemmological Conference (IGC 2015), Vilnius, Lithuania, 121-124.
- Sturman, N., Bergman, J., Poli, J., Homkrajae, A., Manustrong, A., Somsa-ard, N., 2012. Bead-cultured and non-bead-cultured pearls from Lombok, Indonesia. *Gems & Gemology*, 52 (3), 288-297.
- Sturman, N., A., Manustrong, A., Pardieu, V., 2016. The Cultured Pearls of Mergui with an Emphasis on their Internal Structures. Proceedings of the 5th International Gem and Jewelry Conference, GIT 2016, 143-145.

Natural pearls found from *Pinctada radiata* in the Kingdom of Bahrain: Characteristic structures, comparison and identification

Stefanos Karampelas, Abeer Tawfeeq Al-Alawi, Ali Al-Attawi, Kenneth Scarratt

The Bahrain Institute for Pearls & Gemstones (DANAT), WTC East Tower, Manama, Kingdom of Bahrain ;
Stefanos.Karampelas@danat.bh

Bahrain was, and still is, considered a centre for the natural pearl trade. It is the only country in the world which by law bans the trade of cultured pearls. Prior to the early 1930's the natural pearl fishing and trade was very active. However, at this time the newly introduced cultured pearls and oil industry activities started to gain traction the natural pearl industry of the country started to decline. Bahraini 'pearl industry' today is not like at early 1930s. However, pearl trade continues, albeit on a smaller scale and most diving is carried out on a hobby/leisure-time. Annually, around 10 kilos of gem quality natural pearls were harvested mainly from the shallow areas in the waters around Bahrain.

There are two types of pearl producing molluscs in the waters around Bahrain: *Pinctada radiata* (*P. radiata*) and some Pinnidae (a.k.a. pen shells) bivalves. The vast majority of high quality pearls are found in *P. radiata*. Most of the gem quality pearls are found in the waters 50 km NNE of Bahrain. The beds in these areas have an average of about 4-30 shells per square meter. According to the survey recently conducted most of the beds are still in excellent environmental conditions. To protect these beds, the government has implemented strict laws and regulations on mollusc fishing. Moreover, the three main pearl fishing areas north of the island as part of the Bahrain Pearling Trail project which has been included by the UNESCO as a World Heritage Site on 2012.

Natural pearls found in *P. radiata* have a wide range of shapes (e.g. round, oval and button), luster and colors (the most common are white, cream, light yellow, light grey, yellow and others with various overtones). Their average size is 5-7 mm; round pearls bigger than 9 mm are rare. Blister natural pearls could be found in bigger sizes. The last years though identification of the natural saltwater pearls (SWNPs) sometimes is an issue. This is because some saltwater cultured pearls (SWCPs) without bead are sometimes difficult to identify (Hänni, 2006; Sturman & Al-Attawi, 2006; Sturman, 2009, Karampelas et al., 2010, Krzemnicki et al., 2010, Scarratt et al., 2012). Some of the SWCPs without bead present structures similar to those observed in natural pearls. The samples which show "cavities/voids" cause occasionally great difficulties to gemmological laboratories (see some examples in Sturman, 2009). Such internal features could be very confusing as can be observed in SWCPs without bead as well as in saltwater natural pearls (SWNPs). Additionally, some SWCP with natural pearls used as beads appeared in the market recently; sometimes difficult to identify (Scarratt et al., 2017).

For the present study a series of SWCPs without bead from *Pinctada maxima* (*P. maxima*) with voids, SWCPs from *P. maxima* with natural pearls as bead and natural pearls (SWNPs) from *P. radiata* -with and without voids-, were selected, from the National Museum of Bahrain pearl collection acquired during dives organized directly by them the last years, in order to study in detail the "voids" using X-radiography and/or micro-CT. Some of the samples were cut in two pieces in order to check their internal structures under the microscope. The colour of these samples spanned from white to white silver to white cream colour, with shapes ranging from near round, oval, button to baroque, and maximum dimension of around 9 mm.

Regarding the samples with voids, SWNPs from *P. radiata* present in general irregular cavities which match to a degree the external shape of the pearls and in parallel they present low to medium lustre. SWCPs without bead from *P. maxima* present cavities which in general do not match samples' external shape and they present medium to high lustre. In most of cases, micro-CT measurements should be acquired to identify properly these samples.

Identification of SWCPs from *P. maxima* with natural pearls as bead could be sometimes difficult (Figure 1). However, in most of cases traces of cultivation can be observed in micro-CT slides and sometimes in X-radiographs (Figure 1b). For example, the position where the tissue graft was placed, during the insertion of the bead, can be observed (Figures 1c). Sometimes growth structures of the natural pearl used as bead are different compared to those of produced after the cultivation. However, samples with a thin nacre deposition on the natural pearl used as bead are the most problematic to identify.



Figure 1a. A 2.34 ct. cream near round SWCP from *P. maxima* with a bead made of *P. maxima* natural pearl. Photo: Ayoob Bahman.



Figure 1b. X-radiograph of the SWCP showing concentric growth lines in the natural *P. maxima* pearl used as bead. A demarcation is observed along with a dark coloured area, due to tissue graft used during cultivation. This demarcation is often seen in CPs with bead.

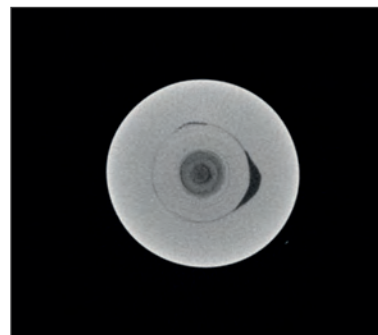


Figure 1c. A slice (2-D) from the μ CT model of the SWCP showing concentric growth lines in the natural *P. maxima* pearl used as bead. A demarcation is observed along with a dark coloured area on the outer ring next to the demarcation. This is due to tissue graft used during cultivation and it is often seen in CPs with bead.

In most of cases, it is important to acquire high quality-resolution micro-CT images in order to better monitor samples' structures and look for potential differences. It is, in general, possible to identify studied natural pearls. However, identification of some SWCPs with natural pearls as bead remains sometimes much more challenging.

References

- Hänni H.A., 2006. A short review of the use of 'keshi' as a term to describe pearls. *Journal of Gemmology*, 30 (1-2), 51-58.
- Karampelas S., Michel J., Zheng-Cui M., Schwarz J.-O., Enzmann F., Fritsch E., Leu L.,
- Krzemnicki M. S., 2010. X-ray Computed Micro-Tomography Applied to Pearls: Methodology, Advantages, and Limitations. *Gems & Gemology*, 46 (2), 122-127.
- Krzemnicki M.S., Friess D., Chalus P., Hänni H.A., Karampelas S., 2010. X-ray computed micro-tomography: Distinguishing natural pearls from beaded and non-beaded cultured pearls. *Gems & Gemology*, 46 (2), 128-134.
- Scarratt, K., Bracher P., Bracher M., Attawi A., Safar A., Saeseaw S., Homkrajae A., Sturman N., 2012. Natural pearls from Australian *Pinctada maxima*. *Gems & Gemology*. 48 (4). 236-261.
- Scarratt, K., Sturman, N., Tawfeeq Al-Alawi, A., Bracher P., Bracher M., Homkrajae, A., Manustrong, A., Somsaard, N., Zhou, C., 2017. Experiments in using atypical 'beads' and mantle interference in the production of cultured pearls with Australian *Pinctada maxima*. GIA report, <https://www.gia.edu/gia-news-research/atypical-beading-production-cultured-pearls-australian-pinctada-maxima>
- Sturman N., 2009. The microradiographic structures on non-bead cultured pearls. GIA Thailand, Bangkok, www.gia-thai.net/pdf/The_Microradiographic_structures_in_NBCP.pdf.
- Sturman N., Al-Attawi A., 2006. The "Keshi" pearl issue. *Gems & Gemology*, 42(3), 142.

Past and present situation of freshwater pearls from North Western Russia

Elisabeth Strack

Gemmologisches Institut Hamburg, Hamburg, Germany
info@strack-gih.de

Introduction

Freshwater pearls from *Margaritifera margaritifera* (L., 1758), also called the „European pearl mussel“, are part of European cultural history. The mussels originally ranged from the north-western Iberian Peninsula to north-western Russia but significant pearl production occurred only in a few countries, such as parts of Germany (especially Bavaria and Saxony), Great Britain (especially Scotland) and Russia. During the last century, populations have diminished by more than 90%, due to environmental influences and the species is listed as endangered on the IUCN Red List since 1996.

In north-western Russia, particularly from the 18th and 19th centuries until 1917, the pearls were used abundantly for both secular and ecclesiastical purposes and commonly incorporated into embroideries, traditional headdresses, jewellery and various objects of religious significance.

Interest in pearls waned after the Russian Revolution, and interviews conducted during the 2000s with people in former pearling centres in Karelia and on the Kola Peninsula showed that local knowledge about pearls has nearly disappeared, and only a few items have been preserved at local museums.

Distribution of the pearl mussel in North-Western Russia

The occurrence of *Margaritifera margaritifera* is confined to the northern hemisphere, situated between approximately 40° and 70° northern latitude. The mussel has a high life expectancy of 200+ years and needs clean, summer-cool waters with high oxygen and low nutrient and Ca contents. It requires for its parasitic glochidial (larval) stage a host fish that is exclusively of the genus *Salmo*, in central Europe it is the brown trout (*Salmo trutta fario*) and in western and northern Europe it is the Atlantic salmon (*Salmo salar*).



Figure 1. The map shows the main rivers and former pearling centres in Karelia and on the Kola Peninsula in North Western Russia.
Source: *The Journal of Gemmology*, 34(7), 2015, p. 585.

Originally, the pearl mussel occurred in a wide area of north-western Russia that stretched from Lithuania in the west to the slopes of the Ural Mountains in the east and from the tributaries of the Don and Volga Rivers in the south to the White Sea in the north. The mussels formerly were especially abundant in rivers and streams flowing into the White Sea

(Figure 1). Today, large populations of ca. 6 and ca. 140 million mussels, respectively, remain only in the Keret River in Karelia and the Varzuga River on the Kola Peninsula (Makhrov et al., 2014). In 1985, harvesting of pearl mussels was completely prohibited and today the species is listed as endangered in the *Red Data Book of the Russian Federation* (Strack, 2015).

The history of pearl usage in Russia

The use of freshwater pearls for decoration and adornment in north-western Russia goes back to the Middle Ages. Pearls came into fashion towards the end of the 18th century, and this lasted until the end of the Russian empire under the Romanoff dynasty in 1917 (Korago, 1981). Traditional festive dresses were embroidered with pearls which also were used to embellish kokoshniks, often in combination with pearl necklaces and pearl earrings. Since the 10th century, pearls were used in the Russian Orthodox Church for embroidering chasubles and antependia and for decorating chalices, book covers, crosses, mitres and icons

Pearling centres developed along the Dvina River near the city of Arkhangelsk, on the Keret and Kem Rivers in Karelia and on the Kola Peninsula, particularly near the Umba and Varzuga Rivers (Figure 1). Apart from the villages, where local women did the craftwork, professional workshops opened up in some cities. The city of Kem, founded in 1783 and situated on the White Sea was important, as was the small city of Olonez, capital of a governorate with the same name, situated near Lake Ladoga (Figure 1).

The first two decades of the Soviet era (1922-1991) saw a decline that went hand in hand with a decline in mussel populations due to pollution by various industries. Moreover, the new political system led to an increasing lack of interest as those who had appreciated pearls in the past no longer existed and the Church had lost its function. Interest in pearls decreased further in the decades after World War II.

Field Research

The Russian Museum of Ethnography in St Petersburg hosts today the most exquisite collection of pearl works, followed by the Armoury Chamber of the Kremlin in Moscow, which focuses on ecclesiastical treasures. Both collections were visited in 1998.

In order to get further on-site information, several visits in 2001, 2006 and 2008 to the former pearling centres in Karelia (Keret Village, Kem, Olonez, Petrosavodsk and Arkhangelsk) and on the Kola Peninsula (Umba village, Varzuga and Kuzomen village) served to conduct interviews with local government, museum and church authorities and fisheries biologists. A number of elderly village citizens were also included. All those interviewed agreed that pearls were an item of the past, knowledge of which had disappeared in the Soviet era. Only rumours had remained of a pearl find made by a government delegation in 1974.

The small town of Umba and the city of Kem both host a museum on the history of pearling and both museums own a 19th century kokoshnik each, while museums in Pedrosawodsk and Arkhangelsk have only collections of shells of *Margaritifera* species.

Three loose 20th century pearls from the Varzuga River were made available by Valery Ziuganov, a fisheries biologist who had worked at the salmon station in Varzuga village.

The Pearls – testing results

The kokoshnik at the Umba museum was examined on-site with the aid of a 10x lens and a UV-Lamp (366nm and 254nm), the small pearls could be identified as imitation pearls while the off-round pearls in sizes of up to 7mm, arranged in rosettes, are freshwater pearls (Figure 2).



Figure 2. This late 19th century kokoshnik is embroidered with small imitation pearls, together with larger Russian freshwater pearls, in sizes up to 7mm and off-round shapes. Courtesy of the Museum of History, Culture and Life of Tersky Pomors, Umba. Photo by E. Strack.

Several pearl items (a selection of earrings and necklaces, a kokoshnik and a belt) kept at the Ethnographic Museum in St. Petersburg, were examined on-site in 1998, with the help of a UV-lamp and an optical microscope (magnification up to 80x). Pearl sizes range on average from 1-4mm, going up to 9mm, colours go from white to light „cream“ to light grey, a few pearls showed brown colours. Shapes included off-round, flat, barrel, button and baroque, flat areas often showed a wrinkled growth pattern and lustre is generally dull (Figure 3).



Figure 3. These earrings containing Russian freshwater pearls (5-6mm in diameter) are dated to the late 19th century. Courtesy of The Russian Museum of Ethnography, St. Petersburg. Photo by E. Strack.



Figure 4. The figure shows three pearls from Varzuga River, dating from the 20th century. From left to right: Barrel shape, 2.68 ct., 7.08 x 6.77 x 6.72mm - Drop shape, 1.28 ct., 10.96 x 4.82 x 4.40mm - Intergrowth of three pearls, 1.83 ct., 3.18mm/3.77mm/5.62mm each - Photos by E. Strack.

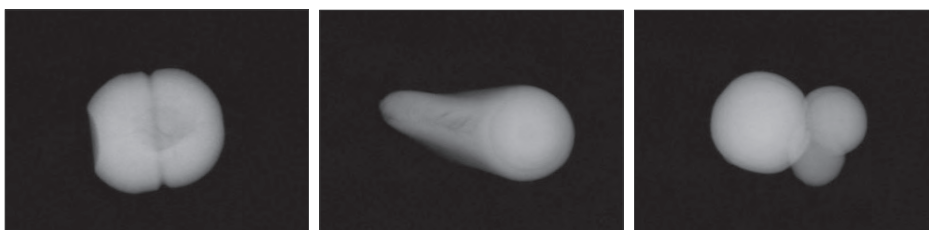


Figure 5. Radiographs of three pearls shown in Figure 4. They reveal irregular areas of organic substance that appear dark (left and centre pearl) and linear deposits of organic material just underneath the outer rim (bulb of centre pearl and triple pearls on the right). Radiographs by E. Strack.

The three loose pearls from the Varzuga River have barrel, drop and intergrown shapes, weighing 2.68 ct., 1.27 ct. and 1.83 ct. each. Measurements are in the range of 3-10mm, and colours are mainly greyish-brown with purplish tinges (Figure 4). Radiographs taken with a Kodak 2200 digital X-ray system (60-70 KV, 49 W), showed irregular and linear deposits of organic substance (Figure 5).

Conclusion

The European freshwater pearl mussel *Margaritifera margaritifera* has largely disappeared from its original distribution area in north-western Russia, only the Varzuga and Keret Rivers still hold large stocks. Listed as endangered in the IUCN Red List since 1996, fishing of the pearl mussel is prohibited in Russia since 1985. Moreover, field research has shown that local knowledge of pearls has waned in the decades since 1917, it is practically non-existent.

The limited number of pearl items available for study included 18th - 19th century objects from museums in St. Petersburg and Umba and three loose pearls from the Varzuga River, collected in the 20th century. Pearl sizes go from ca. 1 to 11mm, colours range from white to grey, some brownish hues are also present. Shapes include off-round, barrel, button and baroque, a wrinkled growth pattern on flat surfaces is characteristic. X-radiography of three loose 20th century pearls revealed irregular and linear deposits of organic substance.

References

- Bespalaya, Yu.V. et al., 2012. Historical geography of pearl fishing in rivers of the southern White Sea region (Arkhangelsk Oblast). *Regional Research of Russia*, 2 (2), 172-181.
- Kaliuzhin, S.M., 2004. *Atlantitscheskii Losos Belewo Moria (The Atlantic Salmon of the White Sea Basin)*. Petropress, Petrosawodsk, Russia, 263 pp.
- Korago, A.A., 1981. *Retschnoi Tschemtschug (Freshwater Pearls)*. Nedra Publishing House, St. Petersburg, Russia, 120 pp.
- Makhrov, A. et al., 2014. Historical geography of pearl harvesting and current status of populations of freshwater pearl mussel *Margaritifera margaritifera* (L.) in the western part of northern European Russia. *Hydrobiologia*, 735 (1), 149-159.
- Popov I.Yu., Ostrovsky A.N., 2014. Survival and extinction of the southern populations of freshwater pearl mussel *Margaritifera margaritifera* in Russia (Leningradskaya and Novgorodskaya oblast). *Hydrobiologia*, 735 (1), 161-177.
- Reis J., 2003. The freshwater pearl mussel [*Margaritifera margaritifera* (L.)] (Bivalvia Unionoida) rediscovered in Portugal and threats to its survival. *Biological Conservation*, 114 (3), 447-452.
- Srepodolski B.I., 1985. *Tschemtschug [Pearls]*. Nauka, Moscow, Russia, 136 pp.
- Strack E., 2006. *Pearls*. Rühle-Diebener-Verlag GmbH, Stuttgart, 696 pp.
- Strack E., 2015. European Freshwater Pearls: Part 1-Russia. *The Journal of Gemmology*, 34 (7), 580-592.

Acknowledgements

The author thanks Dr. V.Ziuganov (Inst. of Biology, Russ. Academy of Sciences, Moscow), S.M. Kaliuzhin (Varzuga Fisheries Cooperative), S.P. Kitaev (Inst. of Biology, Russ. Academy of Sciences, Pedrosavodsk), Mitrofan Badanin (Bishop of Severomorsk and Uмба), A. Radnikova and Dr. Dimitri Baranov (The Russian Museum of Ethnography, St. Petersburg).

Feather and Insect inclusions in Burmese amber and its impact on origin determination

Liu Shang I, Edward

The Gemmological Association of Hong Kong, Hong Kong SAR, PRC. gemedward@hotmail.com

Introduction

Burmese amber (also called burmite) seems to become more popular in the market. Since its age has been reinvestigated and proved to late Cretaceous by Cruickshank and Ko (2003) and Shi et al. (2012), many new discoveries in paleontology on its inclusions were published in recent years. Although some spectroscopic studies have been reported by Shi (2015) and Tay (2015), few works have been done on its gemmological microscopic study. Grimaldi et al., (2002, 2010) discovered that Burmese amber preserves the most diverse Cretaceous paleofauna in amber relative to other Cretaceous amber deposits in Lebanon, France, New Jersey (USA), Siberia (Russia), and Canada (Poinar & Milki, 2001). Insect inclusions in amber can be used for its age and origin determination. After examining more than 3000 pieces of Burmese amber with insects with the use of gemmological microscope and comparing the data (insect taxa) of other major amber deposits, the presence of dinosaur feathers, ancient ants, some distinct insect species and other extinct cretaceous insect inclusions may help, to a certain extent, to characterize Burmese amber.

All specimens were obtained from two main amber deposits in the Hukawng Valley of Myanmar – Zee Phyu Gone mine in Noije Bum (Grimaldi et al., 2002; Cruickshank & Ko, 2003) and Aung Bar mine near Tanai.

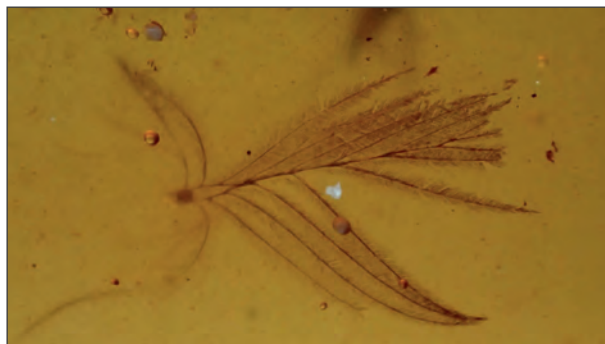


Figure 1. Feather inclusion displays a clear structure of barbs and barbules with poorly defined rachis.

Dinosaur feather

Two amber specimens with bird feathers and three specimens with dinosaur feathers are found from Aung Bar mine in this study. They are all transparent and honey yellow in color. The dinosaur feathers are characterized by lacking of clear central shaft (rachis) and three tiers of branching structure of flight feather of birds (Figure 1) (Xing, 2016).

Haidomyrmex & Ceratomyrmex (Unicorn ants)

In Burmese amber, ants are exceedingly rare and highly unusual. It only comprises approximately 0.2% of all insect inclusions (Grimaldi et al, 2002; Grimaldi & Nascimbene, 2010). Haidomyrmex is one of the extinct genera of Cretaceous ants in the tribe Haidomyrmecini. This genus contains three distinct species Haidomyrmex Cerberus (Dlussky, 1996) Haidomyrmex scimitarus, and Haidomyrmex zigrasi (Barden & Grimaldi, 2012). All of them were discovered as inclusions in Burmese amber. However, Haidomyrmex scimitarus is the only species that has been found in Myanmar. Haidomyrmex was described as a specialized solitary trap-jaw predator which has a pair of long scythe to L-shaped mandibles displaying in vertical-plane movement (Dlussky & Grimaldi, 1996; Barden & Grimaldi, 2012).

In 2013, Perrichot (2016) discovered a new extinct unicorn ant called *Ceratomyrmex ellenbergeri* in Burmese amber. This genus belongs to the Haidomyrmecini, with an oversized mandibles and a long extreme modified clypeus (horn) (Figure 2A). During the study of unicorn ants from Burmese amber, we discovered two other special “species” with clear morphological variation with shared characters of scythe-like mandible and wings (reproductive ants) from eleven Haidomyrmecini samples. One of them displays a large round flat setose lobe at the clypeus apex (Figure 2B) and the other has a relatively short clypeal horn with an extra horn coming out behind the scapes (Figure 2C). It is believed that they are new species of *Ceratomyrmex* (pers. comm. Wong, 2017).

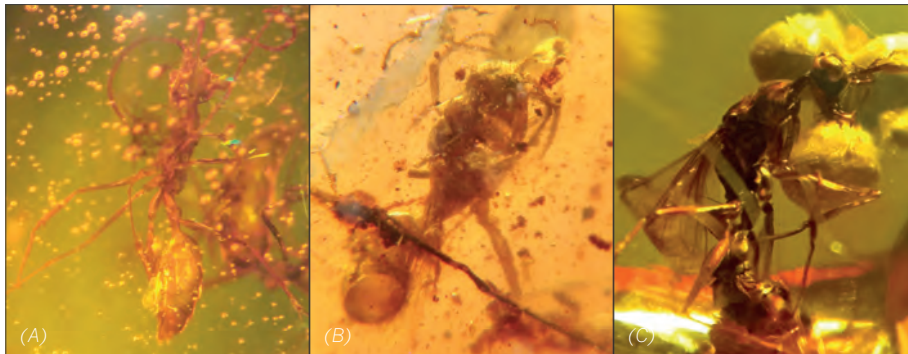


Figure 2. (A) New worker ant *Ceratomyrmex ellenbergeri*
(B)(C) Two newly discovered reproductive ant species of *Ceratomyrmex*

Coccoidea (Scale insects)

Scale insects (Ortheziidae family) have long been discovered as common inclusions in Burmese amber (Grimald et al, 2002). Few of them have been found in Baltic amber. Most scale insects are characterized by its oval shape body with six dark coloured legs and a pair of dark antennae (Figure 3). They can produce a special “scale cover” made of waxy secretion in twenty-four (twelve pairs) radiated thin and long strips which can be used to resemble flower and protect their bodies. Rounded 2-phase (liquid and gas bubble) inclusions are commonly found around them especially at the end of the waxy strips.

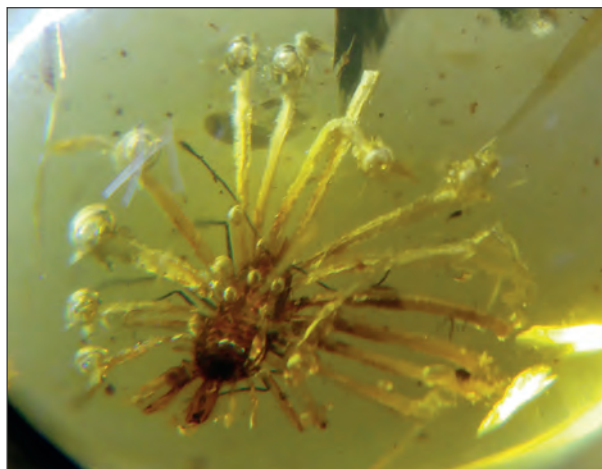


Figure 3. Scale insect inclusion

Other special extinct insects - Alienoptera, Aethiocarenodea, “Carnivorous cricket”

Alienopterus brachyelytrus is an extinct species of Alienoptera (a new created insect order) in the roach-mantis transition zone (Bai et al., 2016). It has characters that showing a mixture of cockroaches and mantis. It has shortened forewings with long and fully developed operational hindwings (Figure 4A). *Aethiocarenum burmanicus* is an extinct sole species of the newly created order Aethiocarenodea (Poinar & Brown, 2017). It has a typical triangular head with big bulging eyes which resemble alien, long neck and long flat body with very thin legs (Figure 4B). “Carnivorous cricket” is a newly discovered extinct insect which possess roach head with a cricket body. It has a pair of big compound eyes and long antennae, two powerful hind legs with all femurs and tibiae are armed with spurs (Figure 4C). It has only been found as inclusion in Burmese amber. No detailed research has been reported on it before.

Conclusion

Burmese amber was formed under special paleoenvironment that was probably more tropical than any other major deposit of Cretaceous amber (Grimaldi et al, 2002). It harbors the most diverse biota in amber from Cretaceous now known. Many distinct tropical taxa like scorpions, centipedes, millipedes and Coccoidea are relatively common in Burmese amber. However, temperate taxa likes Aphidoidea is rare.



Figure 4. Special extinct insect of (A) Alienoptera, (B) Aethiocarenodea and (C) “Carnivorous cricket”

References

- Bai M. et al., 2016. Alienoptera — A new insect order in the roach–mantodean twilight zone, *Gondwana Research*, 39, 317–326.
- Cruickshank, R. D., Ko, K., 2003. Geology of an amber locality in the Hukawng Valley, Northern Myanmar. *Journal of Asian Earth Sciences*, 21, 441–455.
- Dlussky G.M., Grimaldi D., 1996. Ants (Hymenoptera: Formicidae) from Burmese amber. *Paleontological Journal*, 30(4), 449-454.
- Grimaldi D.A., Engel M.S., Nascimbene P.C., 2002. Fossiliferous Cretaceous Amber from Myanmar (Burma): Its Rediscovery, Biotic Diversity, and Paleontological Significance. *American Museum Novitates* 3361, 1-71.
- Grimaldi, D.A., Nascimbene P.C., 2010. Raritan (New Jersey) amber. In: Penney, D. (Ed.), *Biodiversity of Fossils in Amber from the Major World Deposits*, 167–191, Siri Scientific Press, 304pp.
- Perrichot V., Wang B., Engel M.S., (2016). Extreme Morphogenesis and Ecological Specialization among Cretaceous Basal Ants. *Current Biology*, 26 (11), 1468–1472.
- Poinar G., Brown A.E., 2017. An exotic insect *Aethiocarenum burmanicus* gen. et sp. nov. (*Aethiocarenodea* ord. nov., *Aethiocareniidae* fam. nov.) from mid-Cretaceous Myanmar amber. *Cretaceous Research*, 72, 100–104.
- Poinar G., Milki R., 2001. *Lebanese Amber: The Oldest Insect Ecosystem in Fossilized Resin*. Oregon State University Press, 96pp.
- Shi G., Grimaldi D.A., Harlow G.E. et al., 2012. Age constraint on Burmese amber based on U-Pb dating of zircons. *Cretaceous Research*, 37, 155-163.
- Shi G. et al., 2015. Infrared spectral characteristics of ambers from three main sources (Baltic Sea, Dominican Republic and Myanmar) and their implications. *Proceeding of IGC 2015*, 152-153.
- Tay T.S. et al., 2015 Burmese amber from Hti Lin. *Proceeding of IGC 2015*, 26-29.
- Wang B, pers. Comm., 2017. In the process of finishing his paleontological research paper on *Haidomyrmex* & *Ceratomyrmex* in Burmese amber.
- Xing L. et al., 2016. A Feathered Dinosaur Tail with Primitive Plumage Trapped in Mid-Cretaceous Amber. *Current Biology*, 26 (24), 3352–3360.

Ammolite, Canada's Unique Fossil Gemstone

Willow Wight

Canadian Museum of Nature, Ottawa, Canada, wwight@mus-nature.ca

Introduction

Ammolite from Alberta, Canada, has been used as a gemstone since the late 1960s, but it became a commercial success for Korite Minerals Ltd. of Calgary, Alberta, in the early 1980s. The iridescent fossil shell material occurred in significant quantities near Lethbridge, Alberta, though most was buried too deeply (~120 m) for easy extraction. Fortunately, Korite Minerals was able to open a quarry in a more accessible area adjacent to the St. Mary River (Figure 1), from which it produced both ammonite fossils of interest to palaeontologists, and broken pieces of fossil shell showing bright and attractive iridescent colours ranging from red to green and sometimes blue.

A few lapidaries knew of the iridescent shell in the 1960s. For several years, Thomas McArthur marketed a triplet featuring a thin slice of the ammonite shell as "Calcentine", named in honour of Calgary's Centennial in 1975. When Korite Minerals began mining in the late 1970s, they first called their polished material "Korite". In 1981, CIBJO approved the name "Ammolite". (Wight, 1981; Vandervelde, 1993; Wight, Q., 1993). Depending on the stability of the rough shell, Korite produces some doublets, but mostly triplets, with a colourless synthetic spinel cap as protection for use in jewellery.



Figure 1. The original Korite Minerals diggings, St. Mary River Valley, SW of Lethbridge, Alberta, 1992. Photo: Q. Wight.



Figure 2. The Canada 150 Logo design executed as a pendant featuring Ammolite by Korite Minerals (www.korite.com). The Canada 150 Logo is built from four-sided "kite" shapes positioned to form Canada's iconic Maple Leaf symbol.

Canada's 150th Anniversary

The year 2017 is the 150th anniversary of the Confederation of Canada, and the Federal Government has chosen a number of Canadian companies as official suppliers of souvenir items. Among them is Korite Minerals, who have introduced official souvenir jewellery featuring ammolite, including a special Maple Leaf design pin and pendant. This is appropriate, since ammolite is the official gemstone of Alberta, and other than nephrite jade and diamond, the only commercial Canadian gemstone (Figure 2).



Figure 3. Thin layers of whitish bentonite in the Bearpaw Formation are visible in cliffs along the St. Mary River Valley. Photo: Q. Wight.

Ammonites

Ammonites are extinct molluscs of the class Cephalopoda, subclass Ammonoidea. Ammonites were numerous in the Western Interior Seaway that covered much of the western United States and Canada during the Late Cretaceous Age (about 70-75 million years ago), late in the age of the dinosaurs. During that time, shells of deceased ammonites were buried by layers of marine sediments made up of dark grey clays, claystones, shales, silts, sandstones and bentonite (Figure 3) —now known as the Bearpaw Formation. The ammonites discussed below are found in sediments of both onshore and offshore zones of the Seaway. The bentonite, a silicic clay derived from volcanic ash, occurs in thin layers throughout. It stabilized the aragonite in the shells, preventing it from converting into the more common calcite (Mychaluk, et al, 2001).

The Alberta ammonites providing the gem material are *Placenticerus meeki* (Figure 4). Found in specific layers in the shale, the average specimen is 20-25 cm in diameter, with shell thickness less than 6 mm. Another smaller and rarer species, *Placenticerus intercalare*, also provides iridescent shell (Figure 5).



Figure 4. René Vandervelde, founding president of Korite Minerals Ltd., with a fine ammonite specimen (*Placenticerus meeki*), Tucson, 1992. Photo: W. Wight. - Figure 5. Ammonite specimen (*Placenticerus intercalare*) displayed by Korite Minerals, Canadian Gemmological Association Conference, Vancouver, 2007. Photo: W. Wight.

Ammonites showing some iridescence in their shells are found in other parts of the world, notably Madagascar, Russia, and South Dakota, USA. They are of different species and of different geological ages. When compared to the iridescent ammonites from the Bearpaw Formation, however, these materials typically have weak and patchy iridescence, and a shell layer that is too thin and fragile to be used in jewellery. The ammonites themselves are often used as decorative objects, and many are polished on the surface to enhance their iridescence. Such is the *Cleoniceras sp.* ammonite from Madagascar, Middle Cretaceous (100-113 million years old). Cabochons have been made rarely from *Craspedodiscus sp.* ammonite shell from the Volga river area, Ulyanovsk region, Russia (~153 million years old).

Ammonite Shell Structure

The nacreous layer of an ammonite shell is composed of closely packed, microscopic crystals of tabular aragonite in an organic matrix (conchiolin), resulting in essentially a “brick-wall” structure in three dimensions (Wight, 1981). The thickness of the horizontal layers is of the same order of magnitude as the wavelengths of the visible spectrum. When white light hits ammonite’s regularly spaced thin layers, it produces flashes of colours, the result of constructive interference as the white light passes through and diffracts back from multiple layers of uniform thickness. This effect is comparable to that seen with modern pearl shells. The *Nautilus*, which is considered a modern relative of the ammonites, has a similar nacreous layer with tabular aragonite microcrystals.

Types of Ammolite

Researchers have divided the Bearpaw Formation into zones, each identified by a numeric or alphabetic designator, which help identify the provenance of different types of ammonites. The original Ammolite showed small iridescent zones of one colour separated by thin “healed” fractures (“stained-glass” window effect). This fractured material (type 1) was found in concretions in the K Zone, close to the centre of the Bearpaw Formation. The shell of the ammonite was crushed and rehealed during ~70 million years of natural geological processes (Figures 6, 7). Sheet material (type 2) has not been fractured, and can exhibit larger flat areas of uniform colour called colour panes. Sheet Ammolite tends to have stronger iridescence and more areas of blue colour than the fractured material, and is often more popular with buyers. Most type 2 is found in Zone 4, which is closer to the bottom of the Bearpaw. As reported by Mychaluk, 2009, the Ammolite being mined has changed over the years from predominantly fractured to sheet type as more extraction has been done from Zone 4.



Figure 6. Concretion from K Zone of Bearpaw Formation, typically containing fractured (type 1) Ammolite. Photo: Q. Wight.



Figure 7. Both sides of a fine example of a double-sided, Ammolite (shell on both sides with a very thin layer of shale in between) (CMNGE 22088, 11.40 ct, 22.9 x 16.8 x 2.7 mm). This is fractured (type 1) Ammolite typically found in concretions such as shown Figure 6. Photos: W. Wight.

New Developments at Korite Minerals (See Korite website: < www.korite.com>)

The company changed hands in 2016, and the new management has been busy expanding production and marketing of Ammolite and Ammolite jewellery. They recently signed a deal with China's Mahasida Jewelry, which will ensure distribution of its ammolite jewellery to the China market. Ammolite has long had a special appeal in Asia because of its recognition by *feng shui* masters, who believe the gemstone's many colours signify good luck and prosperity. At the Tucson Gem and Mineral Show in 2016, Canada Fossils (Korite's sister company) exhibited many examples of complete ammonites suitable for decorative uses (Figure 8). In Canada we expect brisk sales of Canada's 150th birthday jewellery designs. The new abundance of sheet Ammolite is very appropriate in this regard.

To support this new activity, Korite recently completed a significant expansion of their mine south of Lethbridge, increasing it in size from two to eight acres. That should allow for an increase in annual production of ammolite gems from six million carats in 2016 to eight million carats in 2017. They plan further development to meet the growing demand for this unique phenomenal material that they offer as "one of the rarest gemstones in the world".

References

Korite Minerals website < <http://www.korite.com>>

Mychaluk, K.A., Levinson, A.A., Hall, R.L. 2001. Ammolite: iridescent fossilized ammonite from southern Alberta, Canada. *Gems & gemology*, 37(1), 4–25.

Mychaluk, K.A. 2009. Update on Ammolite production from southern Alberta, Canada. *Gems & Gemology*, 45(3), 192–196.

Paré, P. 2007. Ammolite: birth of a gem. *Canadian Gemmologist*, 28(1), 12-19.

Vandervelde R. 1993. Ammolite, an organic gemstone from Alberta. *Canadian Gemmologist*, 14(2), 53–57.

Wight Q. 1993. Canadian Ammolite—The high, dry sea floor yields opal-like material. *Rock & Gem*, 23(12), 42, 43, 45–47.

Wight W. 1981. "Korite"—Fossil Ammonite shell from Alberta, Canada. *Journal of Gemmology*, 17(6), 406–415.

Acknowledgements

The author thanks Quintin Wight, Ottawa; Karen Fox, Waterloo; and her very helpful colleagues at the Canadian Museum of Nature for their continuing support.

A gemstone occurrence map for Greenland

Anette Juul-Nielsen, Arent Heilmann

Department of Geology, Ministry of Mineral Resources, Government of Greenland, Imaneq 1A – 201, P. O. Box 930, 3900 Nuuk, Greenland; anjn@nanoq.gl

Introduction

Publications on, and in-depth knowledge about, Greenlandic gemstone occurrences are scarce. Historically, exploration companies have focused on exploration for metals and other minerals over gemstones, which has in turn directed public research funds toward projects related to, for example, iron ore, lead-zinc, REE deposits etc. An exception to this is the “diamond rush” in West Greenland in the 1990’s triggered by the diamond finds in Canada.

Consequently, a Greenland mineral occurrence database and interactive map (greenmin.gl) was launched in 2005 based on known mineral occurrences. Diamond, ruby, sapphirine and tourmaline occurrences were the only gemstone occurrences featured in the database. The recent increased interest in exploring for gemstones in Greenland has generated a need for delivering free and easy online access to occurrence information for other types of gemstones for the use of gemstone exploration companies and small scale miners.

In 2015 the Department of Geology initiated a project to create a database of gemstone occurrences; including field work follow-up’s starting in summer 2016 with the Maniitsoq and Fiskefjorden area (Figure 1).

Method

A large literature compilation was made based on registrations dating back to the early 1800s, e.g. Giesecke (1878), Bøggild (1953), Petersen & Secher (1993), Appel & Ghisler (2014), and a new database structure was set up to fit the existing mineral occurrence database, www.greenmin.gl. Data entries include information about type of gemstone, host rock, location, gemstone characteristics and references. Focus was primarily on West Greenland, where the data could be directly used in connection with a larger mapping project in the Maniitsoq area with the aim of generating a geological map at 1:100 000 scale and to map the gemstone occurrences.

The first season of field work was carried out in the Maniitsoq and Fiskefjorden area in summer 2016, where 29 localities were visited by boat and reference samples were taken. The known gemstone occurrences were visited to gain new information about the occurrences and in particular the gemstone characteristics. Areas with potential for hosting gemstones were also investigated and documented.

Based on the database entries, a gemstone occurrence map was generated in Arc-GIS.

Gemstone occurrence database

The literature compilation revealed that most of the information on the gemstone occurrences was related to host rock descriptions while gemstone characteristics and size were seldom mentioned. The new gemstone occurrence map (Figure 1) shows that known gemstone occurrences are concentrated around the more populated areas in West Greenland and South Greenland, where local knowledge of occurrences are abundant and where much exploration and research has taken place. As a consequence of this, the database was, and is, far from complete and only in its very early stages. There is a need for follow-up visits to the gemstone occurrences where information is lacking to generate up to date locality descriptions. Additionally, a new registering guideline for government geologists encountering gemstones in the field needs to be developed to allow for more detailed gemstone occurrence descriptions in the future.

To date, about 300 gemstone occurrences have been registered in the gemstone occurrence database and new data will be added continuously, based on further literature search and field mapping.



Figure 1. The new gemstone occurrence map of Greenland, showing location of the major cities.

Mapping gemstones in the field

The first follow-up field visits were made in summer 2016, where we visited known gemstone occurrences in the Maniitsoq and Fiskefjorden area (Figure 2). Selection of these occurrences was primarily based on the information within the gemstone occurrence database.

The different types of gemstone occurrences included ruby, tourmaline, sphene, sapphirine, diopside, labradorite, garnet, microcline, moonstone, kyanite and scapolite. In addition to the known occurrences, other areas were targeted based on geological environment; primarily areas with ultramafic rocks in proximity to metasedimentary rocks, pegmatites or anorthosites.

The gemstones found were generally either very small or not of good gem quality. However, suitable geological environments are present in the Maniitsoq and Fiskefjorden area and gemstones do occur, indicating that there is a potential for finding gem-quality gemstones; especially the potential for ruby and labradorite seems promising. Labradorite was found on many of the visited localities in the Maniitsoq and Fiskefjorden area. Some of the gemstone localities could be used for geotourism.



Figure 2. Geological map of the Maniitsoq and Fiskefjorden area with visited localities (red dots), modified after the 1:500,000 scale digital geological map of Greenland (Pedersen et al., 2003; greenmin.gl). Pale yellow: Gneiss. Pink: Granodiorite. Green: Amphibolite. Brown: Metasedimentary rocks. Dark Blue: Metanorite. Turquoise: Carbonatite. Grey: Anorthosite.



Figure 3. Field work at Kangerdluarsuk, Maniitsoq in August 2016.

Conclusions

Generating a gemstone database is an ongoing process where new data is added continuously. Generally it is difficult from the descriptions in the publications alone to obtain all relevant information about the occurrences, such as size and quality of the gemstones. Most of the localities need to be re-visited, both for confirmation of the locations and for characterization of the sites. This is a huge and expensive task, but is achievable if done in connection with other field work. Though the field work in 2016 did not give that many promising results with regards to gemstone exploration, there is gemstone potential based on both known occurrences and geological environments; especially for ruby and labradorite. Also geotourism has potential.

The gemstone database, used in combination with geological maps, has proved to be a useful tool for mapping gemstones, and has already provided us with new target areas to follow up upon; e.g. sapphire in basalts in the Disko Bay area, which will be investigated in 2017. Hopefully the information from the gemstone database and occurrence map will not only benefit the gemstone industry in Greenland, but also give us a better understanding of the geological environments in which these gemstones are found.

References

Appel, P. W., Ghisler, M., 2014. Ruby- and sapphirine-bearing mineral occurrences in the Fiskenaeset, Nuuk and Maanitsoq Regions, West Greenland. Danmarks og Grønlands Geologiske Undersøgelse Rapport 2014/72, 71 pp.

Bøggild, O. B., 1953. The Mineralogy of Greenland, Meddelelser om Grønland, Bd. 149, nr. 3.

Giesecke, K. L., 1878. Karl Ludwig Gieseckes Mineralogiske Rejse i Grønland, ved F. Johnstrup: Med et Tillæg om de grønlandske Stednavnes Retskrivning og Etymologi af H. Rink, København, pp. 372.

Ghisler, M., 1990. Geographical subdivision of Greenland. Rapport Grønlands Geologiske Undersøgelse, 148, p. 8-10.

Pedersen M., Weng W.L., Keulen N., Kokfelt, T.F., 2013. A new seamless digital 1:500 000 scale geological map of Greenland. Geological Survey of Denmark and Greenland Bulletin 28, p. 65–68.

Petersen, O. V., Secher, K., 1993. The minerals of Greenland. The Mineralogical Record, March-April 1993, Vol. 24, no. 2, 65 pp.

Acknowledgements

The authors would like to thank Walter A. Balmer (SSEF Swiss Gemmological Institute, Switzerland) for taking part in the field work as well as Julie Hollis (Ministry of Industry and Mineral Resources, Greenland) for helpful suggestions and Jan Schulz Adolfsen (Ministry of Industry and Mineral Resources, Greenland) for ArcGIS-assistance.

Imitations of Tianhuang and Shoushan stones

Stephen Kennedy¹, Jens Najorka²

¹Gem & Pearl Laboratory, Unit 23, 43 Kirby Street, London EC1N 8TE info@thegemlab.co.uk

²X-ray Laboratory, Natural History Museum, Cromwell Road, London SW7 5BD j.najorka@nhm.ac.uk

The challenge from an eBay dealer was whether a collection of twelve orange emperor seals could be determined to be Tianhuang stones. In the event these were returned to the seller without the need for testing to obtain his refund. However, interest had been piqued and the gentleman concerned was asked if he could bring some other carvings into the Gem Laboratory. He was of the belief that the yellow stones were Tianhuang stones and the darker orange, green and brown stones were Shoushan stones.

A yellow seal carving (Figure 1) and an orange seal carving (Figure 2) were selected as examples of a 'Tianhuang stone' and a 'Shoushan stone' from which to take powder scrapings for X-ray powder diffraction analyses. Another carving stood out as having heavily dyed green areas.

The second author analysed the two powders on a Panalytical X'Pert Pro X-ray diffractometer. He carried out two types of measurement to better reveal the nature of the materials and to be more certain about clay mineral assignments. The first being in transmission mode using a mount with more randomly oriented powder grains, which is suitable for identifying the overall mineralogy. The second in reflection mode using an oriented mount, (with and without ethylene glycol), which is more suitable for identifying and distinguishing clay minerals.

In transmission mode the minerals present were identified as chlorite for the 'Tianhuang stone' and chlorite with some talc for the "Shoushan stone'. In reflection mode both the 'Tianhuang stone' and the "Shoushan stone' revealed two types of chlorite with some talc. In reflection mode the presence of other clay minerals such as illite, smectite, kaolinite, and nacrite, can be excluded.

The two types of chlorite show differences in the unit cell parameter c ($c_{\text{chlorite1}}$ 14.2 Å, $c_{\text{chlorite2}}$ 14.3 Å) but no clear differences in unit cell parameters a and b . It is known that substitution of Al for Si, Mg and Fe in chlorite decreases the c parameter (Deer et al. 1992).



Figure 1. 'Tianhuang stone'

Figure 2. 'Shoushan Stone'

It can be concluded that the two chlorites have different compositions (chlorite1 Al high, chlorite2 Al low). The presence of two types of chlorite in a rock is unusual, but not unknown. It more likely points to the possible artificial combination of differing chlorites.

The 'Shoushan stone' powder was white but the "Tianhuang stone" powder was yellow in colour, whereas chlorite or talc powder is white, reflected by the fact the streak of even green chlorite is white. It seemed likely that a yellow pigment had been used to give the yellow colour to the 'Tianhuang stone'. The yellow colour could not be attributed to any crystalline component and there was no time to obtain further material to determine the composition of the dye. The problem from the outset for both authors was what was Tianhuang stone and Shoushan stone. Searches on the internet reveal valuable items that have come up for sale at Christies, Sothebys, Bonhams and smaller auction houses, where the value is related more to the provenance rather than their composition. Not surprisingly most research on the stones has been carried out in China.

Shoushan stones are named after the river and village of the same name in Fujian Province, China. Agalmatolite is used as an older cover all term. There are supposedly over 100 varieties of Shoushan stone with different structures and appearance. Shoushan Stone is postulated to have formed through the replacement of volcanic rock by hydrothermal solutions which were derived from the volcanic rock itself and migrated along faults or shatter zones after the eruption of acid volcanic rock in the late Jurassic period. Shoushan stones have been subdivided according to their major compositions as nacrite-type, dickite-type, illite-type, sericite-type, and pyrophyllite-type (Zou Tian-ren et al, 2010) There seems a consensus that Tianhuang stones, originally sourced from the Bantian Gravel Bed, Shoushan, Fujian Province are predominantly composed of nacrite and dickite with some illite. The dickite can be present as a colourless surface layer, which is highly desirable (Ren Leifu, 1988). However nacrite has also been found in Jimuwo stone, a so-called ordinary Shoushan stone although it is not specified if it is to a minor or major degree (Li Yujuan, 2005). It seems clear that identifying an original Shoushan or Tianhuang stone is problematic but the mineral components provide a starting point in recognizing imitations of these natural carving materials. It is proposed that similarly composed materials with presumably similar appearance could be called Shoushan or Tianhuang even if they are from other areas (Zou Tian-ren et al, 2010).

The imitations of Tianhuang and Shoushan stones appear to be in more abundance than natural materials. A Shoushan stone called larderite (area 30 km from Fuzhou) was found to consist of gypsum and calcined gypsum, and was considered to be an imitation as dickite, nacrite, pyrophyllite, and illite were not found (Liang Bao-yu et al, 2012). A Tianhuang stone was found to consist of pyrophyllite with a lead-glass coating. So at best a coated Shoushan stone (Li Jian-jun et al, 2010). A yellow to brownish yellow Tianhuang stone was found to consist of Clinoclhorite (or Clinochlor) (Pan Xiao-qing, 2011). The variety of imitations probably matches the variety of the natural rocks involved.

As with all ornamental materials the experience of seeing known natural materials is vital. In the absence of such experience it is still fair to conclude both carvings are imitations as they consist of chlorite, which is not a component attributed to either Tianhuang or Shoushan stones. The presence of a yellow colourant to the 'Tianhuang stone' powder is an additional confirmation. The structures of both figures is a very even cloudy structure, which is different to the claimed much more mottled iron-stained nature of the natural rocks. Collectors of tianhuang stone refer to 'radish lines' and 'red line' as structures to look out for. But even these can be imitated (Pan Xiao-qing, 2011) and red lines were noticed in our Tianhuang imitation.

References

Deer, W. A., Howie, R.A., Zussman, J., 1992. An Introduction to the Rock Forming Minerals. 2nd ed., Addison Wesley Longman Limited, p 334.

Liang Bao-yu, Yu Wan-li, Cao Yuan-yuan, Luo Yong-an, Dong Huan, Wang Jia-sheng, 2012. Study on Gemmological Characteristics of a Kind of Imitated Larderite, *Journal of Gems & Gemmology*, 2012-02.

LI Jian-jun, Wang Yue, Li Ting, Liu Hua-feng, 2010. Identification of an imitation of the yellow Tianhuang stone covered by chalkiness, *Superhard Material Engineering*, 2010-05.

Li Yujuan, 2005. On the Mineral Constituent and Characteristics of Shoushan Stone. *Geology of Fujian*, 2005-02.

Pan Xiao-qing, Shen Zhong-yue, Zhang Zhi-liang, Yu Dan-yan, 2011. Clinochlorite:A New Type of Tian Huang Imitation, *Journal of Gems & Gemmology*, 2011-03.

Ren Leifu, 1988. Mineralogy of Tianhuang Gem. *Acta Petrologica et Mineralogica*, 1988-02.

Zou Tian-ren, Guo Li-he, Xu Wen-yi, Xu Hai-ming, Li Chuan, Li Hong-wei, 2010. Mineral composition of Shoushan Stone and nomenclature of Tianhuang Stone, *Acta Petrologica Et Mineralogica* 2010-S1.

Gemological Terminology Issues: An Ongoing Battle...

Çiğdem Lüle

Independent Researcher
PO Box 6007, Buffalo Grove, IL 60089, USA
cigdemlule@yahoo.com

Gemological terminology has presented challenges for the gem trade since the beginning of modern gemology. Although rooted in mineralogy, in the broadest sense, gemology exists to facilitate trade. As a result, certain gemstone nomenclature is influenced by commerce and not by mineralogical standards (Lule, 2012).

Research gemologists attempt to explore and resolve certain issues regarding gem names and treatment disclosure. Laboratory report language has revealed this to be a complicated subject with little consensus within the global gemological community. In most cases, meaningful and practical standards are overlooked or ignored. The lack of application of discernible standards has resulted in practices that can be not only confusing but also misleading to the gemologists, dealers and the consumer.

Research gemologists are expected to provide the most accurate answer to any gemstone related question with the simplest terms since most market participants do not have a science background. Ideally, researchers operate in an area whereby trade needs are taken into consideration without compromising scientific principles. This is not easy, especially when it comes to expressing the work to the public (Lule, 2014).

International Mineralogical Association (IMA) established The Commission on New Minerals and Mineral Names (CNMMN) in 1959 for the purpose of regulating the introduction of new mineral names and of rationalizing mineral nomenclature. It is important to understand that CNMMN does not impose an arbitrary set of rigid rules but rather provide coherent guidelines that offer a reasonably consistent approach to the introduction of the new minerals and the application of mineral nomenclature. CNMMN does not publish anything regarding mineral varieties. Its publications only define mineral species. Besides CNMMN, there are staple publications such as Hey's Mineral Index and Fleischer's Glossary of Mineral Species to be used as reference for varietal names.

Although formidable organizations, such as CIBJO (The World Jewellery Confederation) and AGTA (The American Gem Trade Association) exist to promote gem business, each has also ventured into the area of nomenclature and treatment disclosure, while their positions, if any, regarding issues to gem names and laboratory report language are less clear. Instead, these organizations concentrate on ethics and professional practices. Currently the international gem trade lacks a body empowered to resolve issues of basic gem terminology similar to IMA's CNMMN. Similarly, LMHC (Laboratory Manual Harmonization Committee) works on unifying the language of lab reports, yet this body has not addressed the issues created by using trade terms on lab reports, i.e. pigeon's blood (Robertson & Lule, 2013).

It appears that the IMA took initiative and formed a Commission on Gem Materials (CGM) in order to regulate gem terminology, including organics, simulants and synthetic gem materials prior to 2010. However, the finalized glossary of gem materials has yet to be published following their 2010, 2012 and 2016 reports. The 2016 report was published with an updated list of gem materials. It also indicated that the committee work is ongoing (IMA Website).

The following points appear to be the major concerns in gemological terminology:

- 1- Naming newly discovered gem materials
- 2- Branded gems
- 3- Color descriptions on gemological laboratory reports
- 4- Treatment disclosure

The international gem industry has functioned reasonably well in marketing its gem products with defined and meaningful names. However, there are exceptions and where these exist, they often represent a significant departure from traditional practices. If a more meaningful standard is not identified and embraced, consumer confidence will continue to fade (Richbourg, 2016). A set of gem names based on mineral nomenclature and clear reporting language used by the laboratories would support the scientific credibility of gemology. There have been a number of attempts at producing a comprehensive gem glossary. Additional attempts have been made to standardize color nomenclature and lab report language. These efforts should be accelerated and supported by not only mineralogists but also gem trade associations. However, it must also represent the interests of the various sectors of the gem industry if it is to be functional. There is a dire need for a more unified action for gemologists to address these issues in a more forceful manner with gemology labs. Although most research gemologists would recognize the problem, attempts to resolve these issues have proven futile. Today, labs exert the least independence of the trade then at any point in modern times. Since many established gemologists within IGC audience are part of reputable labs of the international gem trade, their efforts in collaboration to define color terms, varietal names and treatment disclosure terms beyond what LMHC publishes time to time would be very effective (SSEF-Gübelin, 2015). Digital printing industry is a good example that have resolved color description issues by using RGB and/or CMYK codes which are universal now. Why not use it as an example for color terminology, or at least to establish meaningful color boundaries? Such systems are broadly accessible and can be used to define borders based on already published color systems even for even vague terms such as pigeon's blood, royal blue etc. The author can demonstrate that it is possible to achieve with the existing color grading systems and applicable to varietal names beyond IMA's CMNMM gem materials lists (Munsell, 1905, Kelly & Judd, 1955, Rubin & Levine, 1997, Gemworld, 2014, Smith & Lule, 2017).

References

- Gemworld, 2014. World of Color, Gemworld International, Inc. Glenview, IL, USA.
- IMA Website: http://www.ima-mineralogy.org/CGM_activities.htm
- Kelly, K.L., Judd, D.B., 1955. The ISCC-NBS (Inter-Society Color Council and National Bureau of Standards) method of designating colors and a dictionary of color names. NBS Circ. 553. US Government Printing Office. Washington DC, USA.
- Lule, C., 2012. What's In A Name: Gem Terminology. World of Gems Conference III Proceedings. Chicago, IL, USA.
- Lule, C., 2014. Can Mineralogy Resolve Gemstone Nomenclature Issues? GSA Annual Meeting. Vancouver, CANADA. <https://gsa.confex.com/gsa/2014AM/webprogram/Paper249791.html>
- Munsell, A. H., 1905. A Color Notation. Boston, USA.
- Richbourg, C., 2016. What's in a name? The use of historical terminology to describe colour. Jewellery Business, June Issue, pp.12-18. Canada.
- Robertson, S., Lule, C., 2013. A Matter of Opinion -The Science and Guesswork of Origin Reports. The GemGuide, Vol.32, Issue:5. Glenview, USA.
- Rubin, H. and Levine, G., 1997, Gem Dialogue, Color Toolbox. Reno Park, NY, USA.
- Smith, C. P., Lule, C., 2017. The ColorCodex, an innovative approach for establishing the color of gemstones. Rapaport Magazine, Vol. 40, No.1, January Issue, pp. 52-55. Rapaport USA Inc., Las Vegas, Nevada, USA.
- SSEF-Gubelin Press Release, 2015. www.ssef.ch/fileadmin/Documents/PDF/Press_release_Pideonblood_Royalblue_SSEF_GGL_final.pdf

Gem quality emeralds from Ethiopia

Klaus Schollenbruch¹, Lore Kiefert¹, Klemens Link¹, Tewodros Sintayehu²

¹ Gübelin Gem Lab, Maihofstrasse 102, 6006 Luzern, Switzerland lore.kiefert@gubelingemlab.com

² Orbit Ethiopia plc, P.O. Box 23115 Code 1000, Addis Ababa, Ethiopia

Although Ethiopian emeralds already found their way into the literature in 1801 by Esslinger, they were mostly known by locals, but internationally they were of no importance. This changed when in September 2016 a promising deposit was found in the South of Ethiopia (Renfro et al., 2017), with best quality emeralds comparing to very high quality emeralds from Brazil or Zambia, lifting them into the same league as those classical emerald deposits.

The emerald deposit is located approximately 250 km north of the Kenyan border on a small hill, near the village of Shakiso (Figure 1). The area has been extensively investigated over more than 30 years because of major gold, tantalum and other rare metal deposits. They are part of the Proterozoic Pan-African orogeny, and the emerald deposit is closely related to the Kenticha tantalum mine. The area is dominated by Neoproterozoic pegmatites within strongly deformed units of low-grade metamorphic volcano-sedimentary successions, high-grade schists and quartzo-feldspatic gneisses. The N-S striking pegmatites are dated to an age of approximately 530 Ma (Beraki et al., 1989; Tadesse, 1999; Küster et al., 2007).

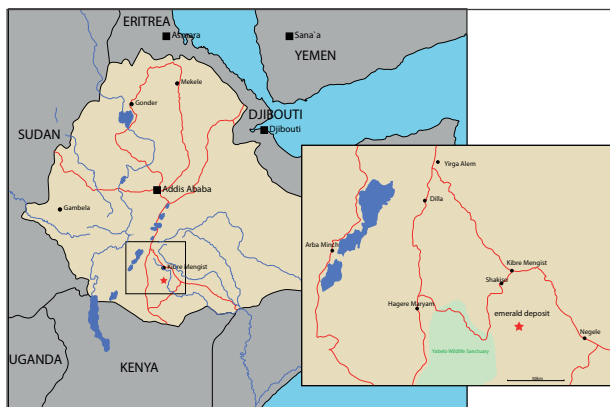


Figure 1. Location of the emerald deposit in Southern Ethiopia.
Artwork: K.Schollenbruch.



Figure 2. (left) One of the shafts in the mining area -
(right) Emerald crystals with matrix.

The discovery was an unexpected find by a local couple looking for tantalum. To follow the primary deposit, many vertical shafts were dug in an area covering several hundred square meters. The depth of the shafts ranges between five and ten meters (Figure 2 left), being deeper towards the top of the hill. The emerald occurs mostly in the form of broken pieces, single crystals, or specimen with host rock and several emerald crystals (Figure 2 right).

Over 50 of these samples, ranging from commercial quality to gem quality, were investigated. The colour ranges from light blue-green to intense saturated pure green. The measured specific gravity ranged from 2.70-2.73 g/cm³, average refractive indices are 1.580 ± 0.001 for n_e and 1.589 ± 0.001 for n_o with a birefringence of 0.009. These data are in good accordance with iron-rich emeralds from Brazil and Zambia.

The emeralds show very similar inclusions than the ones observed in Zambia and Brazil, with two-phase inclusions, where the shape ranges from strongly elongated (growth-tube-like) to nearly square when viewed perpendicular to the c-axis, and roundish to irregular when viewed parallel to the c-axis. Some of the negative crystals also contain three phases, with two fluid and one gas phase. By heating the stone to about 60 degrees C, one of the fluids evaporates (Figure 3).

In addition, growth tubes of various length are observed which are terminated by perpendicular oriented platelets at one end. The growth tubes thicken towards the platelets, giving it a similar look than the “nailhead spicules” observed in hydrothermally grown synthetic emeralds (Figure 4).

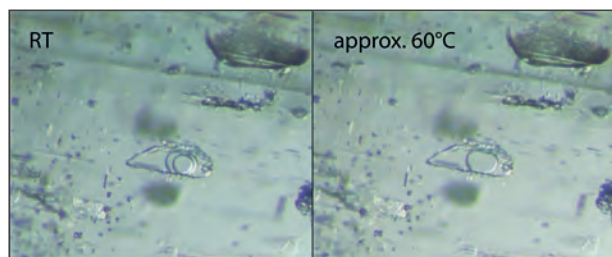


Figure 3. Three-phase inclusions become 2-phase inclusions upon heating.

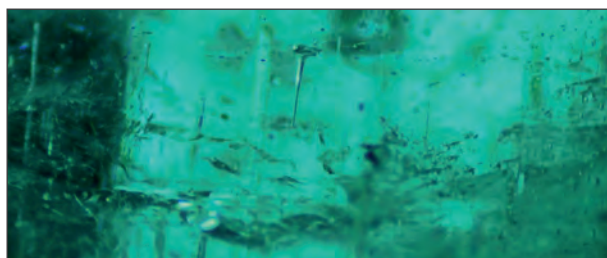


Figure 4. Nail-like inclusion in Ethiopian emerald.

The most prevalent mineral inclusions are brown mica platelets of various size. Some of the micas are surrounded by a milky, corroded looking rim. Other solid inclusions are short, prismatic, colourless oligoclase crystals with a well-developed crystal shape. Another colourless mineral with an irregular shape has not yet been identified. Tiny black mineral inclusions with corroded outlines are similar to the resorbed hematite inclusions observed in Zambian emeralds. The mica and oligoclase crystals were identified by Raman spectroscopy.

Other inclusions are thin films oriented perpendicular to the c-axis, with a grainy look. Similar films are also observed in Zambian emeralds. Open fissures are often stained by brownish-orange iron oxide.

Most of the emeralds show straight growth structures perpendicular to the c-axis, often accompanied by pronounced colour inhomogeneities. When viewed parallel to the c-axis, the growth structures appear hexagonal with many swirly layers.

Oriented UV-vis spectra show a strong broad absorption band at 840 nm caused by elevated amounts of Fe²⁺. The presence of Cr³⁺ was confirmed by typical bands at 684, 637, 609 and 429 nm (Figure 5). Absorption bands related to V³⁺ were not observed, which was confirmed later by chemical testing, which gave very low V-contents, usually below 130 ppm. Altogether, the UV-Vis spectrum of Ethiopian emerald is nearly identical to UV-Vis spectra of other high-Fe emeralds such as from Zambia, Zimbabwe, Madagascar, Brazil or Russia.

While it is difficult to differentiate these emeralds by UV-Vis spectroscopy and also XRF analysis, LA-ICP-MS analysis, performed on three different spots of 12 samples, shows a clear distinction between them and other origins when looking at different element combinations. Ethiopian emeralds generally have elevated Li, Na and Cs content compared to Brazilian emeralds, but the values are only marginally lower than in emeralds from other East African sources. Rb and K concentrations overlap with other East African, as well as the Brazilian origins. However, when comparing Rb/Li ratios to Cs contents a clear distinction of Ethiopian emeralds from the other sources can be made. The ranges obtained for the various elements are shown in Table 1.

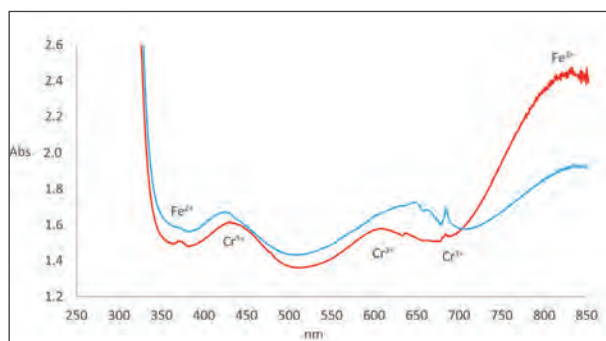


Figure 5. Typical UV-Vis spectrum of Ethiopian emerald.

Table 1: Minimum and maximum values for trace elements of Ethiopian emerald.

| (ppm) | Li | Na | Mg | K | Sc | Ti | V | Cr | Mn | Fe | Co | Zn | Ga | Rb | Cs |
|---------|-----|-------|-------|-----|-----|-----|-----|------|------|------|-------|----|----|----|-----|
| min | 145 | 8727 | 9040 | 103 | 32 | 39 | 68 | 32 | 8,59 | 2681 | 0,988 | 28 | 14 | 21 | 174 |
| max | 327 | 16003 | 13235 | 511 | 123 | 161 | 129 | 4871 | 65 | 4998 | 2,44 | 75 | 26 | 79 | 512 |
| average | 232 | 11834 | 11171 | 247 | 60 | 109 | 102 | 1714 | 17 | 3658 | 2 | 42 | 20 | 48 | 329 |

References

Beraki W.H., Bonavia F., Getachew, T., Tarekegn T., 1989. The Adola Fold and Thrust Belt, southern Ethiopia: a reexamination with implications for Pan-African evolution. *Geological Magazine*, 126(06), 647-657.

Küster D., Romer R.L., Tolessa D., Zerihun D., Bheemalingeswara, K., 2007. Geochemical Evolution and Age of the Kenticha Tantalum Pegmatite, southern Ethiopia. *International Symposium on Granitic Pegmatites: The State of the Art*, May 2007, Porto, Portugal, Abstract Volume, pp. 50–51.

Renfro N., Nemeth M., Sun Z., 2017. A New Discovery of Emeralds from Ethiopia. *Gem News International, Gems & Gemology*, 53(1), 114-115.

Tadesse S., 1999. Geology and Gold Mineralization in the Pan-African Rocks of the Adola Area, Southern Ethiopia. *Gondwana Research*, 2(3), 439-447.

Acknowledgements

The authors would like to express their gratitude to the officials and workers at the emerald mine for making it possible to visit this new deposit. All photos are from the authors unless otherwise specified.

Canadian Gem-Grade Cordierite

Karen E. Fox¹, Chris Yakymchuk²

Earth and Environmental Science, University of Waterloo, Waterloo, Canada

¹kefox.ca@gmail.com; ²cyakymchuk@uwaterloo.ca

Introduction

Cordierite is familiar to gemmologists as a blue gemstone called iolite, while geologists recognize it as a common rock-forming mineral developed during contact and high grade regional metamorphism, and more rarely in pegmatites. Within Canada, relatively few localities have yielded gem-grade material, and attractive cut stones are sufficiently rare that they are preserved in museums and private collections (Figure 1).

The current work examines gemmological properties and elemental composition of gem-grade material from 15 localities in five provinces across Canada (Figure 2), and compares the results with published literature.



Figure 1. Canadian iolite.
Photos: K. Fox



Figure 2. Canadian gem cordierite localities.
Image: modified from Google Earth.

Localities

Many of the sites from which material has been sourced for this project are or were active mining localities, and all the cordierite is associated with metamorphic environments. The Northwest Territories has been heavily mapped in search of gold and base metals, and accompanying reports note the widespread occurrence of cordierite formed by both regional and contact metamorphism in the Archean Yellowknife Supergroup, particularly north of Great Slave Lake (Kamineni & Divi, 1977). Within Manitoba, the Flin Flon-Snow Lake and the Lynn Lake metavolcanic greenstone belts comprise a large Paleoproterozoic volcanogenic massive sulphide (VMS) district from which many ore deposits have been identified, including the Lalor Lake auriferous deposit (Simard et al, 2010). Six of the 15 gem cordierite-bearing sites are in this region. The Geco Mine of Ontario is also a VMS deposit. Baffin Island, Nunavut, hosts four of the gem-cordierite sites, two on the south coast in the metasedimentary rocks of the Lake Harbour group. Further inland, the Turner River site is near the iron-formation magnetite beds of the Archean Mary River group, where metamorphism has reached amphibolite- to granulite-facies.

Gem Material

Gems cut from Canadian cordierite range from deep blue-violet through medium blue to grayish blue, and display the blue-violet/blue/yellow-to-colourless pleochroism typical of iolite. Partially healed fractures are common, as are opaque inclusions identified by Energy Dispersive X-Ray Spectroscopy as iron-oxides, and various Fe-Cu-Ni sulphides. Included flakes of mica are often observed, and diagnostic yellow haloes surrounding monazite and other radioactive minerals appear in the material from Baffin Island (Figure 3). Sillimanite inclusions appear in lower quality material from Walton Lake and Carp Lake.

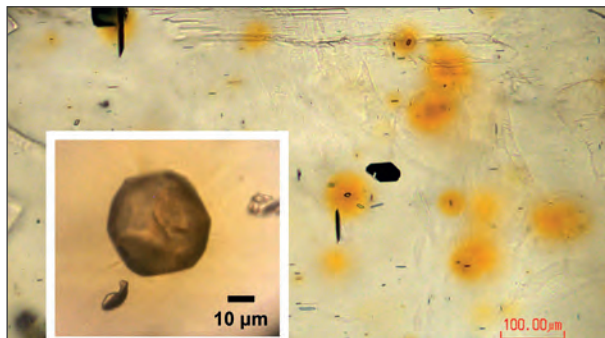


Figure 3. Yellow haloes are caused by the presence of radioactive minerals such as monazite. Photo: K. Fox.

Chemistry and Material Characteristics

The simplified chemical formula for cordierite is $(\text{Mg,Fe})_2\text{Al}_4\text{Si}_5\text{O}_{18} \cdot (\text{H}_2\text{O,CO}_2)$. It is an orthorhombic framework aluminosilicate composed of six-membered rings of tetrahedra cross-linked by additional tetrahedra. Mg^{2+} , Fe^{2+} , Mn^{2+} and Li^{2+} occupy octahedral M-sites, and open channels form parallel to [001] (Bertoldi et al, 2004).

The chemical composition of the cordierite was studied using electron microprobe analysis (EMPA) for major/minor elements, and laser ablation inductively coupled plasma mass spectrometry (LA-ICP-MS) for trace elements. Atoms per formula unit [a.p.f.u.] were calculated based on 18 oxygens. Deer et al. (1997) report that most natural cordierite is Mg-rich, with the molar ratio of Fe / [Fe+Mg+Mn] rarely exceeding 0.5. The Canadian material is no exception: EMPA shows the material from British Columbia and the Ruttan Mine of Manitoba to have the lowest iron ratios, at about 0.15, while the highest ratios were observed south of Ghost Lake in the Northwest Territories, at 0.4. Note that although measurements across chips from a given locality appear reasonably consistent, samples from south of Ghost Lake show a large difference in iron ratios, and greater variability might be observed with a larger sample set (Figure 4).

Specific gravity measurements were done on gem rough using the hydrostatic weighing method with a scientific-grade electronic balance. Efforts were taken to avoid large inclusions, but much of this material is included and fractured to varying degrees. Nevertheless, there is a general trend toward higher specific gravity as Mg is replaced by Fe (Figure 5).

The channels in the structure of cordierite can be occupied by Na^+ (or K^+), as well as by water or CO_2 . In addition, Li and Be tend to partition preferentially into cordierite. Na, Li and Be are all present above the detection limit of the ICP-MS in most of the samples, but K is normally low to absent. Figure 6 has been scaled to match a figure from Bertoldi et al. (2004), who combined data from other workers with their own. The range of values that has been observed for natural cordierites is shaded in blue. Although the concentrations of Li, Be and Na in the Canadian material are on the very low end, they are not atypical.

The presence of water and CO_2 in the channels of cordierite causes shifts in 2V angle, and variability in refractive index values. Preliminary results using the spindle stage techniques of Bloss (1981) show 2V values between 73° and 87°, and similar techniques will be explored for refractive index measurement.

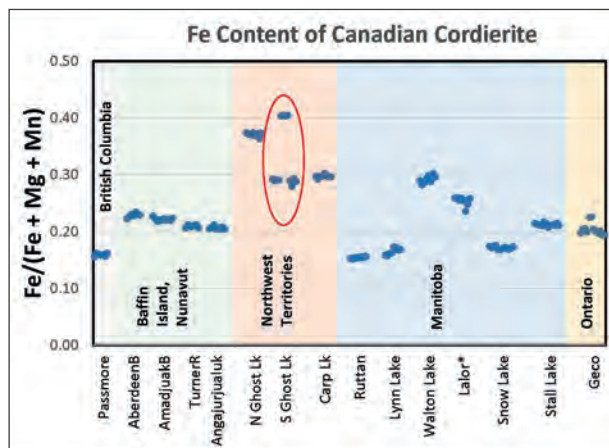


Figure 4. The molar ratio of Fe to other minerals on the M-site rarely exceeds 0.5 in natural cordierite.

Conclusions

The results of this investigation indicate that the elemental composition and gem characteristics of Canadian cordierite are typical of the cordierite of metamorphic origin reported in the literature (Bertoldi et al., 2004; Deer et al., 1997).

Acknowledgements

We thank Brad Wilson for providing cordierite rough from known localities; the Canadian Museum of Nature and the Royal Ontario Museum; Joel Grice, for introducing the principles of the spindle stage for optical mineralogy; Willow Wight, for multi-faceted support; and many people at U of Waterloo.

References

- Bertoldi, C., Proyer, A., Garbe-Schönberg, D., Behrens, H., Dachs, E., 2004. Comprehensive chemical analyses of natural cordierites: implications for exchange mechanisms. *Lithos*, 78, 389 – 409.
- Bloss, F.D., 1981. *The spindle stage: principles and practice*. Cambridge University Press, Cambridge. 340pp.
- Deer, W.A., Howie, R.A., Zussman, J., 1997. *Rock-Forming Minerals, Volume 1B, Disilicates and Ring Silicates*, 2nd Ed. The Geological Society, London, 629 pp.
- Google Earth. "Canadian Gem Cordierite Localities". 60°30'07.52"N 90°22'00.59"W. Dec 13, 2015. Accessed: May 22, 2017.
- Kamineni, D.C., Divi, S.R., 1977. Growth of cordierite in the Archean metasediments near Yellowknife, District of Mackenzie, Canada. *Geologische Rundschau*, 66(1), 255-263.
- Simard, R-L., McGregor, C.R., Rayner, N., Creaser, R.A., 2010. New geological mapping, geochemical, Sm-Nd isotopic and U-Pb age data for the eastern sub-Phanerozoic Flin Flon Belt, west central Manitoba (parts of NTS 63J3-6, 11, 12, 14, 63K1-2, 7-10). In: Report of Activities 2010, Manitoba Innovation, Energy and Mines, Manitoba Geological Survey, 69-87.

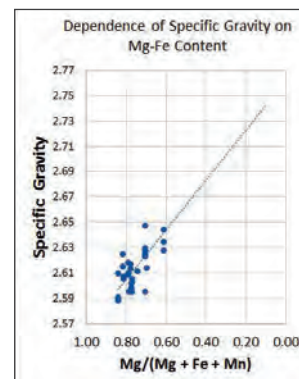


Figure 5. Specific gravity rises as Fe replaces Mg.

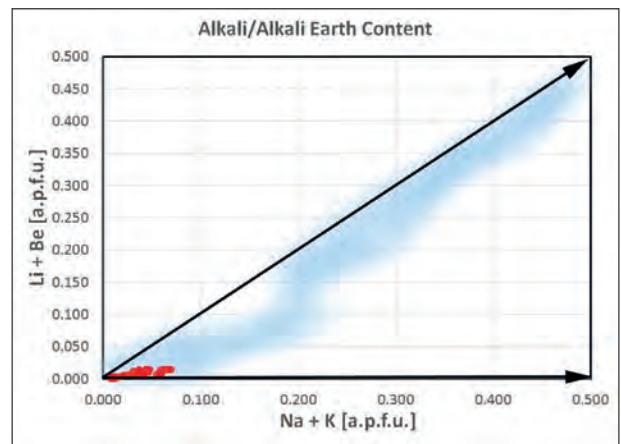


Figure 6. Alkali content (red) in Canadian cordierite is on the low end of that reported by Bertoldi et al (2004) (blue).

Jadeite jade from Japan: its history, gemmology and comparison with jadeite from other sources

Ahmadjan Abduriyim¹, Kazuko Saruwatari², Yusuke Katsurada²

¹Dr. Abduriyim is president of Tokyo Gem Science., LLC and director of GSTV Gemological Laboratory.

²Dr. Saruwatari is a staff gemologist and Dr. Katsurada is a scientist and staff gemologist at GIA's laboratory in Tokyo.

The production of jadeite jade as historical oriental treasure is very limited in Japan. Even though jadeite jade does not show a high transparency as compared to the highest quality of Burmese imperial jadeite jade, because of its rarity and surface features it became a highly valued gemstone in the gem market. Itoigawa-Omi region in Niigata prefecture, is one of the jadeite sources worldwide. The Kotaki area, at the upstream part of the Hime River, in the Itoigawa region, was the first area where natural occurrences of gem-quality jadeite and jadeite-bearing rocks were reported in Japan.

The area is located in the high-pressure and low-temperature type Renge metamorphic Belt within a Late Paleozoic subduction zone. Tsujimori (2002) suggested that blueschist to eclogite metamorphism may be related to the subduction of oceanic crust. Miyajima et al. (1999) and Morishita (2005) suggested that the fluids related to the formation of jadeite in the Itoigawa-Omi region were related to subduction zones. U-Pb zircon dating of jadeite-natrolite rocks in the Itoigawa-Omi area revealed ages of about 519 ± 17 Ma, which are interpreted to be the age of jadeitization. (Kunugiza et al., 2002).

The main goal of this study is to introduce the historical background of an oriental treasure called "*Magatama*", a curved jadeite jade pendant, and the locations it is from, and to describe the color variety, internal texture and chemical features by quantitative analysis (using EPMA and LA-ICP-MS). In this study, Jadeite from Itoigawa-Omi region in the Niigata prefecture and from Wakasa in the Tottori prefecture are divided into several types in terms of variations in color corresponding to chromophores and mineral phases, such as white jadeite jade (nearly pure jadeite), green jadeite jade (Fe-rich, Cr-bearing jadeite), lavender (violet) jadeite jade (Ti-bearing jadeite), blue jadeite jade (Ti- and Fe-bearing jadeite) and black jadeite jade (graphite-bearing jadeite). White jadeite jade from Itoigawa-Omi region is close to a pure jadeite ($X_{jd}=98$). Green jadeite jade from the same location shows a range of $X_{jd}=98$ to 82, the maximum of CaO content is up to 5 wt.% (omphacite component) and its coloring chromophores are Fe and Cr (confirmed by UV-Vis spectroscopy and chemical analysis). Lavender jadeite jade has a range of $X_{jd}=98$ to 93, and tends to be high in TiO_2 and FeO_{tot} and low in MnO content. Blue jadeite jade contains significant TiO_2 (with highest concentration 0.65 wt.%), while X_{jd} ranges from 97 to 93. A similar blue colored jadeite jade from Wakasa region in Tottori prefecture shows $X_{jd}=97$ to 91 and a similarly high TiO_2 content.

In trace element analytical study, Chondrite-normalized and primitive mantle-normalized patterns in Japanese lavender, violetish blue and blue jadeite jade showed higher large-ion lithophile element contents (Sr, Ba) and high field strength element contents (Zr, Nb) than in green jadeite, while the white and black jadeite are relatively low in REE contents, also compared to green jadeite. Furthermore, jadeite jades from other sources of Myanmar, Guatemala and Russia are compared.

Our studies confirmed that the gemological properties such as RI, SG and the spectral absorption lines of Cr and Fe in Itoigawa green jadeite jade are similar to the green jadeite jade from Myanmar and Russia, whereas Guatemala grayish green jadeite does not contain chromium. Lavender jadeite from Guatemala shows a similar coloration to Japanese lavender jadeite jade and its colour is also caused by the chromophores Ti (high content) and Fe and minor amount of Mn. Thin section study revealed that Burmese jadeite jade contains various minerals, such as kosmochlor, amphibole, albite, nepheline and vesuvianite. Russian jadeite jade typically has magnetite in matrix and has analcime in veinlets. Guatemala jadeite jade is characterized by grossular garnet, albite, and rutile inclusions, but may contain other minor minerals as well. Also, Guatemala jadeite containing abundant REEs and heavy trace elements, where Burmese jadeite had much lower values.



Figure 1. Representative samples from Itoigawa-Omi region in Niigata prefecture, Japan.: Magatama jadeite (25.51–63.88 ct).



Figure 2. Left: A 4.6 ton jadeite rough boulder is displayed at the Fossa Magna Museum in Itoigawa. This eroded and rounded boulder from the Kotaki area is mostly white with some green areas of jadeite; the fibrous structure in the black area is amphibole. Thin fault-like veins are filled with white minerals. Right: These rounded jadeite pebbles, found along the coast in Itoigawa-Omi, are approximately 2 to 15 cm long. Courtesy of the Fossa Magna Museum and the Jade Ore Museum (Hisui Gensekikan).

References

Kunugiza, K., Nakamura, E., Miyajima, H., Goto, A., Kobayashi, K., 2002. Formation of jadeite-natrolite rocks in the Itoigawa-Ohmi area of the Hida marginal belt inferred from U-Pbzircon dating. Abstract of annual meeting of the Japanese Association of Mineralogist, Petrologist and Economic Geologists in 2002, GP20 (in Japanese).

Miyajima H., Matsubara S., Miyawaki R., Ito K., 1999. Itoigawa, a new mineral, the Sr analogue of lawsonite, in jadeite from the Itoigawa-Ohmi district, central Japan. *Mineralogical Magazine*, 63, 909–916.

Morishita T., 2005. Occurrence and chemical composition of barium feldspar in a jadeitite from the Itoigawa-Ohmi district in the Renge high-P/T-type metamorphic belt, Japan. *Mineralogical Magazine*, 69, 39–51. Tsujimori T., 2002. Prograde and retrograde P-T paths of the Late Paleozoic glaucophane eclogite from the Renge metamorphic belt, Hida Mountains, south-western Japan. *International Geological Review*, 44, 797–818.



GemRam™

Raman Gemstone Identification System

Quick verification & identification of
both raw and polished gemstones

Spectral library of over 450 gemstones

Supports user-defined spectral libraries

Carat Balances

Sparkling Performer



XPE Precision Balance



JP Carat Balance



JE Carat Balance

Swiss
Weighing
Technology

► www.mt.com/jewelry

METTLER **TOLEDO**



M&A GEMOLOGICAL INSTRUMENTS

MADE BY
GEMOLOGISTS
FOR
GEMOLOGISTS



WWW.GEMMORAMAN.COM



亞洲寶石學院及鑑定所有限公司

Asian Gemmological Institute and Laboratory Limited

Website : www.agil.com.hk Email : agil@agil.com.hk Telephone : +852-27230429
707-708, 7/F, Hang Seng Tsimshatsui Building, No.18 Carnarvon Road, Kowloon, Hong Kong

Motic GM171 Series Trinocular Gemmological Microscope for Gemmologist Set

The Gemmologist Set of GM171 includes:

- Motic GM171 Trinocular Gemmological Microscope
- 1.5X Objective Lens (Can be magnify to 15X-100X)
- Gemstone Rounded Edge Stone Holder
- Diamond Wire Stone Holder
- 0.5X C-mount camera adapter



www.agil.com.hk

Enquiry for Microscope Demo and shipping charge,
please feel free to contact AGIL.



Optional Accessories



A. Moticam BTU8
Camera and Tablet



MotiConnect App



B. Polarizing Filter Set



C. Immersion Cell



D. C-Clamp for Diamond Inscription



E. 0.75X Objective Lens

AGIL is the sole agent of Motic Gemmological Microscope in Namibia and Australia as well as one of the International Distributors.

GemRam for simple gem ID

Daniel Barchewitz

B&W Tek, Lübeck, Germany, danielb@bwtek.com

Although a highly skilled jeweler can be qualified to identify and evaluate gemstones with classical gemological instruments, scientific study is within reach for nearly anyone else to identify an unknown gemstone or verify the identity of a known gemstone. As a nondestructive technique that requires no sample preparation, Raman spectroscopy is the perfect tool to determine the identification of synthetic or natural gemstones and identify inclusions when attached to a microscope. Raman technology, which can be used on uncut gemstones (Figure 1), unmounted and mounted gems and pieces of jewelry, is capable of providing gemstone spectra for all mineral classes, including: borates, carbonates, oxides, phosphates, silicates, sulfates and sulfides.



Figure 1. A lot of rough gem minerals to identify with GemRam in the field.



Figure 2. GemRam ready for identifying on all kinds of gemstones.

The GemRam™ is a lightweight, portable Raman spectrometer (Figure 2 and 3) dedicated to both the verification of known gemstones as well as the identification of unknown gemstones. It comes equipped with B&W Tek's GemID™ identification software, powered by GemExpert's spectral library of greater than 450 different gemstones, as well as unlimited space for user-defined spectra that can be added at any time.

The GemRam utilizes a spectrum stabilized 785nm diode laser and high resolution TE cooled spectrometer to provide unrivaled performance and repeatability. It comes complete with a fiber optic probe and X-Y-Z positioning stage, all in a convenient carrying case.

For users who need a more compact solution to take onto show floors or into shops for quick identification before purchase, B&W Tek also offers the handheld GemRam Mini (Figure 4).



Figure 3. Video Microscope BAC151B connected to the GemRam.



Figure 4. GemRam Mini confirms the "Blue Moon Diamond, 12.03 ct, to be a diamond.

References

GEORAMAN-96, Institut des Matériaux de Nantes, Nantes, France, 10-12 June 1996. In: Terra abstracts. Abstract supplement No. 2 to TERRA nova, Vol. 8, p. 19.

Hänni, H.A., Kiefert, L., Chalain, J-P., Wilcock, I.C., 1997. A Raman microscope in the gemmological laboratory: first experiences of application.- J. Gemmol., 25(6), 394-406.

Traceability of gemstones: challenges and opportunities

Laurent E. Cartier¹, Michael S. Krzemnicki¹, H.A.O. Wang¹, Henry A. Hänni^{1,2}

¹ Swiss Gemmological Institute SSEF, Aeschengraben 26, CH-4051 Basel, gemlab@ssef.ch

² GemExpert, Basel, Switzerland

The tracking and traceability of gemstones is an increasingly important issue. Consumers are ever more interested in knowing where and how the materials they consume are extracted and manufactured (Cartier, 2011; Archuleta, 2016; Nash et al., 2016). Media and NGOs are increasingly scrutinizing the gemstone industry about the origin and sustainability footprint of different gemstones (Global Witness 2015; RESP, 2016). Governments want to improve the management and revenue collected from gemstone resources and global governing bodies have highlighted issues such as smuggling and money laundering in recent years (Schroeder, 2010; UNICRI, 2013). Documenting the provenance and source of gemstones is one way of addressing these concerns; and tracking and traceability are two available mechanisms to achieve this. Although a multi-folded approach – for example a strengthening of specific ethical and sustainability standards within mining, processing and sale of gemstones worldwide - is required to address these issues, the development of techniques to track and trace gemstones is vital to the accountability and credibility of such schemes.

The recent appearance of undisclosed synthetic diamonds on the market further highlights this, how are, could and should different types of gemstones be separated on their journeys through the supply chain? Correct disclosure of sold gemstones, for example treatments in emeralds, is already required in the CIBJO Blue Books. Being able to provide information about the source of a gemstone is set to become more and more critical for jewellery houses, gemstone miners and gemstone traders, if experiences from other sectors are anything to go by. Tracking and traceability can be considered both a growing requirement for some and for others a competitive advantage. The industry today already has clear pricing gradients for natural vs. imitation (turquoise vs. imitation turquoise), natural vs. synthetic (natural spinel vs. synthetic spinel), untreated vs. treated goods (untreated ruby vs. heat treated ruby), and gemstones of different origins (Colombian emerald vs. Zambia emerald). A further level is being added by claims from mining companies, traders and jewellery houses that certain gemstones are “ethical”, “sustainable”, “fair trade”, “conflict-free” or “traceable” gemstones. In order to provide these claims with further credibility, independent verification may be required.

Gemmological science may provide assistance in such cases and this research offers an overview of possible strategies, opportunities and limitations of tracking (downstream “from mine to market”) or tracing gemstones (upstream “from market to mine”) using gemmological approaches. Advances in new technology to map unique gemstone inclusion features and characterise their chemical and spectroscopic properties can aid in these traceability measures. Advances in multi-variate statistics and whole isotope analysis at ultra-trace levels with LA-ICP-MS technology is opening up new insights in chemical fingerprinting of gemstones from different geological and geographic settings (Wang et al., 2016). At another level, the ability to combine precise multiple trace-element data points of a stone with spectroscopic measurements and machine learning technology, opens up research directions in finding unique fingerprints for unique stones. Other approaches involve physical tracing or marking a gemstone either at the mine or at a subsequent stage in the supply chain, simply involving hologramming or laser inscribing a stone or in more complex cases to use uniquely marked nanoparticles injected into fissures that will remain in an emerald even after the cutting and treatment process (Hänni & Cartier, 2013; WWD, 2017). The different marking and tracing technologies available have different approaches, there is not one unique solution for the gemstone industry.



*Figure 1. Miner with rough corundum in Zazafotsy, Madagascar. How could such material be tracked from the mine to consumer?
Photo: Laurent E. Cartier.*

However, gemmologists are well placed to assist in developing such solutions through their detailed knowledge of gemstones. Gemmological science can contribute with complimentary approaches and technology in offering additional information about a gemstone and its provenance.

References

- Archuleta, J.L., 2016. The color of responsibility: ethical issues and solutions in colored gemstones. *Gems & Gemology*, 52(2), 144-160.
- Cartier L.E., 2010. Environmental stewardship in gemstone mining: Quo vadis? *InColor* (Fall/Winter), pp. 2–9.
- Cartier, L.E., 2011. Gemstones. In Sarah Fredericks, Lei Shen, Shirley Thompson, & Daniel Vasey (Eds.), *The Encyclopedia of Sustainability: Vol. 4. Natural Resources and Sustainability* (pp. 174–177). Great Barrington, MA: Berkshire Publishing.
- Global Witness, 2015. Jade: Myanmar’s “big state secret,” <https://www.globalwitness.org/en/campaigns/oil-gas-and-mining/myanmarjade/>
- Hänni, H. A., Cartier, L. E., 2013. Tracing cultured pearls from farm to consumer: A review of potential methods and solutions. *Journal of Gemmology*, 33(7-8), 239-245
- Nash J., Ginger C., Cartier L.E., 2016. The Sustainable Luxury Contradiction Evidence from a Consumer Study of Marine-cultured Pearl Jewellery. *The Journal of Corporate Citizenship*, 63, 73-95
- Responsible Ecosystems Sourcing Platform, 2016. Challenges to advancing social and environmental responsibility in the coloured gems industry, Jan. 31, <http://www.resp.ch/resources/publications/challenges-advancing-environmental-and-social-responsibility-coloured-gems>
- Schroeder R., 2010. Tanzanite as conflict gem: Certifying a secure commodity chain in Tanzania. *Geoforum*, 41, 1, 56–65, <http://dx.doi.org/10.1016/j.geoforum.2009.02.005>
- United Nations Interregional Crime and Justice Research Institute (2013) Expert meeting to discuss a new initiative on coloured gemstones traceability and certification of ethical origin, April 11, www.unicri.it/news/article/2013-04-11_Expert_meeting_Gemstones
- Wang H.A.O., Krzemnicki M.S., Chalain J-P, Lefèvre P., Zhou W., Cartier L.E., 2016. Simultaneous High Sensitivity Trace-Element and Isotopic Analysis of Gemstones Using Laser Ablation Inductively Coupled Plasma Time-of-Flight Mass Spectrometry. *Journal of Gemmology*, 35(3), 212-223.
- WWD, 2017. Gemfields Partners With Gübelin Gem Lab on New Emerald Traceability Technology. Accessed 26 April 2017, <http://wwd.com/fashion-news/fashion-scoops/gemfields-partners-gubelin-gem-lab-emerald-traceability-technology-10851799/>

Aquaprase™: An interesting green-blue variety of chalcedony

Gagan Choudhary

Gem Testing Laboratory, Jaipur, India; gagan@gjepcindia.com

Introduction

In 2014 a light 'aqua' blue to greenish blue or bluish green variety of chalcedony was established in the market by Yianni Melas. The material is marketed under the trade name 'Aquaprase' and has gained a lot of popularity in the recent past, especially amongst the jewellery designers and consumers alike. The name 'aquaprase' however has been given arbitrarily. This material is reportedly being mined in an African locality with opals (Renfro, 2015; Bates, 2016) and solely cut and polished in Jaipur, India by the promoter Avant Chordia. However, similar material such as chrome green chalcedony from Zimbabwe referred to as 'mtorolite' has been known since 1953 (Philips & Brown, 1989; Hyrsl, 1999) as well as from Australia (Willing & Stocklmayer, 2003); dark bluish green chalcedony is also reported from Anatolia, Turkey (Lule-Whipp, 2006; Henn et al, 2016); greenish blue chalcedony coloured by copper impurity such as chrysocolla, referred as 'chrysocolla chalcedony' or 'gem-silica' is also a well-known variety (Shen et al, 2006). There also exist dyed and treated counterparts in similar colours. Due to the existence of these types of chalcedonies, interest in the study of this new type of chalcedony marketed as 'aquaprase' was generated, whose characterization is briefed here.

Seven polished samples (Figure 1) in the weight range 3.00 to 9.18 ct., kindly donated by Mr. Chordia, were used to measure gemmological as well as spectroscopic and chemical characteristics (infrared, Raman, visible absorption, EDXRF).



Figure 1. These greenish blue to bluish green chalcedonies (3.00 - 9.18 ct.) being mined in Africa, solely cut & polished in Jaipur are marketed under the trade name 'Aquaprase'. Photo by G. Choudhary.

Results and Discussion

Visual appearance

The studied samples of Aquaprase ranged from 'aqua' blue to bluish green to greenish blue to green - mostly in low to medium saturation; diaphaneity ranged from semi-transparent to translucent. Most of the samples were unevenly coloured, associated with sharp white banding, whitish clouds and brown areas (matrix); the latter was present in the form of veins as well as patches, showing a granular texture. One light greenish blue sample was evenly coloured. The whitish clouds were more prominently present in greenish blue samples, while, green samples interestingly displayed patches of green colour against a milky body colour, suggesting presence of some mineral inclusion. One semi-transparent sample also displayed minute green-blue spots against a white background of the stone, giving an overall greenish blue body colour.

Inclusions

The inclusion pattern observed in these specimens included botryoidal banding patterns with some whitish material on their surface, pockets of transparent drusy quartz crystals often associated with banded edges, brown patches of hematite (as identified by Raman spectroscopy), and scattered white clouds. These clouds appeared to be pockets of drusy quartz as some of these were breaking on the surface and displayed a typical granular structure, with hexagonal to pseudo-hexagonal grain boundary. The most interesting feature in these chalcedonies was presence of green patches (Figure 2), also responsible for the green colour in these samples. These green patches appeared to be concentrations of some chromium-based mineral along the boundaries or spaces in between drusy quartz crystals, within the pockets. Samples with higher concentration of these patches had deeper green body colour. Raman spectroscopy, however, could not reveal any spectral feature from this material, but appeared deep red under Chelsea filter, confirming presence of chromium; the light blue to greenish blue samples without these obvious green patches also appeared pink to red.

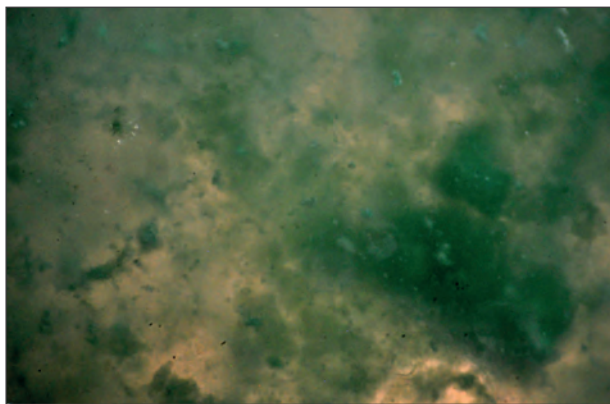


Figure 2. Presence of a green mineral phase along the crystal boundaries within drusy pockets was responsible for the green component in these "Aquaprase" samples.

Greener samples had higher concentrations of these patches and vice versa for bluish samples. Photomicrograph by G. Choudhary; image width 8.46 mm.

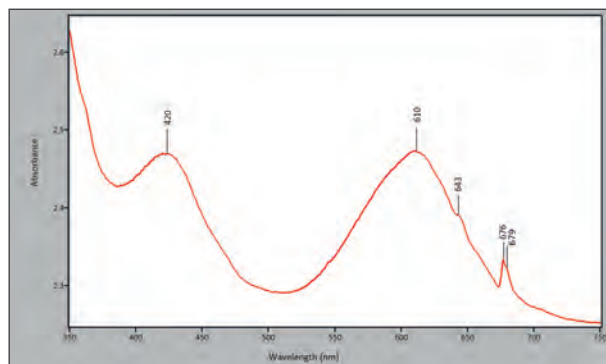


Figure 3. The absorption spectra in the region 400 - 700 nm showed two broad absorption bands centred at ~420 and 610 nm, a shoulder at ~643 nm with the latter absorption band, and sharp peaks (doublet) at ~676 /679 nm, related to chromium.

Properties

The gemmological properties of the studied samples of 'Aquaprase' are summarised in Table 1. Raman and infra-red spectra were consistent with those for chalcedony present in our database. No additional feature was recorded for colour-causing green patches or inclusions. Qualitative EDXRF analysis revealed presence of Ca, Cr, Fe and Ni in traces, in addition to Si. The absorption spectra (Figure 3) in the region 400 - 700 nm showed two broad absorption bands centred at ~420 and 610nm, a shoulder at ~643 nm with the latter absorption band, and sharp peaks (doublet) at ~676 /679 nm. This absorption pattern is similar to that previously reported for chrome chalcedony and hence, suggested the presence of chromium (e.g. Hyrsl, 1999).

Table 1: Properties of the blue-green chalcedony 'Aquaprase' from Africa

| Property | Description |
|--|---|
| Colour range | 'Aqua' blue - greenish blue - bluish green - to green (low to medium saturation) - with and without banding / matrix |
| Diaphaneity | Semi-transparent to translucent |
| RI (spot) | 1.53 - 1.54 |
| SG (hydrostatic) | 2.50 - 2.58 |
| Desk-model spectroscope | Absorption band in yellow region; sharp lines in red |
| Chelsea filter | Patchy brownish-red (green inclusions appeared stronger red); bluer samples - red to pink |
| UV fluorescence | Bluish green to yellowish green (long wave and short wave) |
| FTIR analysis (400 - 7000 cm ⁻¹) | Consistent with chalcedony: Absorption bands at ~5330-4920 and ~4570-4260 cm ⁻¹ ; complete absorption below ~4150 cm ⁻¹ |
| EDXRF analysis | Major: Si; Traces: Ca, Cr, Fe, Ni |
| Raman spectra (200 - 2000 cm ⁻¹) | Consistent with chalcedony: Peaks at ~ 205, 260, 355, 400, 463, 501 (moganite), 692, 798, 1162 cm ⁻¹ |
| Absorption spectra (200 - 800 nm) | Broad absorption bands centred ~ 420 and 600 nm; a shoulder at ~ 643 nm; doublet at ~676 and 679 nm |

Conclusions

The bluish green to green chalcedony coloured by chromium impurity has been known as 'Mtorolite' or 'chrome chalcedony' in the trade for years, while similar bluish green chalcedony is also reported from Turkey, whose properties correspond to those measured for 'aquaprase'. However, this new material being marketed as 'aquaprase' has a range of colours including light 'aqua' blue and light greenish blue, making these chalcedonies an interesting find. 'Aqua' blue or light greenish blue chalcedony already exists in the trade as 'gem-silica' but is coloured by copper impurity (chrysocolla), as against 'aquaprase' which is coloured by chromium. Therefore, these chalcedonies are interesting for two factors - first, the 'aqua' blue to light greenish blue colour is unusual for a chrome chalcedony, and second, the blue colour which was known to occur due to copper impurities, is coloured by chromium-nickel impurities. Further, dyed chalcedony in this colour range is widely available, which can be separated on the basis of absorption spectrum and red reaction under chelsea filter; the treated counterparts do not appear red / pink under chelsea filter and lack typical absorption patterns.

The 'aqua' blue to greenish blue variety of 'aquaprase' chalcedony is an interesting find, and offers an additional choice for the consumers, from a range of natural-coloured gemstones. Currently, this material is solely cut and polished in Jaipur, which adds to the importance of Jaipur as a gem centre, however, it will be interesting to see its consistent supply in the years to come.

References

Bates R., 2016. The Story Behind the New Gemstone: Aquaprase. <http://www.jckonline.com/editorial/article/the-story-behind-the-new-gemstone-Aquaprase/>

Henn U., Schultz-Güttler R., Stephan T., 2016. Grüne undurchsichtige Quarze mit besonderer Berücksichtigung bestrahlter Achate und Aventurisiertem Quarzit aus Brasilien. *Z. Dt. Gemmol. Ges.*, 65(1-2), 9-22 (German; Figure captions in English).

Hyrsl J. (1999). Chrome chalcedony - a review. *Journal of Gemmology*, 26(6), 364-370.

Lule-Whipp C., 2006. Chrome chalcedony from Turkey and its possible archaeological connections. *Gems & Gemology*, 42(3), 115.

Philips G., Brown G. (1989). Mtorolite. *Australian Gemmologist*, 17(5), 205-207.

Renfro N. (2015). Gem News International: A new natural-color bluish green chalcedony. *Gems & Gemology* 51(4), 452-454.

Shen A., Fritz E., DeGhionno D., McClure S., 2006. Identification of dyed chrysocolla chalcedony. *Gems & Gemology*, 42(3), 140.

Willing M.J., Stocklmayer S.M., 2003. A new chrome chalcedony occurrence from Western Australia. *Journal of Gemmology*, 28(5), 265-279.

Acknowledgement

The author is grateful to Mr. Avant Chordia for providing samples for this study.

Figure captions

Sannan-Skarn: a new ornamental gemstone from Pakistan

Henry A. Hänni¹, Leander Franz², Zhou Wei¹

¹ SSEF Swiss Gemmological Institute, Aeschengraben 26, CH-4051 Basel, gemlab@ssef.ch

² Mineralogisch-Petrographisches Institut, University of Basel, Bernoullistrasse 30,
CH-4056 Basel
leander.franz@unibas.ch

At the Hong Kong Jewellery and Gem Fair September 2015 a significant volume of complex fine grained green rock material from Western Pakistan was sold to gemstone dealers under the name Maw Sit Sit. The new material originates from a remote area in Belochistan, about 60 km from the Muslim Bagh Chromite mine. The productive area lies in a thrust zone (Kazmi & Snee, 1989) known as Karakorum Suture Zone. There, sediments from the Tethys were welded on the Eurasian Plate when the Indian continent collided some 65 Mio years ago. Triassic carbonate sediments and oceanic crust were imbricated in a tectonic movement going along with strong brecciation and mylonitization of the rocks. During this imbrication, intense fluid activity led to a replacement of carbonate by calcsilicate minerals. A common term to name the material is skarn, as it describes a rock formed by metasomatic replacement of a parent rock. Sannan is a specific modifier that describes the skarn from the new occurrence.

After a preliminary test, it became clear that this material has nothing in common with Maw Sit Sit, i.e. kosmochlor jade (e.g. Hänni & Meyer, 1997; Franz et al., 2014), although specific gravity (SG) and refractive index may show overlapping data. Three samples (JG1– JG3) were selected and prepared for petrographic thin sections and investigated by polarization microscopy and micro-Raman spectroscopy. Each sample has a strongly different mineralogical composition.

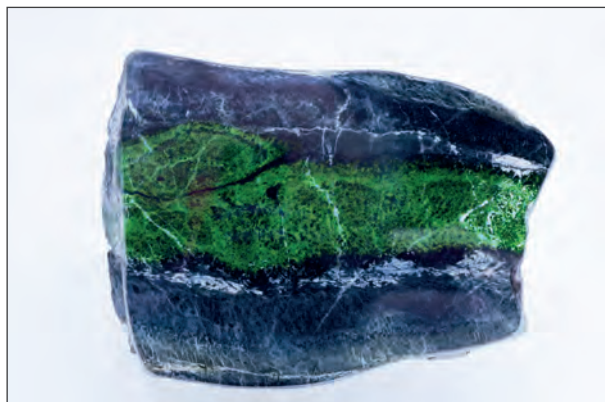


Figure 1. A representative sample (JB11) of Sannan Skarn from Balochistan, Pakistan. Width 12 cm.

Sample JG 1 (SG 3.26) is of greenish-grey to dark green colour and has a fine grained, randomly oriented texture. Euhedral crystals of zoned green, up to 0.6 mm wide hydrogrossular $(\text{Ca}_3(\text{Al,Fe}^{3+})_2(\text{OH})_4/(\text{SiO}_3)_2)$ are surrounded by large prismatic diopside. Streaks and bands of chlorite are often cut by veins filled with calcite. The rock is a calcite-chlorite-hydrogrossular-diopside skarn. Sample JG 2 (SG 2.98) is of medium green colour with a light green margin. Radiating clusters of short prismatic, up to 0.3 mm long aegirine crystals $(\text{Na-Fe-pyroxene, NaFe}^{3+}\text{Si}_2\text{O}_6)$ show a strong pleochroism from luminous green to yellow-green. In interspaces, subordinate fillings of agglomerated, yellow-brown prismatic pectolite crystals $(\text{NaCa}_2\text{Si}_3\text{O}_8(\text{OH}))$ occur. The lighter green margin shows a mylonitic texture with lenticular and linear concentrations of pectolite and chlorite as well as heavily fractured aegirine. The rock is a chlorite-pectolite-aegirine skarn. Sample JG 3 (SG 2.67) shows an inhomogeneous patchy texture with green, dark greyish-green and whitish domains. Pale green winchite crystals (sodic-calcic amphibole, $(\text{CaNa})\text{Mg}_4(\text{Al,Fe}^{3+})\text{Si}_8\text{O}_{22}(\text{OH})_2$) of up to 1 mm size are intergrown with smaller, dark green aegirine crystals. In the darker areas, winchite prisms and fine aegirine needles lie in a groundmass of colourless natrolite $(\text{Na}_2\text{Al}_2\text{Si}_3\text{O}_{10} \cdot 2\text{H}_2\text{O})$. The white zones consist purely of sodalite $(\text{Na}_8(\text{Al}_6\text{Si}_6\text{O}_{24})\text{Cl}_2)$. The rock is thus an aegirine-natrolite-winchite skarn with sodalitic parts. The results of the crystal-optical analysis were confirmed by micro-Raman spectroscopy.

Qualitative chemical results were performed with ED-XRF. The analyses vary from sample to sample, due to their inhomogeneous composition. In all samples, the presence of Cr is identified and Ca is a main constituent, which represents a main difference to Maw Sit Sit.

The rocks described in this paper mainly consist of calc-silicates, which formed by tectonic movements and metasomatic processes in a thrust zone between carbonate sediments and descendants from the oceanic crust. The minerals that are identified are typical for metasomatic processes leading to skarn formation (e.g. Henmi et al., 1971; Nysten & Skogby, 1994). The green colour is due to chromium that is present in most of the constituent minerals.

Sannan-Skarn will have its position among other green stones, such as jadeite, Maw Sit Sit, nephrite a.s.o. It seems, however, clear that it has to be identified correctly and shall be sold under its correct name Sannan-Skarn, the recommended trade name for this new ornamental gemstone. The opaque material is suitable for cabochons, spheres, carvings and other jewellery items. Sannan-Skarn can either be differentiated from Maw Sit Sit by polarization microscopy of thin sections, by EDXRF by checking for Ca, or by micro-Raman spectroscopy through the identification of aegirine, winchite, hydrogrossular and the other minerals listed above.

References

- Franz, L., Tay, T.S., Hänni, H.A., De Capitani, C., Theerapongs, T., Atichat, W., 2014. A comparative study of jadeite, omphacite and kosmochlor jades from Myanmar, and suggestion for a practical nomenclature. *J. Gemmol.*, 34, 210-229.
- Hänni, H.A., Meyer, J., 1997. Maw-sit sit (kosmochlor jade): A metamorphic rock with a complex composition from Burma. *Proceedings of the 26th International Gemmological Conference Idar-Oberstein, Germany*, 22-24.
- Henmi, K., Kusachi, I., Numano, T., 1971. Contact minerals from Kushiro, Hiroshima prefecture, (I) gehlenite and hydrogrossular. *J. Min. Soc. Japan*, 10, 160-169 (in Japanese).
- Kazmi, A.H., Snee, L.W., 1989. *Emeralds of Pakistan, geology, gemology and genesis*. Geological survey of Pakistan. Van Nostrand Reinhold Company, Melbourne, Australia, ISBN 0-442-30328-9.
- Nysten, P., Skogby, H., 1994. Manganese ferro-ferri-winchite from Harstigen, Filipstad, central Sweden. *Mineral. Mag.*, 58, 168-172.

Chemistry and gemmological features of spinels from Sri Lanka and Vietnam

Arūnas Kleišmantas¹; Gamini E. Zoysa²; Edward Liu Shang I³

¹Department of Geology and Mineralogy, Vilnius University, M. K. Čiurlionio St. 21/27, LT-03101 Vilnius, Lithuania; arunas@kleismantas.eu

²Ceylon Gemmological Sciences, 32, Joseph Lane, Colombo 4, Sri Lanka; gaminigz@hotmail.com

³The Gemmological Association of Hong-Kong; gemedward@hotmail.com

Chemistry and colour

The chemical analysis was carried out using the scanning electron microscope Quanta 250/450/650. The chemical composition of various colour hues from Ratnapura of Sri Lanka and Luc Yen of Vietnam were investigated. Various research books claim that the colour of spinel is determined by chromophores Cr^{3+} , Fe^{2+} , Fe^{3+} and Co^{2+} (Bukanov, 2001; Henn, 1995; Karanth, 2000). In the articles of some researchers are mentioned, that Cr^{3+} , V^{3+} , and Fe^{2+} , Fe^{3+} are responsible for the dominant red colour (Gorghian et al., 2013) and red (orange), of various hues purple, grey, purplish blue, bluish green (Schmetzer, et. al. 1989), and Fe^{2+} , Fe^{3+} , Co^{2+} blue, purplish or greyish blue, and bluish green or grey (Schmetzer, et. al. 1989). After chemical analyses of spinels from these 2 localities, we would like to complement this statement, since V^{3+} determines brown and yellow colour of spinel. The highest content of V_2O_3 (0.44 – 0.88 wt.%) was found in four spinel samples from Ratnapura, Sri Lanka (Table 1).

Table 1. Chromophore oxides (weight percent) in orangy pink and pinkish orange spinels from Sri Lanka.

| No/Colour | $\text{V}_2\text{O}_3\%$ | $\text{Cr}_2\text{O}_3\%$ | $\text{FeO}\%$ | $\text{CoO}\%$ |
|-------------------|--------------------------|---------------------------|----------------|----------------|
| 1. Orangy pink | 0.50 | 0.32 | 0.19 | 0.07 |
| 2. Orangy pink | 0.53 | 0.36 | 0.28 | 0.20 |
| 3. Orangy pink | 0.44 | 0.11 | 0.08 | 0.05 |
| 4. Pinkish orange | 0.88 | 0.05 | 0.08 | 0.08 |

(*-submitted together with FeO and Fe_2O_3 contents)

The colour is orangy pink or pinkish orange, and not red, as claimed by the abovementioned authors (Gorghian et al., 2013). We believe that the orangy hue is determined by V^{3+} , together with low or medium, content of Cr_2O_3 (0.05 – 0.36 wt.%), where Cr^{3+} determines the red and pink colour (Bukanov, 2001; Gorghian et al., 2013; Henn, 1995; Karanth, 2000). As expected, these samples feature a relatively low content of iron oxide (0.08 – 0.28 wt.%) and cobalt oxide (0.05 – 0.20 wt.%), as Fe^{2+} and Co^{2+} determine the purple and the blue colour of spinel (Bukanov, 2001; Chauviré et al., 2015; Henn, 1995; D'Ippolito et al., 2015; Karanth, 2000, Schmetzer et al., 1898). Hence together with Cr^{3+} these minerals can acquire pink hue. It is a fact that V^{3+} also influences the green colour of various minerals, such as beryl (emerald), tourmaline, garnet (demantoid), which are coloured by Cr^{3+} , and V^{3+} (Feral, 2015; Henn, 1995). Cr^{3+} determines the red colour of spinels, however our opinion is that V^{3+} , differently than Cr^{3+} , can determine yellow colour. Accordingly we can claim that if V^{3+} determined the red colour of spinel or, as in the case of other minerals, green colour, the tested samples would not have orange hue. It is perfectly illustrated by the pinkish orange spinel sample from Ratnapura locality (Sri Lanka) (Table 1, No. 4), which features a high content of vanadium oxide 0.88%, whereas the contents of chrome, iron and cobalt oxides (respectively 0.05 wt.% 0.08 wt.% and 0.08 wt.%) are very low (Table 1). Vanadium ions can determine yellow and brown colour as example in unheated Tanzanite (zoisite) (Feral, 2015). Thus, we believe that V^{3+} can determine the yellow and brown colour of spinel.

The red colour of dark red spinel is determined by a high content of Cr³⁺ (Table 2). Purple/violet colour of samples is determined by Fe²⁺ and a low content of Co²⁺, whereas the pink hue of samples is determined by Cr³⁺ and high content of Fe²⁺, which saturation depends on the quantitative ratio of Fe²⁺ and Cr³⁺ (Table 3). Relatively low contents of chromophores V³⁺, Cr³⁺, Fe²⁺ and Co²⁺ (respectively 0.02 – 0.08 wt.%, 0.02 – 0.04 wt.%, 0.18 – 0.31 wt.% and 0.03 – 0.04 wt.%) were found in the pinkish grey spinel, thus their hue is grey.

Table 2. Chromophore oxides in dark red spinel from Sri Lanka.

| No/Colour | V ₂ O ₃ % | Cr ₂ O ₃ % | FeO% | CoO% |
|-------------|---------------------------------|----------------------------------|------|------|
| 1. Dark red | 0.29 | 1.63 | 0.09 | 0.02 |
| 2. Dark red | 0.26 | 1.85 | 0.11 | 0.08 |

(*-submitted together with FeO and Fe₂O₃ contents)

Table 3. Chromophore oxides in purple/violet, pink spinels.

| No/Colour | Locality | V ₂ O ₃ % | Cr ₂ O ₃ % | FeO% | CoO% |
|-----------------------|-----------|---------------------------------|----------------------------------|-----------|-----------|
| 1.Purple/violet | Vietnam | 0.02-0.04 | 0.01-0.06 | 1.86-2.86 | 0.06-0.08 |
| 2.Light purple/violet | Vietnam | 0.08 | 0.13-0.14 | 0.62-0.65 | 0.02 |
| 3.Purple/violet | Sri Lanka | 0.02 | 0.04 | 1.16 | 0.03 |
| 4.Light purple/violet | Sri Lanka | 0.02-0.03 | 0-0.15 | 0.58-0.65 | 0.03-0.11 |
| 5.Vivid pink | Vietnam | 0.05-0.23 | 0.10-0.20 | 0.86-2.17 | 0.02-0.07 |
| 6.Pink | Vietnam | 0.05-0.22 | 0.04-0.11 | 0.74-0.76 | 0.03-0.06 |
| 7.Light pink | Vietnam | 0.04-0.33 | 0.10-0.11 | 0.22-0.24 | 0.05-0.10 |
| 8.Light pink | Sri Lanka | 0.06-0.23 | 0.03-0.11 | 0.07-0.24 | 0.02-0.08 |

(*-submitted together with FeO and Fe₂O₃ contents)

The content of V₂O₃ in pink spinels is varying from 0.04 to 0.33 wt.%, however it may not influence the colour. The content of V₂O₃ 0.4 wt.%, supposedly determines the yellow and brown colour. According to Schmetzer et. al. (1989) the colour of spinel contain distinct amounts of vanadium, orange red to orange colours were observed. V₂O₃ content of the tested spinels, the assumption can be made that the content of V₂O₃ that can determine the brown or yellow colour starts at 0.4 wt.%, whereas together with a low content of Cr³⁺, it determines orange colour. It can be related to the magnetic features of vanadium. Vanadium is not magnetically detectable, when concentration is not less than approximately 0.4 wt.% of vanadium oxide (Feral, 2015). When vanadium become magnetic, it could also has influence for the spinel colour.

Mineral inclusions

The chemical analysis of the minerals inclusions were carried out using the scanning electron microscope Quanta 250/450/650. According to Chauviré et.al. (2015) and Malsy et. al. (2012) blue and orangey-red to orangey-pink spinels from Vietnam were identified these mineral inclusions: dolomite, calcite, titanite, rutile, zircon, graphite, apatite, pyrrhotite, pentlandite, violarite, clinocllore, phlogopite, graphite, magnesite and chondrodite. After comparison with before mentioned authors about spinels from Vietnam, we identified other minerals inclusions: corundum and zoisite inclusions in the pink spinel, as well clay minerals inclusions in the blue spinel. And after comparison with Gubelin et. al. and before mentioned authors about spinels from Sri Lanka, we identified other minerals inclusions: allanite, paragonite (Figure 1), zoisite, K-feldspar, plagioclase, florencite (Figure 2) inclusions in the grey or near-colorless spinels, as well biotite, pyrite diopside inclusions in the pink, red and purple spinels.

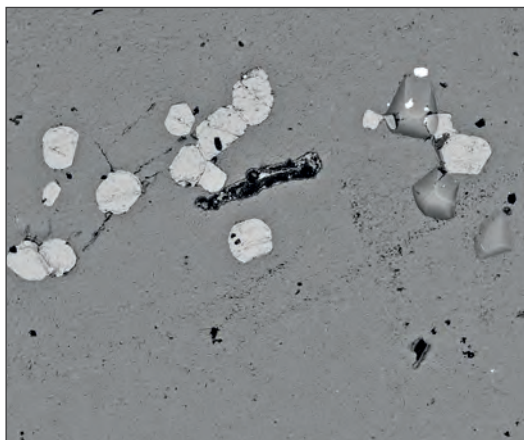


Figure 1. Paragonite (grey), clinochlorite (black), phlogopite (light grey) inclusions in spinel from Sri Lanka.

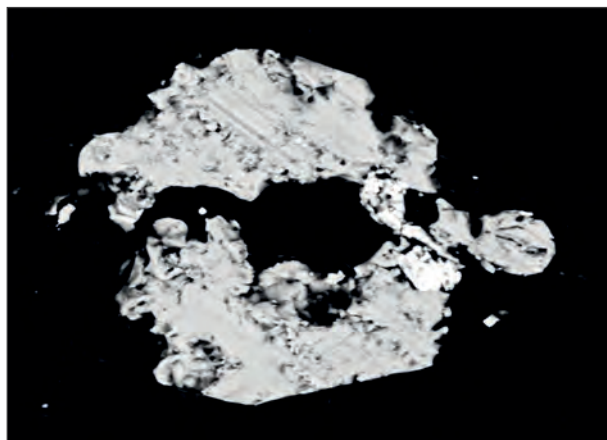


Figure 2. Florensite inclusion in spinel from Sri Lanka.

References

- Bukanov, V., 2001. Colored stones, Gemological Dictionary, 66.
- Chauviré, B., Rondeau, B., Fritsch, E., Ressigeac, P., Devidal, J.-L., 2015. Blue Spinel from the Luc Yen District of Vietnam, *Gems & Gemology*, 51(1).
- Feral K., 2015. http://www.gemstonemagnetism.com/spinel_pg_2.html.
- Gorghian, A., Mottana, A., Rossi, A., Oltean, F.M., Esposito, A., Marcelli, A., 2013. Investigating the colour of spinel: 1. Red gem-quality spinels („balas“) from Ratnapura (Sri Lanka), *Accademia Nazionale dei Lincei*, 14, 127-140.
- Gubelin, E.J., Koivula, J.I., 2004. Photoatlas of Inclusions in Gemstones, Spinel and its inclusions, 372-382.
- Henn, U., 1995. Spinel. *Gemmologie, Z. Dt. Gemmolog. Ges.*, 44(4), 54-57.
- D'Ippolito, V., Andreozzi, G.B., Halenius, U., Skogby, H., Hametner, K., Günther, D., 2015. Color mechanisms in spinels: cobalt and iron interplay for the blue color, *Physics and Chemistry of Materials*, <http://dx.doi.org/10.1007/s00269-015-0734-0>
- Karant, R.V., 2000. Spinel. *Gems and gem industry in India*; Geological Society of India, 205-208.
- Malsy, A.-K., Karampelas, S., Schwarz, D., Klemm, L., Armbruster, T., Tuan, D.A., 2012. Orange-red to orange-pink gem spinels from a new deposit at Lang Chap (Tan Huong-Truc Lau), Vietnam *The Journal of Gemmology*, 33, 1-4, 19-27.
- Schmetzer, K., Haxel, C., Amthauer, G., 1989. Colour of natural spinels, gahnospinel and gahnites, *Neues Jahrbuch für Mineralogie Abhandlungen*, 160(2), 159-180.

Cobalt diffusion-treated spinel

Michael Krzemnicki, Hao Wang¹,
Tom Stephan, Ulrich Henn²

¹SSEF – Swiss Gemmological Institute, Basel
michael.krzemnicki@ssef.ch

²German Gemmological Association, Idar-Oberstein

Since 2015 dark blue spinel which is diffusion-treated with cobalt is encountered in larger quantities especially in the Asian gem market. First information and gemmological characteristics were given by [Saeseaw et al. \(2015\)](#) und [Peretti et al. \(2016\)](#). Both conclude, that this treatment is easy to detect by a trained gemmologist and that these stones in many aspects clearly differ from natural untreated Co-spinels, highly appreciated and valued in the trade.

Generally, diffusion treatment causes artificial colouration or colour modification on colourless to pale coloured source material by admixing colouring substances/elements during a specific heat process.

Diffusion close to the surface, i.e. with a shallow penetration depth (generally < 1 mm) of colouring transition metals such as Fe and Ti, Cr or Co is known for corundum but not so much for spinels since the 1970s. By using light and small ions such as Be, a deeper penetration of diffusion (so-called lattice diffusion) is reached– with the effect of activating and stabilizing colour-centers in corundum.

We report here about our findings of spinels treated by surface-related diffusion with cobalt to produce a deep blue colour.

Results

For this study, two sample series were investigated, compiled from material before and after treatment process. Figure 1 shows one sample series; from left to right: untreated rough (2.86 ct), untreated pre-cut (2.23 ct; 8.03 x 6.86 x 4.04 mm), diffusion-treated pre-cut (2.43 ct; 9.03 x 6.93 x 4.82 mm) and diffusion-treated polished (2.24 ct; 9.01 x 7.00 x 4.42 mm).



Figure 1. Series of spinels before (2 samples on the left) and after diffusion-treatment with Co (two samples on the right).

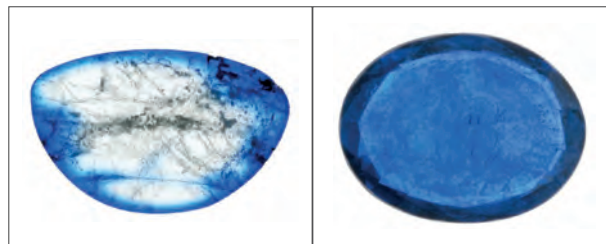


Figure 2. Cross-section of a Co diffusion-treated spinel with distinct deep blue colouration close to the surface and colour concentration in surface-reaching fissures. Width of cross section 12.4 mm

Figure 3. Patchy colour distribution and deep blue colour concentrations in surface-reaching fissures. Weight: 2.24 ct (length 9 mm).

The cross-section (Figure 2) cut from a research sample reveals in detail the penetration depth of the surface-related diffusion of cobalt (about 1 mm). Furthermore we can see that the diffusion acts also along in surface-reaching fissures, resulting in a deep blue colour along such a fissure. An irregular, partly patchy colour distribution can be observed when a cut sample is immersed in water (Figure 3). As in the cross-section, the surface-reaching fissures are characterized by a deep blue colour concentration.

Refractive index and density

The physical characteristics such as the refractive index and density are in the known range of natural spinel: $n = 1.715$ and $D = 3.59 \text{ g/cm}^3$.

Microscopic features

Studies with a gemstone microscope (immersion) determine numerous tension cracks and neo-healing cracks with flux residues. Both clearly indicate heat treatment at a relatively high temperature. Figure 4 shows large flux residues in neo-healed fissures with tiny colourless needles as a result of a devitrification process during the cooling stage of the treatment.

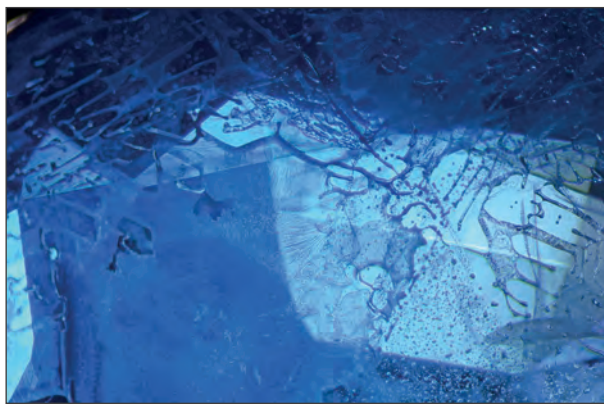


Figure 4. Artificially healed fissure with flux residues containing small devitrification needles. Magnification 35x

Chemical characteristics

A chemical profile was measured across one cross-section of a diffusion-treated blue spinel with a GemTOF (see <http://www.gemtof.ch>) operating at SSEF. This new and highly versatile analytical method is using a laser (193 nm) which ablates small particles from the gemstone which are then ionized (ICP) and subsequently analyzed in a time-of-flight mass spectrometer (Wang et al., 2016 and references therein).

The surface diffusion of cobalt is clearly apparent in Figure 5. The chemical profile from rim to core to rim shows Co concentrations up to 3894 ppm on the rim. 4-6 ppm Co in the core were possibly present before treatment and had no influence on the original colour, given the very high concentration of iron. Ni and less strongly Ti show positive correlation with Co.

Figure 6 shows strong concentration variation of elements presumably originating from vitreous residues in artificially healed fissures (especially Na, B and Si).

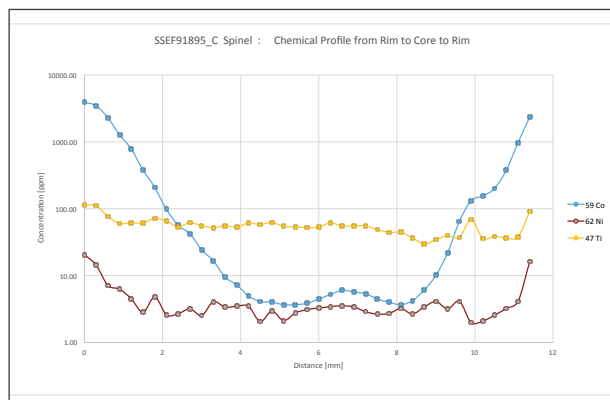


Figure 5. Chemical profile showing high Co-concentrations on the rim and positive correlation with Ni and Ti.

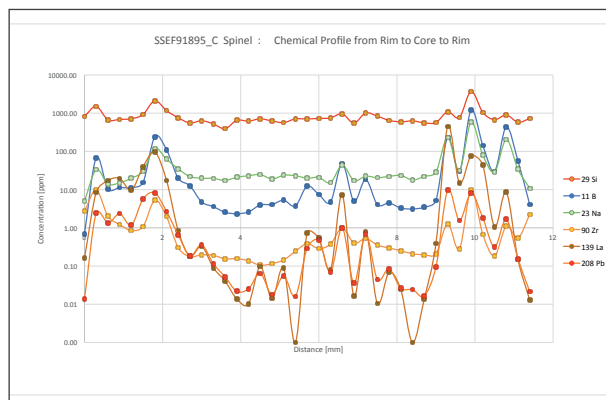


Figure 6. Chemical profile with strong concentration variation of elements (Na, B and Si) presumably originating from residues in artificially healed fissures.

Absorption spectra

The visible absorption spectrum of the Co diffusion-treated deep blue spinel is dominated by Co^{2+} -bands with maxima at 348, 581 and 623 nm (Shigley & Stockton 1984, Hanser 2013, Chauvire et al. 2015). Additional absorption bands at 388 nm as well as 458 and 475 nm (weak) are due to Fe^{2+} of the original grey-violet material.

References

- Chauviré, B., Rondeau, B., Fritsch, E., Ressigeac, P., Devidal, J-L., 2015. Blue Spinel from the Luc Yen District of Vietnam. *Gems & Gemology*, 51(1), 2-17.
- Hanser C., 2013. Blue Co-spinel from Luc Yen, Vietnam: a spectroscopic study. Unpublished Bachelor thesis (supervision M.S. Krzemnicki), Univ. Freiburg i. Br., Germany.
- Krzemnicki M.S., 2016. Cobalt diffusion-treated spinel. SSEF Facette, No. 22, p. 24. www.ssef.ch/fileadmin/Documents/PDF/640_Facette/SSEF-FACETTE22-Bd.pdf
- Peretti, A., Günther, D., Haris, M. T. M., 2016. New spinel treatment discovered involving heat- and cobalt-diffusion. www.gemresearch.ch
- Saeseaw, S., Weeramonthonlert, V., Khowpong, C., Ng-Pooresatien, N., Sangsawong, S., Raynaud, V., Ito, C., 2015. Cobalt Diffusion of Natural Spinel: a report describing a new treatment on the gem market. www.gia.edu/gia-news
- Shigley, J.E., Stockton C.M., 1984., 'Cobalt-blue' gem spinels. *Gems & Gemology*, 20(1), 34-41.
- Wang H.A.O., Krzemnicki M.S., Chalain J-P., Lefèvre P., Zhou W., Cartier L.E., 2016. Simultaneous high sensitivity trace-element and isotopic analysis of gemstones using laser ablation inductively-coupled plasma time-of-flight mass spectrometry. *Journal of Gemmology*, 35(3), 212–223, <http://dx.doi.org/10.15506/JoG.2016.35.3.212>

Acknowledgements

Part of the studied samples were kindly donated by Thamrong Charasaiya, A. Di Salvo, and Jeffery Bergman, all from Bangkok (Thailand).

Kosmochlor-bearing jadeite rocks from Kenterlau-Itmurundy (Lake Balkhash, Kazakhstan)

Leander Franz¹, Michael Krzemnicki², Kristina Ernst³, Christian de Capitani⁴,
George E. Harlow⁵, Nicolai Kouznetsov⁶

¹Mineralogisch-Petrographisches Institut, University of Basel, Switzerland, leander.franz@unibas.ch

²SSEF Swiss Gemmological Institute, Basel, Switzerland

³ETH Zürich, Switzerland

⁴Mineralogisch-Petrographisches Institut, University of Basel, Switzerland

⁵American Museum of Natural History, New York, U.S.A

⁶Jade Resources, LTD, Hong Kong

Petrographic, petrologic and geochemical investigations on Cr-jadeite rocks from Kenterlau-Itmurundy near Lake Balkhash (Kazakhstan) reveal five different rock groups. *Jadeitites* show irregular, medium-grained white sections made up of decussate jadeite crystals and fine-grained sections made up of aligned Cr-jadeite. *Omphacite jadeitites* show a homogeneous, pale green colour with randomly oriented jadeite crystals, which are overgrown by omphacite on their rims and along fractures. *Phlogopite-analcime jadeitites* show decussate, white sections made up of jadeite and foliated, partially microfolded green layers and spots consisting of Cr-jadeite. Analcime and phlogopite formed late in fractures in the jadeite-rich sections. *Phlogopite-omphacite jadeitites* reveal an inhomogeneous mineral distribution with a dark-green matrix made up of sheaf-like aggregates of Cr-omphacite and white spots of decussate prismatic jadeite crystals. Post-crystallization deformation is evident by bent and twisted pyroxenes while phlogopite formed post-tectonically on fractures and grain boundaries. Due to the extreme textural inhomogeneity, transitions between these four groups are blurred. *Kosmochlor-analcime-albite-omphacite jadeitites* reveal an inhomogeneous fabric with decussate, white sections, pale-green shear bands, and dark green layers. Again, white jadeite-rich sections formed pre-tectonically while shear bands display aligned Cr-omphacite, and in rare cases small aggregates of kosmochlor (identified by Raman spectroscopy, see Fig. 1). The main occurrence of kosmochlor is in the dark green layers, where it mantles strongly corroded chromite grains (Fig. 2). Microprobe investigations of two kosmochlor-bearing rocks and one phlogopite omphacite jadeite reveal extreme mineral compositional variability. Pyroxene zoning with jadeite cores and rim sections of omphacite or Cr-omphacite are wide spread. Similarly, kosmochlor aggregates are very inhomogeneous covering a wide range in the pyroxene plots (Figs. 3 A&B). Similar textures have been observed by other investigations (e.g. Shi et al., 2005) and are due to pre-, syn- and post-tectonic crystallization processes. Distinct inhomogeneities are also revealed by ED-XRF spot analyses, which show a strong compositional variability from section to section.

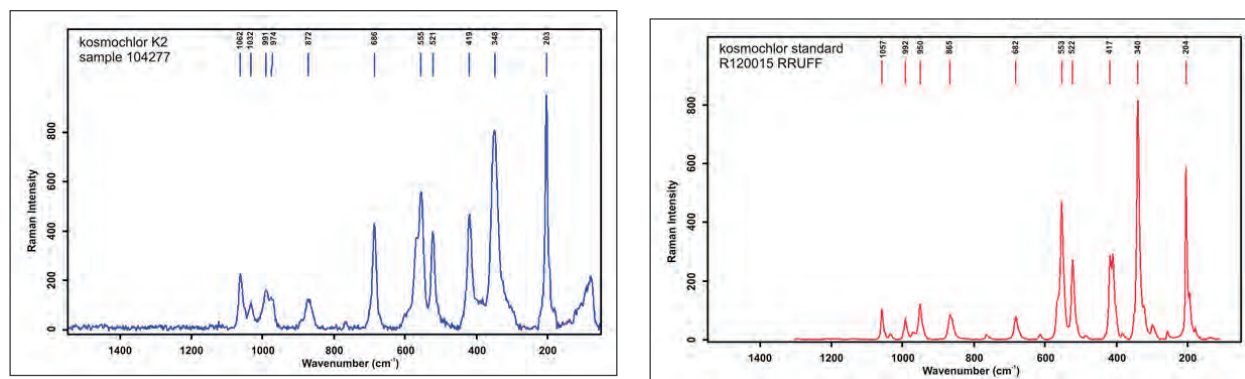


Figure 1. Raman spectra of kosmochlor from sample 104277 and of kosmochlor standard R120015 from the RRUFF database.

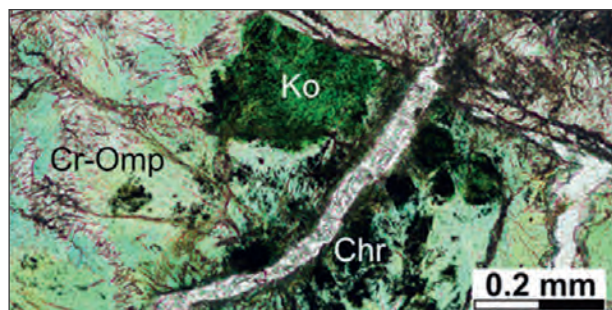


Figure 2. Microphotograph of sample 104277 (II polarizers) showing kosmochlor-aggregates (Ko) with chromite (Chr) surrounded by Cr-omphacite (Cr-Omp), Cr-jadeite (Cr-Jd) and jadeite (Jd) in. Fractures are filled with albite and analcime.

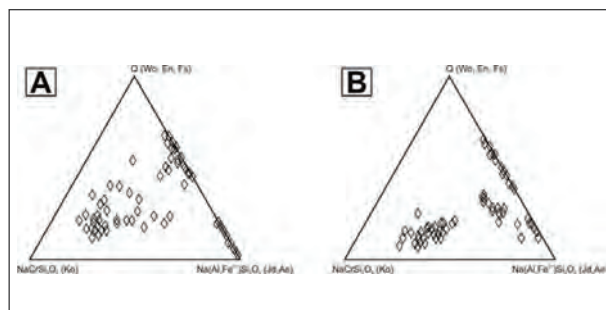


Figure 3. Microprobe analyses from the kosmochlor-bearing samples 104276 (A) and 104277 (B) reveal the great compositional variability of pyroxene in these rocks.

As evident from these investigations, nearly pure jadeite formed pre-tectonically. During subsequent deformation, Ca- and Cr-rich fluids led to the formation of omphacite, Cr-omphacite, Cr-jadeite and eventually to kosmochlor. The largest modal amount of kosmochlor formed pre- and syn-tectonically in chromite-bearing layers of the rocks. Analcime, albite and phlogopite formed post-tectonically and during late brittle deformation.

Until now, terrestrial kosmochlor has been described from Burma (Ou Yang 1984; Hänni & Meyer 1997), New Zealand (Ikehata & Arai 2004), Japan (Anthony et al., 1995), Kola peninsula and Lake Baikal, Russia (Zozulya et al. 2003; Reznitskii et al., 1999). Similar to these occurrences, the presence of kosmochlor in Cr-rich jadeitites from Kenterlau-Itmurundy, is explained by appropriate rock composition, pervasive HP/LT conditions (i.e. 600°C at 1.2 GPa; Dobretsov & Ponomareva 2009). According to their rock fabrics and to the geology of the area we interpret the Kazakhstan jadeitites as P-types as defined by Tsujimori & Harlow (2012).

References

- Anthony, J.W., Bideaux, R.A., Bladh, K.W., Nichols, M.C., 1995. Handbook of Mineralogy. Volume 2: Silica, silicates. Part one, 430 pp.
- Dobretsov, N.L., Ponomareva, L.G., 2009. Comparative characteristics of jadeite and associated rocks from Polar Ural and Prebalkhash region. *International Geology Review* 10, 221-242.
- Hänni, H. A., Meyer, J., 1997. Maw-sit-sit (kosmochlore jade): A metamorphic rock with a complex composition from Burma. *Proceedings of the 26th International Gemmological Conference Idar-Oberstein, Germany*, 22-24.
- Ikehata, K., Arai, S., 2004. Metasomatic formation of kosmochlor-bearing diopside in peridotite xenoliths from North Island, New Zealand. *American Mineralogist*, 89, 1396-1404.
- Ou Yang, C.M. 1984., Terrestrial source of ureyite. *American Mineralogist*, 69, 1180-1183.
- Reznitskii, L.S., Sklyarov, E.V., Karmanov, N.S., 1999. The first find of kosmochlor (ureyite) in metasedimentary rocks. *Doklady Akademii Nauk*, 363, 1049-1053.
- Shi, G.H., W., Stöckhert, B., Cui, W.Y., 2005. Composition and texture of kosmochlor and chromium clinopyroxenes in rocks from the Myanmar jadeite area. *Mineralogical Magazine*, 69, 1059-1075.
- Tsujimori, T., Harlow, G.E., 2012. Petrogenetic relationships between jadeite and associated high-pressure and low-temperature metamorphic rocks in worldwide jadeite localities: a review. *European Journal of Mineralogy*, 24, 371-390.
- Zozulya, D.R., Gavrilenko, B.V., Savchenko, Y.E., 2003. Kosmochlor from coastal sediments of Tersky coast in the White Sea, Kola Peninsula. *Zapiski Vserossijskogo Mineralogicheskogo Obshchestva*, 132, 101-108.

Rare Fancy Sapphires from Bo Phloi Gem Field, Kanchanaburi, Western Thailand

Thanong Leelawatasuk, Tasnara Sripoonjan*, Namrawee Susawee,
Pornsawat Wathanakul and Visut Pisutha-Arnond

The Gem and Jewelry Institute of Thailand (Public Organization),
Bangkok 10500 Thailand; *Email: stasnara@git.or.th

Introduction

Over the past few decades, the Bo Phloi gem field of Kanchanaburi province in the western Thailand was one of the important sources of blue sapphires supplied to the world market. Blue sapphires from Kanchanaburi have long been well known for their deep blue colour and large variations in sizes. Those sapphires occur in subsurface gem-bearing gravel beds of a secondary alluvial deposit. The sapphire gravels were derived from a weathered alkaline basalt nearby. As of the present days, the production has dramatically been decreased due to the depletion of the resources in the areas. In the past decades, however, the very rare and less well-known varieties of fancy sapphires were also collected by a mine owner during the active mining activity. Those materials are pink, violet-purple, yellow, green and parti-colour varieties of sapphires that allowed to be used for this study by the owners. In this study, 10 representative samples (Figure 1) were selected from the owner's collection (totally 15 stones). The stones' gemological properties were collected by basic gem equipment and various advanced instruments, such as UV-Vis-NIR, FTIR, Raman and EDXRF spectroscopy.

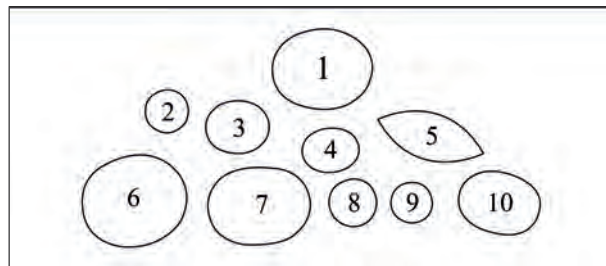


Figure 1. Fancy sapphire samples from Bo Phloi gem field, Kanchanaburi, Thailand: (1) violet, 7.65 ct; (2) pale green, 0.78 ct; (3) parti-colour, 2.60 ct; (4) green, 1.39 ct; (5) yellow, 2.72 ct; (6) pale pink, 9.38 ct; (7) pink, 6.35 ct; (8) pink, 1.07 ct; (9) purple, 0.71 ct; (10) pink, 2.99 ct. Photo by T. Sripoonjan.

Gemological Properties

The stones had the RI of 1.760-1.770, SG of 3.92-4.01 and mostly were inert to moderate orangey red under LWUV radiation and mostly inert under SWUV radiation. Microscopic observation revealed that the most common internal features were fingerprint-like inclusions which were sometimes filled with orange-brown iron oxides (Figure 2A, B). Almost all the samples contained cloud-like inclusions as well as brown silks identified by Raman spectroscopy as hematite (Figure 2C, D). Some samples showed iridescent platelets (Figure 2E) and mineral inclusions such as a nepheline also by Raman spectroscopy (Figure 2F).

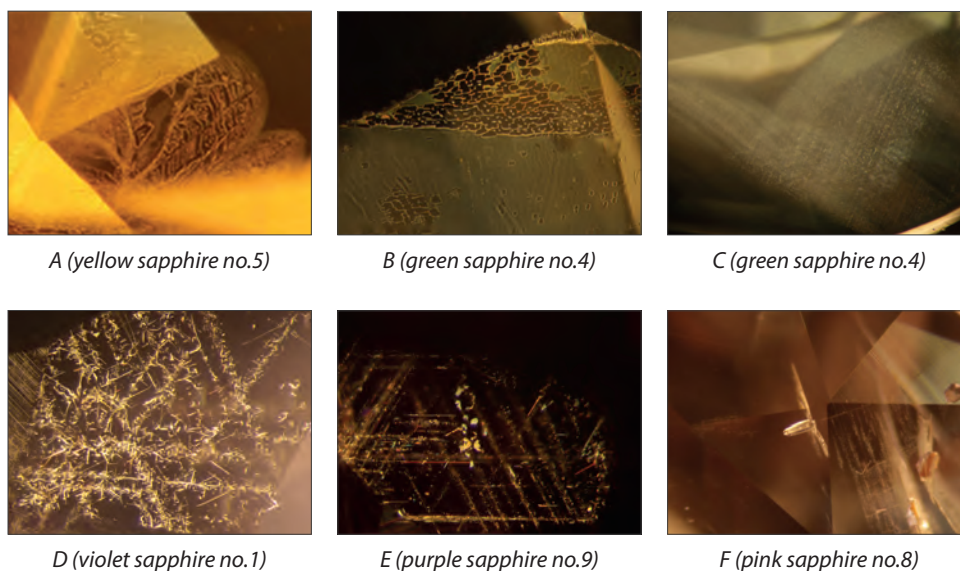


Figure 2. Microscopic features of inclusions in fancy sapphires from Bo Phloi, Kanchanaburi (see text for further details) Photos by T. Sripoonjan.

Advanced spectroscopy

UV-Vis-NIR spectra (Figure 3) clearly showed different absorption bands diagnostic of colour varieties as well as peaks at 378, 387 and 450 nm due to Fe^{3+} appeared in all varieties. Cr^{3+} - related absorption bands were usually observed in violet-purple and pink varieties, whilst $\text{Fe}^{2+}/\text{Ti}^{4+}$ IVCT absorption bands were commonly present in blue and green stones (as suggested by Burn, 1993; Fritsch and Mercer, 1993). The spectra in Mid-IR region displayed absorption peaks related to AlOOH (Bowersox et al., 2000) at 3360, 3090, 2622 and 2416 cm^{-1} (see Figure 4). EDXRF analyses (Table 1) gave high iron content in all colour varieties (av. 0.54 wt.% Fe_2O_3). High titanium contents are found in green and parti-colour samples (av. 0.02 wt.% TiO_2), whereas high chromium contents appeared in violet, purple and pink varieties (av. 0.03 wt.% Cr_2O_3). Gallium and vanadium contents typically averaged 0.02 wt.% Ga_2O_3 and 0.01 wt.% V_2O_5 .

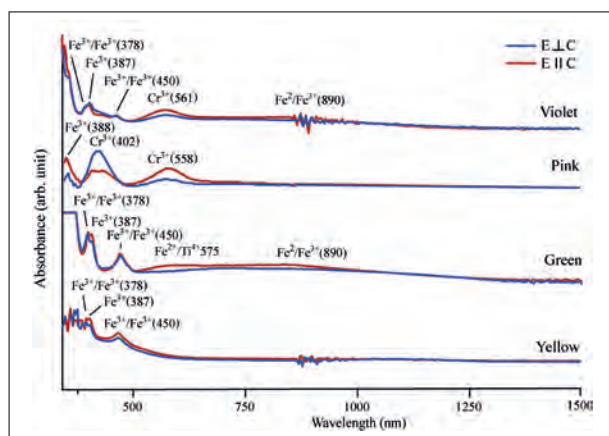


Figure 3. UV-Vis absorption spectra of various coloured sapphires from Bo Phloi gem field.

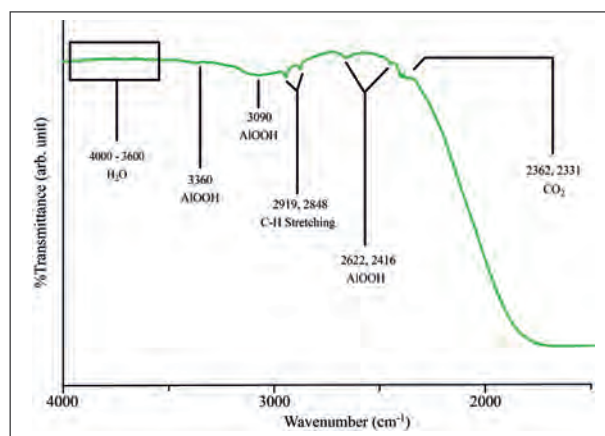


Figure 4. FTIR spectrum of a representative fancy sapphire showing absorption peaks related to AlOOH .

Table 1. EDXRF analyses of fancy sapphires from Bo Phloi, Kanchanaburi (wt.%).

| Oxides\Colours | Pink (4) | Yellow (1) | Green (2) | Violet-Purple (2) | Parti (1) |
|--------------------------------|-------------|------------|-------------|-------------------|-----------|
| TiO ₂ | 0.007-0.018 | 0.008 | 0.018-0.025 | 0.014-0.023 | 0.017 |
| V ₂ O ₃ | 0.004-0.016 | 0.010 | 0.003-0.029 | 0.007-0.013 | 0.040 |
| Cr ₂ O ₃ | 0.015-0.033 | 0.010 | 0.002-0.006 | 0.024-0.088 | 0.089 |
| Fe ₂ O ₃ | 0.055-0.428 | 0.093 | 0.935-0.937 | 0.358-0.410 | 0.438 |
| Ga ₂ O ₃ | 0.013-0.021 | 0.027 | 0.026-0.026 | 0.021-0.025 | 0.022 |

Discussion and Conclusion

The colors of fancy sapphires from Bo Phloi, Kanchanaburi are related well to the amounts of their trace element constituents; (1) the pink hue is caused mainly by the Cr³⁺-related absorption that correspond well to its high Cr but low Ti contents; (2) the yellow hue is due mainly to Fe³⁺ transitions that correspond well to its high Fe but low Ti and Cr contents (3) the violet-purple hue is caused by the combination of the blue coloration from Fe²⁺/Ti⁴⁺ and Fe²⁺/Fe³⁺ IVCT plus pink from the Cr³⁺-related absorption that correspond well to its high Cr, Fe and Ti contents; (4) the green hue is caused by the combination of the blue coloration from Fe²⁺/Ti⁴⁺ and Fe²⁺/Fe³⁺ IVCT plus yellow from Fe³⁺ transitions that correspond well to its high Fe and Ti but low Cr contents. Moreover, the high Ga contents (130-252 ppm) of our pink-violet-purple samples are comparable to those (170-310 ppm) of the rare alluvial ruby–sapphire transition megacrysts found in Australia; thus, the chemical data obtained from this study may suggest that the pink-violet-purple sapphires could involve in a magmatic-related metasomatic process as proposed by Sutherland et al. (2017). It is noteworthy that the presence of the nepheline inclusion in the pink sapphire also supports a model that the Bo Phloi fancy sapphires was likely to originate from a syenetic-melt as suggested by Khamloet et al. (2014).

References

- Bowersox, G.W., Foord, E.E., Laurs, B.M., Shigley, J.E. and Smith, C.P., 2000. Ruby and Sapphire from Jegdalek, Afghanistan. *Gems & Gemology*, 36(2), 110-236.
- Burns, R.G., 1993. *Mineralogical applications of crystal field theory*, 2nd ed., Cambridge, Great Britain: Cambridge University Press, 576 p.
- Fritsch, E., and Mercer, M., 1993. Blue Color in sapphire caused by Fe²⁺/Ti⁴⁺ intervalence charge transfer, *Letters, Gems & Gemology*, 29(3), 151 and 226.
- Khamloet, P., Pisutha-Arnond, V. and Sutthirat, C., 2014. Mineral inclusions in sapphire from the basalt-related deposit in Bo Phloi, Kanchanaburi, western Thailand; indication of their genesis. *Russian Geology and Geophysics*, 55, 1087-1102.
- Sutherland, F.L., Graham, I.T., Harris, S.J., Coldham, C., Powell, W., Belousova, E.A. and Martin, L. 2017. Unusual ruby–sapphire transition in alluvial megacrysts, Cenozoic basaltic gem field, New England, New South Wales, Australia. *Lithos* 278–281, 347–360.

Acknowledgements

We are gratitude to Mr. Paiboon Pimpisitthavorn, the S.A.P. mine owner, for providing the stones. This study was fully funded by the GIT. The authors would like to sincerely thank to Mrs. Wilawan Atichat for her suggestion and kind reviewing the manuscript.

Characteristics of exceptionally gem-quality untreated blue sapphires from Bo-Phloi gemfield, Kanchanaburi-Thailand

Thanapong Lhuaamporn, Saengthip Saengbuanglam, Nataya Nilhud, Thanong Leelawatanasuk

The Gem and Jewelry Institute of Thailand; thanapongl1986@gmail.com

Introduction

The Bo-Phloi gemfield in the Kanchanaburi province of Western Thailand has been known as one of the world important sources of blue sapphire related to basaltic origin. Nowadays, the production output becomes scarce due to the depletion of the resource. In the past decades, majority of the raw materials from this deposit needed to be enhanced by heating to improve their inferior quality, because the commercially gem-quality untreated stones are very rare. As such, the characteristics of those untreated materials have not been well documented in literatures. In early April 2017, the GIT Gem Testing Laboratory (GIT-GTL) had an opportunity to study 29 exceptionally rare gem-quality cut stones of unheated blue sapphires weighing from 0.73 to 2.66 ct (Figure 1) declared to be mined from the Bo-Phloi gemfield by a mine owner. The overall colour of this set of blue sapphires are light to very deep blue. In contrast, the majority of sapphires from this deposit commonly show grayish hue with silky appearance that requires heat treatment, while the unheated gem-quality stones from this source are usually found in medium tone of blue color rather than deep blue like the stones shown in Figure 1.



Figure 1. The representative of blue sapphire samples from Bo-Phloi, Kanchanaburi-Thailand.

Basic properties

The gemological properties of all specimens collected by basic instruments showed RI values of 1.770-1.762 and inert under SWUV and LWUV lights. Their inclusions under 60x microscope displayed silks, clouds, fingerprints, strong blue color banding, twinning planes, crystals and iron stains as shown in Figure 2. No indications of heating were observed in these stones.

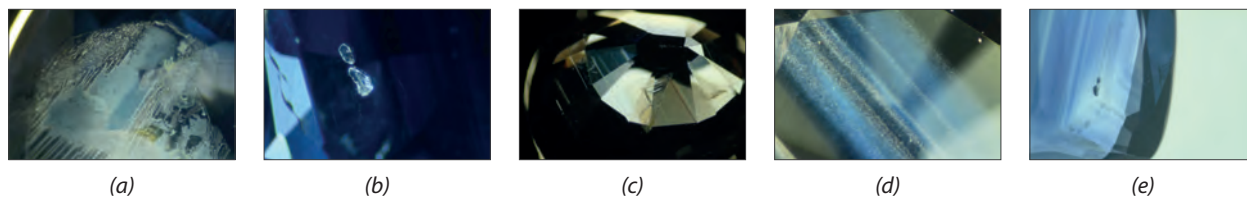


Figure 2. The inclusions of blue sapphire from Bo-Phloi: (a) fingerprint with iron stain, (b) crystal inclusions, (c) repeated twinning planes, (d) silks and clouds, (e) angular color banding.

Advanced instruments

The Mid-IR spectra of some samples collected by a FTIR-Nicolet 6700 showed peaks at 3619 cm^{-1} , 3650 cm^{-1} , 3695 cm^{-1} (Figure 3) that indicate a type of mica or kaolinite (Balmer et al., 2007). The OH stretching peak displayed at 3309 , 3232 cm^{-1} (Beran et al., 2006.). Nevertheless, some samples did not show any significant peaks.

The UV-Vis-NIR spectra (see Figure 4) of all samples measured by a PerkinElmer spectrometer model Lambda 950 displayed the dominant Fe^{3+} -related absorption peaks at 330 , 388 , 377 and 450 nm as well as the strong absorption bands caused by $\text{Fe}^{2+}/\text{Ti}^{4+}$ and $\text{Fe}^{2+}/\text{Fe}^{3+}$ IVCT around 900 and 575 nm , respectively, that are responsible for its blue colouration (Nassau & Valente, 1987; Burn, 1993; Fritsch & Mercer, 1993; Schmetzer & Schwarz, 2004). These are the typical absorption pattern of blue sapphires from basaltic-type origin.

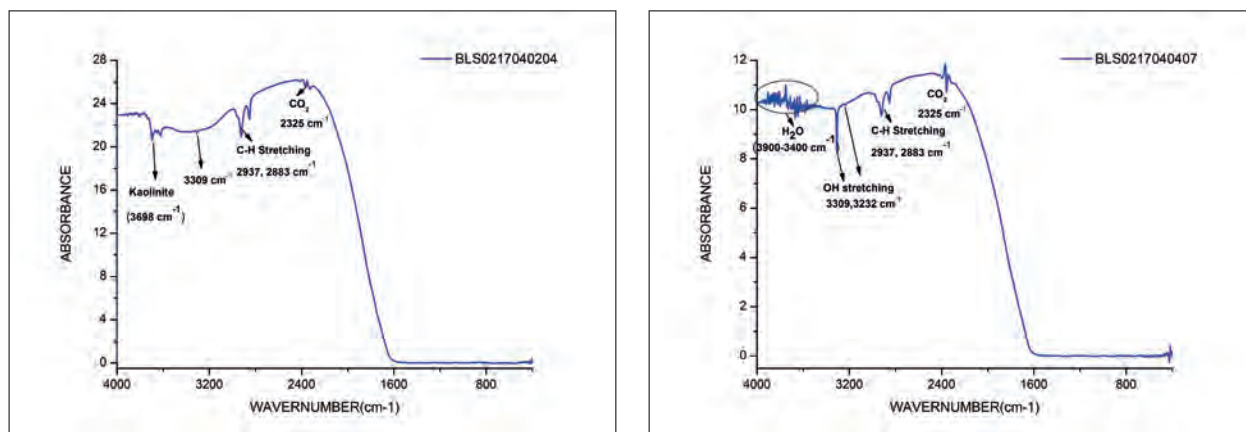


Figure3. FTIR spectra of Bo-Phloi blue sapphires: (a)kaolinite and OH stretching peak (b)strong OH stretching peak.

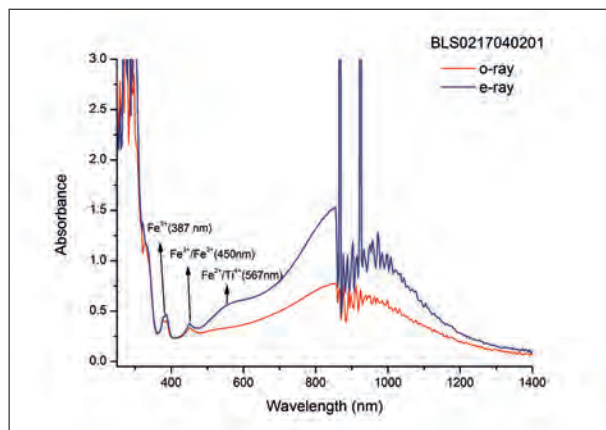


Figure4. A representative UV-Vis-NIR spectra of Bo-Phloi blue sapphire.

The chemical compositions of the stones analyzed by EDXRF-EDAX Eagle III (Table 1) gave rather high Fe contents and moderate Ga contents. The Ti, Ga and Ti/Fe were compared with blue sapphires from other sources in Thailand (Figure 5).

Table 1. Chemical compositions of 29 Bo-Phloi blue sapphires by EDXRF.

| Element oxide | Concentration range (wt%) | Mean (29 samples) |
|--------------------------------|---------------------------|-------------------|
| Al ₂ O ₃ | 99.66-99.36 | 99.56 |
| TiO ₂ | 0.02-bdl | 0.01 |
| V ₂ O ₅ | 0.01-bdl | 0.01 |
| Cr ₂ O ₃ | 0.01-bdl | 0.01 |
| Fe ₂ O ₃ | 0.58-0.31 | 0.40 |
| Ga ₂ O ₃ | 0.03-0.01 | 0.02 |

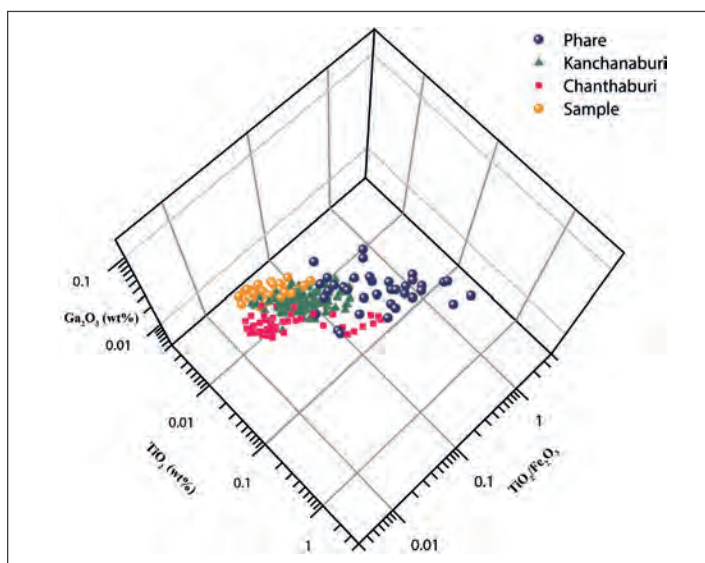


Figure 5. The 3-D comparison plot of the samples and blue sapphires from other sources in Thailand.

Conclusion

The diagnostic characteristics of these exceptional gem-quality untreated blue sapphires from Bo-Phloi gemfields are 1) their intense blue coloration and the prominent color banding without any indication of heat-treatment, 2) occasionally with the presence of some kaolinite absorption peaks at 3619 cm⁻¹, 3650 cm⁻¹, 3695 cm⁻¹ on the FTIR spectrum. However, the remaining properties, such as their inclusion features, their chemical compositions and the UV-Vis-NIR absorption patterns are consistent with those of blue sapphires from basaltic origin elsewhere. The 3D comparison plot of the chemical data reveals that these stones fall within the area of Kanchanaburi sapphires and can be discriminated from those of Phare and Chanthaburi.

References

Balmer, W.A., Leelawatanasuk, T., Atichat, W., Wathanakul, P., Somboon, C., 2006. Update on characteristics of heated yellow sapphires. Poster, Proceedings of the 1st International Gem and Jewelry Conference, 3pp.

Beran, A., Rossman, G.R., 2006. OH in naturally occurring corundum. *European Journal of Mineralogy*, 18(4), 441–7.

Fritsch, E., Mercer, M., 1993. Blue Color in Sapphire Caused by Fe²⁺/Fe³⁺ Intervalence Charge Transfer, *Letters. Gems & Gemology*, 29(3), 151 and 226.

Nassau, K., Valent, G.K., 1987. The seven types of yellow sapphire and their stability to light. *Gems & Gemology*, 23(4), 221-231.

Schmetzer, K., Schwarz, D., 2004. The causes of colour in untreated, heat treated and diffusion treated orange and pinkish orange sapphires- a review. *Journal of Gemmology*, 29(3), 149–82.

Smith, C. P., Kammerling, R.C., Keller, A.C., Peretti, A., Scarratt, K.V., Khoa, N.D., Repetto, S., 1995. Sapphires from southern Vietnam. *Gems & Gemology*, 31(3), 168-186.

Transparent gemstones and the most recent supercontinent cycle

John M. Saul

ORYX, Paris, France; john.saul@wanadoo.fr

Certain hard and normally opaque minerals, both rare and common, occasionally crystallize as transparent or partly transparent “gem” crystals. Such stones, designated “crystalline colored gemstones” (CCGs), form under highly constrained just-so “Goldilocks” conditions that did not exist prior to the last supercontinent cycle.

- One set of gem-forming conditions arises during continent-to-continent collisions and the *amalgamation of continents*.
- Another, which produces distinctively different gems, comes into existence during crustal extension and the *breakup of continents*.

CCGs are defined as minerals with a Mohs hardness of 6 or more, which, after faceting, have produced transparent stones weighing a half carat or more (Saul, 2007, 2014, 2017). Quartz gems are excluded from the definition of CCGs, originally as a matter of convenience, with the later justification that gems should be rare. Also excluded from the working definition of CCGs are those emeralds and alexandrites that formed in contact-metamorphic deposits in which crystal growth was cushioned by massive mica. The gem beryl and topaz deposits at Volodarsk (Korosten), Ukraine and at Luumäki in Finland are also special cases where crystal growth within watery bubbles was cushioned by granitic magma of unusual composition while still locally viscous (Touret, 1992; Peter Lyckberg, personal communication, March 2012; Saul, 2014). The rubies and pink sapphires from Aappaluttoq, Greenland, are not reliably dated (Smith et al., 2016) and are also excluded.

Type 1 CCGs

Type 1 CCGs form at depth in 3-D sites where the temperature was greatly elevated. Elevated temperature allows minerals to crystallize higher in the crust, hence with lower constraining pressure, thereby allowing the growth of crystals of superior quality, i.e. gems.

The requisite heat is produced by friction when one continental plate begins to pass (subduct) beneath another, as in the Kenya/Tanzania border region, the Himalayas, the Hindu Kush, the Pamirs, and the Urals.

A 3-D “craterform” scar is present in each of these CCG-producing areas (Figures), vestiges of the Late Heavy Bombardment (which is the episode that also scarred the face of the Moon, c.4100-3800 Ma). This provided a slanting zone of crustal weakness that guided the down-going plate. Clusters of primary CCG deposits formed on the upper plate in areas of weak crust and greatest heating just inside the circumferences of the craterform scars.

Aside from the special cases mentioned above, the world’s oldest CCGs are those formed during the Pan-African ‘Event’ (which was an extended episode of continent-to-continent collisions, not a singlet event) from c.640 Ma to perhaps 520 Ma. Such ages have been obtained for the crystallization of CCGs in the Gondwanan lands of eastern Africa, Sri Lanka, Madagascar, western Namibia, and eastern Brazil. These dates are interpreted as signaling the first doubling of the continental crust, or the first (and possibly concurrent) oblique continent-to-continent collisions, or the first (and possibly concurrent) episodes of deep subduction. (There is no consensus concerning the time when deep subduction first occurred, as was made clear by a show of hands at the end of the International Workshop on the Origin and Evolution of Plate Tectonics held at Monte Verità, Locarno, 17-22 July 2016.)

In sum, the first appearance of Type 1 CCGs (as defined to exclude special cases) signals the initiation of modern style plate tectonics, with deep subduction first occurring in zones of weakness dating to the formation of our planet. Type 1 CCGs are associated with the amalgamation of continents.

Type 2 CCGs

Blue-green-yellow magmatic (BGY-mag) sapphires, the oldest of which is apparently not older than 300 Ma, are the prime example of Type 2 CCGs. Such gems are known from eastern Australia, far eastern Russia, eastern China, Cambodia, Laos, Vietnam, Thailand, Rwanda, Cameroon, NW Kenya, Madagascar, France, Germany and elsewhere, with some localities intriguingly close to Gondwanan Type 1 CCG areas, but mostly not. Such occurrences are associated with crustal extension and the *break-up of continents*.

The mode of formation of BGY-mag sapphires is incompletely understood, but can be roughly outlined. During extension and supercontinent break-up, high-density pure CO₂ is released in great quantities, “an important mechanism for transferring deep mantle fluids towards the Earth’s surface” (Touret and Huizenga, 2012).

When a CO₂ bubble-domain invades a silicic melt or magma containing Fe and Mg, the magma becomes oversaturated in aluminum (Guo et al., 1996). Exsolution forces the crystallization of corundum crystals that incorporate trace amounts of Fe and Ti that give the characteristic color to BGY-mag sapphires. Corundum crystals are subsequently brought to the Earth’s surface by alkali basaltic lava, to which they readily adhere (Baldwin 2015). Gem quality crystallization is due to the cushioning effect on crystals growing partly or entirely within the dense CO₂ fluid. When pressure varies under such circumstances, the change is transmitted equally in all directions, with no shearing or folding, but with production of color zones within individual crystals of BGY-mag sapphires where the uptake of traces of Fe and Ti did not keep pace with the exsolution of the aluminum. Some BGY-mag sapphires form in near ideal circumstances as unattached “floaters”, entirely surrounded and cushioned by CO₂.

References

Baldwin, L.C., 2015. Origin and formation of alkali basalt-hosted sapphire megacrysts from the Cenozoic Siebengebirge Volcanic Field, W Germany [Ph.D. thesis]: University of Bonn, 211pp.

Guo, J., O’Reilly, S.Y., and Griffin, W.L., 1996. Corundum from basaltic terrains: a mineral inclusion approach to the enigma: *Contributions to Mineralogy and Petrology*, 22, 368–386.

Saul, J.M., 2007. On the Origin of deposits of Crystalline Colored Gemstones: 30th International Gemmological Conference, Moscow, Abstract.

Saul, J.M., 2014. *A Geologist Speculates: Les 3 Colonnes*, Paris, 159pp. ISBN 978-23-7081-004-5.

Saul, J.M., 2017. Transparent gemstones and the most recent supercontinent cycle, *International Geology Review* (submitted).

Smith, C.P., Fagan, A.J., and Clark, B., 2016. Ruby and pink sapphire from Aappaluttoq, Greenland: *Journal of Gemmology*, 35(4), 94-306.

Touret, L., 1992. Les pegmatites de Volhynie (Ukraine): *Revue de Gemmologie, A.F.G.*, 110, 25-26.

Touret, J.L.R., and Huizenga, J.M., 2012. Fluid-assisted granulite metamorphism: A continental journey: *Gondwana Research*, 21, 224-235.

The author thanks the Richard Lounsbery Foundation for backing this project, and Lauriane Pinsault for mapwork.

A single caption for all figures:

Maps showing primary deposits of Type I crystalline colored gemstones (CCGs) and their relationship to the edges of former continental plates, to orogenic belts, and to large 3-D circular scars.

Color origin of color-changing diaspore from Turkey

Andy H. Shen, Cuihong Liu, Tian Shao, Min Ye

Gemmological Institute, China University of Geosciences, Wuhan, China; ahshen1@live.com

Diaspore from Turkey (known as “zultanite” or “csarite” in the trade) can produce a decent color changing effect - when viewed in D65 light source it appears to be yellowish-brown; in incandescent light, orange pink (Figure 1). We used two rough crystals from Turkey (Lüle, 1996, Lüle, 2012) and orient them according to the perfect cleavage plane {010} in diaspore and other crystallographic characteristics. Six thin slabs perpendicular to specific crystallographic axis (three from each crystal), each about 1.5mm in thickness, were made. These slabs were checked with their refractive indices along the crystallographic axes to ensure the orientations were correct. We then conducted conventional gemological testing, polarized ultraviolet-visible (UV-Vis) spectroscopy and laser ablation inductively coupled plasma mass spectrometry (LA-ICP-MS) to obtain further gemological properties, polarized UV-Vis spectra and trace element concentrations.



Figure 1. The color-changing effect of diaspore sample B-1.

Table 1. LA-ICP-MS data of diaspore samples.

| Sample number | unit: ppm | | | | | |
|---------------|-----------|------|-----|------|-----|------|
| | Si | Fe | Ti | Cr | Ga | V |
| B-1-1 | 2780 | 5840 | 436 | 152 | 131 | 23.5 |
| B-1-3 | 2820 | 5600 | 401 | 145 | 135 | 22.5 |
| B-1-4 | 2680 | 5710 | 384 | 135 | 129 | 22.5 |
| B-2-2 | 2829 | 6631 | 563 | 101 | 143 | 24.9 |
| B-2-3 | 2427 | 6315 | 598 | 99.6 | 142 | 23.8 |

The results from LA-ICP-MS showed that the main trace elements of these samples are Fe, Si, Ti together with minute amount of Cr and Ga (Table 1). These values are consistent with what we previously reported (Ye et al., 2016). A JASCO MSV-5200 microscopic polarized UV-Vis spectrometer was used in UV-Vis spectroscopy study. The absorption band positions in green-yellow area are different when samples are tested with the polarized light's electric vector aligned with different crystallographic directions (Figure 2). In 'E//a' direction, the absorption band peaked at 567.6nm; while in 'E//b' and 'E//c' direction the absorption band peaked at 574 nm and 546.6 nm respectively; bands are all broad and weak but the 'E//b' is the strongest. This absorption band in green-yellow area is the main cause of the color-changing effect. Additionally, in the violet-blue area, strong absorption near 371nm, 385nm, 391nm and 447nm are seen and are most likely due to d-d electronic transition of Fe³⁺ and coupled Fe³⁺- Fe³⁺ transition (Ye et al, 2016 and the references therein).

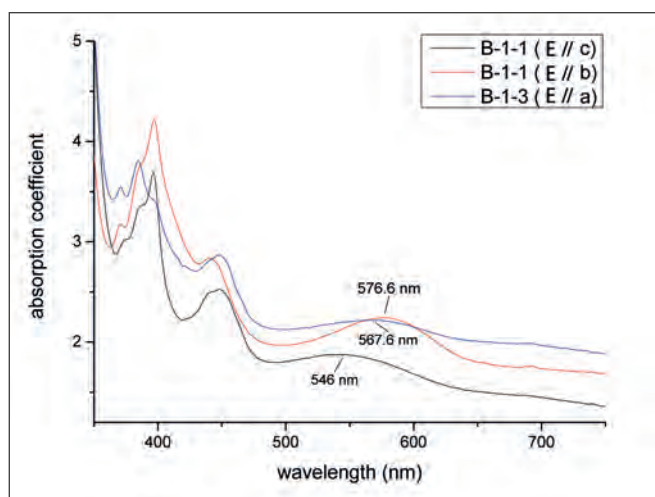


Figure 2. UV-Vis polarized absorption spectra of diaspore sample B-1.

Compared with the polarized UV-Vis absorption spectra of an oriented blue sapphire, both diaspore and blue sapphire have an absorption band near 576 nm. From Burns (1993), an Fe²⁺ - Ti⁴⁺ pair located in two adjacent edge-sharing octahedra in a corundum structure has a separation of 0.279 nm and with IVCT energy of 17,400cm⁻¹, which corresponding to light with wavelength of 574.7 nm. In the case of a blue sapphire, additional band of 14,000 cm⁻¹ (714 nm in wavelength), which is attributed to Fe²⁺ - Ti⁴⁺ pair located in two adjacent face-sharing octahedra (with an Al-Al distance of 0.265 nm) has made the blue sapphire blue.

The crystal structure of diaspore consists of an essentially hexagonal close-packed array of O atoms with Al occupying one half of the available octahedral interstices. Each Al occupied octahedron shares four edges with four adjacent Al occupied octahedra to form the 'double rutile strings' parallel to the c-axis (Ewing, 1935). These strings are then linked by corner-sharing oxygen atoms to equivalent strings (Figure 3). The A1- A1 distance between two adjacent octahedra is 0.2845 nm, and that of the other two edge-sharing adjacent octahedra is 0.3098 nm, as to the corner-sharing adjacent octahedra, the A1- A1 distance is 0.3289 nm (Hill, 1979). Therefore, the shortest distance between Al-Al in diaspore is comparable to those in the edge-sharing octahedral sites in corundum and, in diaspore structure, there is no face-sharing octahedral sites.

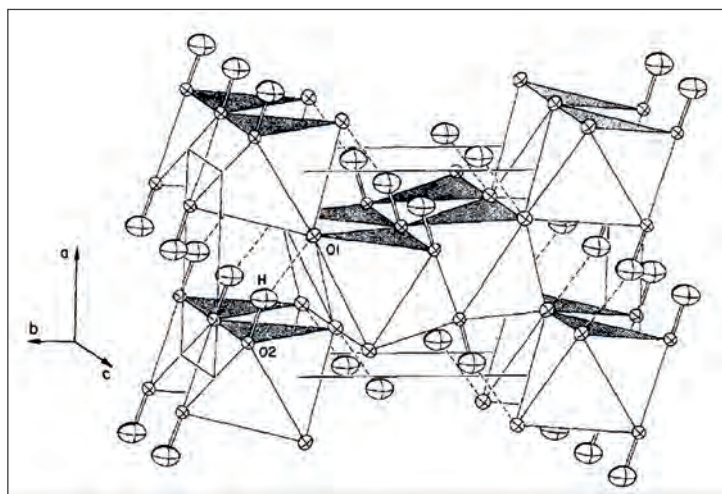


Figure 3. The structure of diaspore (Roderick J. Hill, 1979).

Therefore, from comparing the polarized spectra of these color-changing diaspore and analyzing the similarity and difference between the corundum and diaspore structure (Hänni, 1983, Hänni, 2017), we believe there is good evidence to show the color-changing effect in the diaspore is caused by Fe^{2+} - Ti^{4+} pairs located in the adjacent edge-sharing octahedra. The lack of face-sharing octahedral sites in diaspore has prevented diaspore to develop blue body color. Additionally, in all color-changing diasporites we have analyzed, $[\text{Fe}] \gg [\text{Si}] + [\text{Ti}]$. Thus, even though the Si^{4+} may take up some Fe^{2+} instead of forming useful color absorbing Fe^{2+} - Ti^{4+} pairs, there are plenty of Fe^{2+} in the crystal to fully take up Ti^{4+} to form Fe^{2+} - Ti^{4+} pairs.

References

- Burns, R.G., 1993. Mineralogical Applications of Crystal Field Theory (second edition). Britain: Cambridge university press, 1993: 105-153.
- Ewing, F. J., 1935. The Crystal Structure of Diaspore. *Physics and Chemistry of Minerals*, 3, 203-207.
- Hänni, H.A., 1983. Weitere Untersuchungen an einigen farbwechselnden Edelsteinen. *Z. Dt. Gemmol. Ges.* 32(2/3), 99-106.
- Hänni, H.A., 2017. Diaspor mit Farbwechsel und eine Glas-Imitation. *Z.Dt.Gemmol.Ges.* 66(1/2), 5-12.
- Hill, R.G., 1979. Crystal Structure Refinement and Electron Density Distribution in Diaspore. *Physics and Chemistry of Minerals*, 5, 179-200.
- Lüle, C., 1996. Mineralogy, crystallography, formation, conditions and gemmological features of diaspore occurrences of Küçükçamlitepe Bauxite Deposits within the region of Milas-Mugla , Turkey, Master Thesis, Ankara University, Ankara, Turkey
- Lüle, C. & Sayili S., 2012. Gem quality diaspore from turkey. *Abstract Proceedings, GIT, Bangkok, Thailand*, 86 – 89.
- Ye, M., Shen, A.H., Peng, W., 2016. Gemmological and Spectral Characteristic of Zultanite: Colour Changing Diaspore. *Journal of Gems and Gemmology*, 18(5), (in Chinese with English abstract).

Research of Jadeite Inclusions: Graphite and Zircon

Jian Mao¹, Elizabeth Su²

¹Gemstone Testing Centre of ECUST, Shanghai, China, jmao@ecust.edu.cn

²Gemsu Rona (Shanghai) Jewellery Co., Ltd., Shanghai, China, esu_gems@yahoo.com

In this paper, we discuss a type of special jadeite sample with distinct black veiny texture composed of minute graphitic materials, in which zircon inclusions are observed clearly under microscope. Zircon and carbonaceous materials (CM) occur in various igneous and metamorphic rocks as common accessory minerals. Previous researches revealed that direct correlation exists between the degree of graphitization of CM and metamorphic grade of host rocks. Otherwise, zircon is regarded as ideal U-Pb dating mineral for its good stabilization, which can be able to remain chemically closed under extreme geological conditions. A suite of formation ages of jadeite rocks were given by different geologists on the basis of respective U-Pb dating analysis of zircon inclusions in Myanmar jadeite samples. Apparently, there are obvious difference between these published results. It may be attributed to different loss quantity of radiogenic Pb of zircons during multi-period deformation and metamorphism and hydrothermal activities of jadeite formation. The goal of this paper is to analysis graphitic matters and zircon inclusions in the Myanmar jadeite samples and to provide useful information on estimating the form process of host jadeite rocks by Raman microprobe, incorporating BSE and CL imaging methods.

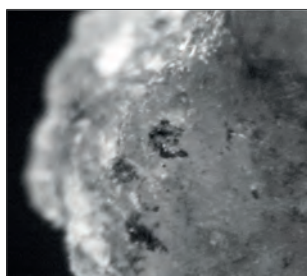


Figure 1



Figure 2



Figure 3



Figure 4

Photomicrograph of internal features of jadeite samples (30X). Figure 1 Black graphitic matters on the surface and cross section (20X, reflected light). Figure 2 and Figure 3 Zircons with different morphologies marked by the circles (30X, transmitted light). Figure 4 the biggest zircon inclusion "HTZN" (160X, plain-polarized light). Each zircon inclusion is verified by Raman microprobe.

Conclusion

Raman spectroscopy is an effective analytical method of geology and genetic mineralogy and can provide useful information and convictive evidence to the research on the Myanmar jadeitite formation process. Raman spectral parameters of graphitic inclusions in the jadeite samples illustrate that graphitic matters formed from hydrothermal fluids in the late stage of jadeitite formation. The hydrothermal fluids also give rise to alternation and structure recovery of zircon inclusions in the jadeitite rocks based on the Raman micro-analysis and BSE imaging of different areas (rims and cores). In practice, we suggest that the intensities of Raman bands assigned to laser-induced luminescence of REE (from 1053 to 1460 cm^{-1}) can be regarded as important index for distinguishing between hydrothermal and hydrothermal-altered zircon rims and remnant cores. Raman spectroscopy can be used as pre-analysis and selection of test point for zircon trace-element compositions analyzing.

References

- Cui, W.Y., Shi, G.H., Yang, F.X., and Zhang, L.C., 2000. A new viewpoint-magma genesis of jadeite jade, *Journal of Gems and Gemmology*, 2(3), 16-21.
- Dawson, P., Hargreave, M.M., and Wilkinson, G.F., 1971. The vibrational spectrum of zircon (ZrSiO_4), *J. Phys. C: Solid State Phys.*, 4, 240-256.
- Gaft, M., Panczer, G., Reisfeld, and R., Shinno, I., 2000. Laser-induced luminescence of rare-earth elements in natural zircon, *J. Alloy. Compd.*, 300-301, 267-274.
- Hoskin, P.W.O., and Black, L.P., 2000. Metamorphic zircon formation by solid-state recrystallization of protolith igneous zircon, *Metamorphic Geol.*, 18, 423-439.
- Hoskin, P.W.O., and Schaltegger, U., 2003. The Composition of Zircon and Igneous and Metamorphic Petrogenesis, *Rev. mineral. Geochem.*, 53, 27-55.
- Hoskin, P.W.O. 2005. Trace-element composition of hydrothermal zircon and the alteration of Hadean zircon from the Jack Hills, Australia. *Geochim. Cosmochim. Acta*, 69(3), 637-649.
- Mao, J., Chai, L.T., Liu, X.L., Fan, J.L., Xu, J.Y., and Jin, Z.Y., 2013. Research of Genesis of Black Bands in Burma Jadeite, *Spectroscopy and spectral analysis*, 33(9), 2411-2415.
- Nasdala, L., Wenzel, M., Vavra, G., Irmer, G., Wenzel, T., and Kober, B. 2001. Metamictisation of natural zircon: accumulation versus thermal annealing of radioactivity-induced damage, *Contrib. Mineral. Petrol.*, 141, 125-144.
- Nasdala, L., and Hanchar, J.M. 2005. Comment on: Application of Raman spectroscopy to distinguish metamorphic and igneous zircon, *Anal. Lett.*, 38, 728-734.
- Pasteris, J.D. 1989. In Situ Analysis in Geological Thin-Sections by Laser Raman Microprobe Spectroscopy: A Cautionary Note, *Appl. Spectrosc.*, 43, 567-570.
- Pasteris, J.D., and Chou, I.M. 1998. Fluid-deposited graphitic inclusions in quartz: Comparison between KTB (German Continental Deep-Drilling) core samples and artificially reequilibrated natural inclusions, *Geochim. Cosmochim. Acta*, 62(1), 109-122.

- Qiu, Z.L., Wu, F.Y., Yang, S.F., Zhu, M., Sun, J.F., and Yang, P. 2008. *Chin. Sci. Bull.*, 53(24), 3104-3111.
- Shi, G.H., and Cui, W.Y. 2004. Textures and Microstructures of Myanmar Jadeitite: Implications for formation of Jadeitic Fei-ts'ui, *Journal of Gems and Gemmology*, 6(3): 8-11.
- Shi, G.H., Cui, W.Y., Cao, S.M., Jiang, N., Jian, P., Liu, D.Y., Miao, L.C., and Chu, B. 2008. Ion microprobe zircon U–Pb age and geochemistry of the Myanmar jadeitite, *Journal of the Geological Society*, 165, 221-234.
- Wopenka, B., and Pasteris, J.D. 1993. Structural characterization of kerogens to granulite-facies graphite: Applicability of Raman microprobe spectroscopy, *Am. Mineral*, 78, 533-557.
- Xian, W.S., Sun, M., Malpas, J., Zhao, G.C., Zhou, M.F., Ye, K., Liu, J.B., Phillips, D.L. 2004. Application of Raman Spectroscopy to Distinguish Metamorphic and Igneous Zircons, *Anal. Lett.*, 37(1), 119-130.
- Xiong, D.X., Sun, X.M., Zhai, W., Shi, G.Y., and Wang, S.W. 2006. Graphite Inclusions with High Crystallinity in the Auriferous Quartz Veins from Daping Gold Deposit in Yunnan Province, China: Evidence for Involvement of Metamorphic Fluid from Granulite-Facies Lower Crust in the mineralization, *Acta Geologica Sinica*, 80(9), 1448-1457.
- Yui, T.F., Maki, K., Usuki, T., Lan, C.Y., Martens, U., Wu, C.M., Wu, T.W., and Liou, J.G. 2010. Genesis of Guatemala jadeitite and related fluid characteristics: Insight from zircon, *Chem. Geol.*, 270, 45-55.

Acknowledgments

We thank for the support from Prof. S. G. Guo, Y. Q. Wang, Dr. X. L. Liu, L. Y. Shi, X. Z. Han. Thanks Dr. J. L. Fan for providing distinctive research samples and innovative ideas. We also thank Y. Kan for Raman Micro-analysis.

Gem materials from upper Northern Thailand: potential in jewellery

Panjawan Thanasuthipitak¹, Kanyarat Kwansirikul, Weerapan Srichan, Phisit Limtrakun, Opor Saidum and Theerapongs Thanasuthipitak

¹Gemmology Programme, Department of Geological Sciences, Faculty of Science, Chiang Mai University, Chiang Mai, Thailand; panjawan.t@cmu.ac.th

A number of gem materials (minerals and rocks) found in upper Northern Thailand (Figure 1) could be used for jewellery. The best known are the alkali basalt-related sapphires from the deposit in the Denchai District of Phrae Province. The material and the deposits have been extensively studied by e.g. Limtrakun, 2003; Limtrakun et al., 2001; Wathanakul et al., 2012; Amphon, 2016.

Because of the unfavourable quality of the sapphires (mostly rather dark blue with some greenish blue, brown and dark trapiche-like core) only sporadic small scale mining activities took place since about 1957.

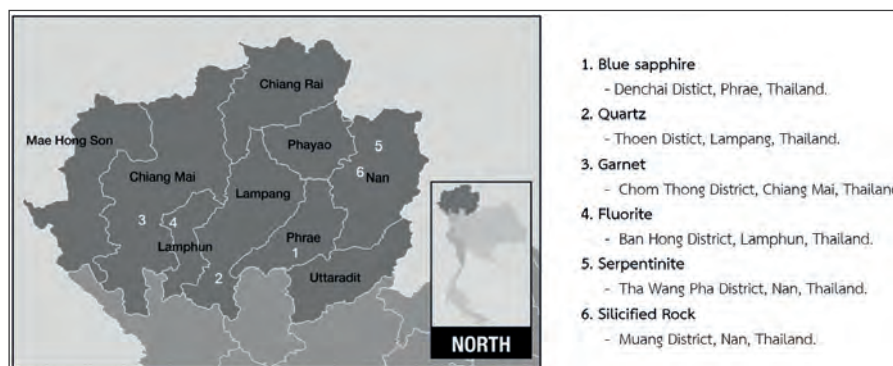


Figure 1. Distribution of some gem materials in upper Northern Thailand.

1. Blue sapphire (Denchai District, Phrae), 2. Quartz (Thoeng District, Lampang),
3. Garnet (Chom Thong District, Chiang Mai), 4. Fluorite (Ban Hong District, Lamphun),
5. Serpentinite (Tha Wang Pha District, Nan), 6. Silicified Rock (Muang District, Nan).

Even though, regardless of the quality, sapphire is a high potential gemstone, this study will concentrate on other gem materials of upper Northern Thailand and their potential to be used in jewellery.

These are: included quartz/rock crystal, garnet, fluorite, serpentinite and silicified volcanic rocks. They were selected on the basis of availability and the fact that they do not require any treatment or enhancement in terms of colour and/or clarity.

Examples of Lanna style jewellery including these gem materials are shown. Since at least the 14th century Thailand formed a principal part of the Lanna Kingdom which also includes parts of Southwest China, Northeast Myanmar and Northwest Laos.

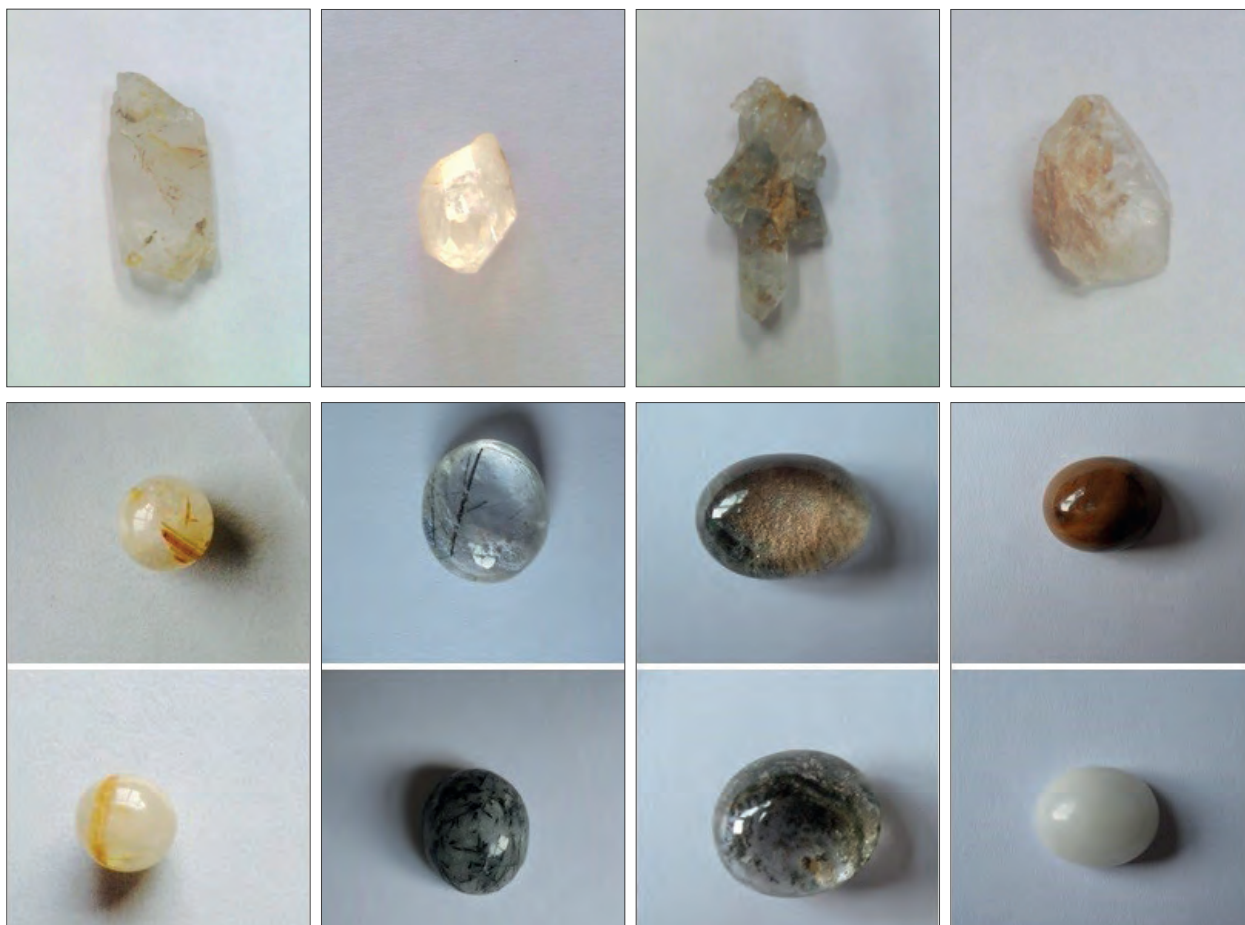


Figure 2. Rough and cabochon cut included quartz/rock crystal.

Included quartz/rock crystal (#2 in Figure 1)

The deposit of predominantly rock crystal and few amethyst is located in the Thoen District of Lampang Province forming hydrothermal or pneumatolytic veins in metamorphic country rocks (schist and gneiss).

The quartz crystals are generally 1-2 cm in size or bigger. They are transparent, although some are slightly cloudy white with tint of bluish gray. The mineral inclusions identified in the rock crystal are rutile, crocidolite, tourmaline, chlorite, hematite, and limonite. The specific gravity (SG) of 2.64-2.66 and RI of 1.54-1.55 are characteristic for of common quartz. The rock crystals to be set in Lanna style jewellery are cabochon cut with the inclusions at their base so that their yellow, green, or brownish red colour is observed on the surface (Figure 2). Examples of Lanna style jewellery using the included rock crystals are shown in Figure 3.



Figure 3. Lanna style jewelry with included rock crystal.

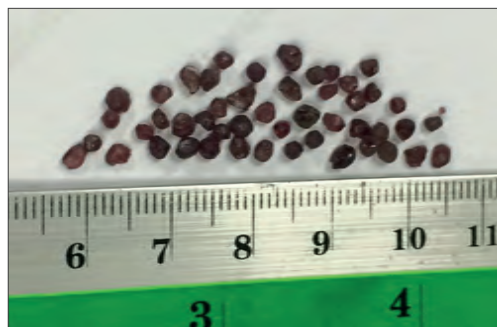


Figure 4. Almandine garnet rough from Chom Thong, Chiang Mai.

Garnet (#3 in Figure 1)

Almandine garnet of purplish red and strong pinkish red colour is found as alluvial heavy mineral fraction in a small stream bed in the Chom Thong District of Chiang Mai Province. The gem mineral most likely occurs as porphyroblast in gneiss. Some of the garnet samples show a good trapezohedron crystal habit. Most crystals are less than 0.5 cm in diameter (Figure 4) and hence are not suitable for use in the jewellery designed for this study. The garnet SG varies from 3.73 to 4.26, averaging at 4.00, while RI varies between 1.78 and 1.80.



Figure 5. Fluorite: rough and cabochon cut.

Fluorite (#4 in Figure 1)

Fluorite samples collected for this study originate from an old fluorite mine in the Ban Hong District of Lamphun Province. The mineralization is due to hydrothermal vein filling in limestone and shale of Permo-Carboniferous age. The samples show massive granular or botryoidal forms and are either transparent, green, or purple in colour (Figure 5) with SG from 3.06 to 3.18, averaging at 3.12 and RI of 1.43-1.44. Inclusions observed in the fluorite are iron oxide, two-phase inclusion, and liquid fingerprints. The mineral is cabochon cut and set in Lanna style jewellery (Figure 6).



Figure 6. Lanna style jewelry with fluorite.

Serpentinite (#5 in Figure 1)

Serpentinite is a metamorphosed mafic or ultramafic rock (for example peridotite or gabbro). The samples were collected from the Tha Wang Pha District of Nan Province. They are emerald green to dark green or brown to black in colour and composed mainly of serpentine group minerals and chlorite. Therefore they are quite soft and have a waxy or silky luster. SG varies between 2.44 and 2.89. The stones are cabochon cut (Figure 7) and also set in Lanna style jewellery.



Figure 7. Serpentinite and silicified volcanic rocks samples and cabochon cut samples.

Silicified volcanic rock (#6 in Figure 1)

The samples were collected from a Triassic-Jurassic volcanic belt in the Muang District of Nan Province comprising mainly andesite, rhyolite, and tuff/welded tuff. The rocks of the belt were locally silicified what makes them harder and sometimes adding a glassy luster. The colour varies from green and grayish green to purplish red (Figure 7). The rock samples are also cabochon cut and used in Lanna style jewellery (Figure 8).



Figure 8. Lanna style jewelry with silicified rhyolite.

Conclusion

The minerals and rocks, whose detailed gemmological properties (petrographic examination in case of rock samples) had been studied, were used in jewellery designed and created for this study. The aim is to introduce options available for the region jewellery cottage industry regarding both, raw materials and design.

References

- Amphon, R., 2016. Heat treatment of blue sapphires from Den Chai district, Phrae province. Master thesis, Chiang Mai University, 112 p.
- Limtrakun, P., 2003. Origin and distribution of corundum from an intraplate alkali basaltic province in Thailand: evidence from field and inclusion studies. PhD thesis, University of Tasmania, 274 p.
- Limtrakun, P., Khin, Z.K., Ryan, C.G., and Meruagh, T.P., 2001. Formation of the Denchai gem sapphires, northern Thailand: evidence from mineral chemistry and fluid/melt inclusion characteristics. *Mineralogical Magazine*, 65(6), p. 725-735.
- Wathanakul, P., Atichat, W., Ingavanija, S., Satitkune, S., Lhuaaporn, T., Monarumit, N. and Nanthasin, P., 2012. Blue sapphires from Phrae, northern Thailand. *Proc. 3rd GIT, Bangkok, Thailand*.

Acknowledgements

Funds for this study provided by the Thailand Research Fund and the National Research Council of Thailand are greatly appreciated. Thanks are also due to the Department of Geological Sciences, CMU for providing facilities needed for this study.

IGC 2017



NAMIBIA